Chemical Sensing and Catalytic Properties of Water-Stable Metal-Organic Frameworks Constructed from Dicarboxylate Ligands

A Dissertation Submitted to the

Indian Institute of Technology Guwahati

as Partial Fulfillment for the Degree of

DOCTOR of PHILOSOPHY

by

Rana Dalapati

DEPARTMENT OF CHEMISTRY

INDIAN INSTITUTE OF TECHNOLOGY GUWAHATI

GUWAHATI, INDIA

December 2018

Chemical Sensing and Catalytic Properties of Water-Stable Metal-Organic Frameworks Constructed from Dicarboxylate Ligands

A Dissertation Submitted to the

Indian Institute of Technology Guwahati

as Partial Fulfillment for the Degree of

DOCTOR of PHILOSOPHY

by

Rana Dalapati

Roll No. 146122002

DEPARTMENT OF CHEMISTRY

INDIAN INSTITUTE OF TECHNOLOGY GUWAHATI

GUWAHATI, INDIA

February 2019

Declaration

I hereby declare that the submitted thesis titled as "**Chemical Sensing and Catalytic Properties of Water-Stable Metal-Organic Frameworks Constructed from Dicarboxylate Ligands**" is the output of entire investigations carried out by me in the Department of Chemistry, Indian Institute of Technology Guwahati, under the proper guidance of Dr. Shyam P. Biswas. The result included in this thesis obtained from collaborative work has been acknowledged.

On following the scientific tradition all information provided in this thesis are correct to the best of my knowledge.

IIT Guwahati — Rana Dalapati

February 2019 — Candidate

Dr. Shyam P. Biswas
Associate Professor
Department of Chemistry
Indian Institute of Technology Guwahati
Guwahati – 781039, India
Tel: +91 – 361 – 258 3309
Email: sbiswas@iitg.ernet.in

Certificate

Certified that the work described in this thesis entitled "**Chemical Sensing and Catalytic Properties of Water-Stable Metal-Organic Frameworks Constructed from Dicarboxylate Ligands**" by Mr. Rana Dalapati, Department of Chemistry, Indian Institute of Technology Guwahati has been carried out under my supervision and has not been submitted elsewhere for a degree.

IIT Guwahati
February 2019

Dr. Shyam P. Biswas
Thesis supervisor
Department of Chemistry
Indian Institute of Technology Guwahati
Guwahati – 781039, Assam, India

Acknowledgment

I would like to express my gratitude and appreciation to all those who gave me the opportunity to complete the longest journey of my academic career as a Ph.D. student in the Department of Chemistry at the Indian Institute of Technology Guwahati. I like to express my deepest gratitude to my supervisor Dr. Shyam P. Biswas for his excellence guidance, caring, patience and providing me with an excellent atmosphere for doing my research work.

I would like to extend my heartiest appreciations to the doctoral committee members, Prof. V. Manivannan, Prof. Gopal Das and Dr. Chandan Mukherjee for their constant evaluation of my work and valuable suggestions. I would also like to thank all faculty members and staff members of the Chemistry department.

I take this opportunity to show my deep gratitude to our collaborators, Prof. Christoph Janiak, Prof. Norbert Stock, Dr. Helge Reinsch, Dr. Amarajothi Dhakshinamoorthy, Dr. Vishal Trivedi, Dr. Biman B. Mandal and Dr. Chinnakonda S. Gopinath for their invaluable contribution to my research work.

I am thankful to the Department of Chemistry and Central Instrument Facility (CIF) of IIT Guwahati for providing me the various sophisticated instrument for characterization of many of my compounds. I am also thankful to the entire technical officer and the operator in the Chemistry Department and CIF, who helped me to collect the data.

I have really enjoyed the friendly work environment in the lab with my group members Amlan, Kaustuv Da, Mostakim, Aniruddha, Soutick, Chiranjib and Masud. I also like to thank Laxmikanta, Mreedu and Nazeef who helped for my research during their project work.

I am grateful to my friends who helped me throughout my research work. I want to thank Subhankar, Sayanta, Bapan, Nilotpal, Ashalata, Dilip, Pallabita, Sabyasachi, Adil for their help during my research work.

I am grateful to the Ministry of Human and Research Development (MHRD), Govt. of India for providing me the fellowship and other financial support.

Finally, I want to thank my parents, Ekata and other family members. Without your love and support, I could not have completed my Ph.D. program.

Dedicated to my Family

Table of Contents

Table of Contents

Thesis Title:	**Chemical Sensing and Catalytic Properties of Water-Stable Metal-Organic Frameworks Constructed from Dicarboxylate Ligands**
Name of the Candidate:	Rana Dalapati
Roll No.:	146122002
Thesis Supervisor:	Dr. Shyam P. Biswas
Department:	Chemistry
Institute:	Indian Institute of Technology Guwahati, Assam, India

Thesis Overview:

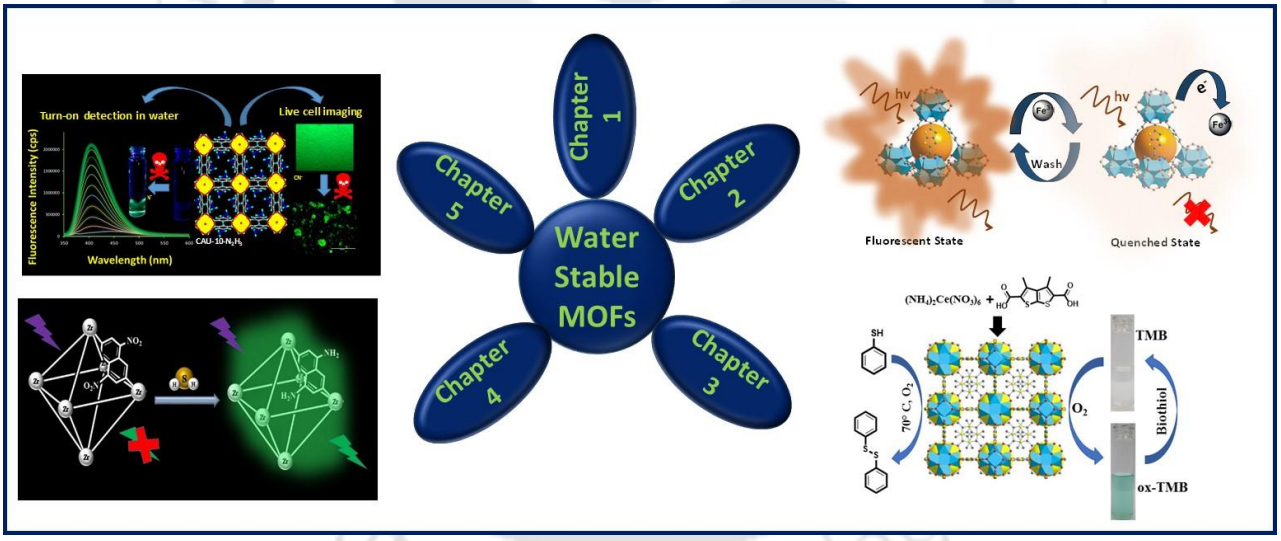

Chapter 1 describes the design principles of water-stable MOFs and their applications in adsorption, sensing and catalysis. The construction of secondary building units (SBUs) of MOFs with an inert metal ion (Cr(III), Al(III) or Fe(III)) is a well-accepted strategy for the synthesis of water-stable MOFs. The metal-ligand coordination bond strength also plays a key role for the hydrolytic stability of MOFs. Pearson's hard/soft acid/base principle can be a rough approximation for the metal-ligand bond strength. Carboxylate-based ligands can be regarded as hard bases and they form strong coordination bonds with high valent metal ions e.g. Cr(III), Al(III), Fe(III), Zr(IV), Hf(IV), Ce(IV), Ti(IV), which can act as hard acids. The hydrolytic stability of a MOF material also largely depends on the coordination geometry, extent of orbital overlap, high connectivity of metal cluster and steric factors. The high connectivity of metal cluster in the framework provides high thermal and chemical stability. Use of hydrophobic ligands during the synthesis is a simple and single-step protocol for the synthesis of hydrophobic and water-stable MOFs. Other than direct synthesis, post-synthetic modification also imparts hydrophobicity in the MOF, which increases the hydrolytic stability. The water-stable MOFs have been employed as high-capacity adsorbents of gases, water, organic molecules, oil, cation, anion, etc. The detection of targeted analytes present in water can be achieved by water-stable fluorescent MOFs. The hydrolytically stable MOFs have been also applied as reusable heterogeneous catalysts for various industrially relevant organic reactions.

Chpater 2 describes the synthesis of four isoreticular thienothiophene-based Zr(IV) MOF materials (**1′**, **2′**, **3′** and **4′**) under solvothermal conditions. All the MOFs possess the UiO-66 (UiO = University of Oslo) framework topology and contains $[Zr_6O_4(OH)_4]^{12+}$ building units (Figure 1). The μ_3-O and μ_3-OH groups occupy the triangular faces of the Zr_6 octahedron. Every Zr atom is coordinated with eight O atoms, forming a square antiprismatic coordination environment. The 3D, cubic framework is constructed by the interconnection of the $[Zr_6O_4(OH)_4]^{12+}$ units with the -CO_2 groups of twelve ligands. The hydrophobicity and fluorescence properties of all the MOF compounds have been tuned in a systematic fashion by attaching methyl and phenyl groups to the thienothiophene-based ligands. As verified by the fluorescence titration experiments, all the MOF materials featured selective, fast, and sensitive sensing of Fe^{3+} ions in water through the fluorescence quenching mechanism (Figure 2). The quenching efficiencies of the materials towards Fe^{3+} ions decreased in the order: **4′** (98%) > **3′** (96%) > **2′** (91%) > **1′** (86%). This trend in the quenching efficiency of the compounds can be correlated with the electron density available

in their frameworks. Thorough experimental studies indicate that the transfer of electrons from the π-conjugated, electron-rich thienothiophene-based frameworks to the half-filled 3d orbitals of Fe^{3+} ions accounts for the fluorescence quenching of MOF compounds.

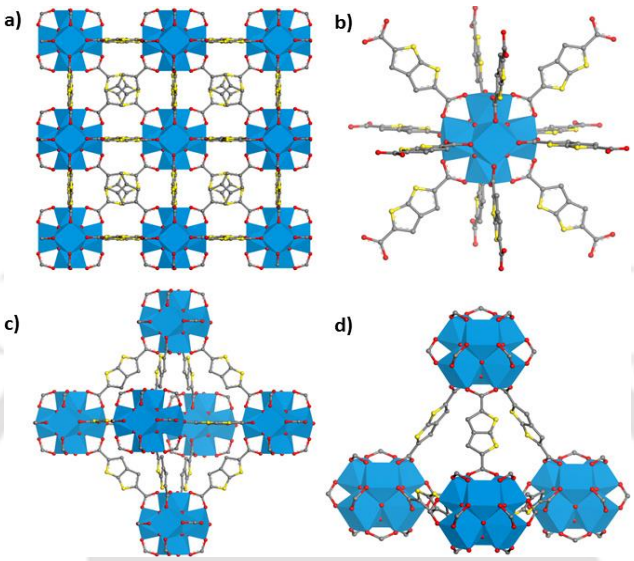

Figure 1. (a) Cubic 3D framework structure of **1** with Zr_6 node. (b) Node connectivity for the framework structure of **1**. Views of the (c) octahedral and (d) tetrahedral cages. Colour codes: Zr, blue polyhedra; C, grey; O, red; S, yellow).

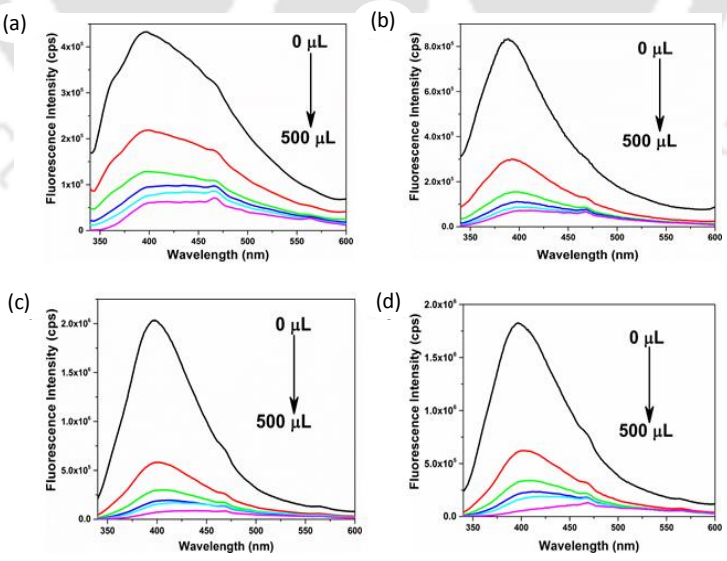

Figure 2. Quenching of fluorescence intensity with gradual addition of Fe^{3+} solution to a 3 mL aqueous suspension of **1′** (a), **2′** (b), **3′** (c) and **4′** (d).

In addition, molecular logic gates were designed by employing the MOFs for distinguishing between Fe^{3+} and Fe^{2+} ions. Overall, high photostability and reusability in Fe^{3+} sensing as well as the ability to discriminate between Fe^{3+} and Fe^{2+} ions through logic operations make the MOFs suitable for real-life applications.

Chapter 3 describes the solvothermal synthesis and characterization of a Ce(IV)-based MOF (**5**) material incorporating 3,4-dimethyl thieno[2,3-b]thiophene-2,5-dicarboxylic acid. The XPS study reveals the presence of both Ce(III) and Ce(IV) ions in the framework.

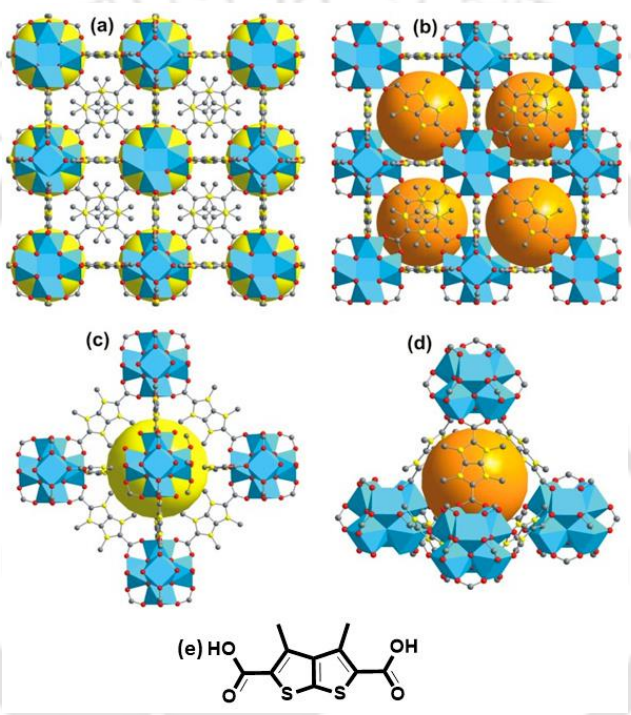

Figure 3. Cubic 3D framework structure of **5** in ball-and-stick representation. (a, b) Depiction of octahedral (yellow spheres) and tetrahedral (orange spheres) cages. (c, d) are the magnified views of (a, b), respectively. (e) Structure of the H_2DMTDC ligand. Colour codes: Ce, blue polyhedra; C, grey; O, red; S, yellow.

The cubic framework structure (Figure 3) of the compound comprises hexanuclear cluster cores having a $[Ce_6O_4(OH)_4]^{12+}$ composition. In these cluster cores, the six cerium atoms are situated at the corners of an octahedron. The eight faces of each octahedron are bridged by the O atoms of μ_3-O and μ_3-OH groups, which are arranged in an alternating fashion. Eight O atoms are

coordinated with each Ce atom. The latter has a square antiprismatic geometry in which the O atoms from the carboxylate, μ_3-O and μ_3-OH groups occupy the square faces.

Remarkably, the activated compound (**5′**) mimics the catalytic activity of biological oxidase enzymes due to the existence of redox-active cerium atoms in the framework. The excellent oxidase-like catalytic properties of the material were demonstrated by employing characteristic chromogenic peroxidase substrates: TMB and AzBTS. Based on the oxidase-mimicking activity of MOF, a colorimetric sensing platform for biothiols in NaAc buffer (0.2 M, pH = 4) was established. It can be seen from Figure 4 that the absorbance of ox-TMB decreased dramatically upon gradual addition of 0.5 mM solutions of cysteine. The sensing ability of biothiols by the MOF was employed to detect cysteine in human blood plasma. A significant heterogeneous catalytic performance of the mixed valence state Ce-MOF was also observed in the oxidation of thiol compounds using molecular oxygen (Scheme 1). The hot filtration experiments confirmed the heterogeneity of the oxidation catalysis reaction. The conversion of thiophenol observed in the 1st, 2nd, 3rd and 4th cycles after 12 h corresponded to 100%, 98%, 97% and 96%, respectively, which confirms the recyclability of **5′**.

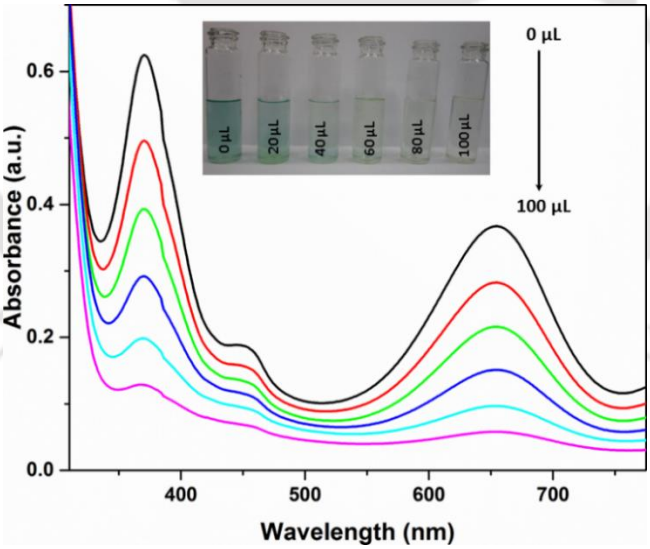

Figure 4. Change in the absorption spectrum of ox-TMB upon gradual addition of 0.5 mM cysteine solution in NaAc buffer (0.2 M, pH = 4). Inset: corresponding change in color of the ox-TMB solution.

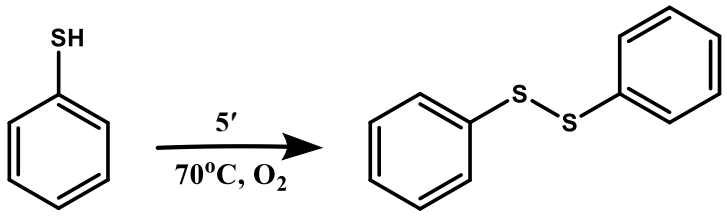

Scheme 1. Oxidation of thiophenol to 1,2-diphenyldisulfide in presence of catalyst **5′** and molecular oxygen.

Chapter 4 describes the synthesis, characterization of dinitro-functionalized Zr(IV)-based DUT-52-$(NO_2)_2$ MOF (**6**) (DUT = Dresden University of Technology). The activated material (**6′**) acts as a colorimetric and fluorogenic turn-on probe for the sensing of H_2S under physiological conditions (HEPES buffer, pH = 7.4, temperature = 37 °C) (Scheme 2). As confirmed by the steady-state fluorescence titration experiments, the MOF compound features significant capabilities for the highly selective and sensitive (detection limit: 20 µM) detection of H_2S.

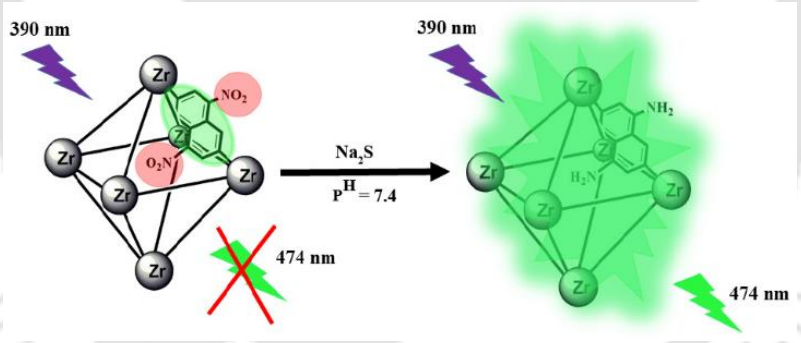

Scheme 2. Sensing of H_2S sensing by **6′** under physiological conditions (HEPES buffer, pH = 7.4, temperature = 37 °C) through fluorescence turn-on mechanism.

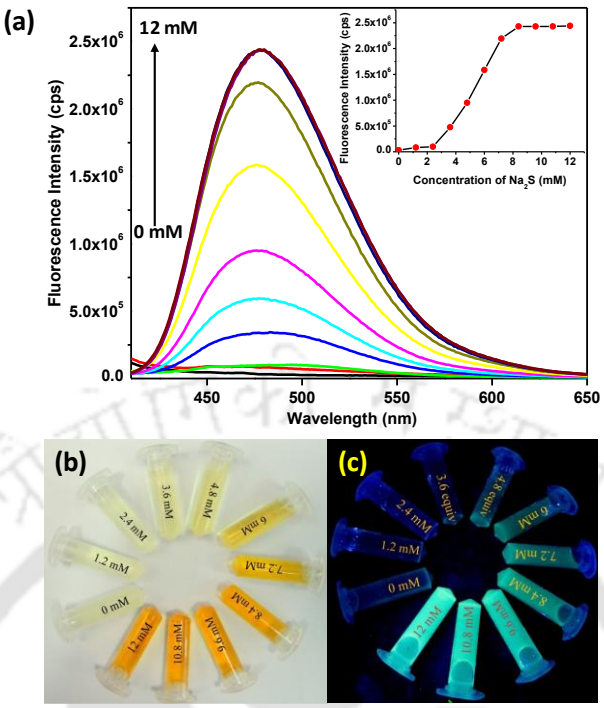

Figure 5. (a) Fluorescence turn-on response of **6′** (0.04 M) with increasing concentrations of Na_2S. Concentration-dependence of the emission intensity (monitored at 474 nm) is shown in the inset. The corresponding naked-eye colorimetric responses of **6′** towards H_2S under (b) day light and (c) UV light are also displayed.

The presence of two nitro functional groups per H_2NDC-$(NO_2)_2$ ligand completely quench the fluorescence of the naphthalene moiety in dinitro-functionalized Zr-based DUT-52 (Figure 5a). The corresponding diamino-functionalized MOF compound, formed through H_2S-mediated reduction, is expected to be more fluorescent than the dinitro-functionalized material. Remarkably, the compound exhibited visually detectable colorimetric and fluorogenic responses towards H_2S under day light as well as under UV irradiation (Figure 5b and 5c). In addition, the probe could be used for the detection of H_2S in human blood plasma and as well as living cells.

Chapter 5 describes the synthesis and systematic characterization of a hydrazine-functionalized Al(III) MOF namely CAU-10-N_2H_3 (**7**). The framework structure of **7** is presented in Figure 6. As revealed from the figure, the framework of CAU-10-N_2H_3 is formed by the interconnection of cis-corner sharing [AlO_6] octahedra with the hydrazine-functionalized isophthalate ligands. This

structural connectivity leads to the formation of helical chains. Two adjacent helices are related by a mirror plane.

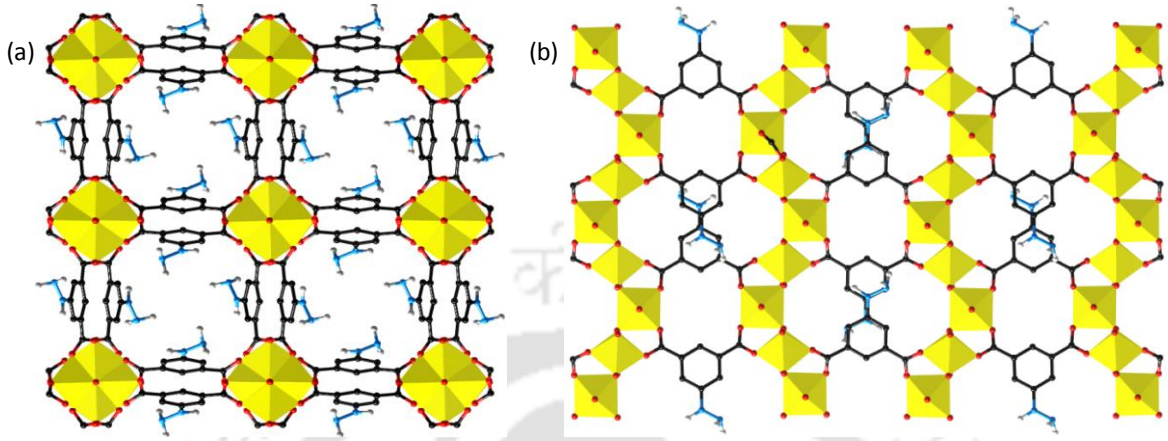

Figure 6. The simulated structure of the framework of CAU-10-N_2H_3 (**7**) compound (a). Hydrogen atoms have been omitted from phenyl ring of the structural diagram for clarity. Helical arrangement of [AlO_6] octahedra in the framework of CAU-10-N_2H_3 as seen along the b-axis (b). Colour codes: C, black; O, red; N, blue; Al, yellow polyhedra; H, white.

The activated material **7′** is capable of sensing CN^- ions even in the presence of other competitive anions present in water (Figure 7). The appearance of green fluorescence under UV light upon cyanide addition makes this material a naked-eye fluorescent sensor for CN^- ions in aqueous medium. The cyanide induced deprotonation of the acidic -NH proton present in hydrazine-functional group was confirmed by ^1H NMR titration experiment. This deprotonation leads to the fluorescence turn-on signal of the MOF probe. A very low detection limit of 0.48 μM was obtained for this MOF, which is lower than the allowable cyanide concentration (2 μM) in drinking water according to the WHO. The live cell imaging experiments with non-toxic Al(III) MOF clearly establish that the MOF is capable of intracellular CN^- ions.

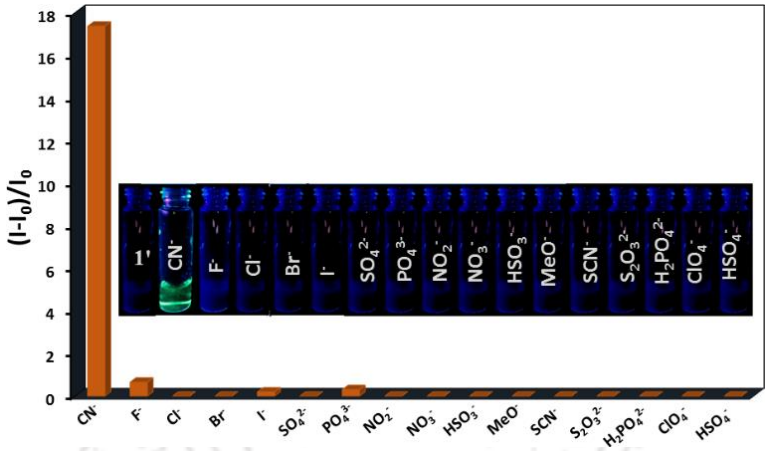

Figure 7. Relative fluorescence enhancement behaviour of **7′** towards addition of different anions. Inset: naked-eye fluorogenic response of **7′** towards different anions.

Chapter 1

Design principles of water-stable metal-organic frameworks (MOFs) and their applications in adsorption, sensing and catalysis

Stability of MOF is a topic with important significance considering its application in real field under humid conditions. The different types of strategies have been used to the synthesis of a water stable MOFs, which are mainly based on use of inert metal ion, effect of metal-ligand coordination, use of hydrophobic ligand, surface functionalization and so on. A brief description of these strategies is provided in this chapter. With the advantage of stability in a water medium, water stable MOFs can be efficiently applied in a broad range of areas. Few applications of water stable MOFs in adsorption, sensing and catalysis will be discussed in this chapter.

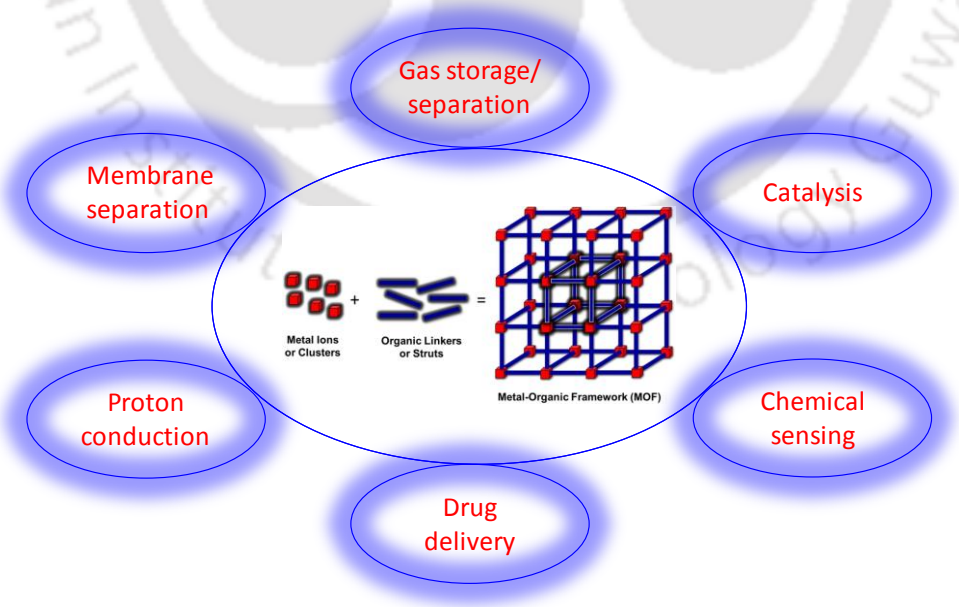

Chapter 1

1.1 Introduction

The systematic investigation of coordination compounds was started from the time of Alfred Werner (1893). However, the first coordination compound was firstly synthesized accidentally in the early eighteenth century by Heinrich Diesbach at Berlin in 1704.[1] The first synthesized coordination compound is known as 'Prussian Blue'. After ~270 years of synthesis, the 3D cubic structure of 'Prussian Blue' was identified in the year 1977.[2] At the end of 70's, the research based on coordination compound was accelerated. The representation and classifications of inorganic compounds were pioneered by Prof. A. F. Wells. In 1977, Prof. A. F. Wells introduced the concept of node and connections in inorganic crystal system.[3] The phrase 'coordination polymer' was introduced in the year 1964 by Prof. J. C. Bailar.[4] Design of inorganic and organic polymer based on node connectivity was increased in surprisingly short time.

Introduction of the concept of supramolecular chemistry by Prof. Lehn further gave a real impulse towards the design, synthesis and crystal engineering of inorganic compounds.[5] In 1989, Prof. Robson has introduced the synthesis of infinite and ordered framework structure *via* connecting the octahedral or tetrahedral nodes by rod-like connecting units.[6] In the year 1990, Prof. M. C. Etter identified the importance of hydrogen bond as a determinant factor of a crystal structure.[7] At the same time, the pioneered research was carried out by Prof. G. Desiraju based on the strong hydrogen bonding interaction in crystal systems.[8] The concept of node connectivity for the synthesis of the 3D supramolecular framework was further extended by Prof. O. M. Yaghi. In 1995, Prof. Yaghi reported the hydrothermal synthesis route to a crystalline, metal-organic, open framework system having extended channel and composed of uncommon metal coordination.[9] The copper (I) centers of the compound $Cu(4,4'\text{-bpy})_{1.5}\cdot NO_3(H_2O)_{1.25}$ (4,4'-bpy = 4,4'-bypyridine) is linked by rod-like 4,4'-bpy ligands to form porous and 3-D networks with three different size channels. The channels were occupied by nitrate anions that are hydrogen bonded to solvent water molecules. This new type of porous material with 3D-network structure was named as Metal-Organic Framework (MOF).

The large potential of MOF material was unexpected initially when Prof. Yaghi introduced the terminology called 'MOF'. After that, a number of MOFs have been reported at an unprecedented rate until this date. During these years, a number of terminologies were used by for this class of porous materials by several research groups such as coordination polymers,

coordination networks, MOFs and organic analogues of zeolites. The different nomenclatures used to name the porous frameworks were not consistent among research groups, causing further unnecessary confusions. In the year 2012, the International Union of Pure and Applied Chemistry (IUPAC) task group has published a provisional definition of MOF as: 'Metal-Organic Framework, abbreviated to MOF, is a Coordination Polymer (or alternatively Coordination Network) with an open framework containing potential voids'.[10]

The synthesis and characterization of new porous materials with open framework structures were further taken care by other research groups. Kitagawa *et al.* showed a reversible uptake of CH_4, N_2 and O_2 by a three-dimensional framework $\{[M_2(4,4'\text{-bpy})_3(NO_3)_4]\cdot xH_2O\}_n$ (M = Co, Ni, Zn).[11] The channeling cavity present in the framework was occupied by water molecules, which didn't show any significant interaction with crystal framework. Rosseinsky *et al.* attempted to synthesize framework structures with desolvated form. In 1999, Rosseinsky *et al.* reported a coordination polymer framework of $Ni_2(4,4'\text{-bipy})_3(NO_3)_4$, which showed a small relaxation of the crystal structure on guest desolvation.[12] In the same year, Prof. Yaghi reported a metal-organic framework called MOF-5, which remained stable when fully desolvated and when heated up to 300 °C. MOF-5 is the very first example of a MOF material with permanent porosity and has been extensively studied until date.[13] The research based on MOF materials with permanent porosity was accelerated after this breakthrough result.

In the last 20 years, the Cambridge Crystallographic Database Centre (CCDC) has recorded more than 80,000 MOF structures. In the early stage of MOF development, MOF-5 showed many interesting properties with exceptional surface area. But, it has been observed that many reported MOF materials including MOF-5 are not stable in water.[14,15] In spite of huge prospect of MOF materials, the instability in aqueous medium restricts their commercialization and applications in industrial scale. Currently, the design and synthesis of water-stable MOF materials are in high demand based on their practical applications. More than 6000 articles have been published in recent years related with MOF materials (Figure 1.1). Among them, only few papers highlight the synthesis and applications of water-stable MOF materials.

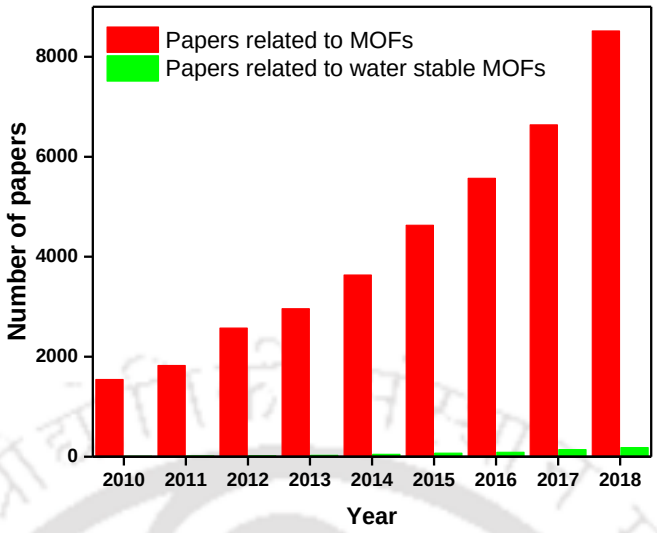

Figure 1.1 Number of publications per year from 2010-2018 for articles on the topic of "metal-organic framework" or "water stable metal-organic framework". The numbers were determined based on a Scifinder search in December 2018 spanning from 2010 to 2018 using keywords: 'metal-organic framework' and 'water stable metal-organic framework'.

1.2 Design principles of water-stable MOFs

Stability of MOFs in the presence of water is a topic with important significance considering their applications in real field under humid conditions. Due to 3D structures, porosity and other factors, MOF materials are used in gas storage and gas separation.[16,17] In industry, the ubiquitous presence of water vapor in various gas stream must be accounted. On the other hand, water stability is a crucial issue for the use of MOFs as a heterogeneous catalyst in aqueous medium. Recently nano-sized MOFs are used in biological applications,[18,19] which also demand the water stability of MOFs in aqueous biological environment. Clearly, considering the design and synthesis of new MOFs for practical applications, the stability in water medium or in humid environment is an essential property that must be considered.

Recording of X-ray powder diffraction (XRPD) pattern of MOFs after the treatment with water or water vapor and comparing the XRPD pattern with the pristine sample before exposure is the simplest method to determine the water stability of a crystalline MOF. The partial loss of porosity of MOFs can be identified by measuring the nitrogen adsorption isotherms of water-exposed MOFs and determining the specific surface area. The metal clusters present in MOFs are

susceptible to the attack by nucleophilic water molecules, which lead to partial ligand displacement. Measuring the NMR or UV-Vis spectra of the supernatant liquid also informs about the dissolution of the solid phase of MOFs. Different types of strategies have been used for the synthesis of water-stable MOFs, which are mainly based on: use of inert metal ions, effect of metal-ligand coordination, use of hydrophobic ligands, surface functionalization and so on. A brief description of these strategies is provided in the next section.

1.2.1 Inertness of metal clusters

Since a metal cation can act as an electrophilic center, the nucleophilic water molecule can attack the metal center easily. Therefore, the construction of secondary building units (SBUs) of MOFs with an inert metal ion is a well-accepted strategy for the preparation of water-stable MOF compounds. It was found that the use of inert Cr(III), Al(III) or Fe(III) metal ions for the synthesis of MOFs imparts the resistivity towards the water-based hydrolysis. In 2005, Férey *et al.* reported the synthesis strategy of a new MOF with a combination of Cr(III) metal ion and 1,4-benzene dicarboxylic acid (H_2BDC) ligand.[20] This Cr(III)-based MOF, MIL-101 (MIL = Material of the Institute Lavoisier) showed an exceptional stability in air atmosphere. The super tetrahedron (ST) framework structure of Cr-MIL-101 is constructed from the linkage of BDC dianions with inorganic trimeric $[Cr_3O(H_2O)_2F(CO_2)_6]$ building units. The inorganic trimeric secondary building units consist of the three Cr atoms in an octahedral environment and the six coordination sites are occupied by four O atoms from the bridging bidentate BDC^{2-}, one μ_3-O atom and one oxygen atom from the terminal water or fluorine group. The structure of Cr-MIL-101 features corner-sharing ST, which are made from the linkage of inorganic trimers and BDC dianions. A 3D network of "corner-sharing" super tetrahedra with an augmented MTN zeotype architecture was established by the connection between the ST through vertices (Figure 1.2). The MOF called Al-MIL-101 shows a similar structure with Cr-MIL-101 and it is also highly stable in water.[21]

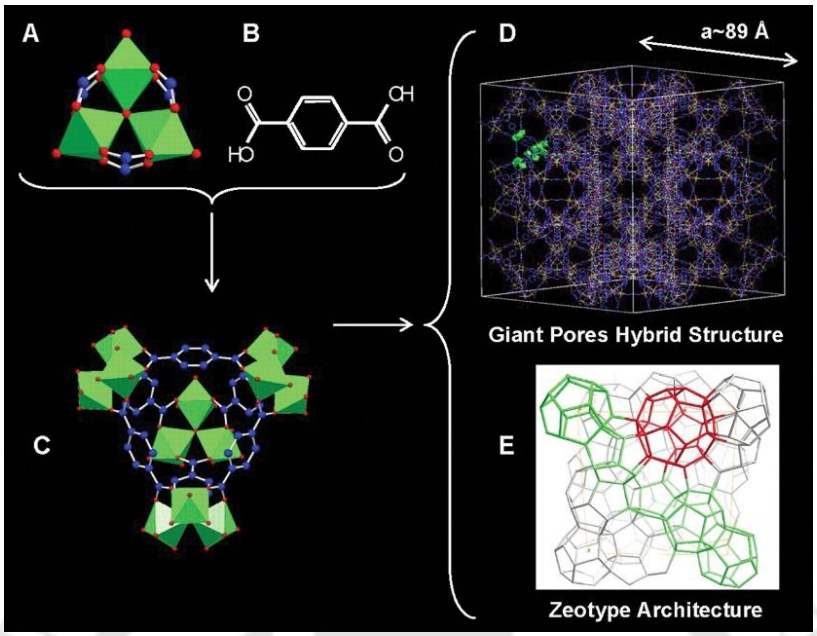

Figure 1.2 (A) The trimeric building block of Cr-MIL-101 chelated by three carboxylic functional group designed by computer simulation. The super tetrahedron (ST) was constructed with (B) terephthalic acid, which lies (C) on the edges of the ST. (D) Ball and stick representation of one unit cell of Cr-MIL-101. (E) Framework structure of Cr-MIL-101 having MTN topology with the medium (green) and large (red) cages delimited by the vertex sharing of the ST. Color codes: Chromium octahedra, oxygen, fluorine and carbon atoms are in green, red, and blue, respectively. Reproduced with permission from ref. 20. Copyright 2018 American Association for the Advancement of Science.

Another MOF called Cr-MIL-53 is one of the popular MOFs among the Cr(III)-based MOFs.[22] The MIL-53 framework shows a reversible breathing behavior upon dehyhydration and rehydration. The as-synthesized form (MIL-53as) shows a one-dimensional large-pore channel filled with free disordered terephthalic molecules (Figure 1.3). On removal of guest molecules, it leads to a nanoporous solid (MIL-53ht) with a Langmuir surface area over 1500 m^2/g. The hydration at room temperature results in a narrow-pore material (MIL-53lt). The isostructural Al-MIL-53 also shows a high stability.[23] Other than MIL-101 and MIL-53, a large number of MOFs synthesized with inert Cr(III) and Al(III) metal ions are summarized in Table 1.1.

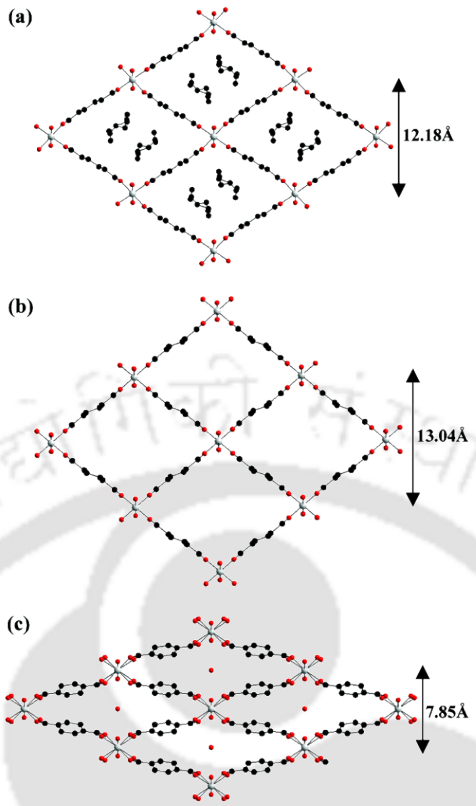

Figure 1.3 View of the one-dimensional pore channel system of (a) MIL-53as, (b) MIL-53ht and (c) MIL-53lt. Reproduced with permission from ref. 22. Copyright 2002 American Chemical Society.

Table 1.1 Summary of some representative stable MOFs constructed with Cr(III) and Al(III) ions.

MOF	Cluster/Core	Ligand	Ref.
Cr-MIL-101	$[Cr_3(\mu_3\text{-}O)(COO)_6]$	BDC	20
Cr-MIL-53	$[Cr(OH)(COO)_2]_n$	BDC	22
Cr-MIL-100	$[Cr_3(\mu_3\text{-}O)(COO)_6]$	BTC	24
Cr-MIL-101-NDC	$[Cr_3(\mu_3\text{-}O)(COO)_6]$	2,6-NDC	25
Cr-MIL-88A	$[Cr_3(\mu_3\text{-}O)(COO)_6]$	FUM	26
Cr-MIL-88B	$[Cr_3(\mu_3\text{-}O)(COO)_6]$	BDC	26
Cr-PCN-333	$[Cr_3(\mu_3\text{-}O)(COO)_6]$	TATB	27
Cr-PCN-426	$[Cr_3(\mu_3\text{-}O)(COO)_6]$	TMQPTC	28
Al-MIL-53	$[Al(OH)(COO)_2]_n$	BDC	29
Al-MIL-101	$[Al_3(\mu_3\text{-}O)(COO)_6]$	$BDC\text{-}NH_2$	21

Al-MIL-100	$[Al_3(\mu_3\text{-}O)(COO)_6]$	BTC	30
DUT-5	$[Al(OH)(COO)_2]_n$	BPDC	31
CAU-1	$[Al_8(OH)_4(OCH_3)_8(COO)_{12}]$	BDC-NH_2	32
CAU-10	$[Al(OH)(COO)_2]_n$	1,3-BDC	33
Al-PCN-333	$[Al_3(\mu_3\text{-}O)(COO)_6]$	TATB	34

Linkers are abbreviated as: BDC = 1,4-benzene dicarboxylate; FUM = fumarate; 2,6-NDC = naphthalene-2,6-dicarboxylate; BTC = benzene-1,3,5-tricarboxylate; BDC-NH_2 = 2-aminoterephthalate; BPDC = biphenyl-4,4′-dicarboxylate; TATB = 4,4′,4″-s-triazine-2,4,6-triyl-tribenzoate; 1,3-BDC = 1,3-benzenedicarboxylate; TMQPTC = 2′,3″,5″,6′-tetramethyl-[1,1′:4′,1″:4″,1‴- quaterphenyl]-3,3‴,5,5‴-tetracarboxylate.

1.2.2 Metal-ligand bond strength

Metal-ligand coordination bond strength plays a key role for determining the stability of MOFs in water. The stability of MOFs are governed by acid-base coordination chemistry. Strong coordination bonds are expected between hard Lewis acids and bases or soft Lewis acids and bases. Pearson's hard/soft acid/base principle can be rough approximation for the metal-ligand bond strength. Carboxylate-based ligands can be regarded as hard bases and they form strong coordination bonds with high valent metal ions e.g. Cr(III), Al(III), Fe(III), Zr(IV), Hf(IV), Ce(IV) or Ti(IV), which can act as hard acids.[35,36] A highly stable mesoporous metalloporphyrin MOF called PCN-600(Fe) was synthesized by Zhou *et. al* based on this strategy.[37] The **stp-a** network of PCN-600(Fe) contains four-connected square planar tetrakis (4-carboxyphenyl) porphyrin (TCPP) ligand with D_{4h} symmetry and six-connected $Fe_3O(OOC)_6$ metal cluster with D_{3h} symmetry (Figure 1.4).

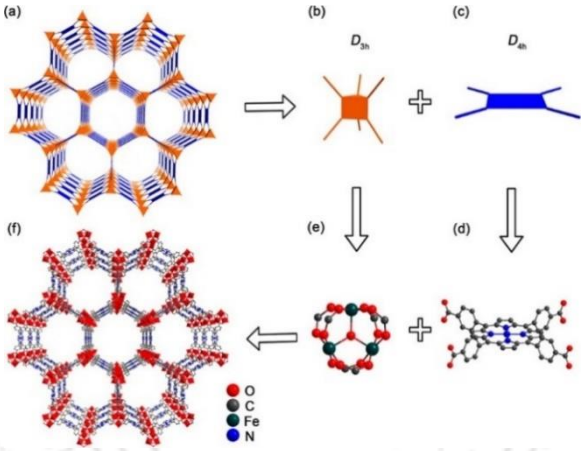

Figure 1.4 (a) The **stp-a** network of PCN-600(Fe), (b) the view of D_{3h} symmetric six-connected and (c) D_{4h} four-connected nodes, and (d, e) corresponding nodes commonly seen in other MOFs and PCN-600. Reproduced with permission from ref. 37. Copyright 2014 American Chemical Society.

The soft acidic metal cations (such as Zn^{2+}, Cu^{2+}, Ni^{2+}) can coordinate with soft basic N-donor ligands, which form much stronger metal-N bonds than those of metal-O bonds by coordination with the hard-base carboxylate ligands. The ZIF-8 framework constructed from Zn^{2+} and 2-methylimidazole ligands received widespread interests because of its excellent thermal and hydrothermal stability.[38]

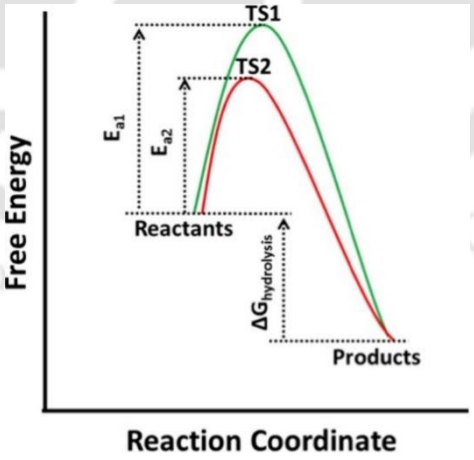

Figure 1.5 The reaction coordinate diagram representing the importance of kinetic factors in controlling the stability of MOFs in aqueous system. Reproduced with permission from ref. 39. Copyright 2014 American Chemical Society.

1.2.3 Local environment and steric factors

The isolated properties of metal ions and ligands are not solely responsible for the stability of a framework system. The hydrolytic stability of a MOF material also largely depends on the coordination geometry, extent of orbital overlap, high connectivity of metal cluster and steric factors. Two MOFs with similar thermodynamic stabilities governed by the metal-ligand coordination may show different rates of hydrolysis controlled by kinetic effects.[39] Figure 1.5 shows a reaction coordinate diagram for two different MOFs with same thermodynamic stabilities. The MOF following reaction path 1 (green) during hydrolysis is more stable than the other following reaction path 2 (red). Therefore, the kinetic factor controlled by the local environment (steric effect or hydrophobicity) is equally important for the hyrolytic stability of MOFs.

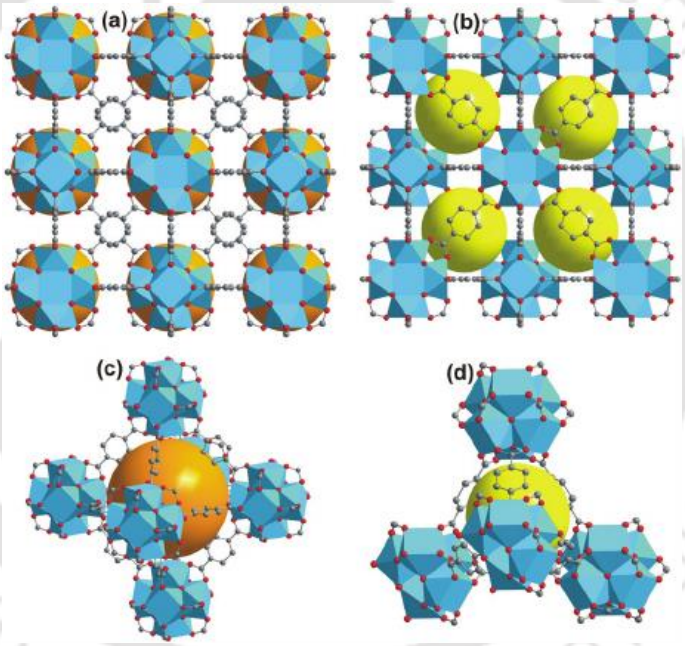

Figure 1.6 The representations of the 3D cubic framework structure of UiO-66 in ball-and-stick model. (a, b) The framework showing spatial arrangements of the octahedral and the tetrahedral cages present in the MOF, represented by orange and yellow spheres, respectively. (c, d) Magnified views of the octahedral and the tetrahedral cages. Zr atoms are displayed as octahedra (color codes: Zr, blue; C, gray; O, red). Reproduced with permission from ref. 40. Copyright 2013 Royal Society of Chemistry.

Zr(IV)-based UiO (UiO = University of Oslo) type MOFs with an inner $Zr_6O_4(OH)_4$ metal core show exceptional stabilities. Zr_6-octahedron are alternatively capped by μ_3-O and μ_3-OH

groups. The edges of Zr_6-octahedron are bridged by carboxylates (-CO_2) originating from the H_2BDC ligand forming $Zr_6O_4(OH)_4(CO_2)_{12}$ cluster. The eight oxygen-coordinated zirconium atoms form a square-antiprismatic coordination. One square face of the antiprism is formed by oxygen atoms supplied by carboxylates while the second square face of the antiprism is formed by oxygen atoms coming from the μ_3-O and μ_3-OH groups (Figure 1.6).[40] The high connectivity of metal clusters in the UiO type framework provides high thermal and chemical stability. The isostructural framework constructed by Hf(IV), Ce(IV), Th(IV) also show good stability in water. This high coordination number also relates with the stability reported in a range of other MOFs including the Zr/Hf-based DUT-51, -53, -67-69, -84,[41-43] PCN-56-59, -222, -224, -225,[44-47] MIL-140,[48] and MOF-525, -545.[49]

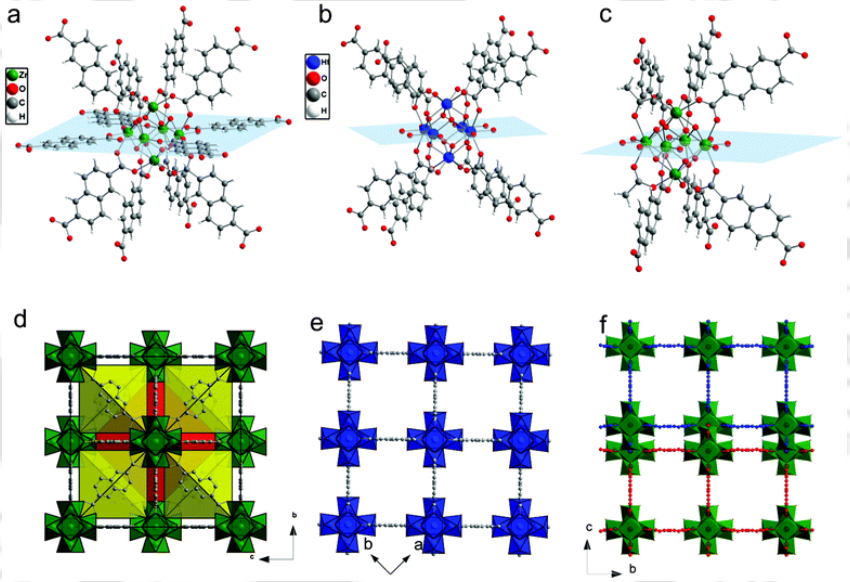

Figure 1.7 The view of coordination environment of SBU (a - DUT-52; b - DUT-53(Hf); c - DUT-84(Zr).) and 3D framework structure (d - DUT-52; e - DUT-53(Hf); f - DUT-84(Zr). Reproduced with permission from ref. 43. Copyright 2013 Royal Society of Chemistry.

A series of water-stable Zr(IV) and Hf(IV) MOFs namely DUT (DUT = Dresden University of Technology) were synthesized by Kaskel *et al.* with linear and bent carboxylic acid ligands. The MOF called DUT-51(Zr) was synthesized using a bent dithieno[3,2-b;2′,3′-d]thiophene-2,6-dicarboxylate (DTTDC), which contains an eight-connecting Zr-cluster with an overall composition of $[Zr_6O_6(OH)_2(DTTDC)_4(BC)_2(DMF)_6](DMF)_{12}(H_2O)_{19}$ (BC = benzoic acid and DMF = *N*,*N*-dimethylformamide).[41] The isomorphous Hf(IV) analogue called DUT-51(Hf)

with the same composition $[Hf_6O_6(OH)_2(DTTDC)_4(BC)_2(DMF)_6](DMF)_{12}(H_2O)$ was also reported. DUT-52 and DUT-53 were synthesized with linear 2,6-naphthalenedicarboxylate (2,6-NDC) as a ligand.[43] DUT-52 synthesized using Zr(IV) salt shows a 12-connected $[Zr_6O_4(OH)_4]^{12+}$ SBU, which is isoreticular with UiO-66. DUT-53(Hf) structure is built up with $[Hf_6O_6(OH)_2]^{10+}$ SBUs (Figure 1.7b) interconnected by eight 2,6-NDC linkers giving rise to an 8-connected framework. The structure of DUT-84(Zr) is composed of double layers and involves 6-connected $[Zr_6O_8(CH_3COO)_2]^{6+}$ SBUs (Figure 1.7c). The structure of DUT-67, similar to DUT-51, contains an 8-connected cluster. The structures of DUT-68(Zr) and DUT-68(Hf) also contain 8-connected clusters.[41] The structure of DUT-69 is based on the uninodal 10-connected framework.[42] Similar high connectivity was also observed in highly stable Zr_6-based PCN MOF.[50]

1.2.4 Hydrophobicity

Water-based hydrolysis of MOFs occurs mainly in two primary steps. At first, the water molecule comes close to the metal cluster, which allows the interaction between the electrophilic metal ion and nucleophilic water molecule. In the second step, the energetics of this interaction must be greater to overcome the activation energy barrier of the hydrolysis reaction.[39] The framework hydrophobicity can play a key role to control the first step of the reaction. It has been observed that the stability of MOFs under humid conditions can be improved by incorporating hydrophobic functional groups in the ligands.[51] The direct installation of ligands during MOF synthesis or post-synthetic modification (PSM) of ligands was widely adopted for the synthesis of hydrophobic frameworks.

1.2.4.1 Hydrophobic ligands

The use of hydrophobic ligands during the synthesis is a simple and single-step protocol for the synthesis of hydrophobic MOFs. The presence of hydrophobic groups in the framework structure increases the pore hydrophobicity and repeal the water molecules, which prevents further interactions of water molecules with metal ions. Methyl, ethyl, phenyl or long chain alkyl groups including fluorinated functional groups are commonly used for the design of hydrophobic ligands. The pore hydrophobicity decreases the water adsorption, which can be directly verified by performing the water adsorption isotherms on the sample. The fluorous metal-organic frameworks

(FMOFs) synthesized by Omary *et al.* with a fluorous ligand, 3,5-bis(trifluoromethyl)-1,2,4-triazolate showed no detectable water adsorption even at near 100% relative humidity, confirming the hydrophobicity of the framework.[52] Few water-stable MOFs constructed with hydrophobic ligands are summarized in Table 1.2.

Table 1.2 Summary of some representative stable MOFs constructed with hydrophobic ligands.

MOFs	Surface Modification Type	Synthesis Method	Structure of Organic Ligand	Water Contact Angle [°]	Ref.
PESD-1	aromatic ring	direct synthesis	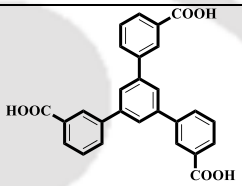	>150	53
UPC-21	multi-aromatic rings	direct synthesis	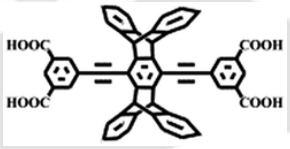	145 ± 1	54
FMOF-1/ FMOF-2	fluorinated aromatic ring	direct synthesis	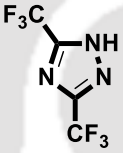	-	52
MOFF-1	fluorinated aromatic ring	direct synthesis	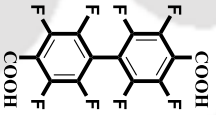	108 ± 2	55
MOFF-2	fluorinated aromatic ring	direct synthesis	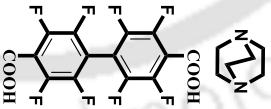	151 ± 1	55
MOFF-3	fluorinated aromatic ring	direct synthesis	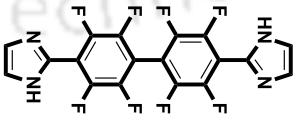	135±2	55
UHMOF-100	fluorinated aromatic ring	direct synthesis	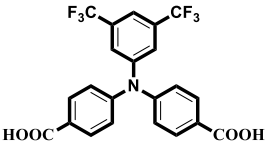	176	56

Al-MIL-53-AM4	alkyl (C_4) chain	post-synthetic modification	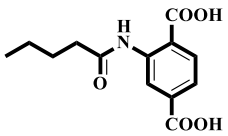	>150	57
Al-MIL-53-AM6	alkyl (C_6) chain	post-synthetic modification	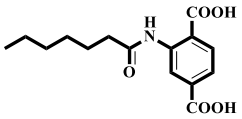	>150	57
F-ZIF-90	fluorinated aromatic ring	post-synthetic modification	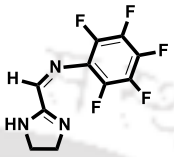	159.1	58, 59

1.2.4.2 Post-synthetic modification

Post-synthetic modification (PSM) is another well accepted method to tune the surface functionality of MOF materials. The transformation of hydrophilic to hydrophobic MOFs *via* PSM method was accomplished by several research groups. This transformation can be accomplished by mainly two methods. First, the ligand present in MOFs can be functionalized by PSM method. Second, the surface of the MOF material can be coated by various techniques.

1.2.4.2.1 Post-synthetic functionalization of ligands

Cohen *et al.* showed post-synthetic covalent modification of metal-organic frameworks with long alkyl substituents to protect these materials against moisture.[57] The MOF constructed with polar 2-amino-1,4-benzenedicarboxylate (NH_2-BDC) displayed hydrophilic properties. The amino group was modified with different alkyl anhydrides to form amide-functionalized MOFs. The introduction of hydrophobic alkyl chains *via* PSM improves the water resistance and change the physical properties (i.e., hydrophobicity) of the MOF. Contact angle measurements are commonly used to examine the hydrophobic properties of materials. The materials with water contact angles (WCA) >150° are considered as superhydrophobic. After modification, Al-MIL-53-NH_2 MOF possessed superhydrophobic properties with contact angles greater than 150°.

Superhydrophobic zeolitic imidazole framework (F-ZIF-90) was reported by Huang *et al.* by using a fluorine-functionalized imidazolate as an organic linker.[58,59] PSM of ZIF-90 with

pentafluorobenzylamine *via* amine condensation reaction resulted in superhydrophobis surface of the MOF material, which showed high steam stability.

1.2.4.2.2 Post-synthetic surface modification

The hydrophobic surface coating of MOF material is another method to stabilize MOFs under humid conditions. A well-known MOF called UiO-66-NH_2 was coated with microporous organic network (MON). The MON-coated UiO-66-NH_2 was synthesized *via* Sonogashira coupling of tetra(4-ethynylphenyl)methane with 1,4-diiodobenzene or 4,4′-diiodobiphenyl (Figure 1.8).[60] The MON thickness on UiO-66-NH_2 was controlled by changing the amount of tetra(4-ethynylphenyl)methane. Water contact angle measurement showed the chemical changes of the surface properties of MOF@MONs as compared to the original UiO-66-NH_2 MOF. The water contact angle increased up to 145° for the MON-coated MOF material and it showed an adsorption of a model organic compound, toluene, in water.

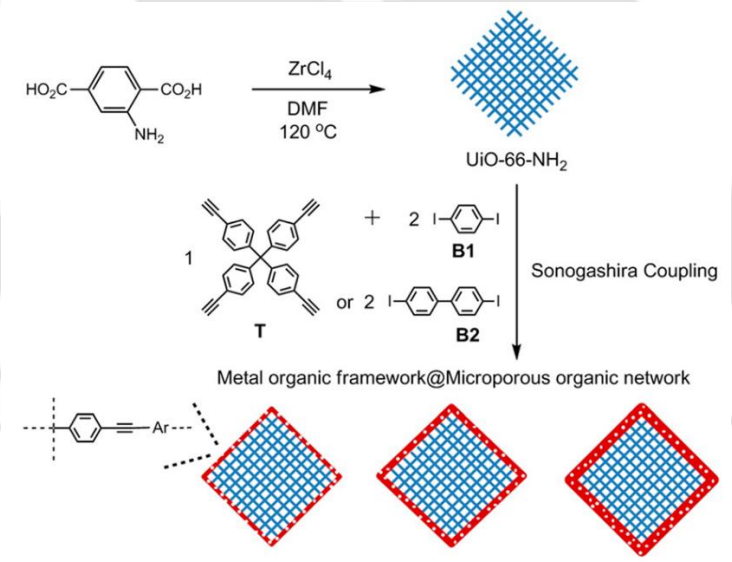

Figure 1.8 Schematic presentation for the synthesis of MOF@MON hybrid materials. Reproduced with permission from ref. 60. Copyright 2014 American Chemical Society.

Vapor deposition technique was also adopted to modify the MOF surface with hydrophobic polydimethysiloxane (PDMS) materials to enhance their moisture or water resistance. Yu *et al.* developed a general strategy for PDMS coating on MOF-5, HKUST-1 and ZnBT as representative vulnerable MOFs (Figure 1.9).[61] The PDMS-coated MOFs showed nearly 100% retention of

porosity as confirmed by surface area analysis. Compared to the pristine MOFs, all PDMS-coated samples displayed water contact angles of 130 ± 2°, which revealed hydrophobic character of the surface.

A plasma-enhanced chemical vapor deposition (PECVD) of perfluorohexane on Cu-BTC MOF was used for the pore surface modification with hydrophobic -CF_3 group.[62] The plasma-treated MOF showed enhanced stability against degradation by water. The Monte Carlo simulations suggested that the perfluorohexane sites prevent the formation of water clusters within the Cu-BTC MOF, thereby improving the water stability.

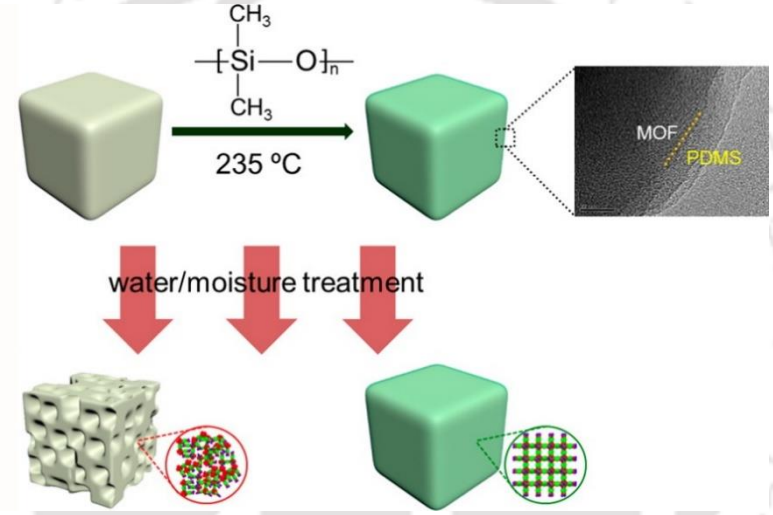

Figure 1.9 Schematic presentation of PDMS-coating on the surface of MOFs and the enhancement of water resistance of MOFs. Reproduced with permission from ref. 61. Copyright 2014 American Chemical Society.

Park *et al.* described the formation of amorphous carbon coatings on the surface of MOFs that prevented hydrolysis.[63] The controlled heat treatment of IRMOF-1 under nitrogen atmosphere led to the formation of an amorphous carbon coating on its surface, which shielded the framework from decomposition under humid conditions. The overheated MOF produced ZnO@carbon material that did not display microporosity or chemical characteristics of MOFs. The carbon-coated MOF prepared at 510° C showed undamaged crystalline structure after 2 h of soaking in water (Figure 1.10).

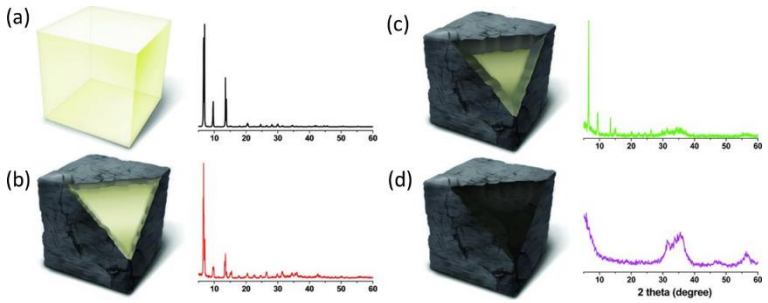

Figure 1.10 Schematic presentations and XRPD patterns of IRMOF-1 (a) and carbon-coated IRMOF-1 after thermal treatment at increasing temperatures (b and c). At a temperature of 550 °C, the structure of IRMOF-1 transforms into ZnO nanoparticles@amorphous carbon (d). Reproduced with permission from ref 63. Copyright 2012 Wiley Online Library.

1.3 Applications of water-stable MOFs

With the advantage of stability in aqueous medium, water-stable MOFs can be efficiently applied in a broad range of areas.[64] Adsorption in both gaseous and liquid phases is a classical example for the applications of the water-stable MOFs.[65-69] The sensing of different analytes in pure aqueous medium by MOFs opens up enormous opportunities for the monitoring of water health as well as medicinal diagnoses.[70-76] Water-stable MOFs as heterogeneous catalysts further promote the opportunity of the commercialization of MOF materials in industrial scale.[77-79] The other important applications of water-stable MOFs include proton conduction, cell imaging and drug delivery.[80-84] Few applications of water-stable MOFs in adsorption, sensing and catalysis will be discussed in the next sections.

1.3.1 Adsorption

Adsorption is one of the prime applications of porous materials. Porous materials including activated carbons, mesoporous silicas and zeolites are largely used in the chemical industry. The exceptional structural features, variable functionalization and tunable porosities of MOFs make these materials to be superior over other conventional porous materials. Highly porous water-stable MOFs with great structural diversity can be used as high-capacity adsorbents. Current literature survey suggests that water-stable MOF materials have been also successfully employed for gas

storage and separation, water adsorption and adsorptive removal of various targeted compounds from water-based systems.

1.3.1.1 Adsorption of water

Poor stability of MOFs under humid conditions restrict their applications as adsorbents for water. The water-stable MOFs have been employed for the adsorption of water in recent years. The water adsorption of a representative set of MOFs with various hydrolytic stability was systematically examined by Kaskel *et al.* The water stability and water adsorption capacity of the metal-organic frameworks such as HKUST-1 ($Cu_3(BTC)_2$; BTC = benzene-1,3,5-tricarboxylate), ZIF-8, MIL-101, Fe-MIL-100 and DUT-4 (Al(OH)(NDC); NDC = naphthalene-2,6-dicarboxylate) were studied.[85] In this study, HKUST-1 showed the highest water adsorption affinity although it is unstable in direct contact with water. The MIL-101, Fe-MIL-100 and ZIF-8 materials showed good stability in water. The water adsorption isotherms of Fe-MIL-100 and MIL-101 MOF suggested that these materials show high water uptake only at higher concentrations. The pore size and the 'bridging effect' played crucial roles in water adsorption.

Stock *et al.* studied the effect of functionalization on the water adsorption capacity of the highly water-stable Al(III)-based MOF called CAU-10 (CAU = Christian-Albrechts-University).[86] The decoration of the inner walls of CAU-10 by different functional groups (-NH_2, -NO_2, -CH_3, -OCH_3 and -OH groups) strongly affected the water adsorption capacity and the shape of the water adsorption isotherms (Figure 1.11). The water adsorption capacity decreased upon increasing the size of the functional group. Hydrophilic groups (-NH_2, -OH) showed adsorption at a lower relative humidity whereas hydrophobic substituents (-NO_2, -OCH_3, -CH_3) exhibited adsorption at higher relative humidity with a lower adsorption capacity.

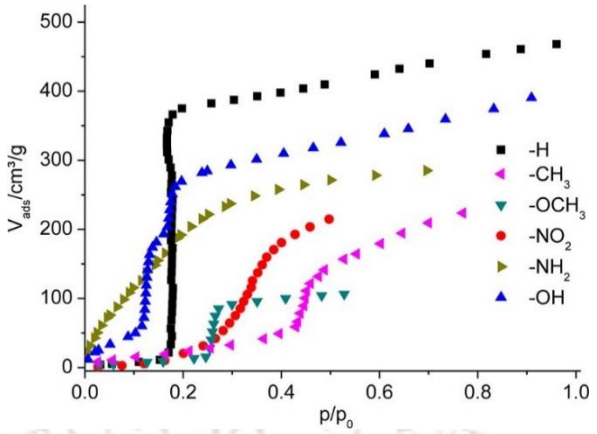

Figure 1.11 Water adsorption isotherms at 298 K of a series of functionalized (-NO_2, -NH_2, -CH_3, -OCH_3, and -OH) CAU-10 MOFs. Reproduced with permission from ref. 86. Copyright 2013 American Chemical Society.

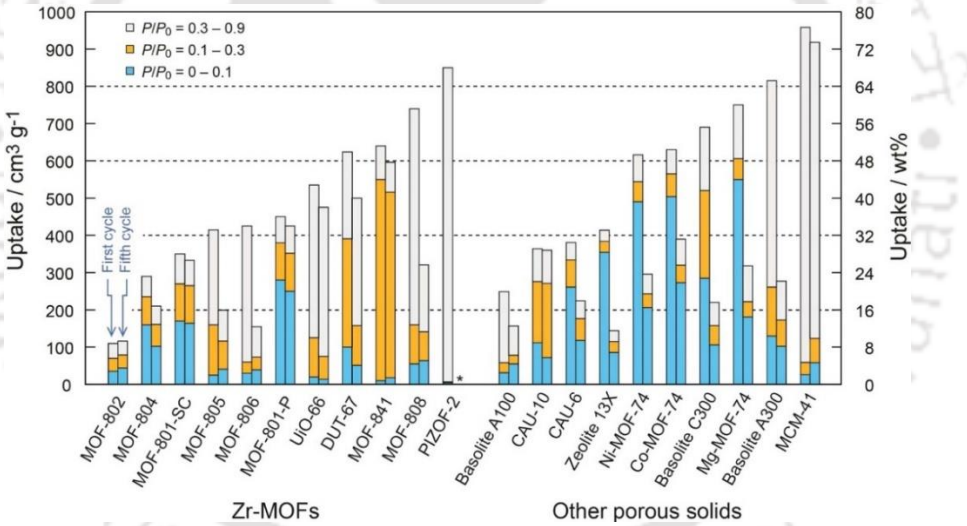

Figure 1.12 Water uptake capacities for Zr-based MOFs in different pressure ranges (left) and other MOF materials (right) at 298 K. Left and right bars represent the first and fifth cycles, respectively. The asterisk (*) mark indicates no data. Reproduced with permission from ref. 87. Copyright 2013 American Chemical Society.

Yaghi *et al.* identified the three main criteria for attaining high performing porous materials for water adsorption application based on a comparative water adsorption study of 23 materials, 20 of which are MOFs including 10 Zr(IV) MOFs (Figure 1.12).[87] Other than high water stability, these criteria include condensation pressure of water in the pores, uptake capacity, and

recyclability. Zr(IV)-based MOF-801-P and MOF-841 are the highest performers which are constructed with fumaric acid and 4,4′,4″,4‴-methanetetrayltetrabenzoic acid, respectively.

Table 1.3 Summary of reported MOFs with porous features and water adsorption capacities measured at 298 K.

MOF	Pore Diameter (nm)	S_{BET} (m^2 g^{-1})	Pore volume (cm^3 g^{-1})	Water Uptake (cm^3 g^{-1})	Ref.
HKUST	0.9/0.6	1270	0.62	0.51	88
Al-MIL-53-NH_2	n.d.	n.d.	n.d.	0.09	89
Al-MIL-53-OH	n.d.	n.d.	n.d.	0.40	89
Al-MIL-100	2.5/2.9	1814	1.14	0.50	90
Cr-MIL-101	2.9/3.4	3017	1.61	1.28	85
Cr-MIL-101	2.9/3.4	3124	1.58	1.40	91
Cr-MIL-101-NH_2	< 2.9/3.4	2690	1.6	1.06	92
Cr-MIL-101-NO_2	< 2.9/3.4	1245	0.7	0.44	92
Fe-MIL-100	2.5/2.9	1549	0.82	0.81	85
CAU-6	0.5/1.0	625	0.25	0.32	93
CAU-10	0.7	635	0.25	0.31	86
CAU-10	0.7	600	0.26	0.3	87
CAU-10-CH_3	n.d.	n.d.	n.d.	0.15	86
CAU-10-OCH_3	n.d.	n.d.	n.d.	0.07[a]	86
CAU-10-NH_2	n.d.	n.d.	n.d.	0.19[a]	86
CAU-10-NO_2	n.d.	440	0.18	0.15[a]	86
CAU-10-OH	n.d.	n.d.	n.d.	0.27	86

UiO-66	0.75/1.2	1160	0.52	0.40	88
UiO-66	0.75/1.2	1290	0.49	0.42	87
UiO-66-NO_2	< 0.75/1.2	792	0.4	0.37	94
UiO-66-NH_2	< 0.75/1.2	1123	0.52	0.34	94
UiO-66-2,5-$(OMe)_2$	n.d.	868	0.38	0.42	94
MOF-841	0.9	1390	0.53	0.48	87

[a] Measured at lower relative humidity p/p_0 = 0.5– 0.7.

1.3.1.2 Adsorption of other molecules/ions

Other than water adsorption, the water-stable MOFs have been also utilized for the adsorption and separation of gases under humid conditions. Water-stable MOFs can be applied to separate gases including different volatile organic compounds (VOCs). The adsorptive separation of dyes, oils, metal ions and anions by water-stable MOFs have been also demonstrated.

1.3.1.2.1 Adsorption of gases

In last two decades MOFs have shown remarkable progress in gas adsorption and separation.[95-98] Dehumidified and pure gas are generally required for any practical application. Eddaoudi *et al.* have reported a fluorinated hydrolytically stable MOF called AlFFIVE-1-Ni (KAUST-8), which can selectively remove water vapor from gas streams containing CO_2, N_2, CH_4, and higher hydrocarbons.[99] The MOF material is also capable to remove both H_2O and CO_2 in N_2-containing streams.

MOFs have attracted much interests for hydrogen or methane storage in vehicles. Both methane and hydrogen are promising candidates as replacements for gasoline (petrol). Zr-based MOF, NU-1100 reported by Farha *et al.* exhibited very promising gas uptake for hydrogen and natural-gas storage.[100] The total volumetric hydrogen adsorption at 65 bar and 77 K is 43 g L^{-1} (0.092 g g^{-1}), which is promising for hydrogen storage application by NU-1100 at low temperature. The methane gravimetric deliverable capacity of NU-1100 is 0.24 g g^{-1}, which is significantly high.

Carbon dioxide (CO_2) is a main greenhouse gas, which is released through human activities such as deforestation and burning fossil fuels including natural processes such as volcanic eruptions.[101] The annual global emission of CO_2 has been increased by approximately 80% between 1970 and 2004. The porous and robust MOF materials have shown remarkable progress for CO_2 adsorption in last decades.[102] The capture of CO_2 gas in presence of water have been accomplished by several water-stable MOFs. The selective capture of CO_2 in 65% RH was reported by Yaghi *et al.* for IRMOF-74-III-CH_2NH_2 and IRMOF-74-III-$(CH_2NH_2)_2$.[103,104] The high affinity towards CO_2 gas by amine functional groups was attributed to the strong dipole-quadrupole interactions between amine functional group and CO_2. Am amide-CO_2 hydrogen bonding interaction was also suggested for CO_2 adsorption by a flexible metal-organic framework, $\{[Mn_2(2,6\text{-ndc})_2(bpda)_2]\cdot 5DMF\}_n$ (2,6-ndc = 2,6-naphthalene dicarboxylate; bpda = *N,N′*-bis (4-pyridinyl)-1,4-benzene dicarboxamide).[105]

1.3.1.2.2 Adsorption of small molecules

Using isoreticular chemistry, a series of MOFs with tunable aperture size was reported with rare-earth metal ions (Eu^{3+}, Tb^{3+} and Y^{3+}) for the separation of controlled and selective solvent molecules and light hydrocarbons. The fumarate-based **fcu**-MOF displayed complete exclusion of branched paraffins from normal paraffins. The **fcu**-MOF constructed with bulky 1,4-naphthalenedicarboxylate (1,4-NDC) ligand exhibited an exceptionally high selectivity for n-C_4H_{10} over CH_4.[106,107] The copper(II) paddle wheel based hydrolytically stable MOF $[Cu_4(tdhb)]$ (BUT-155), constructed with 3,3′,5,5′-tetrakis(3,5-dicarboxyphenyl)-2,2′,4,4′,6,6′-hexamethylbiphenyl ligand, showed a high performance for selective adsorption of soft-base type aniline over water or phenol.[76]

The fluorous metal-organic framework (**FMOF-1**) constructed from silver(I) 3,5-bis (trifluoromethyl)-1,2,4-triazolate showed hydrophobic behavior with a high capacity and affinity to C_6-C_8 hydrocarbons of oil components.[52] Based on its high water stability, the material could be used for oil-spill cleanup. Another fluorinated ultrahydrophibic MOF called **UHMOF-100** was synthesized by Ghosh *et al.* This MOF exhibited excellent oil adsorption capacities and reusability features.[56] Based on the excellent features of this MOF, a MOF-coated membrane was fabricated for the separation of oil from water (Figure 1.13). Post-synthetically modified MOF@MON hybrid

materials, reported by Son *et al.*, demonstrated an excellent performance for the adsorption of toluene in water.[60]

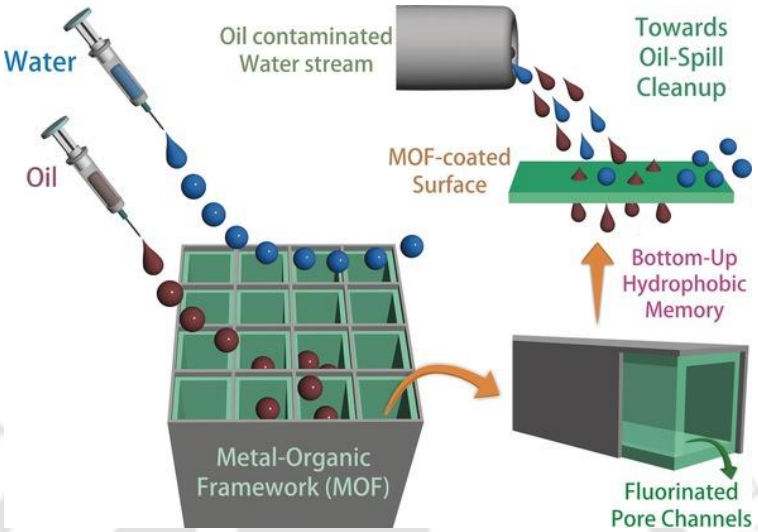

Figure 1.13 Schematic presentation of fluorinated ultrahydrophobic pore surface, utilized as a potential method to obtain ultrahydrophobicity in MOFs. Reproduced with permission from ref. 63. Copyright 2016 Wiley Online Library.

Water-stable MOF materials were successfully utilized for the adsorptive removal of various organics from contaminated water.[108-112] The well-studied Zr(IV)-based UiO-66 MOF was employed for the adsorptive removal of an anionic dye, methyl orange (MO).[112] Experimental data suggested that the adsorption capacity of UiO-66 toward MO was higher than that of methylene blue (MB). The adsorption and removal of phthalic acid and diethyl phthalate from water by UiO-66 and UiO-66-NH_2 MOFs were also investigated.[113] A comparative study supported that ZIF-8 MOF has higher adsorption capacity as compared to UiO-66 framework. The adsorptive removal of naproxen and clofibric acid, two typical PPCPs (PPCP = pharmaceuticals and personal care product) by MOF materials was reported by Jhung *et al.* The Cr-MIL-101 and Fe-MIL-101 compounds showed higher removal efficiency as compared to porous activated carbons.[114]

1.3.1.2.3 Adsorption of ions

Separation of cation mixtures *via* chromatography is another promising application for water-stable MOFs. Zhang *et al.* reported a 3D pillar-layer framework, $[Zn(trz)(H_2betc)_{0.5}]\cdot DMF$,

with uncoordinated carboxyl groups which exhibited exceptional stability.[115] The pillar-layer MOF can selectively adsorb Cu^{2+} ions and it was employed for the column chromatographic separation of Cu^{2+}/Co^{2+} mixture. The selective adsorption of Cu^{2+} over Cd^{2+} and Ni^{2+} ions was studied by Biswas *et al.* with a water-stable thienothiophene based Zr(IV) MOF.[116] Phosphorylurea-derived Zr(IV)-MOFs with UiO-68 topology were synthesized by Lin *et al.*, which showed efficient sorption capacity for uranyl ions.[117] Two isostructural mesoporous MOFs, PCN-100 and PCN-101, constructed with $Zn_4O(CO_2)_6$ secondary building blocks and extended ligands containing amino functional groups, were employed to capture metal ions like Cd^{2+} and Hg^{2+}.[118]

The removal of toxic ionic pollutant such as arsenic was accomplished by Wang *et al.* using Zr-UiO-66 MOF across a broad pH range of 1 to 10.[119] The superior arsenic removal performance of UiO-66 MOF could be attributed to the crystalline structure containing zirconium oxide clusters. These clusters provide active sites along with two binding sites within the adsorbent framework, i.e., hydroxyl group and benzenedicarboxylate ligand. Two MOFs namely $[Zn_2(Tipa)_2(OH)]\cdot 3NO_3\cdot 12H_2O$ (**FIR-53**, Tipa = tris(4-(1H-imidazol-1-yl)phenyl)amine)) and $[Zn(Tipa)]\cdot 2NO_3\cdot DMF\cdot 4H_2O$) (**FIR-54**) were synthesized by Zhang *et al.*, which can efficiently trap the inorganic pollutant ion $Cr_2O_7^{2-}$ *via* single-crystal-to-single-crystal (SC-SC) approach.[120] A mesoporous cationic thorium-based MOF called SCU-8 containing channels with a large inner diameter of 2.2 nm showed a rapid removal of oxo anions like ReO_4^- and $Cr_2O_7^{2-}$ by driving forces including electrostatic interactions, hydrogen bonds, hydrophobic interactions and Van der Waals interactions.[121]

1.3.2 Chemical sensing

The development of fluorescence-based sensors has aroused tremendous scientific interests, since fluorescence techniques are highly sensitive and easy to operate.[70] MOFs are considered for fluorescence sensing applications with remarkable performance because of their specific photoluminescent properties occurring from conjugated ligands and metal ions (e.g. lanthanides), which are further enhanced by their unique structural design, porosity and high surface areas.[122,123] The effectiveness of MOFs for the sensing of different analytes present in water was successfully proven in past years. Due to the unique porous structures, MOFs can act as hosts for fluorescent guest molecules, which is hardly possible for other materials.[124-126] Ghosh. *et al.*

summarized the various possible photophysical processes in MOFs as displayed in Figure 1.14.[127] The sensing of water in organic solvents is important to check the quality of anhydrous solvents. The detection of targeted analytes present is water is another important issue for monitoring the water health. Other than fluorescence sensing, a few MOF materials were also employed for the colorimetric sensing of various target analytes.[128-131]

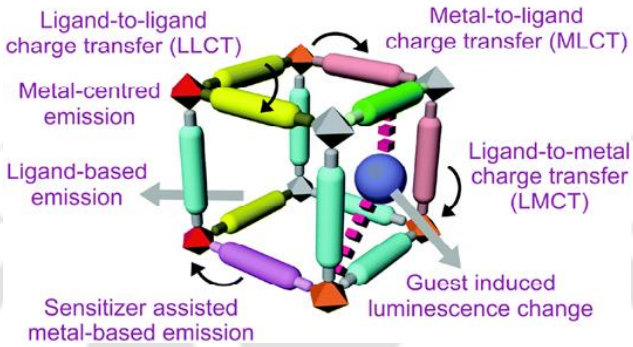

Figure 1.14 Schematic representation of the various possible phenomenon responsible to the emission of MOFs. Reproduced with permission from ref. 127. Copyright 2017 Royal Society of Chemistry.

1.3.2.1 Sensing of water

The robust microporous Zn-MOF called LIFM-CL1, constructed with a ligand that exhibits characteristic excited-state intramolecular proton transfer (ESIPT), was employed for the ultrafast naked eye sensing of water.[132] The Zn-MOF underwent facile single-crystal-to-single-crystal transformation driven by reversible removal/uptake of coordinating water molecules. The interconversion between the hydrated and dehydrated phases could turn the ligand ESIPT process on or off, resulting in a two-color photoluminescence switching. Figure 1.15 shows the schematic presentation of water sensing mechanism *via* different ESIPT processes. This MOF was applied in relative humidity sensing (RH<1%) including the detection of traces of water (<0.05% v/v) in various organic solvents.

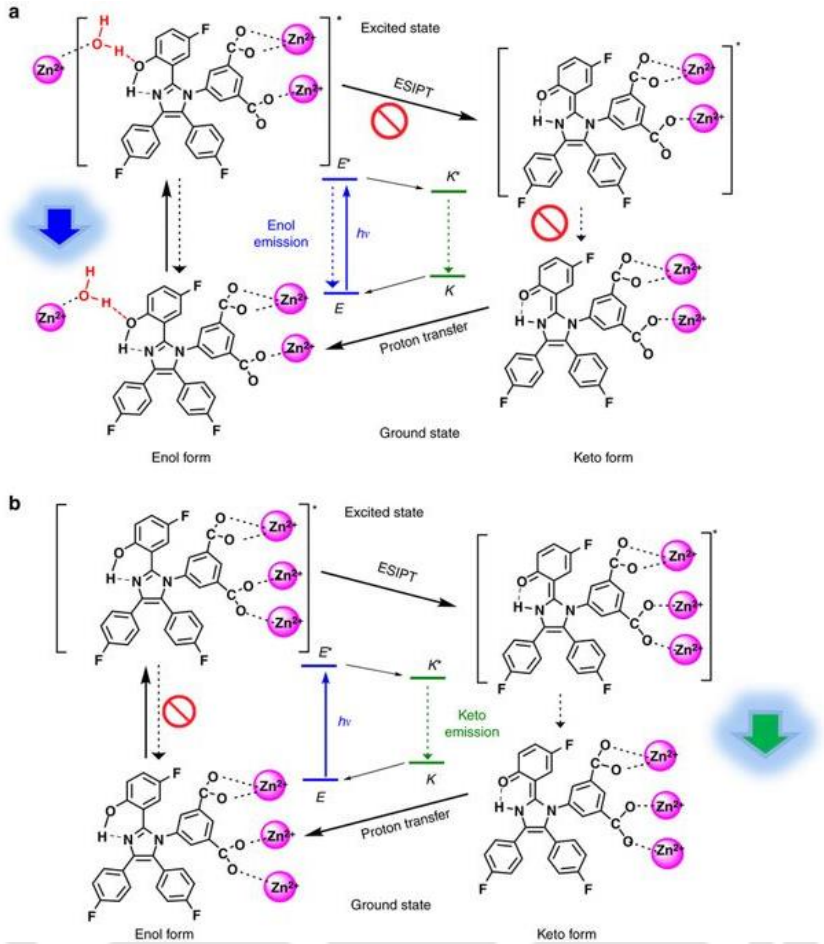

Figure 1.15 Schematic representation of the water sensing mechanism in hydrated LIFM-CL1-H_2O (a) and dehydrated LIFM-CL1 (b) structures, in which the keto-enol tautomerization on excitation is blocked in LIFM-CL1-H_2O by H-bonding, but turned on in LIFM-CL1. Reproduced from ref. 132. Copyright 2017 Nature Publishing Group.

Fluorescent MOFs constructed with lanthanides metal ions have shown great potentials for the sensing of water. Dong and co-workers have synthesized two Ln^{3+}-MOFs which have ellipse-like channels filled with H-bonded water molecules as guests. The water-loaded MOFs showed strong fluorescence whereas the dehydrated framework featured strong fluorescence quenching and the process is reversible in nature.[133] Fluorescent lanthanide-MOF polymer mixed-matrix membranes (LnMOF@MMMs) were synthesized by Buschbaum *et al.* which can be used for the detection of very low relative humidity (only 2%).[134]

1.3.2.2 Sensing of targeted analytes in water

The application of MOFs for fluorescence sensing is a well-established field of research. The lack of stability of many MOFs in aqueous medium restricts their applications in real field. Water-stable MOFs break that restriction as they are hydrolytically stable. Among the various target analytes, the detection of nitroaromatic compounds (NACs) by stable MOFs has been well-studied.[135-139] 2,4,6-Trinitrophenol (TNP), commonly known as picric acid, is one of the most hazardous and water soluble explosive molecules, which acts as a strong fluorescence quencher. Various research suggested different mechanisms for the picric acid induced quenching including photo-induced electron transfer (PET),[140] fluorescence resonance energy transfer (FRET),[141] molecular interactions (such as electrostatic interactions)[142] and inner-filter effect (IFE).[143] A highly fluorescent amine-functionalized Zr(IV)-based MOF with UiO-68 topology was efficiently applied for the selective detection of picric acid in water.[144] A MOF-coated paper test strip was also developed for in-field applications (Figure 1.16). Hou *et al*. reported a Tb-based water-stable MOF, which can detect the NACs even in vapor phase.[145]

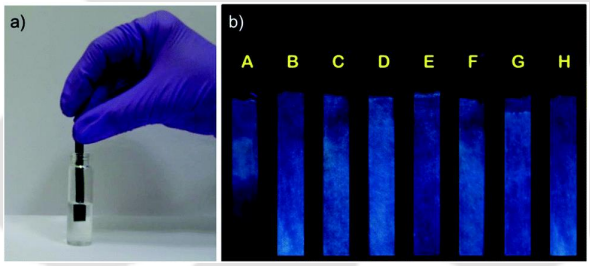

Figure 1.16 (a) Paper strip based detection of explosives in the aqueous phase. (b) Response of MOF-coated paper strips towards various nitro analytes under UV light (A = 2,4,6-trinitrophenol (TNP), B = 2,4,6-trinitrotoluene (TNT), C = 1,3,5-trinitro-1,3,5-triazacyclohexane (RDX), D = 2,4-dinitrotoluene (2,4-DNT), E = 1,3-dinitrobenzene (DNB), F = 2,6-dinitrotoluene (2,6-DNT), G = nitrobenzene (NB), H = 2,3-dimethyl-2,3-dinitrobutane (DMNB)). Reproduced with permission from ref. 144. Copyright 2015 Royal Society of Chemistry.

A few stable MOFs were employed for the sensing of gas molecules. Ghosh *et al.* developed a reaction-based detection methodology for the sensing of toxic hydrogen sulphide (H_2S) gas dissolved in water.[146,147] The presence of nitro (NO_2) or azide (N_3) functional group can act as a reaction site towards H_2S gas. Based on this strategy, few stable MOFs were utilized as

fluorescence turn-on probes for the sensing of H_2S gas.[148-152] Gu *et al.* strategically developed a stable Zr(IV)-based MOF called PCN-224(Pt) containing platinum(II) porphyrin core, which can act as an oxygen-sensitive center.[153] The fluorescent platinum(II) porphyrinic MOF showed a unique response towards dissolved oxygen. The water-dissolved SO_2 gas readily formed a mixture of sulfite and bisulfite (SO_3^{2-} and HSO_3^-) ions. The SO_3^{2-} ion generated from SO_2 gas could be selectively detected by stable MOF-5-NH_2 material.[154] The reusable nature of this MOF probe makes it a potential luminescent sensor to detect SO_3^{2-} for practical applications.

Moreover, a large number of stable MOFs have been recently reported for the detection of cations and anions in water. A water-stable Eu(III)-functionalized Zr(IV)-MOF was constructed by encapsulating Eu^{3+} cations into the pores of Zr-UiO-66-$(COOH)_2$.[155] The Eu(III)-encapsulated MOF system showed a naked eye response for only toxic Cd^{2+} cation over other cations in water. In another report, the Al-MIL-53 MOF was employed to detect the Fe^{3+} ion *via* metal ion exchange mechanism.[156] Furthermore, several water-stable MOFs have been also prepared for the selective detection of anions in water. A stable Zr(IV)-based MOF constructed from C═C bridged di-isophthalate ligand showed high stability in water and it was employed for the sensitive detection of $Cr_2O_7^{2-}$ anion.[157] Cao *et al.* employed another water-stable Zr-MOF for the selective detection of $Cr_2O_7^{2-}$ anion.[158] A cationic dye namely 3,6-diaminoacridinium cation (DAAC) was loaded inside the porous channels of hydrolytically stable bio-MOF-1 by the conventional cation-exchange process by Ghosh *et al.* for the selective detection of lethal cyanide anion (CN^-) in aqueous medium (Figure 1.17).[159]

In addition, a few water-stable MOFs materials have been reported for the selective detection of biologically active small molecules (e.g. ascorbic acid, dopamine, cysteine, glutathione, etc.).[160-164] Post-synthetically modified UiO-66 MOF was also employed for pH sensing application.[165] A few examples of water-stable MOFs are summarized in Table 1.4 with their applications for various sensing processes.

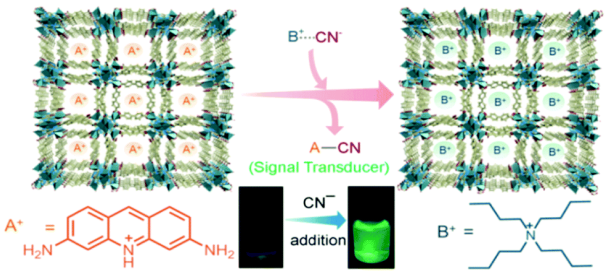

Fig. 1.17 Schematic representation of chemodosimetric approach in bio-MOF-1⊃DAAC prompted by CN^- inducing a turn-on fluorescence response. Reproduced with permission from ref. 159. Copyright 2017 Royal Society of Chemistry.

Table 1.4 Summary of reported MOFs with porous features and water adsorption capacities measured at 298 K.

Type of Targeted Analyte	MOF	Analyte	Limit of Detection	Ref.
nitro-aromatics	BUT-12	TNP	23 ppb	136
	BUT-13	TNP	10 ppb	136
	$\{[Zn_2(L)_2(bpy)]\cdot(DMF)\cdot(H_2O)_2\}_n$	TNP	2.62 ppm	138
	UiO-68	TNP	1.6×10^{-6} M	141
	UiO-68-NH_2	TNP	-	144
	$\{Cd(INA)(pytpy)(OH)\cdot 2H_2O\}_n$	TNP	9.1×10^{-3} mM	166
	bio-MOF-1	TNP	2.9 ppb	167
	$\{[Zn(2,5\text{-tdc})(3\text{-abit})]\cdot H_2O\}_n$	TNP	3.3×10^{-3} mM	168
biomolecules	UiO-66-DNS	cysteine	9.8 μM	163
	UiO-66-PSM	bilirubin	0.59 pmol/L	169
	MN-ZIF-90	amino acids	-	170
	Tb^{3+}@1	dipicolinic acid	3.6 nM.	171
	Eu@MIL-121	hippuric acid	9 μg mL^{-1}	172
	Fe-MIL-88	H_2O_2	46 nm	173

	Cu^{2+}@MIL-91(Al:Eu)	uric Acid	1.6 μmol L^{-1}	174
cations	MIL-53-L	Cu^{2+}	-	175
	UiO-66-NH_2-Eu	Cd^{2+}	0.22 μM	155
	$[In_2(OH)_2(H_2TTHA)(H_2O)_2]_n$	Ru^{3+}	0.26 ppm	176
	$[In_2(OH)_2(H_2TTHA)(H_2O)_2]_n$	UO_2^{2+}	0.42 ppm	176
	$\{Cd(INA)(pytpy)(OH)\cdot 2H_2O\}_n$	Cu^{2+}	3.9×10^{-3} mM	166
	$[Zn(dbp)]_n$	Mn^{2+}	1.80×10^{-4} M	177
	$[Cd(dbp)(H_2O)\cdot 2H_2O\cdot CH_3CN]_n$	Mn^{2+}	5.08×10^{-6} M	177
	NNU-1	Fe^{3+}	0.20×10^{-3} M	178
	$[(CH_3)_2NH_2][In(TNB)_{4/3}]$ ·(2DMF)($3H_2O$) ⊃DSM	Hg^{2+}	1.75 ppb	179
	$[Eu_2L(1,3\text{-bdc})_3]\cdot 5H_2O$	Fe^{3+}	0.023 mM	180
anions	EuCPBDA	MnO_4^-	-	181
	bio-MOF-1⊃DAAC	CN^-	5.2 ppb	159
	Pt(II)TMPyP/rho-ZMOF	S^{2-}	27 nM	182
	$\{Eu_2L_3(DMF)\}\cdot 2DMF$	PO_4^{3-}	6.62 μM	183
	UiO-66-NH_2	PO_4^{3-}	1.25 μM	184
	$[Eu_7(mtb)_5(H_2O)_{16}]^+$	$Cr_2O_7^{2-}$	0.56 ppb	185
	$[(CH_3)_2NH_2][In(TNB)_{4/3}]$ ·(2DMF)($3H_2O$) ⊃DSM	$Cr_2O_7^{2-}$	0.079 μM (23 ppb)	179
	$\{[Zn(2,5\text{-tdc})(3\text{-abit})]\cdot H_2O\}_n$	$Cr_2O_7^{2-}/CrO_4^{2-}$	-	168

Linkers are abbreviated as: pytpy = 4′-(4-Pyridinyl)-2,2′:6′,2″-terpyridine; INA = isonicotinic acid; 2,5-tdc = 2,5-thiophenedicarboxylic acid; 3-abit = 4-amino-3,5-bis(imidazol-1-ylmethyl)-1,2,4-triazole; H_2TTHA = 1,3,5-triazine-2,4,6-triamine hexaacetic acid; H_2dbp = 4′-(4-(3,5-dicarboxylphenoxy)phenyl)-4,2′:6′,4″-terpyridine; TNB = 4,4′,4″-nitrilotribenzoicacid; CPBDA = 3-(6-carboxypyridin-3-yl)benzene-1,4-dioic acid; mtb = 4-[tris(4-carboxyphenyl)methyl]benzoic acid.

1.3.3 Heterogeneous catalysis

MOF materials provide considerably high porosity, which offers suitable spaces for the incorporation of functional groups.[186] The chemical flexibility, modified pore structures and large, readily accessible internal surface areas of MOFs facilitate possible applications in heterogeneous catalysis.[187,188] Xamena *et al.* summarized and nicely explained the main strategies for the inclusion of catalytic activity into a MOF scaffold (Figure 1.18).[189]

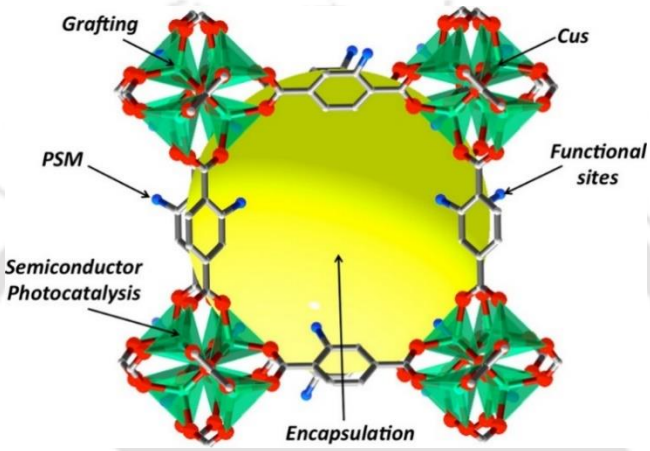

Figure 1.18 Different strategies for the inclusion of catalytic moieties into a MOF scaffold. Reproduced with permission from ref. 189. Copyright 2013 American Chemical Society.

This high versatility of MOF design provides clear advantages for catalysis, since it is possible to rationally design not only the active site but also its environment with an unprecedented degree of precision. The catalytic function can be installed at the organic or at the inorganic component and this can be done by direct synthesis or by post-synthetic modification.[190] Additionally, the porous system of the MOF can also serve as the confined space in which a catalytic species (e.g., metal or metal oxide nanoparticle, metal coordination complex, etc.)[191-195] can be encapsulated, or it can act as the confined space reactor where a chemical reaction can take place. The performances of several MOFs as compared to commercial catalysts are poor due to their instability in the reaction medium. The utilization of hydrolytically stable MOFs as heterogeneous catalysts can overcome such disadvantages, since they are highly adaptable to prevent the structural collapse. Water-stable MOFs have been shown to efficiently catalyze water splitting as well as organic reactions in a large numbers of reports.

1.3.3.1 Catalysis of water splitting reactions

Recently, MOF materials have been used for water splitting application, where water acts as a reactant source.[190] In order to participate in water splitting, a MOF material should exhibit benchmark stability in aqueous medium in a wide pH range. Zhang *et al.* anchored molybdenum polysulfide (MoS_x) on Zr-MOF (UiO-66-NH_2) for the hydrogen evolution reaction (HER).[191] The introduction of MoS_x nanosheets into the MOF dramatically enhanced the HER activity due to the improved electron transport. Matsuoka *et al.* prepared the Ti-MOF-NH_2 photocatalyst using 2-amino-benzenedicarboxylic acid (H_2BDC-NH_2) as an organic linker for the enhanced photocatalytic HER under visible light irradiation.[192] Furthermore, a Ru complex-modified Ti-based MOF (Ti-MOF-Ru(tpy)$_2$; tpy = 4′-(4-carboxyphenyl)-terpyridine) was synthesized, which exhibited high photocatalytic activity for the HER under visible light with a wavelength up to 620 nm.[193] Zhau and co-workers proposed two novel polyoxometalate (POM)-based MOFs, NENU-500 and NENU-501, as electrocatalysts for HER to generate hydrogen from water under acidic conditions.[194]

1.3.3.2 Catalysis of organic reactions

The use of MOFs with coordinatively unsaturated sites (CUS) has been widely explored for catalytic applications.[195-199] In this case, one of the coordination sites of the metal ion is occupied by a weakly coordinated ligand, which can be removed without causing collapse of the crystalline structure. The terephthalate based Cr-MIL-101, UiO-66 and related materials are relevant examples of this type of water-stable MOFs.[200-214] García and co-workers studied the influence of functional groups present in terephthalic acid on the catalytic activity of Cr-MIL-101 in Lewis acid catalyzed reactions.[215] The Cr-MIL-101 materials were utilized as heterogeneous catalysts for epoxide ring opening by methanol, benzaldehyde acetalization by methanol and Prins coupling reaction. The observed results clearly showed the catalytic activity increased as the electron-withdrawing ability of the substituents increased. Up to three folds of enhancement of reaction rate in the presence of the -NO_2 substituent was found for some of these reactions. A similar study was carried out with functionalized UiO-66-X (X = -H, -NH_2, -CH_3, -OCH_3, -F, -Cl, -Br, -NO_2) MOFs for the cyclization of citronellal.[208] While all materials were catalytically active, the rate was dramatically enhanced by the electron-withdrawing groups on the linker (-F, -Cl, -Br,

-NO_2) and UiO-66-NO_2 was found to be the most active material. The functionalized Cr-MIL-101 MOFs were studied by Jainak *et al.* as heterogeneous catalysts for the diacetal formation from benzaldehyde and methanol (B-M reaction) as well as other aldehydes and alcohols. In this reaction, water is formed in the equilibrium reaction (Figure 1.19).[210] The activity decreased in the order: Cr-MIL-101-NO_2 > Cr-MIL-101 > Cr-MIL-101-NH_2. Within different samples of un-functionalized Cr-MIL-101, the activity increased with increasing the surface area. Cr-MIL-101 has two terminal water molecules connected with its octahedral Cr(III) ions, which can be removed under high vacuum, thus creating Lewis acid sites. Cr-MIL-101 and its derivatives show extraordinary stability in water, which make them suitable for catalytic reactions involving water.

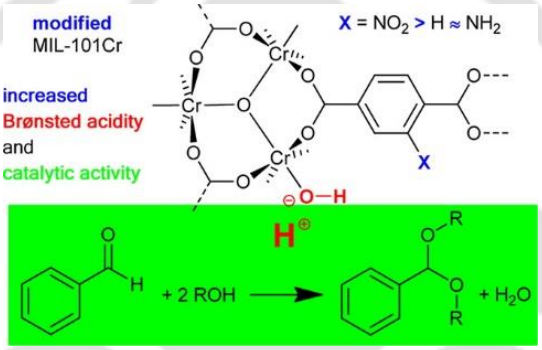

Fig. 1.19 Schematic representation of Brönsted acidity in functionalized Cr-MIL-101 MOFs for heterogeneous catalysis in the condensation reaction of aldehydes with alcohols. Reproduced with permission from ref. 210. Copyright 2014 American Chemical Society.

Water-stable Cr-MIL-101 and Al-MIL-53 MOFs anchored with Brönsted hydrogensulfate acid groups were investigated in the esterification of *n*-butanol with acetic acid.[211] The hydrogensulphated catalyst namely, S-MIL-53(Al), showed the highest performance among the materials tested as acid catalysts in the esterification reaction and can be recycled with slight loss of activity. Control experiments confirmed that the activity of S-MIL-53(Al) was much higher than the same material treated with only one of the reactants (triflic anhydride or H_2SO_4). The results established that hydrogensulfate acid groups anchored on ordered structures became highly stable and consequently displayed high acidity and reactivity. Polyoxometalate (POM)-ionic-liquid-functionalized MIL-100 was developed by Liu *et al.* and used in biodiesel production through the esterification of oleic acid with ethanol.[212] It was found that under the optimal

conditions, the conversion of oleic acid could reach 94.6%, demonstrating a great catalytic activity. Another Keggin-type polyoxometalate (POM), $[CuPW_{11}O_{39}]^{5-}$, a catalyst for air-based organic oxidation was encapsulated in the pores of MOF-199 (HKUST-1).[213] This POM-MOF material, resulted a substantial synergistic stabilization of both the MOF and the POM and catalyzed the rapid chemo- and shape-selective aerobic oxidation of thiols to disulfides. García *et al.* also reported aerobic oxidation of thiols to disulfides using iron metal–organic frameworks as solid redox catalysts.[214]

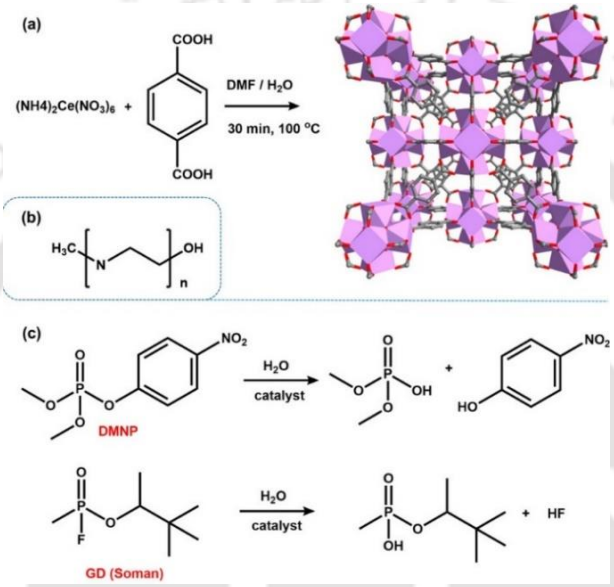

Figure 1.20 The structures of Ce-BDC MOF (a), linear-polyethylenimine (PEI) (b), and the reaction of phosphonate-based nerve agents after hydrolysis (O-pinacolyl methylphosphonofluoridate, GD and a simulant (dimethyl 4-nitrophenyl phosphonate, DMNP) (c). color codes: Carbon (gray), oxygen (red) and cerium (purple). Reproduced with permission from ref. 219. Copyright 2017 American Chemical Society.

In addition, Cr-MIL-101 encapsulated 12-tungstophosphoric heteropolyacid (HPW), HPW@MIL-101(Cr) was studied by Zhong *et al.* as a water-tolerant solid catalyst for hydrolysis.[215] The catalytic activity and reusability of HPW@MIL-101 were evaluated in the liquid-phase hydrolysis of ethyl acetate. The specific activity of HPW@MIL-101 was found to be 377.2 mmol mol_{acid}^{-1} min^{-1}, which is the highest observed in solid acid catalysts. The detoxification of organophosphate nerve agents using MOFs was examined by Farha *et al.*.[216-218] The fast rate of dimethyl 4-nitrophenyl phosphonate (DMNP) hydrolysis was observed for Ce-

UiO-66 compared to Zr-UiO-66 in *N*-ethylmorpholine buffering solution.[219] Polyethylenimine (PEI), a linear polymer, was used to replace the buffer. The half-life for the degradation of O-pinacolyl methylphosphonofluoridate (known as GD) using Ce-UiO-66 was observed to be 3 min whereas Zr-UiO-66 showed ~4 min half-life under the same conditions. DMNP was hydrolyzed at the P-O bond whereas GD was hydrolyzed at the P-F bond, which led to differences in hydrolysis rate between the simulant and agent.

The catalytic activity of Pd/MIL-101 was evaluated for the Suzuki-Miyaura coupling between 4-chloroanisole and phenylboronic acid in water.[220] Here, MIL-101 acted as a support for the nanoparticles and showed high stability in water and other organic solvents. The Pd/MIL-101 catalyst gave 82% yield of 4-phenylanisole when the reaction was performed with tetrabutylammonium bromide using sodium methoxide as a base in 6 h. The catalytic activity of Pd/MIL-101 for the Ullmann homocoupling reaction of 4-chloroanisol in the absence of phenylboronic acid was also studied. Various aryl chlorides were examined as substrates for the Ullmann coupling reaction in air. The conversion was essentially quantitative with 100 % selectivity to the corresponding biphenyl compound at 80 °C. Cohen *et al.* synthesized highly crystalline Zr(IV)-based MOF containing open 2,2′-bipyridine (bpy) chelating sites.[221] The resulting UiO-67-bpydc readily formed complexes with $PdCl_2$ to produce a MOF that exhibited efficient and recyclable catalytic activity for the Suzuki-Miyaura cross-coupling reaction.

MOF-based bifunctional acid-base catalysts were designed for aldol condensation reaction. The Hf-based MOF, Hf-MOF-808 was employed as a heterogeneous catalyst for the highly selective and efficient cross-aldol condensation of biomass-derived furanic carbonyls with acetone.[222] Hf-MOF-808 could be also used in the one-pot synthesis of allylic alcohols by the sequential aldol condensation reaction to yield the α,β-unsaturated methyl ketone. In addition, proline-functionalized Zr-based UiO-67 and UiO-68 type MOF materials were also employed for the diastereoselective aldol addition.[223] High yields (up to 97%) were achieved using ethanol as a solvent. Both MOFs showed reversed diastereoselectivity in aldol addition, preferring *syn*-aldol adduct formation for reaction of cyclohexanone with 4-nitrobenzaldehyde.

1.3.3.3 Biomimetic catalysis

Enzymes are the most sophisticated catalysts with unique features of extraordinary substrate affinity, catalytic efficiency and specificity.[222-224] The biomimetic MOF catalysts present the advantages of extended applicability and enhanced stability and sometimes they display catalytic properties that are not possessed by the natural enzymes.[225,226] Based on these advantages, a large number of biomimetic MOFs were developed in past few years.

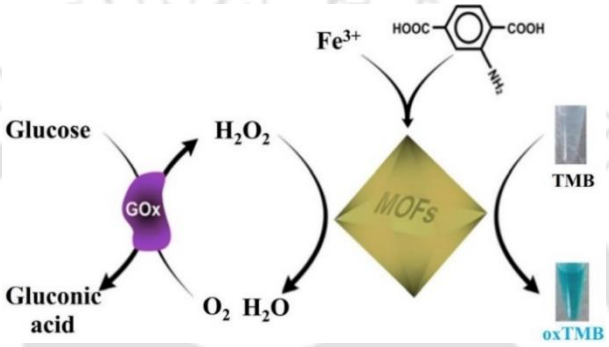

Figure 1.21 Schematic presentation of the glucose detection by Fe-MIL-88-NH_2. Reproduced with permission from ref. 229. Copyright 2013 Royal Society of Chemistry.

Peroxidases are a class of enzymes for degrading H_2O_2 in human bodies and defending against pathogens in plants.[227,228] Nanoscale Fe-MIL-88-NH_2 MOF reported by Li *et al.* was used to mimic the catalytic properties of peroxidase for the oxidation of 3,3′,5,5′-tetramethylbenzidine (TMB) by H_2O_2 (Figure 1.21).[229] Compared to free horseradish peroxidase (HRP), Fe-MIL-88-NH_2 could effectively catalyze this reaction, resulting in a colored product of oxidized TMB, which made Fe-MIL-88-NH_2 a simple alternative for a colorimetric glucose sensor by coupling the oxidation of glucose oxidase. Unfunctionalized Fe-MIL-53 was also employed for glucose sensing.[230,231] An iron-containing porphyrin complex (Hemin) was encapsulated in Al-MIL-101-NH_2 MOF and the composite system showed a peroxidase-like activity. It was applied for the glucose detection.[232] Mesoporous Zr-MOF, PCN-22(Fe) containing Fe-TCPP (TCPP = tetrakis(4-carboxyphenyl)porphyrin) also exhibited excellent peroxidase-like catalytic activity.[233,234] A mixed valence state Ce-MOF was reported by Zhao *et al.*, which exhibited an oxidase like activity due to the Ce^{3+}/Ce^{4+} system present in the MOF. The catalyst could spontaneously recycle and

interchange between the two oxidation states in a redox reaction.[235] The MOF could oxidize TMB to blue-colored oxidized TMB in the absence of H_2O_2. It was applied for the detection of biothiols.

Ma *et al.* successfully encapsulated Microperoxidase-11 (MP-11) into a mesoporous MOF called Tb-mesoMOF consisting of nanoscopic cages. The composite (MP-11@Tb-mesoMOF) demonstrated superior catalytic activity and recyclability in the oxidation of the chromogenic substrate 3,5-di-tert-butyl-catechol (DTBC) to the corresponding *o*-quinone product.[236] In another report, the encapsulation of three heme-proteins (horseradish peroxidase, cytochrome c and MP-11) were achieved by Zhou *et al.* in PCN-333 MOF. These immobilized enzymes maintained or surpassed their catalytic activities over the free enzymes. They exhibited better catalytic performance in organic solvents.[237] These immobilized enzymes showed almost no leaching during catalysis and recycling and maintained high catalytic activity. The immobilization of proteins (e.g. horseradish peroxidase, HRP) and DNA into ZIF-8 was achieved by Falcaro *et al.* through a 'one-pot' biomimetic mineralization strategy.[238] Remarkably, in the presence of trypsin, the ZIF-8/HRP biocomposite retained the bioactivity of HRP showing an 88% conversion of pyrogallol to purporogallin. Under similar conditions, only 20% conversion was observed for the non-protected HRP. The MOF-coated biomolecules maintained enzymatic activity in harsh conditions (e.g. boiling water, boiling DMF), which demonstrated the excellent performance of MOFs as protective coatings for biomacromolecules.

1.4 Motivation and aims of the thesis work

The synthesis and design principles of a large number of MOF materials have been known in literature before the start of this thesis work. At the same time, research activity based on MOF materials has been found to grow enormously due to their various potential applications in a broad range of fields. Whereas many MOFs so far have been synthesized with a great potential of applicability, the area of MOFs with high chemical stability has remained largely unexplored. The development of design principles for stable MOF materials, which can sustain under harsh conditions, is a key challenge for the researchers. Long-term stability of MOF materials is a key factor for the transformation of research based on MOF material from the academic to industrial scale. A few stable MOFs have been commercialized in recent years. Currently, researchers throughout the world are trying to develop water-stable MOFs to utilize their great potentials for

applications in real life. The synthesis of stable MOFs could be possible with the right choice of metal ions and ligands. The use of metal ions with higher oxidation states (e.g. Cr(III), Al(III), Hf(IV), Ti(IV), Zr(IV), Ce(IV), etc.) or use of hydrophobic ligands has been demonstrated to be a successful approach, which results in MOFs having higher physiochemical stabilities (air, water, heat, acid-base, etc.). Other than direct synthetic approach, post-synthetic modification has been also established as a suitable strategy for the stabilization of MOFs. The stable MOFs have been used for the gas adsorption, water adsorption, sensing of different analytes, cell imaging, drug delivery, catalysis, membrane separation etc. Considering the applications of MOF materials in fluorescence sensing, only a few MOF systems have been explored for the detection of various analytes in pure aqueous medium. Other than fluorescence sensing application, the design of MOF based biomimetic catalysts is a very new topic of research. In this thesis, the gas adsorption, fluorometric and colorimetric sensing as well as catalytic applications of highly stable MOFs bearing metal ions in high oxidation states (Al(III), Zr(IV) and Ce(IV) will be presented.

1.5 References

1. A. Kraft, *Bull. Hist. Chem.*, 2008, **33**, 7.
2. H. J. Buser, D. Schwarzenbach, W. Petter, and A. Ludi, *Inorg. Chem.*, 1977, **16**, 2704.
3. A. F. Wells, Three-Dimensional Nets and Polyhedra; Wiley: New York, 1977.
4. J. C. Bailar, *Jr. Prep. Inorg. React.* 1964, **1**, 1.
5. J.-M. Lehn, *Angew. Chem., Int. Ed.*, 1988, **27**, 89.
6. B. F. Hoskins and R. Robson, *J. Am. Chem. Soc.*, 1989, **111**, 5962.
7. M. C. Etter, *Acc. Chem. Res.*, 1990, **23**, 120.
8. G. R. Desiraju, Crystal Engineering. The Design of Organic Solids; Elsevier: Amsterdam, 1989.
9. O. M. Yaghi, and H. Li, *J. Am. Chem. Soc.*, 1995, **117**, 10401.
10. S. R. Batten, N. R. Champness, X. -M. Chen, J. G. -Martinez, S. Kitagawa, L. Öhrström, M. O'Keeffe, M. P. Suh and J. Reedijk, *CrystEngComm*, 2012,**14**, 3001.
11. M. Kondo, T. Yoshitomi, H. Matsuzaka, S. Kitagawa and K. Seki, *Angew. Chem., Int. Ed.*, 1997, **16**, 1725.
12. C. J. Kepert and M. J. Rosseinsky, *Chem. Commun.*, 1999, 375.
13. H. Li, M. Eddaoudi, M. O'Keeffe and O. M. Yaghi, *Nature*, 1999, **402**, 276.

14. J. A. Greathouse and M. D. Allendorf, J. Am. Chem. Soc., 2006, **128**, 10678.

15. S. S. Kaye, A. Dailly, O. M. Yaghi and J. R. Long, *J. Am. Chem. Soc.*, 2007, **129**, 14176.

16. B. Li, H. -M. Wen, W. Zhou and B. Chen, *J. Phys. Chem. Lett.*, 2014, **5**, 3468.

17. H. Li, K. Wang, Y. Sun, C. T. Lollar, J. Li and H. -C. Zhou, *Mater. Today*, 2018, **18**, 108.

18. S. Keskin and S. Kızılel, *Ind. Eng. Chem. Res.*, 2011, **50**, 1799.

19. J. D. Rocca, D. Liu and W. Lin, *Acc. Chem. Res.*, 2011, **44**, 957.

20. G. Férey, C. Mellot-Draznieks, C. Serre, F. Millange, J. Dutour, S. Surble and I. Mirgiolaki, *Science*, 2005, **309**, 2040.

21. P. Serra-Crespo, E. V. Ramos-Fernandez, J. Gascon and F. Kapteijn, *Chem. Mater.*, 2011, **23**, 2565.

22. C. Serre, F. Millange, C. Thouvenot, M. Noguès, G. Marsolier, D. Louër and G. Férey, *J. Am. Chem. Soc.*, 2002, **124**, 13519.

23. S. Biswas, T. Ahnfeldt and N. Stock, *Inorg. Chem.*, 2011, **50**, 9518.

24. G. Férey, C. Serre, C. Mellot-Draznieks, F. Millange, S. Surblé, J. Dutour and I. Margiolaki, *Angew. Chem., Int. Ed.*, 2004, **43**, 6296.

25. A. Sonnauer, F. Hoffmann, M. Fröba, L. Kienle, V. Duppel, M. Thommes, C. Serre, G. Férey and N. Stock, *Angew. Chem., Int. Ed.*, 2009, **48**, 3791.

26. C. Serre1, C. Mellot-Draznieks, S. Surblé1, N. Audebrand, Y. Filinchuk and G. Férey, *Science*, 2007, **315**, 1828.

27. X. Lian, D. Feng, Y. -P. Chen, T. -F. Liu, X. Wang and H. -C. Zhou, *Chem. Sci.*, 2015, **6**, 7044.

28. T. -F. Liu, L. Zou, D. Feng, Y. -P. Chen, S. Fordham, X. Wang, Y. Liu, and H. -C. Zhou, *J. Am. Chem. Soc.*, 2014, **136**, 7813.

29. T. Loiseau, C. Serre. C, Huguenard. G. Fink, F. Taulelle, M. Henry, T. Bataille and G. Férey, *Chem. Eur. J.*, 2004, **10**, 1373.

30. C. Volkringer, D. Popov, T. Loiseau, G. Férey, M. Burghammer, C. Riekel, M. Haouas and F. Taulelle, *Chem. Mater.*, 2009, **21**, 5695.

31. I. Senkovska, F. Hoffmann, M. Fröba, J. Getzschmann, W. Böhlmann and S. Kaskel, *Microporous Mesoporous Mater.*, 2009, **122**, 93.

32. T. Ahnfeldt, N. Guillou, D. Gunzelmann, I. Margiolaki, T. Loiseau, G. Férey, J. Senker and N. Stock, *Angew. Chem., Int. Ed.*, 2009, **48**, 5163.

33. D. Fröhlich, S. K. Henninger and C. Janiak, *Dalton Trans.*, 2014, **43**, 15300.

34. D. Feng, T. -F. Liu, J. Su, M. Bosch, Z. Wei, W. Wan, D. Yuan, Y. -P. Chen, X. Wang, K. Wang, X. Lian, Z. -Y. Gu, J. Park, X. Zou and H. -C. Zhou, *Nat. Commun.*, 2015, **6**, 5979.

35. T. -L. Ho, *Chem. Rev.*, 1975, **75**, 1.

36. M. Bosch, M. Zhang and H. -C. Zhou, *Adv. Chem.*, 2014, **2014**, 8.

37. K. Wang, D. Feng, T. -Fu Liu, J. Su, S. Yuan, Y. -P. Chen, M. Bosch, X. Zou and H. -C. Zhou, *J. Am. Chem. Soc.*, 2014, **136**, 13983.

38. H. Hayashi, A. P. Côté, H. Furukawa, M. O'Keeffe and O. M. Yaghi, *Nat. Mater.*, 2007, **6**, 501.

39. N. C. Burtch, H. Jasuja, and K. S. Walton, *Chem. Rev.*, 2014, **114**, 10575.

40. S. Biswas, J. Zhang, Z. Li, Y. -Y. Liu , M. Grzywa, L. Sun, D. Volkmer and P. V. D. Voort, *Dalton Trans.*, 2013, **42**, 4730.

41. V. Bon, V. Senkovskyy, I. Senkovska and S. Kaskel, *Chem. Commun.*, 2012, **48**, 8407.

42. V. Bon, I. Senkovska, I. A. Baburin and S. Kaskel, *Cryst. Growth Des.*, 2013, **13**, 1231.

43. V. Bon, I. Senkovska, M. S. Weiss and Stefan Kaskel, *CrystEngComm*, 2013,**15**, 9572.

44. H. -L. Jiang, D. Feng, K. Wang, Z. -Y. Gu, Z. Wei, Y. –P. Chen and H. -C. Zhou, *J. Am. Chem. Soc.*, 2013, **135**, 13934.

45. H. -L. Jiang, D. Feng, T. -F. Liu, J. -R. Li and H. -C. Zhou, *J. Am. Chem. Soc.*, 2012, **134**, 14690.

46. D. Feng, Z. -Y. Gu, J. -R. Li, H. -L. Jiang, Z. Wei and H. -C. Zhou, *Angew. Chem., Int. Ed.*, 2012, **51**, 10307.

47. D. Feng, W. -C. Chung, Z. Wei, Z. -Y. Gu, H. –L. Jiang, Y. -P. Chen, D. J. Darensbourg, and H. -C. Zhou,*J. Am. Chem. Soc.*, 2013, **135**, 17105.

48. V. Guillerm, F. Ragon, M. Dan-Hardi, T. Devic, M. Vishnuvarthan, B. Campo, A. Vimont, G. Clet, Q. Yang, G. Maurin, G. Férey, A. Vittadini, S. Gross and C. Serre , *Angew. Chem. Int. Ed.*, 2012, **51**, 9267.

49. W. Morris, B. Volosskiy, S. Demir, F. Gándara, P. L. McGrier, H. Furukawa, D. Cascio, J. F. Stoddart, and O. M. Yaghi, *Inorg. Chem.*, 2012, **51**, 6443.

50. J. Pang, S. Yuan, D. Du, C. Lollar, L, Zhang. M. Wu, D. Yuan, H. -C. Zhou and M. Hong, *Angew. Chem. Int. Ed.*, 2017, **56**, 14622.

51. D. Ma, Y. Li and Z. Li, *Chem. Commun.*, 2011, **47**, 7377.

52. C. Yang, U. Kaipa, Q. Z. Mather, X. Wang, V. Nesterov, A. F. Venero and M. A. Omary, *J. Am. Chem. Soc.*, 2011, **133**, 18094.

53. K. P. Rao, M. Higuchi, K. Sumida, S. Furukawa, J. Duan and S. Kitagawa, *Angew. Chem. Int. Ed.*, 2014, **53**, 8225.

54. M. Zhang, X. Xin, Z. Xiao, R. Wang, L. Zhanga and D. Sun, *J. Mater. Chem. A*, 2017, **5**, 1168.

55. T. -H. Chen, I. Popov, O. Zenasni, O. Daugulis and O. Š. Miljanić, *Chem. Commun.*, 2013, **49**, 6846.

56. S. Mukherjee, A. M. Kansara, D. Saha, R. Gonnade, D. Mullangi, B. Manna, A. V. Desai, S. H. Thorat, P. S. Singh, A. Mukherjee and S. K. Ghosh, *Chem. Eur. J.*, 2016, **22**, 10937.

57. J. G. Nguyen and S. M. Cohen, *J. Am. Chem. Soc.*, 2010, **132**, 4560.

58. C. Liu and A. Huang, *New J. Chem.*, 2018, **42**, 2372.

59. C. Liu, Q. Liu and A. Huang, *Chem. Commun.*, 2016, **52**, 3400.

60. J. Chun, S. Kang, N. Park, E. J. Park, X. Jin, K. -D. Kim, H. O. Seo, S. M. Lee, H. J. Kim, W. H. Kwon, Y. -K. Park, J. M. Kim, Y. D. Kim and S. U. Son, *J. Am. Chem. Soc.*, 2014, **136**, 6786.

61. W Zhang, Y. Hu, J. Ge, H. -L. Jiang and S. -H. Yu, *J. Am. Chem. Soc.*, 2014, **136**, 16978.

62. J. B. Decoste, G. W. Peterson, M. W. Smith, C. A. Stone and C. R. Willis, *J. Am. Chem. Soc.*, 2012, **134**, 1486.

63. S. J. Yang and C. R. Park, *Angew. Chem. Int. Ed.*, 2012, **24**, 4010.

64. S. Yuan, L. Feng, K. Wang, J. Pang, M. Bosch, C. Lollar, Y. Sun, J. Qin, X. Yang, P. Zhang, Q. Wang, L. Zou, Y. Zhang, L. Zhang, Y.Fang, J. Li and H. -C. Zhou, *Adv. Mater.*, 2018, **30**, 1704303.

65. H. Li, K. Wang, Y. Sun, C. T. Lollar, J. Li and H. -C. Zhou, *Mater. Today*, 2018, **21**, 108.

66. I. A. Sung and H. Jhung, *Mater. Today*, 2014, **17**, 136.

67. D. Saha, Z. Bao, F. Jia and S. Deng, *Environ. Sci. Technol.*, 2010, **44**, 1820.

68. Y. He, W. Zhou, G. Qian and B. Chen, *Chem. Soc. Rev.*, 2014,**43**, 5657.

69. K. Vellingiri, J. E. Szulejko, P. Kumar, E. E. Kwon, K. -H. Kim, A. Deep, D. W. Boukhvalov and R. J. C. Brown, *Sci. Rep.*, 2016, **6**, 27813.

70. L. E. Kreno, K. Leong, O. K. Farha, M. Allendorf, R. P. V. Duyne and J. T. Hupp, *Chem. Rev.*, 2012, **112**, 1105.

71. L. -H. Cao, F. Shi, W. -M. Zhang, S. -Q. Zang and T. C. W. Mak, *Chem. Eur. J.*, 2015, **21**, 15705.

72. P. Shi, Y. Zhang, Z. Yu and S. Zhang, *Sci. Rep.*, 2017, **7**, 6500.

73. J. Deng, K. Wang, M. Wang, P. Yu and L. Mao, *J. Am. Chem. Soc.*, 2017, **139**, 5877.

74. W. Qiang, H. Hu, L. Sun, H. Li and D. Xu, *Anal. Chem.*, 2015, **87**, 12190.

75. B. Gole, A. K. Bar and P. S. Mukherjee, *Chem. Commun.*, 2011, **47**, 12137.

76. Y. Chen, B. Wang, X. Wang, L. -H. Xie, J. Li, Y. Xie and J. -R. Li, *ACS Appl. Mater. Interfaces*, 2017, **9**, 27027.

77. M. B. Majewski, A. J. Howarth, P. Li, M. R. Wasielewski, J. T. Huppab and O. K. Farha, *CrystEngComm*, 2017, **19**, 4082.

78. A. H. Chughtai, N. Ahmad, H. A. Younus, A. Laypkovc and F. Verpoort, *Chem. Soc. Rev.*, 2015, **44**, 6804.

79. K. Pirkanniemi and M. Sillanpää, *Chemosphere*, 2002, **48**, 1047.

80. J. M. Taylor, R. K. Mah, I. L. Moudrakovski, C. I. Ratcliffe, R. Vaidhyanathan and G. K. H. Shimizu, *J. Am. Chem. Soc.*, 2010, **132**, 14055.

81. P. Ramaswamy, N. E. Wong, B. S. Gelfand and G. K. H. Shimizu, *J. Am. Chem. Soc.*, 2015, **137**, 7640.

82. J. Zhuang, C. -H. Kuo, L. -Y. Chou, D. -Y. Liu, E. Weerapana and C. -K. Tsung, *ACS Nano*, 2014, **8**, 2812.

83. P. Horcajada, T. Chalati, C. Serre, B. Gillet, C. Sebrie, T. Baati, J. F. Eubank, D. Heurtaux, P. Clayette, C. Kreuz, J. -S. Chang, Y. K. Hwang, V. Marsaud, P. -N. Bories, L. Cynober, S. Gil, G. Férey, P. Couvreur and R. Gref, *Nat. Mater.*, 2010, **9**, 172.

84. P. Horcajada, R. Gref, T. Baati, P. K. Allan, G. Maurin, P. Couvreur, G. Férey, R. E. Morris and C. Serre, *Chem. Rev.*, 2012, **112**, 1232.

85. P. Küsgens, M. Rose, I. Senkovska, H. Frödeb, A. Henschel, S. Siegle and S, Kaskel, *Microporous Mesoporous Mater.*, 2009, **120**, 325.

86. H. Reinsch, M. A. van der Veen, B. Gil, B. Marszalek, T. Verbiest, D. de Vos and N. Stock, *Chem. Mater.*, 2013, **25**, 17.

87. H. Furukawa, F. Gándara, Y. -B. Zhang, J. Jiang, W. L. Queen, M. R. Hudson and O. M. Yaghi, *J. Am. Chem. Soc.*, 2014, 136, 4369.

88. P. M. Schoenecker, C. G. Carson, H. Jasuja, C. J. J. Flemming and K. S. Walton, *Ind. Eng. Chem. Res.*, 2012, **51**, 6513.

89. A. Shigematsu, T. Yamada and H. Kitagawa, *J. Am. Chem. Soc.*, 2011, **133**, 2034.

90. F. Jeremias, A. Khutia, S. K. Henninger and C. Janiak, *J. Mater. Chem.*, 2012, **22**, 10148.

91. G. Akiyama, R. Matsuda, H. Sato, A. Hori, M. Takata and S. Kitagawa, *Microporous Mesoporous Mater.*, 2012, **157**, 89.

92. A. Khutia, H. U. Rammelberg, T. Schmidt, S. Henninger and C. Janiak, *Chem. Mater.*, 2013, **25**, 790.

93. H. Reinsch, B. Marszałek, J. Wack, J. Senker, B. Gil and N. Stock, *Chem. Commun.*, 2012, **48**, 9486.

94. G. E. Cmarik, M. Kim, S. M. Cohen and K. S. Walton, *Langmuir*, 2012, **28**, 15606.

95. J. -R. Li, R. J. Kupplera and H. -C. Zhou, *Chem. Soc. Rev.*, 2009, **38**, 1477.

96. O. K. Farha, A. Ö. Yazaydın, I. Eryazici, C. D. Malliakas, B. G. Hauser, M. G. Kanatzidis, S. T. Nguyen, R. Q. Snurr and J. T. Hupp, *Nat. Chem.*, 2010, **2**, 944.

97. R. B. Getman, Y. -S. Bae, C. E. Wilmer and R. Q. Snurr, *Chem. Rev.*, 2012, **112**, 703.

98. R. E. Morris and P. S. Wheatley, *Angew. Chem., Int. Ed.*, 2008, **47**, 4966.

99. A. Cadiau, Y. Belmabkhout, K. Adil, P. M. Bhatt, R. S. Pillai, A. Shkurenko, C. Martineau-Corcos, G. Maurin and M. Eddaoudi, *Science*, 2017, **356**, 731.

100. O. V. Gutov, W. Bury, D. A. G. Gualdron, V. Krungleviciute, D. Fairen-Jimenez J. E. Mondloch, A. A. Sarjeant, S. S. Al-Juaid, R. Q. Snurr, J. T. Hupp, T. Yildirim and O. K. Farha, *Chem. Eur. J.*, 2014, **20**, 12389.

101. H. Puliyalil, D. L. Jurković, V. D. B. C. Dasireddya and B. Likozara, *RSC Adv.*, 2018, **8**, 27481.

102. K. Sumida, D. L. Rogow, J. A. Mason, T. M. McDonald, E. D. Bloch, Z. R. Herm, T. -H. Bae and J. R. Long, *Chem. Rev.*, 2012, **112**, 724.

103. A. M. Fracaroli, H. Furukawa, M. Suzuki, M. Dodd, S. Okajima, F. Gándara, J. A. Reimer and O. M. Yaghi, *J. Am. Chem. Soc.*, 2014, **136**, 8863.

104. R. W. Flaig, T. M. O. Popp, A. M. Fracaroli, E. A. Kapustin, M. J. Kalmutzki, R. M. Altamimi, F. Fathieh, J. A. Reimer and O. M. Yaghi, *J. Am. Chem. Soc.*, 2017, **139**, 12125.

105. C. -H. Lee, H, -Y. Huang, J. -J. Lee, C. -Y. Huang, Y. -C. Kao, G. -H. Lee, S.-M. Peng, J. -C. Jiang, I. Chao and K. -L. Lu, *ChemistrySelect*, 2016, **1**, 2923.

106. A. H. Assen, Y. Belmabkhout, K. Adil, P. M. Bhatt, D. -X. Xue, H. Jiang and M. Eddaoudi, *Angew. Chem., Int. Ed.*, 2015, **54**, 14353.

107. D. -X. Xue, Y. Belmabkhout, O. Shekhah, H. Jiang, K. Adil, A. J. Cairns and M. Eddaoudi, *J. Am. Chem. Soc.*, 2015, **137**, 5034.

108. Q. Chen, Q. He, M. Lv, Y. Xu, H. Yang, X. Liu and F. Wei, *Appl. Surf. Sci.*, 2015, **327**, 77.

109. M. S. Embaby, S. D. Elwany, W. Setyaningsih and M. R. Saber, *Chin. J. Chem. Eng.*, 2018, **26**, 731.

110. J. Qiua, Y. Fenga, X. Zhanga, M. Jiaa and J. Yaoab, *J. Colloid Interface Sci.*, 2017, **499**, 151.

111. Y. Feng, Y. Li, M. Xu, S. Liu and Jianfeng Yao, *RSC Adv.*, 2016, **6**, 109608.

112. H. Molavi, A. Hakimian, A. Shojaeia and M. Raeiszadeh, *Appl. Surf. Sci.*, 2018, **445**, 424.

113. N. Abedin, K. Beom, K. Jung, Z. Hasan and S. H. Jhung, *J. Hazard. Mater.*, 2015, **282**, 194.

114. Z. Hasan, J. Jeon and S. H. Jhung, *J. Hazard. Mater.*, 2012, **209**, 151.

115. X. Meng, R. -L. Zhong, X. -Z. Song, S. -Y. Song, Z. -M. Hao, M. Zhu, S. -N. Zhaoab and H. -J. Zhang, *Chem. Commun.*, 2014, **50**, 6406.

116. M. SK, M. Grzywa, D. Volkmer and S. Biswas, *J. Solid State Chem.*, 2015, **232**, 221.

117. M. Carboni, C. W. Abney, S. Liub and Wenbin Lin, *Chem. Sci.*, 2013, **4**, 2396.

118. Q. -R. Fang, D. -Q. Yuan, J. Sculley, J. -R. Li, Z. -B. Han and H. -C. Zhou, *Inorg. Chem.*, 2010, **49**, 11637.

119. C. Wang, X. Liu, J. P. Chen and K. Li, *Sci. Rep.*, 2015, **5**, 16613.

120. H. -R. Fu, Z. -X. Xu and J. Zhang, *Chem. Mater.*, 2015, **27**, 205.

121. Y. Li, Z. Yang, Y. Wang, Z. Bai, T. Zheng, X. Dai, S. Liu, D. Gui, W. Liu, M. Chen, L. Chen, J. Diwu, L. Zhu, R. Zhou, Z. Chai, T. E. A. Schmitt and S. Wang, *Nat. Commun.*, 2017, **8**, 1354.

122. Y. Cui, Y. Yue, G. Qian and B. Chen, *Chem. Rev.*, 2012, **112**, 1126.

123. F. -Y, Yi, D. Chen, M. -K. Wu, L. Han and H. -L. Jiang, *ChemPlusChem*, 2016, **81**, 675.

124. R. -B. Lin, S. -Y. Liu, J. -W. Ye, X. -Y. Li and J. -P. Zhang, *Adv. Sci.*, 2016, **3**, 1500434.

125. D. Kukkar, K. Vellingiri, K. -H. Kim and A, Deep, *Sens. Actuators, B*, 2018, **273**, 1346.

126. X. Fang, B. Zong and S. Mao, *Nano-Micro Lett.*, 2018, **10**, 64.

127. W. P. Lustig, S. Mukherjee, N. D. Rudd, A. V. Desai, J. Li and S. K. Ghosh, *Chem. Soc. Rev.*, 2017, **46**, 3242.

128. Y. Zhang, B. Li, H. Ma, L. Zhang and W. Zhang, *J. Mater. Chem. C*, 2017, **5**, 4661.

129. Y. Yu, X. -M. Zhang, J. -P. Ma, Q. -K. Liu, P. Wang and Y. -B. Dong, *Chem. Commun.*, 2014, **50**, 1444.

130. S. Khatua, S. Goswami, S. Biswas, K. Tomar, H. Sekhar Jena and S. Konar, *Chem. Mater.*, 2015, **27**, 5349.

131. A. Mallick, B. Garai, M. A. Addicoat, P. St. Petkov, T. Heinec and R. Banerjee, *Chem. Sci.*, 2015, **6**, 1420.

132. L. Chen, J. -W. Ye, H. -P. Wang, M. Pan, S. -Y. Yin, Z. -W. Wei, L. -Y. Zhang, K, Wu, Y. -N. Fan and C. -Y. Su, *Nat. Commun.*, 2017, **8**, 15985.

133. Y. Yu, J. -P. Maa and Y. -B. Dong, *CrystEngComm*, 2012, 14, 7157.

134. J. M. Stangl, D. Dietrich, A. E. Sedykh, C. Janiak and K. M. Buschbaum, *J. Mater. Chem. C*, 2018, **6**, 9248.

135. L. Zhang, Z. Kang, X. Xin and D. Sun, *CrystEngComm*, 2016, **18**, 193.

136. B. Wang, X. -L. Lv, D. Feng, L. -H. Xie, J. Zhang, M. Li, Y. Xie, J. -R. Li and H. -C. Zhou, *J. Am. Chem. Soc.*, 2016, **138**, 6204.

137. S. S. Nagarkar, A. V. Desai and S. K. Ghosh, *Chem. Commun.*, 2014, **50**, 8915.

138. S. Senthilkumar, R. Goswami, N. L. Obasi and S. Neogi, *ACS Sustainable Chem. Eng.*, 2017, **5**, 11307.

139. J. -S. Hu, S. -J. Dong, K. Wu, X. L. Zhang, J. Jiang, J. Yuan and M. -D. Zheng, *Sens. Actuators, B*, 2019, **283**, 255.

140. D. Banerjee, Z. Hua and J. Li, *Dalton Trans.*, 2014, **43**, 10668.

141. M. SK and S. Biswas, *CrystEngComm*, 2016, **18**, 3104.

142. S. S. Nagarkar, B. Joarder, A. K. Chaudhari, S. Mukherjee and S. K. Ghosh, *Angew. Chem., Int. Ed.*, 2013, **125**, 2953.

143. M. Rong, L. Lin, X. Song, T. Zhao, Y. Zhong, J. Yan, Y. Wang and X. Chen, *Anal. Chem.*, 2015, **87**, 1288.

144. S. S. Nagarkar, A. V. Desai, P. Samanta and S. K. Ghosh, *Dalton Trans.*, 2015, **44**, 15175.

145. J. Qin, B. Ma, X. -F. Liu, H. -L. Lu, X. -Y. Dong, S. -Q. Zang and H. Hou, *J. Mater. Chem. A*, 2015, **3**, 12690.

146. S. S. Nagarkar, T. Saha, A. V. Desai, P. Talukdar and S. K. Ghosh, *Sci. Rep.*, 2014, **4**, 7053.

147. S. S. Nagarkar, A. V. Desai and S. K. Ghosh, *Chem. Eur. J.*, 2015, **21**, 9994.

148. S. Nandi, H. Reinsch, S. Banesh, N. Stock, V. Trivedi and S. Biswas, *Dalton Trans.*, 2017, **46**, 12856.

149. X. Zhang, J. Zhang, Q. Hu, Y. Cui, Y. Yang and G. Qian, *Appl. Surf. Sci.*, 2015, **355**, 814.

150. A. Legrand, A. Pastushenko, V. Lysenko, A. Geloen, E.A. Quadrelli, J. Canivet and D. Farrusseng, *ChemNanoMat*, 2016, **2**, 866.

151. A. Buragohain and S. Biswas, *CrystEngComm*, 2016, **18**, 4374.

152. A. Das, S. Banesh, V. Trivedi and S. Biswas, *Dalton Trans.*, 2018, **47**, 2690.

153. J. Yang, Z. Wang, Y. Li, Q. Zhuang and J. Gu, *Chem. Mater.*, 2016, **28**, 2652.

154. M. Wang, L. Guo and D. Cao, *Anal. Chem.*, 2018, **90**, 3608.

155. X. -Y. Xu and B. Yan, *Sens. Actuators, B*, 2016, **222**, 347.

156. C. -X. Yang, H. -B. Ren and X. -P. Yan, *Anal. Chem.*, 2013, **85**, 7441.

157. M. -M. Xu, X. -J. Kong, T. He, X. -Q. Wu, Li. -H. Xie and J. -R. Li, *Inorg. Chem.*, 2018, **57**, 14260.

158. Z. -J. Lin, H. -Q. Zheng, H. -Y. Zheng, L. -P. Lin, Q. Xin and R. Cao, *Inorg. Chem.*, 2017, **56**, 14178.

159. A. Karmakar, B. Joarder, A. Mallick, P. Samanta, A. V. Desai, S. Basua and S. K. Ghosh, *Chem. Commun.*, 2017, **53**, 1253.

160. D .Yue, D. Zhao, J. Zhang, L. Zhang, K. Jiang, X. Zhang, Y. Cui, Y. Yang, B. Chen and G. Qian, *Chem. Commun.*, 2017, **53**, 11221.

161. Q. Zhu, Y. Chen, W. Wang, H. Zhang, C. Ren, H, Chen and X. Chen, *Sens. Actuators, B*, 2015, **210**, 500.

162. C. Zhao, Z. Jiang, R. Mu and Y. Li, *Talanta*, 2016, **159**, 365.

163. S. Sharma and S. K. Ghosh, *ACS Omega*, 2018, **3**, 254.

164. J. Zhu, T. Xia, Y. Cui, Y. Yang and G. Qian, *J. Solid State Chem.*, 2019, **270**, 317.

165. J. A. Sigalat and D. Bradshaw, *Chem. Commun.*, 2014, **50**, 4711.

166. J. Zhang, J. Wu, G. Tang, J. Feng, F. Luo, B. Xu and C. Zhang, *Sens. Actuators, B*, 2018, **272**, 166.

167. B. Joarder, A. V. Desai, P. Samanta, S. Mukherjee and S. K. Ghosh, *Chem. - Eur. J.*, 2015, **21**, 965.

168. J, Zhang, J. Wu, L. Gong, J, Feng and C, Zhang, *ChemistrySelect*, 2017, **2**, 7465.

169. Y. Du, X. Li, X. Lv and Q. Jia, *ACS Appl. Mater. Interfaces*, 2017, **9**, 30925.

170. H. Li, X. Feng, Y. Guo, D. Chen, R. Li, X. Ren, X. Jiang, Y. Dong and B. Wang, *Sci. Rep.*, 2014, **4**, 4366.

171. Y. Zhang, B. Li, H. Ma, L. Zhang, H. Jiang, H. Song, L. Zhang and Y. Luo, *J. Mater. Chem. C*, 2016, **4**, 7294.

172. J. -N. Hao and B. Yan, *Chem. Commun.*, 2015, **51**, 14509.

173. C. Zhao, Z. Jiang, R. Mub and Y. Li, *Talanta*, 2016, **159**, 365.

174. X. Lian and B. Yan, *Inorg. Chem.*, 2017, **56**, 6802.

175. C. Liu and B. Yan, *Sens. Actuators, B*, 2016, **235**, 541.

176. N. Du, J. Song, S. Li, Y. -X. Chi, F. -Y. Bai and Y. -H. Xing, *ACS Appl. Mater. Interfaces*, 2016, **8**, 28718.

177. Y. Wu, J. Wu, Z. Luo, J. Wang, Y. Li, Y. Hanc and J. Liu, *RSC Adv.*, 2017, **7**, 10415.

178. B. -L. Hou, D. Tian, J. Liu, L. -Z. Dong, S. -L. Li, D. -S. Li and Y. -Q. Lan, *Inorg. Chem.*, 2016, **55**, 10580.

179. H. -R. Fu, Y. Zhao, T. Xie, M. -L. Han, L. -F. Ma and S. -Q. Zang, *J. Mater. Chem. C*, 2018, **6**, 6440.

180. Y. -L. Gai, Q. Guo, X. -Y. Zhao, Y. Chen, S. Liu, Y. Zhang, C. -X. Zhuo, C. Yao and K. -C. Xiong, *Dalton Trans.*, 2018, **47**, 12051.

181. F. Guo, Q.Yang and X. Li, *J. Inorg. Organomet. Polym. Mater.*, 2018, **28**, 1.

182. D. Masih, V. Chernikova, O. Shekhah, M. Eddaoudi and O. F. Mohammed, *ACS Appl. Mater. Interfaces*, 2018, **10**, 11399.

183. P. C. Rao and S. Mandal, *Inorg. Chem.*, 2018, **57**, 11855.

184. J. Yang, Y. Dai, X. Zhu, Z. Wang, Y. Li, Q. Zhuang, J. Shia and J. Gu, *J. Mater. Chem. A*, 2015, **3**, 7445.

185. W. Liu, Y. Wang, Z. Bai, Y. Li, Y. Wang, L. Chen, L. Xu, J. Diwu, Z. Chai and S. Wang, *ACS Appl. Mater. Interfaces*, 2017, **9**, 16448.

186. H. Furukawa, K. E. Cordova, M. O'Keeffe and O. M. Yaghi, *Science*, **341**, 1230444.

187. Y. Zhang and S. N. Riduana, *Chem. Soc. Rev.*, 2012, **41**, 2083.

188. S. Kitagawa, R. Kitaura and S, Noro, *Angew. Chem., Int. Ed.*, 2004, **43**, 2334.

189. J. Gascon, A. Corma, F. Kapteijn and F. X. L. Xamena, *ACS Catal.*, 2014, **4**, 361.

190. W. Wang, X. Xu, W. Zhou and Z. Shao, *Adv. Sci.*, 2017, **4**, 1600371.

191. X. Dai, M. Liu, Z. Li, A. Jin, Y. Ma, X. Huang, H. Sun, H. Wang and X. Zhang, *J. Phys. Chem. C*, 2016, **120**, 12539.

192. Y. Horiuchi, T. Toyao, M. Saito, K. Mochizuki, M. Iwata, H. Higashimura, M. Anpo and M. Matsuoka, *J. Phys. Chem. C*, 2012, **116**, 20848.

193. T. Toyao, M. Saito, S. Dohshi, K. Mochizuki, M. Iwata, H. Higashimura, Y. Horiuchi and M. Matsuoka, *Chem. Commun.*, 2014, **50**, 6779.

194. J. -S. Qin, D. -Y. Du, W. Guan, X. -J. Bo, Y. -F. Li, L. -P. Guo, Z. -M. Su, Y. -Y. Wang, Y. -Q. Lan and H. -C. Zhou, *J. Am. Chem. Soc.*, 2015, **137**, 7169.

195. I. T. Horváth, *Green Chem.*, 2008, **10**, 1024.

196. N. Yan, C. Xiao and Y. Kou, *Coord. Chem. Rev.*, 2010, **254**, 1179.

197. A. Dhakshinamoorthy, A. M. Asiri and H. Garcia, *Chem. Commun.*, 2014, **50**, 12800.

198. P. Valvekens, F. Vermoortele and D. D. Vos, *Catal. Sci. Technol.*, 2013, **3**, 1435.

199. L. Ahrem, G. Scholz, T. Gutmann, B. Calvo, G. Buntkowsky and E. Kemnitz, *J. Phys. Chem. C*, 2017, **121**, 12206.

200. J. Tang and J. Wang, *Environ. Sci. Technol.*, 2018, **52**, 5367.

201. S. Ketrat, T. Maihom, S. Wannakao, M. Probst, S. Nokbin and J. Limtrakul, *Inorg. Chem.*, 2017, **56**, 14005.

202. S. Borah, S. Mishra, L. Cardenas and N. Gogoi, *Eur. J. Inorg. Chem.*, 2018, 751.

203. J. N. Halla and P. Bollini, *React. Chem. Eng.*, 2019, Advance Article.

204. N. V. Maksimchuk, K. A. Kovalenko, V. P. Fedinbc and O. A. Kholdeeva, *Chem. Commun.*, 2012, **48**, 6812.

205. M. Hartmann and M. Fischer, *Microporous Mesoporous Mater.*, 2012, **164**, 38.

206. F. Vermoortele, B. Bueken, G. L. Bars, B. V. de Voorde, M. Vandichel, K. Houthoofd, A. Vimont, M. Daturi, M. Waroquier, V. V. Speybroeck, C. Kirschhock and D. E. D. Vos, *J. Am. Chem. Soc.*, 2013, **135**, 11465.

207. M. Vandichel, J. Hajek, F. Vermoortele, M. Waroquier, D. E. D. Vos and Veronique Van Speybroeck, *CrystEngComm*, 2015, **17**, 395.

208. F. Vermoortele, M. Vandichel, B. V. de Voorde, R. Ameloot, M. Waroquier, V. V. Speybroeck and D. E. D. Vos, *Angew. Chem., Int. Ed.*, 2012, **51**, 4887.

209. A. S. -Portillo, S. Navaljn, P. Concepcijn, M. Álvaro and H. García, *ChemCatChem*, 2017, **9**, 2506.

210. A. Herbst, A. Khutia and C. Janiak, *Inorg. Chem.*, 2014, **53**, 7319.

211. M. G. Goesten, J. J. -Alcañiz, Enrique V. R. -Fernandez, K.B. S. S. Gupta, E. Stavitski, H. Bekkum, J. Gascon, F. Kapteijn, *J. Catal.*, 2011, **281**, 177.

212. H, Wan, C. Chen, Z. Wu, Y. Que, Y. Feng, W. Wang, L. Wang, G. Guan and X. Liu, *ChemCatChem*, 2015, 7, 441.

213. J. Song, Z. Luo, D. K. Britt, H. Furukawa, O. M. Yaghi, K. I. Hardcastle and C. L. Hill, *J. Am. Chem. Soc.*, 2011, **133**, 16839.

214. A. Dhakshinamoorthy, M. Alvaro and H. Garcia, *Chem. Commun.*, 2010, **46**, 6476.

215. Y. Zang, J. Shi, X. Zhao, L. Kong, F. Zhang and Y. Zhong, *React. Kinet. Mech. Catal.*, 2013, **109**, 77.

216. J. E. Mondloch, M. J. Katz, W. C. Isley III, P. Ghosh, P. Liao, W. Bury, G. W. Wagner, M. G. Hall, J. B. DeCoste, G. W. Peterson, R. Q. Snurr, C. J. Cramer, J. T. Hupp and O. K. Farha, *Nat. Mater.*, 2015, **14**, 512.

217. Y. Liu, A. J. Howarth, N. A.Vermeulen, S. -Y. Moon, J. T.Hupp and O. K. Farha, *Coord. Chem. Rev.*, 2017, **346**, 101.

218. S. -Y. Moon,Y. Liu, J. T. Hupp and O. K. Farha, *Angew. Chem., Int. Ed.*, 2015, **54**, 6795.

219. T. Islamoglu, A. Atilgan, S. -Y. Moon, G. W. Peterson, J. B. DeCoste, M. Hall, J. T. Hupp and O. K. Farha, *Chem. Mater.*, 2017, **29**, 2672.

220. B. Yuan, Y. Pan, Y. Li, B. Yin and H. Jiang, *Angew. Chem., Int. Ed.*, 2010, **49**, 4054.

221. H. Fei and S. M. Cohen, *Chem. Commun.*, 2014, **50**, 4810.

222. D. Schilter, *Nat. Rev. Chem.*, 2018, **6**, 0147.

223. R. Callender and R. B. Dyer, *Acc. Chem. Res.*, 2015, **48**, 407.

224. S. Shoda, H. Uyama, J. Kadokawa, S. Kimura and S. Kobayashi, *Chem. Rev.*, 2016, **116**, 2307.

225. Y. Chenab and S. Ma, *Dalton Trans.*, 2016, **45**, 9744.

226. I. Nath, J. Chakraborty and F. Verpoort, *Chem. Soc. Rev.*, 2016, **45**, 4127.

227. B. Halliwell, M. Veronique, C. Lee and H. Long, *FEBS Lett.*, 2000, **486**, 10.

228. M. C. Mehdy, *Plant Physiol.*, 1994, **105**, 467.

229. Y. L. Liu, X. J. Zhao, X. X. Yang and Y. F. Li, *Analyst*, 2013, **138**, 4526.

230. W. Dong, X. Liu, W. Shi and Y, Huang. *RSC Adv.*, 2015, **5**, 17451.

231. T. Lin, Y. Qin, Y. Huang, R. Yang, L. Hou, F. Ye and S. Zhao, *Chem. Commun.*, 2018, **54**, 1762.

232. F. -X. Qin, S. -Y. Jia, F. -F. Wang, S. -H. Wu, J. Song and Y. Liu, *Catal. Sci. Technol.*, 2013, **3**, 2761.

233. D. Feng, Z. -Y. Gu, J. -R. Li, H. -L. Jiang, Z. Wei and H. -C. Zhou, *Angew. Chem. Int. Ed.*, 2012, **51**, 10307.

234. G. Yu, X. Song, S. Zheng, Q. Zhao, D. Yana and J. Zhao, *Anal. Methods*, 2018, **10**, 4275.

235. Y. Xiong, S. Chen, F. Ye, L. Su, C. Zhang, S. Shen and S. Zhao, *Chem. Commun.*, 2015, **51**, 4635.

236. V. Lykourinou, Y. Chen, X. -S. Wang, L. Meng, T. Hoang, L. -J. Ming, R. L. Musselman and S. Ma, *J. Am. Chem. Soc.*, 2011, **133**, 10382.

237. D. Feng, T. -F. Liu, J. Su, M. Bosch, Z. Wei, W. Wan, D. Yuan, Y. -P. Chen, X. Wang, K. Wang, X. Lian, Z. -Y. Gu, J. Park, X. Zou and H. -C Zhou, *Nat. Commun.*, 2015, **6**, 5979.

238. K. Liang, R. Ricco, C. M. Doherty, M. J. Styles, S. Bell, N. Kirby, S. Mudie, D. Haylock, A. J. Hill, C. J. Doonan and P. Falcaro, *Nat. Commun.*, 2015, **6**, 7240.

Chapter 2

The effect of functional groups in the aqueous phase selective sensing of Fe(III) ions by thienothiophene-based zirconium metal-organic frameworks and the design of molecular logic gates

This chapter presents the synthesis of four isoreticular thienothiophene-based Zr(IV) MOF materials under solvothermal conditions. All the MOFs possess the UiO (UiO = University of Oslo) framework topology and contains $[Zr_6O_4(OH)_4]^{12+}$ *building units. The hydrophobicity and fluorescence properties of all the MOF compounds have been tuned in a systematic fashion by attaching methyl and phenyl groups to the thienothiophene-based ligands. As verified by the fluorescence titration experiments, all the MOF materials featured selective, fast, and sensitive sensing of* Fe^{3+} *ions in water through the fluorescence quenching mechanism. In addition, molecular logic gates were designed by employing the MOFs for distinguishing between* Fe^{3+} *and* Fe^{2+} *ions.*

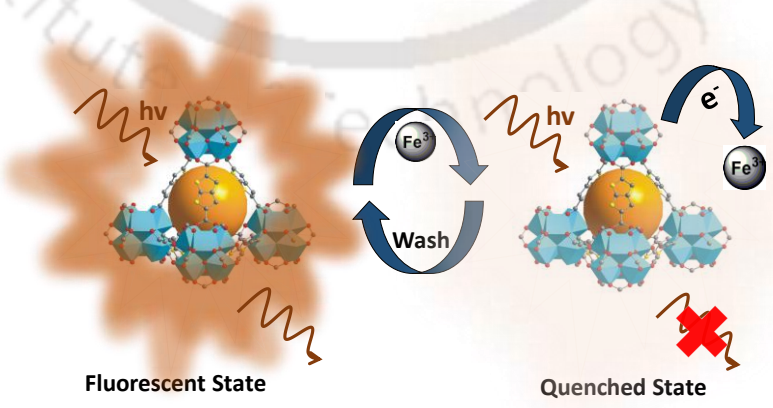

Dalton Transactions

R. Dalapati, Ü. K. Demir, C. Janiak and S. Biswas, *Dalton Trans.*, 2018, **47**, 1159.

2.1 Introduction

The selective recognition and discrimination of biologically active species has been one of the devoted areas of scientific research.[1] Among the various methodologies, due to simplicity and high sensitivity, the fluorescence-based molecular recognition strategy has gained significant attention. Recently, metal-organic frameworks (MOFs)[2] have been efficiently employed in fluorescence sensing applications including chemical separation,[3] gas storage,[4] heterogeneous catalysis,[5] polymerization[6] and drug delivery.[7] Fluorescent MOFs have several advantages over the conventional small-molecule-based sensor materials because of their ultrahigh surface areas, adjustable porosities, functionalizable pore walls and π-conjugated backbones.[8] The ordered orientation of fluorescent ligands and metal clusters in MOFs enhances the rate of electron transfer throughout the porous framework.[9-11] Encouraged by the advantages of MOF-based fluorescent sensor materials, significant research efforts have been devoted to date to prepare MOFs for the optical/fluorescence sensing of ionic species, small organic molecules, volatile organic compounds and energetic materials.[12,13] However, targeted design and synthesis of MOFs having high selectivity towards the detection of a particular analyte is still a challenging task.

Among the biologically active cations, sensing of Fe^{3+} is one of the important areas of research since it is actively involved in important biological processes like storage and transport of oxygen,[14] electron transfer as well as the synthesis of DNA and RNA.[15] The consumption of water with excess levels of iron cause cellular toxicity,[16-18] which can damage biomolecules (such as lipids and proteins)[19] and may be associated with some serious diseases such as Alzheimer's disease.[20] Thus far, several fluorescent MOFs have been developed to recognize Fe^{3+} ions.[21-23] However, the discrimination between Fe^{3+} and Fe^{2+} ions by MOF materials is unexplored so far. For the detection of Fe^{3+} ions, numerous lanthanide-based[23–26] MOFs have been used owing to their excellent luminescence properties. A few non-lanthanide[27,28] MOFs have also been employed for serving the same purpose. However, most of the previously reported lanthanide MOF-based fluorescent sensors for Fe^{3+} ions work *via* cation-exchange with framework metal ions.[28] The cation-exchange mechanism leads to either the collapse of the framework[29] or the generation of mixed-metal frameworks.[30] As a result, these MOF-based fluorescent probes show poor recyclability of their detection performances towards Fe^{3+} ions. Moreover, other cations (e.g. Al^{3+}, Cu^{2+}) have been reported to interfere with the recognition of

Fe^{3+} ions. Therefore, the development of new MOF-based sensor materials for Fe^{3+} ions that can overcome the above-stated problems is still a challenging task. In addition to the fluorescence quenching *via* the cation-exchange mechanism, the interactions of Fe^{3+} ions with the organic ligands and simultaneous electron transfer from the electron-rich frameworks to the electron-poor Fe^{3+} ions can also lead to fluorescence quenching.[31]

Numerous Zr(IV)-based MOFs have been reported to exhibit high physicochemical stabilities.[32,33] Therefore, the synthesis of Zr(IV) MOFs containing fluorescent ligands could be a better choice than the lanthanide-based MOFs in order to resist the structural collapse of the MOFs during the sensing events. Furthermore, the use of highly conjugated ligands might facilitate the electron shuttle from the framework to the electron poor species of interest. Owing to its highly extended π-electron system, there is an extensive use of the thieno[3,2-b] thiophene species for the preparation of high-performance organic polymer semiconductors.[34-36] Therefore, we hypothesized that the construction of Zr(IV) MOFs incorporating thienothiophene units could be very effective for showing fluorescence quenching behaviour towards Fe^{3+} ions through the electron transfer mechanism. In this work, the preparation and thorough characterization of four highly stable Zr(IV) MOFs (three new and one previously reported[37]) containing thienothiophene-based ligands are presented. All the MOFs were capable of performing selective sensing of Fe^{3+} ions in pure aqueous medium by the fluorescence quenching mechanism. The dynamic nature of the fluorescence quenching processes in these MOF systems has been indicated by the fluorescence investigations (both steady-state and time-resolved). The presence of the electron transfer mechanism was confirmed by employing the well-known electron acceptor methyl viologen (MV^{2+}) dications, which exhibited a reverse trend in the fluorescence quenching efficiencies of the MOFs compared to the Fe^{3+} ions. It has been anticipated that both the steric and electronic effects of the functional groups grafted with thienothiophene-based ligands govern the fluorescence quenching mechanism. In addition to the selective sensing of Fe^{3+} ions, molecular logic gates were constructed by using the MOFs for discrimination between Fe^{3+} and Fe^{2+} ions.

2.2 Experimental

2.2.1 Materials and physical measurements

The preparation of H_2TDC, H_2DMTDC, H_2MPTDC and H_2DPTDC ligands was carried out by following literature protocols.[38] All other reagents were procured from the commercial vendors. All the fluorescence titration experiments were conducted by using Milli-Q water as a medium. A PerkinElmer Spectrum Two FT-IR spectrometer (FT-IR = Fourier transform infrared) was employed to collect the FT-IR spectra in the region of 440-4000 cm^{-1}. For characterizing the absorption peaks, the following notations were used: weak (w), medium (m), strong (s), very strong (vs), shoulder (sh) and broad (br). A Mettler-Toledo TGA/SDTA 851e thermogravimetric instrument was utilized to carry out the thermogravimetric analysis (TGA) in the temperature range of 30-700 ℃ in air at a heating rate of 5 ℃ min^{-1}. X-Ray powder diffraction (XRPD) patterns were obtained at room temperature with a Bruker D2 Phaser X-ray diffractometer functioning at 30 kV and 10 mA employing Cu-Kα (λ = 1.5406 Å) radiation. UV-Vis spectra were recorded with a PerkinElmer Lambda 25 UV-Vis spectrometer. A Hitachi S3400N SEM-EDX (SEM-EDX = scanning electron microscope-energy dispersive X-ray) equipment was used to carry out the EDX measurements. Nitrogen adsorption experiments were performed by utilizing a Quantachrome Autosorb iQ-MP volumetric gas adsorption equipment at −196 ℃. The degassing of the samples was accomplished at 120 ℃ under high vacuum for 12 h before the adsorption measurements. The water adsorption measurements were carried out by a volumetric method with a Quantachrome Autosorb iQ MP instrument at 20 ℃. Contact angle experiments were performed by employing a KRUSS Drop Shape Analyzer-DSA25 instrument with an automatic liquid dispenser at ambient temperature. A JASCO V-650 UV-Vis spectrophotometer equipped with a 150 mm integrating sphere was used to record the UV-Vis spectra in the solid state. $BaSO_4$ was employed as an internal standard. Fluorescence investigations were performed with a HORIBA JOBIN YVON Fluoromax-4 spectrofluorometer. An Edinburgh Instrument Life-Spec II instrument was employed for measuring the fluorescence lifetimes by using the time-correlated single-photon counting (TCSPC) procedure. The FAST software supplied by Edinburgh Instruments was utilized to analyse the fluorescence decays by the reconvolution technique. The synthesis and activation of **2** were performed by following the

literature procedure.[37] Regular characterization techniques (N_2 sorption analysis, IR spectroscopy, XRPD as well as TG analysis) were employed for validating the phase-purity.

2.2.2 Synthesis of $[Zr_6O_4(OH)_4(C_8H_2O_4S_2)_6]\cdot DMF\cdot 18H_2O$ (1)

A sealed glass tube containing a mixture of $ZrCl_4$ (50 mg, 0.215 mmol), H_2TDC (49 mg, 0.215 mmol) ligand and benzoic acid (786 mg, 6.45 mmol) in DMF (3 mL) was heated at 150 °C for 24 h by employing a dry block heater. After cooling the tube down to ambient temperature spontaneously, the white precipitate was filtered off and washed several times with acetone. Afterwards, the precipitate was dried in air. Yield: 55 mg (0.02 mmol, 63%) related to the Zr salt. Anal. calcd. For $C_{51}H_{59}NO_{51}S_{12}Zr_6$: C, 25.24 H, 2.45 N, 0.57. Found: C, 24.32 H, 2.88 and N, 0.70%. FT-IR (KBr, cm^{-1}): 3410 (br), 2924 (w), 1507 (m), 1457 (m), 1366 (vs), 1172 (m), 1084 (m), 1021 (m), 884 (m), 771 (m), 721 (s), 658 (m) and 603 (m).

2.2.3 Synthesis of $[Zr_6O_4(OH)_4(C_{15}H_8O_4S_2)_6]\cdot 4DMF\cdot 21H_2O$ (3)

The synthesis procedure for this compound (white powder) was similar to that presented for **1**, except that the H_2MPTDC ligand (68 mg, 0.215 mmol) was used instead of the H_2TDC ligand. Yield: 60 mg (0.018 mmol, 53%) related to the Zr salt. Anal. calcd. for $C_{102}H_{122}N_4O_{57}S_{12}Zr_6$: C, 37.80 H, 3.79 and N, 1.72. Found: C, 38.0 H, 3.68 N, 1.67%. FT-IR (KBr, cm^{-1}): 3422 (br), 3053 (w), 2924 (w), 1573 (m), 1512 (m), 1472(m), 1390 (vs), 1192 (m), 1125 (w), 1027 (m), 775 (m), 720 (m), 666 (s) and 615 (m).

2.2.4 Synthesis of $[Zr_6O_4(OH)_4(C_{20}H_{10}O_4S_2)_6]\cdot 2.5DMF\cdot 11H_2O$ (4)

The synthesis procedure for this compound (white powder) was similar to that presented for **1**, except that the H_2DPTDC ligand (82 mg, 0.215 mmol) was used instead of the H_2TDC ligand and the amount of benzoic acid employed was 262 mg (2.15 mmol) instead of 786 mg (6.45 mmol). Yield: 50 mg (0.015 mmol, 42%) related to the Zr salt. Anal. calcd. For $C_{127.5}H_{91.5}N_{2.5}O_{45.5}S_{12}Zr_6$: C, 46.08 H, 3.14 and N, 1.05. Found: C, 46.8 H, 2.95 N, 1.2%. FT-IR (KBr, cm^{-1}): 3411 (br), 3056(m), 2928 (w), 2858 (w), 1604 (m), 1554 (m), 1515 (s), 1476(m), 1394 (vs), 1222 (m), 1114 (w), 876 (m), 787 (m), 752 (m), 713 (s), 697 (m) and 631 (m).

2.2.5 Activation procedures for the as-synthesized materials

The activation of the as-synthesized forms of all the compounds was carried out in two stages. The stirring of the as-synthesized compounds (0.2 g each) in methanol (30 mL) at room temperature was conducted in the first step. The subsequent step involved collection of the white compounds by filtration and heating them at 100 °C for 24 h under high vacuum. The activated forms of **1**, **2**, **3** and **4** are denoted as **1′**, **2′**, **3′** and **4′**, respectively.

2.2.6 Fluorescence titration experiments

For performing the fluorescence titration experiments, the samples (3 mg each) of **1′**, **2′**, **3′** and **4′** were suspended in water (3 mL) and the mixture was homogenized by ultrasonic treatment for 30 min. Subsequently, 300 μL of each of the suspension was diluted with 2700 μL of water (final concentration = 99 μg mL^{-1}) in a quartz cuvette and 10 mM solutions of different analytes were added in an incremental manner. The calculation of the quenching efficiency (Q) involved the formula: $Q = (1 - I/I_0) \times 100\%$, where I_0 and I are the fluorescence intensity of the aqueous dispersions of the compounds before and after the addition of the analyte. For the Fenton-type reaction, 20 μL of H_2O_2 was added to the aqueous suspension of each compound, accompanied by the addition of Fe^{2+} solution. In the case of the radical scavenging experiment, fluorescence titration measurement was carried out in the presence of 300 μL of isopropyl alcohol (IPA).

2.3 Results and discussion

2.3.1 Preparation and activation procedures

Zr(IV)-based MOFs were prepared by using the following ligands: 3,4-dimethylthieno[2,3-b]thiophene-2,5-dicarboxylic acid (H_2DMTDC), thieno[2,3-b]thiophene-2,5-dicarboxylic acid (H_2TDC), 3,4-diphenylthieno[2,3-b]thiophene-2,5-dicarboxylic acid (H_2DPTDC) and 3-methyl-4-phenylthieno[2,3-b]thiophene- 2,5-dicarboxylic acid (H_2MPTDC). The respective MOF materials were denoted as **1**, **2**, **3** and **4**. The syntheses of all the four MOF compounds involved solvothermal reactions (150 °C, 24 h) in *N*,*N*-dimethylformamide (DMF) using benzoic acid as a modulator. The $ZrCl_4$ to benzoic acid molar ratio was maintained at 1 : 30 for synthesizing **1** and **3**. Compound **4** was prepared by employing a $ZrCl_4$ to benzoic acid molar ratio of 1 : 10. The preparation of **2** was performed by following our formerly reported

procedure.[37] The as-synthesized materials contain guest molecules inside their voids, which were first exchanged with methanol. Subsequently, the methanolexchanged forms of the compounds were subjected to thermal treatment under dynamic vacuum. The thermally activated compounds obtained in this way are termed **1′**, **2′**, **3′** and **4′**.

2.3.2 FT-IR analysis

The activated and as-synthesized forms of **1**, **3** and **4** (Figure 2.1-2.3) display absorption bands with high intensity in the regions of 1560-1600 and 1370-1390 cm^{-1} in their IR spectra. The asymmetric and symmetric stretching vibrations of the coordinated carboxylate groups attached to the ligands give rise to these absorption peaks, respectively.[39-41] The IR spectra of the as-synthesized materials feature absorption peaks at ca. 1655 cm^{-1} with moderate intensity. These absorption peaks are observed due to the stretching vibration of the carbonyl groups of the guest DMF molecules.[42] The IR spectra of all the activated compounds lack peaks due to the DMF molecules. These results confirm that the materials have been completely activated.

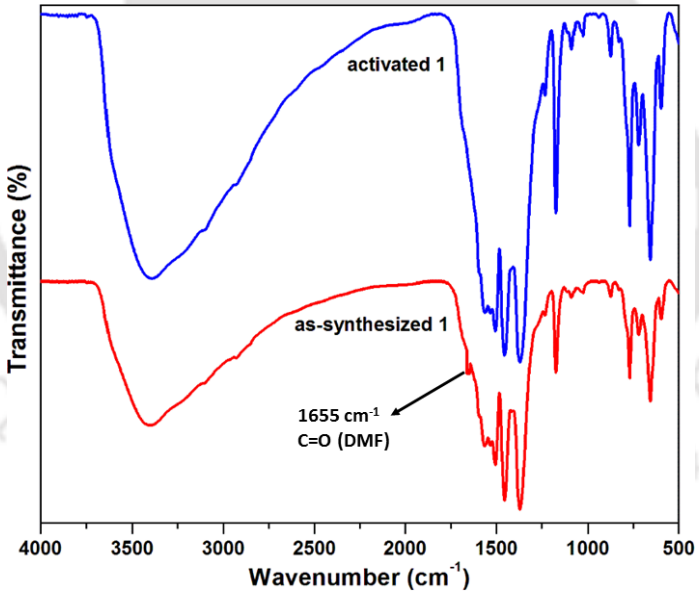

Figure 2.1 FT-IR spectra of as-synthesized and activated **1**.

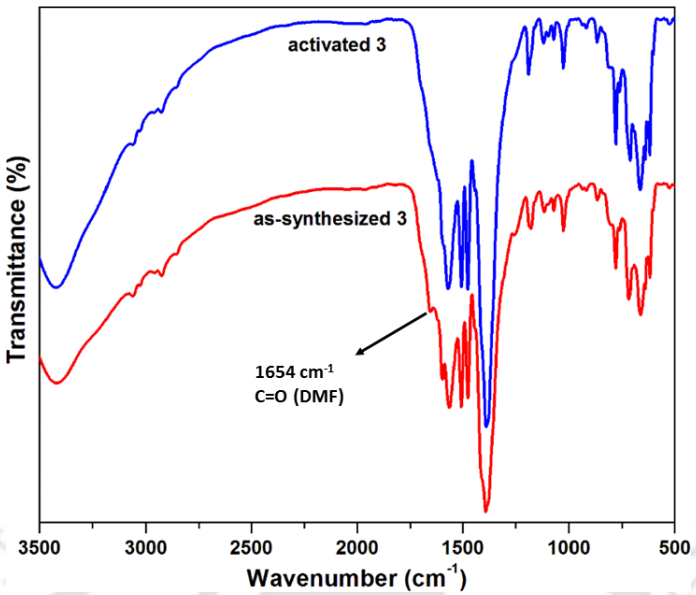

Figure 2.2 FT-IR spectra of as-synthesized and activated **3**.

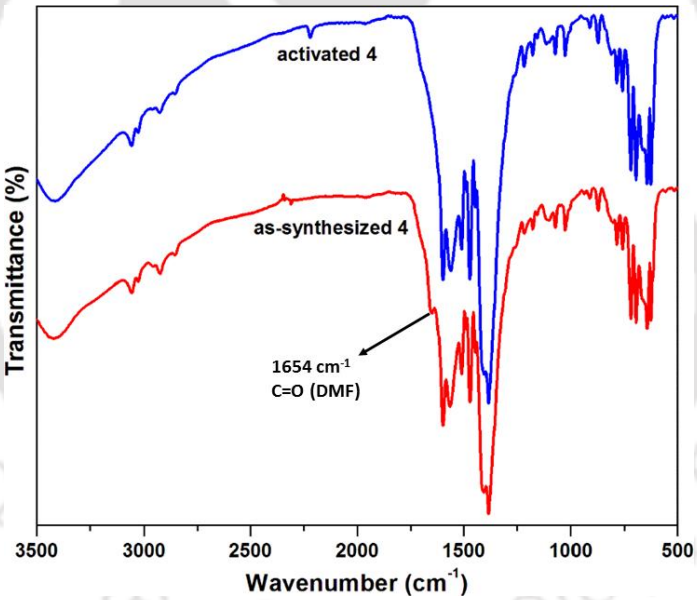

Figure 2.3 FT-IR spectra of as-synthesized and activated **4**.

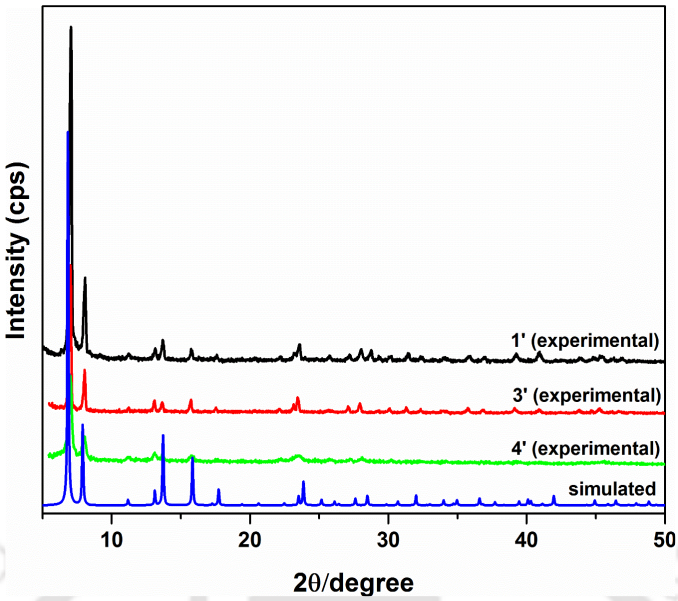

Figure 2.4 Simulated and experimental XRPD patterns of **1′**, **3′** and **4′**.

2.3.3 Structure description

A comparison between the simulated XRPD pattern of the formerly reported, isostructural **2** and the experimental XRPD patterns of the as-synthesized **1**, **3** and **4** reveals that they match quite closely with each other (Figure 2.4).[37,43] The indexing of the XRPD patterns of the as-synthesized materials suggests that each of them bears a cubic structure. The resulting lattice parameters are summarized in Table 2.1.

Table 2.1 Lattice parameters of as-synthesized **1**, **3** and **4** having cubic unit cells. The values are compared with those of the formerly reported, isostructural, dimethyl-functionalized Zr(IV)-based compound

Compound	*a* (Å)	*V* (Å^3)
1	23.0145(3)	12,190.0(7)
3	23.1153(3)	12,350.9(5)
4	22.9783(7)	12,132.6(12)
$[Zr_6O_4(OH)_4(DMTDC)_6]$ [37]	23.0917(6)	12,313.1(3)
Zr-DMTDC[43]	23.12	12,358.43

The unit cell parameters of **1**, **3** and **4** are similar to those of the recently reported Zr-DMTDC material as well as **2**.[37,43] These similarities indicate that **1**, **3** and **4** possess the UiO-66

(UiO = University of Oslo) framework topology as **2**. The framework structure of Zr(IV),[47] Hf(IV)[48] and Ce(IV)[49]-based pristine UiO-66 materials has been described formerly by several research groups. Similar to the parent UiO-66 compound, the cubic network structure of the presented materials contains $[Zr_6O_4(OH)_4]^{12+}$ building units (Figure 2.5). The μ_3-O and μ_3-OH groups occupy the triangular faces of the Zr_6 octahedron. Every Zr atom is coordinated with eight O atoms, forming a square antiprismatic coordination environment. The O atoms from the carboxylate, μ_3-OH and μ_3-O functionalities occupy the square faces of the square-antiprism. The 3D, cubic framework is constructed by the interconnection of the $[Zr_6O_4(OH)_4]^{12+}$ units with the $-CO_2$ groups of twelve ligands. Larger octahedral as well as smaller tetrahedral cages exist in the framework structures. In the neighborhood of every octahedral cage, eight tetrahedral cages are present. Narrow triangular windows connect the two types of cages. The inner side of the cages is decorated by the methyl or phenyl groups attached to the coordinated TDC ligands. It is worth mentioning that compound **4** has less crystallinity (Figure 2.4) compared to the other MOFs. It has been documented that the use of bulky ligands for the MOF synthesis usually leads to an amorphous phase of the MOF material.[44,45] The presence of bulky ligands restricts the connectivity between the building blocks and decreases the long-range order. The formation of a large number of basic building units results in 'humps' in the XRPD pattern.[46] In the case of **4**, the presence of two bulky phenyl substituents is responsible for the absence of long-range order in the crystal structure, which results in an less crystalline feature in the XRPD pattern.

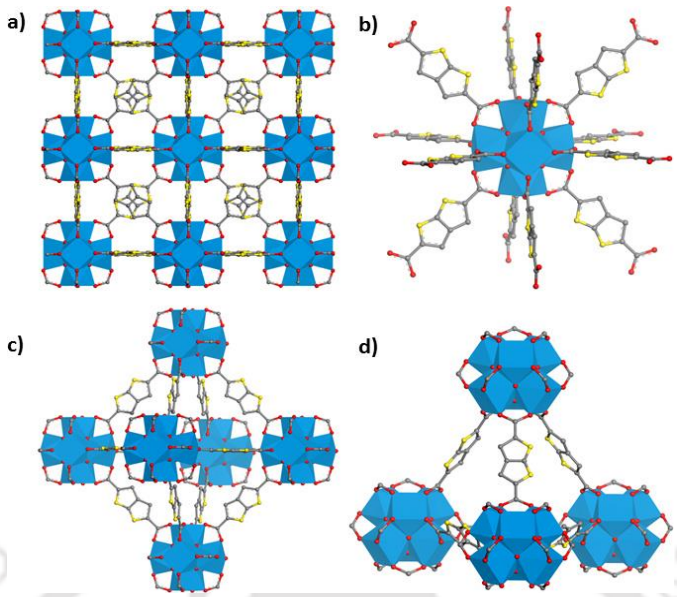

Figure 2.5 (a) Cubic 3D framework structure of **1** with Zr_6 node. (b) Node connectivity for the framework structure of **1**. Views of the (c) octahedral and (d) tetrahedral cages. Color codes: Zr, blue polyhedra; C, grey; O, red; S, yellow).

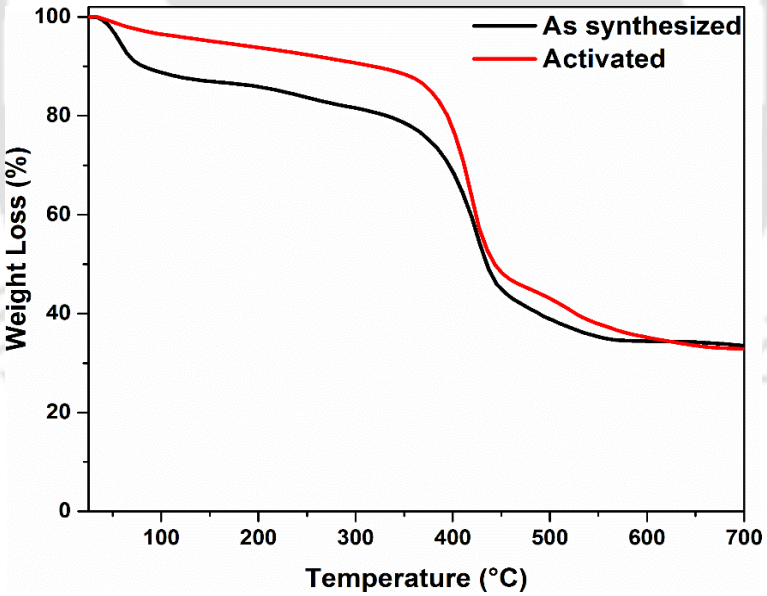

Figure 2.6 TG curves of **1** and **1′** recorded in an air atmosphere in the temperature range of 25-700 °C with a heating rate of 5 °C min^{-1}.

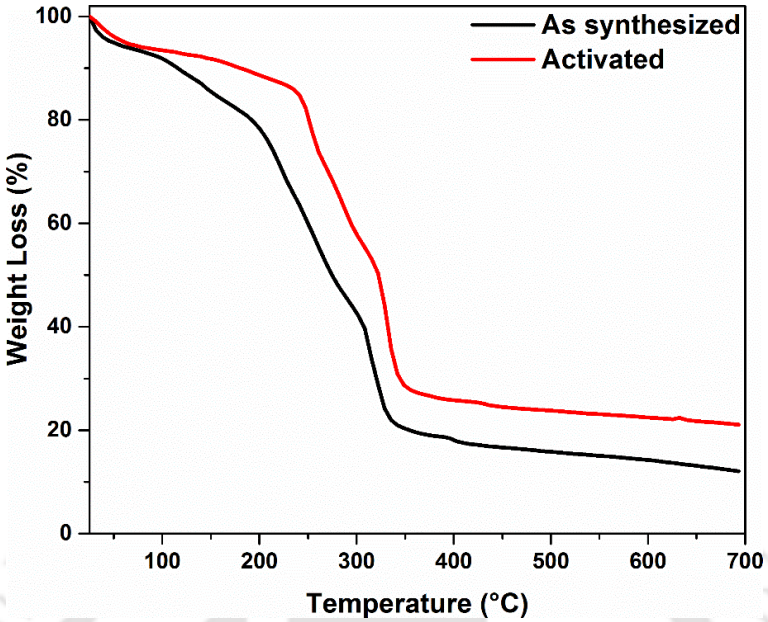

Figure 2.7 TG curves of **3** and **3′** recorded in an air atmosphere in the temperature range of 25-700 °C with a heating rate of 5 °C min^{-1}.

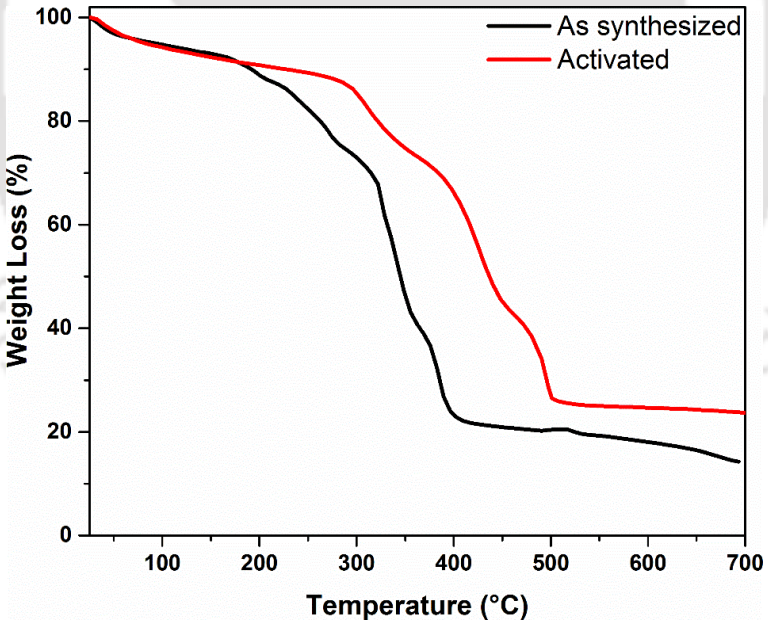

Figure 2.8 TG curves of **4** and **4′** recorded in an air atmosphere in the temperature range of 25-700 °C with a heating rate of 5 °C min^{-1}.

2.3.4 Thermal and chemical stability

Thermogravimetric analyses (TG) were performed for examining the thermal stability of the as-synthesized and thermally activated **1**, **3** and **4** (Figure 2.6-2.8). The TG analyses indicate that **1**, **3** and **4** are thermally stable up to 350, 230 and 300 °C, respectively. We have summarized the results of the TG analyses in Table 2.2.

Table 2.2 Weight loss steps in the TG curves of as-synthesized **1**, **3** and **4**, and their assignments.

Compound	First Weight Loss (%): Obs. / Cal.	No. of H_2O Molecules Removed in First Weight Loss Step	Second Weight Loss (%): Obs. / Cal.	No. of DMF Molecules Removed in Second Weight Loss Step
as-synthesized **1**	13.1 / 13.3	18	3.1 / 2.9	1
as-synthesized **3**	11.7 / 11.6	21	8.9 / 9.0	4
as-synthesized **4**	6 / 5.9	11	5.5/ 5.4	2.5

The initial weight loss step (temperature range: 25-130 °C) in the TG traces of the as-synthesized compounds is observed due to the removal of occluded water molecules. In the temperature range of 130-200 °C, the second weight loss step occurs because of the removal of guest DMF molecules. The initial weight loss step (temperature range: 25-130 °C) in the TG traces of activated compounds is noticed owing to the partial hygroscopic characteristics of the materials which results in hydration upon contact with moisture during storage.

To investigate the chemical stability of **1′**, **3′** and **4′**, we stirred the samples in different liquids like acetic acid, water, 1 M HCl and NaOH (pH = 11) under ambient conditions for 6 h. Then, XRPD measurements were accomplished with the filtered materials to check their crystallinity. The XRPD patterns (Figure 2.9-2.11) unambiguously substantiate the retention of the crystallinity of all of the activated compounds after treatment with these liquids. To check the stability of the framework structures of the compounds in the above-mentioned liquids, we have also recorded the UV-Vis spectra of the supernatants. The absorption bands corresponding to the free ligands were observed in the UV-Vis spectra (Figure 2.12-2.14) of all the supernatants. These results suggest the partial framework collapse of the MOF materials. The extent of

framework collapse is higher in acetic acid and NaOH solution (pH = 11) compared to that in 1 M HCl and pure aqueous solution.

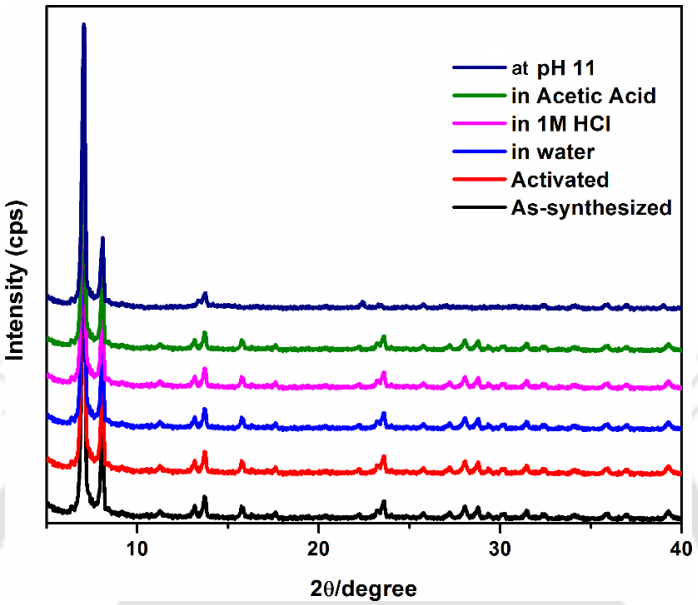

Figure 2.9 XRPD patterns of **1′** in different forms: as-synthesized, activated, treated with water, treated with 1M HCl and treated at pH 11.

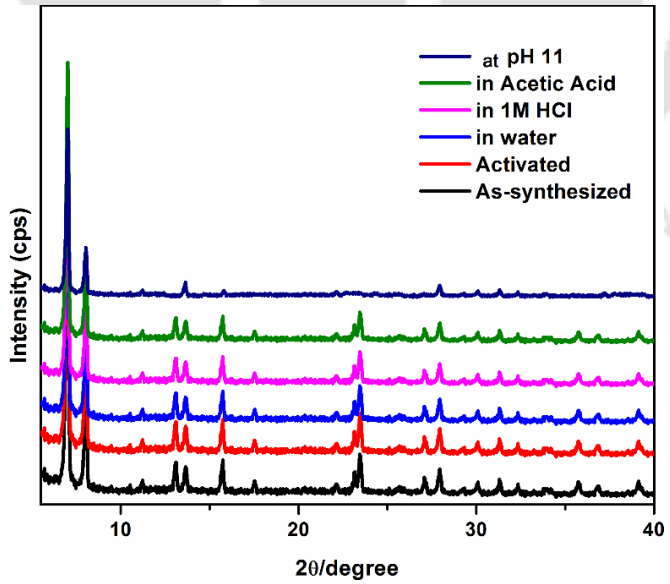

Figure 2.10 XRPD patterns of **3′** in different forms: as-synthesized, activated, treated with water, treated with 1M HCl and treated at pH 11.

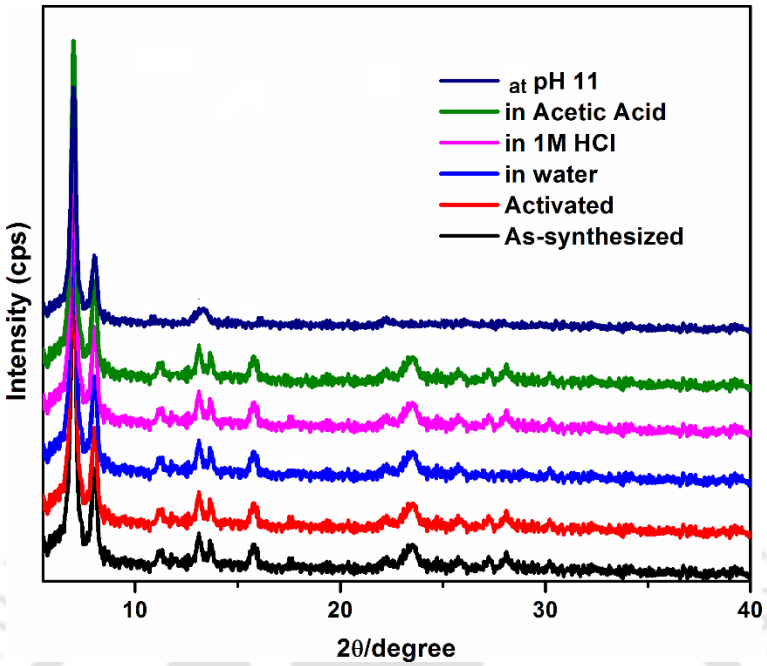

Figure 2.11 XRPD patterns of **4′** in different forms: as-synthesized, activated, treated with water, treated with 1M HCl and treated at pH 11.

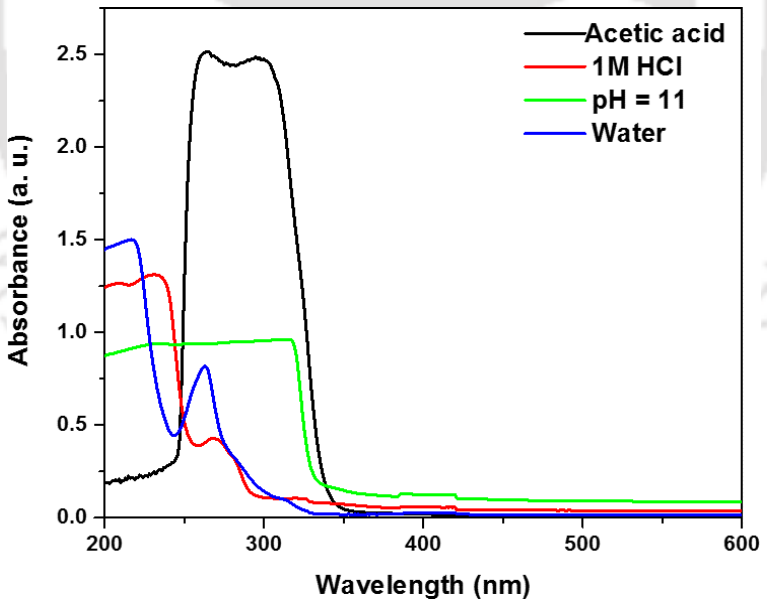

Figure 2.12 UV-Vis spectra different supernatant solution after treatment of **1′**.

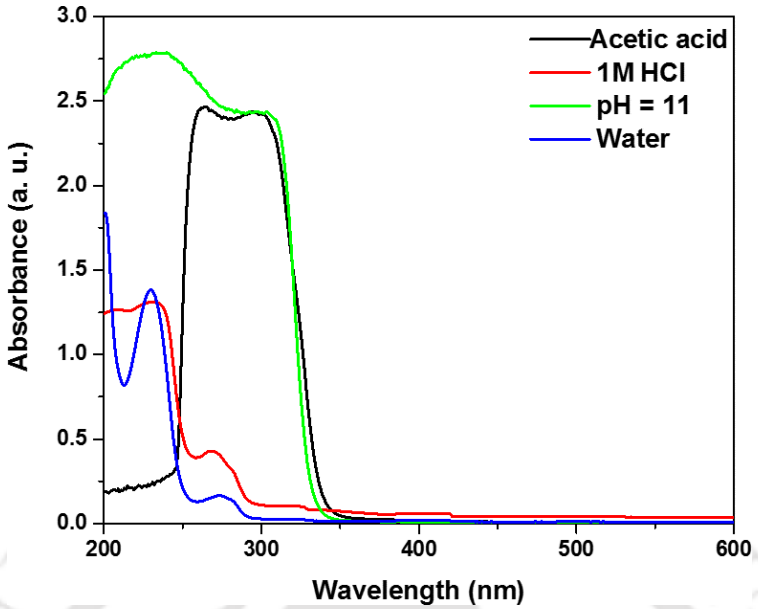

Figure 2.13 UV-Vis spectra different supernatant solution after treatment of **3′**.

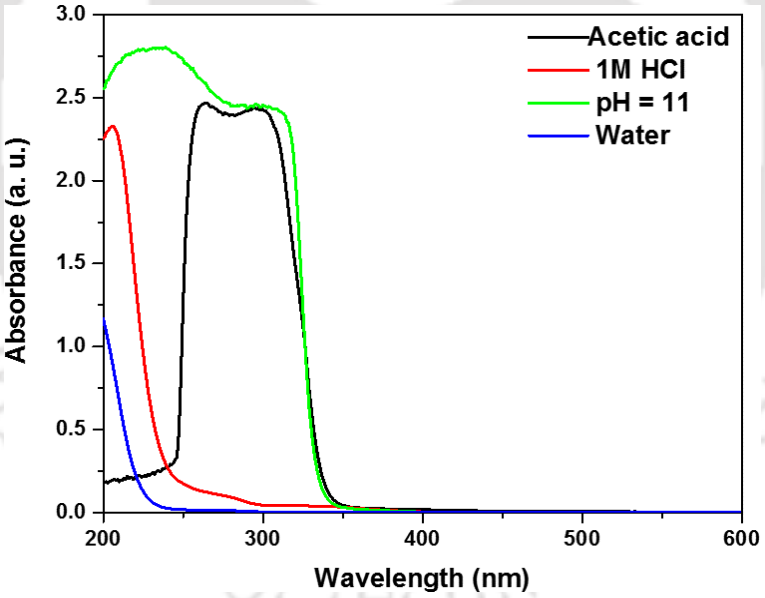

Figure 2.14 UV-Vis spectra different supernatant solution after treatment of **4′**.

2.3.5 Gas sorption properties

For proving the permanent porosity, N_2 sorption experiments were conducted with all the activated compounds. From the type-I shaped N_2 adsorption isotherms (Figure 2.15), the values of the BET surface areas of the compounds were determined. The estimated BET surface areas

of **1′**, **3′** and **4′** correspond to 1299, 978 and 446 $m^2 g^{-1}$, respectively. The micropore volumes of **1′**, **3′** and **4′**, which were calculated at p/p_0 = 0.5, correspond to 0.66, 0.50 and 0.24 $cm^3 g^{-1}$, respectively. Therefore, the activated materials showed a regular decrease in the values of the surface area and micropore volume with the increase in the bulkiness of the functional groups (methyl and phenyl) attached to the TDC ligand.

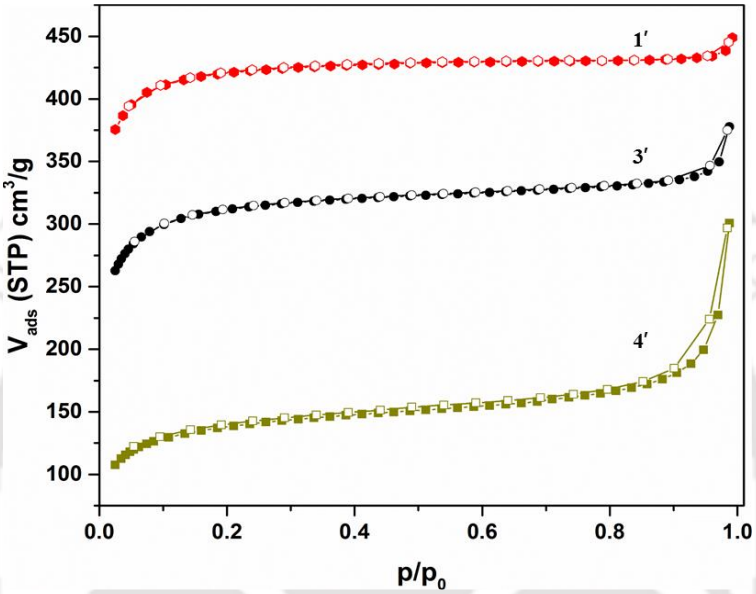

Figure 2.15 Nitrogen adsorption (filled symbols) and desorption (empty symbols) isotherms of **1′**, **3′** and **4′** collected at –196 °C.

2.3.6 Photophysical behavior

The combination of electronically inert Zr(IV) ions (having the d^{10} configuration) with fluorescent organic ligands has been formerly employed in the literature for the preparation of MOF compounds exhibiting strong luminescence properties.[50,51] Furthermore, the S atoms of the MOF materials incorporating thiophene moieties have been previously shown to act as Lewis basic sites for the recognition of small organic molecules (such as acetone, nitrobenzene and p-nitroaniline),[52-54] metal ions (Cu^{2+} and Fe^{3+})[52] and Hg^0 vapour.[43] These observations have inspired us to explore the photoluminescence behavior of the presented Zr(IV)-based MOF compounds containing thienothiophene-based ligands.

The diffuse reflectance (DR) UV-Vis spectra of the free ligands as well as the MOF compounds were recorded under ambient conditions. Remarkably, the absorption spectra of the MOF materials are very similar to their corresponding free ligands (Figure 2.16). The free ligands and the MOF compounds displayed broad absorption bands centred at around 330 nm. These peaks arise owing to the π-π* transition of the ligands.[55-57] These similarities in the absorption spectra point out that the coordinated ligands are solely responsible for the absorption of light in these MOF materials. The optical bandgaps were evaluated for the free ligands and the MOF materials by using the Tauc equation:[58,59]

$$(\alpha h\upsilon)^2 = A\,(h\upsilon - E_g)$$

Here, h stands for the Planck's constant, A is a constant, E_g is the bandgap energy of allowed transitions and υ denotes the frequency of light. The optical bandgaps of **1′**, **2′**, **3′** and **4′** were found to be 3.41, 3.45, 3.44 and 3.43 eV, respectively (Figure 2.17). These values are comparable to those of the previously reported UiO-66 materials.[60,61] The estimated optical bandgaps of H_2TDC, H_2DMTDC, H_2MPTDC and H_2DPTDC ligands are 3.33, 3.36, 3.28 and 3.34 eV, respectively. Therefore, the optical bandgaps of the free ligands increased upon coordination with the Zr^{4+} ions.

The fluorescence characteristics of the free ligands and the MOF compounds were also studied. The free ligands and the corresponding MOF compounds exhibited broad emission bands centered at around 400 nm in their solid-state fluorescence emission spectra (Figure 2.18). These emission bands appear because of the π-π* transition of the framework ligands.[62] The similarities in the emission spectra of the free ligands and the corresponding MOF materials suggest that the luminescence of the MOF compounds arises from the ligand centred π-π* transition. The coordination of the DPTDC ligand with the Zr^{4+} ions is expected to perturb the π-π* transition, causing a blue shift (Δλ = 7 nm) in the emission band of **4′** compared to the free H_2DPTDC ligand.[51]

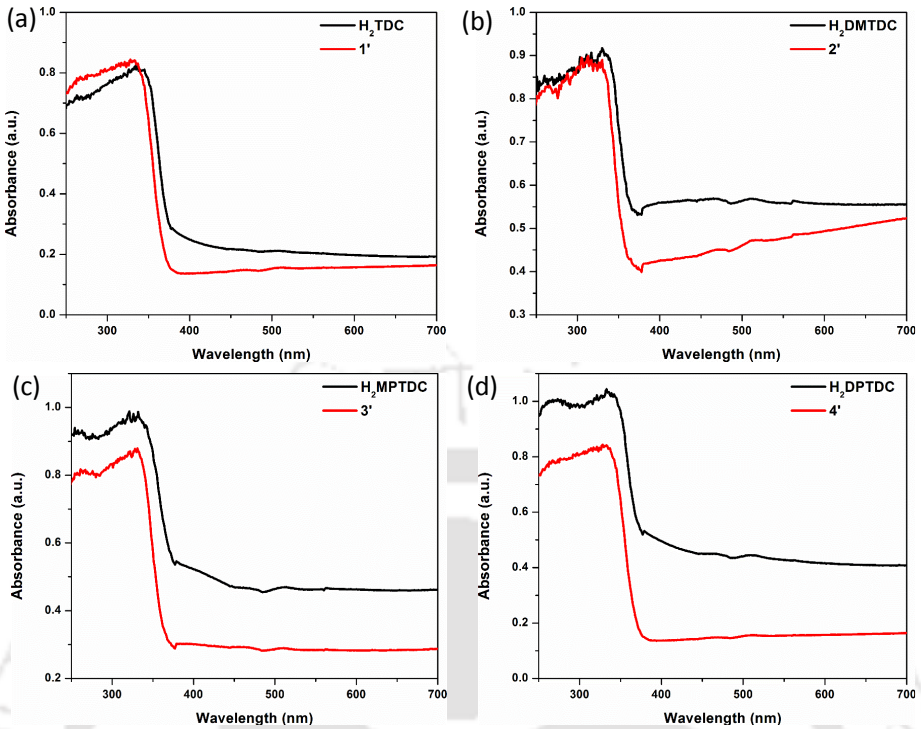

Figure 2.16 Diffuse reflectance UV-visible absorption spectra of (a) TDC ligand and **1′**, (b) H_2DMTDC ligand and **2′**, (c) H_2MPTDC ligand and **3′**, (d) H_2DPTDC ligand and **4′**.

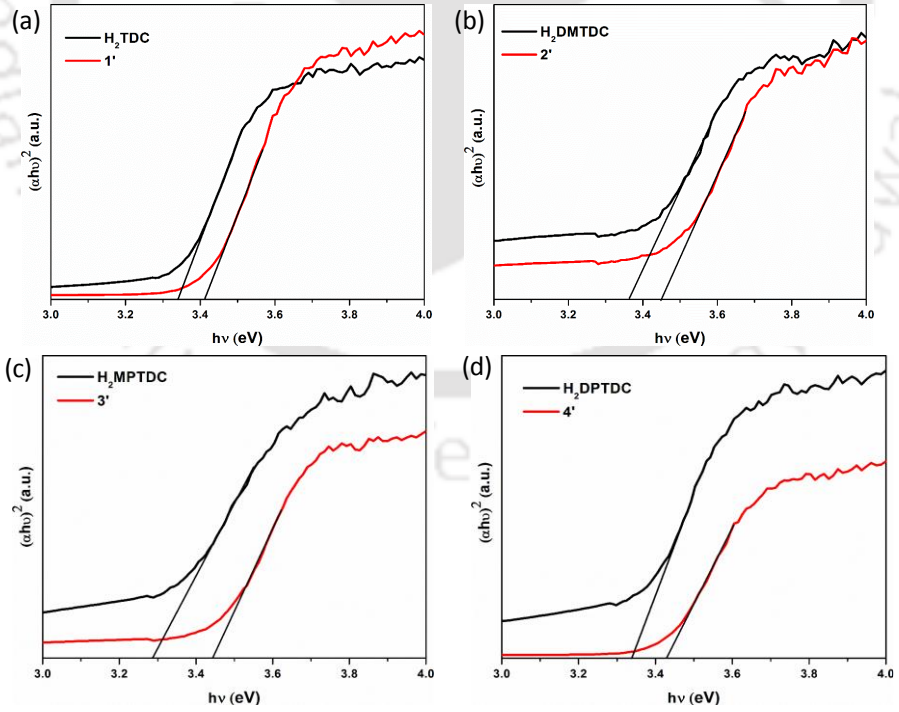

Figure 2.17 Tauc plot for (a) TDC ligand and **1′**, (b) H_2DMTDC ligand and **2′**, (c) H_2MPTDC ligand and **3′**, (d) H_2DPTDC ligand and **4′**.

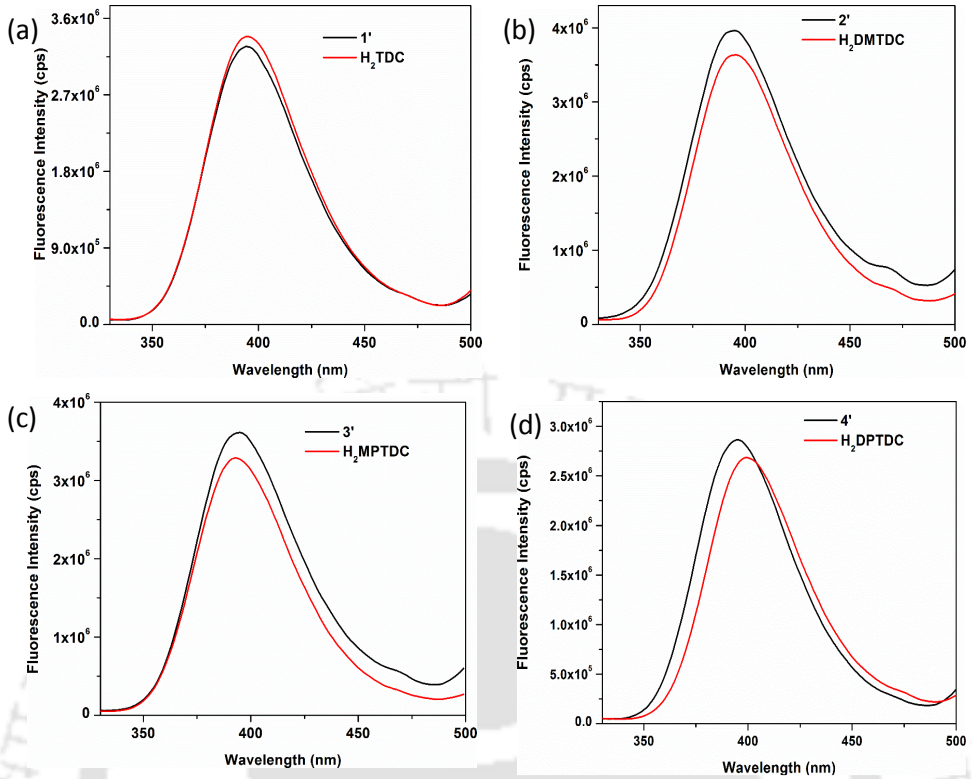

Figure 2.18 Room temperature solid-state fluorescence emission spectra of (a) TDC ligand and **1′**, (b) H_2DMTDC ligand and **2′**, (c) H_2MPTDC ligand and **3′**, (d) H_2DPTDC ligand and **4′** (λ_{ex} = 260 nm).

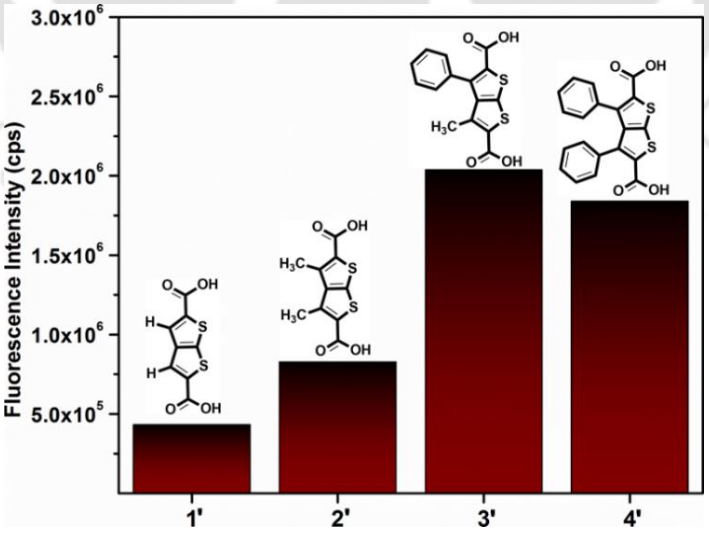

Figure 2.19 Ligand-based fluorescence response of the aqueous suspensions of **1′**, **2′**, **3′** and **4′** at ambient conditions.

The electronic properties of MOFs can be modulated by changing the substituents in the linker molecules.[63] These electronic properties directly influence the other optical properties of MOFs.[64,65] Since all the MOF materials are stable in aqueous medium, their fluorescence properties were explored in pure aqueous medium to check the effect of substitution on their fluorescence behaviour. It can be seen from Figure 2.19 that the fluorescence intensity of the compounds (on going from **1′** to **3′**) increases with the increment of electron density in the frameworks. However, the presence of two phenyl groups makes **4′** more hydrophobic compared to other materials. As a result, the aqueous suspension of **4′** shows a slight decrease in the fluorescence intensity compared to that of **3′**. These results suggest that not only the electronic nature of the functional groups but also their hydrophobicity play a crucial role in governing the fluorescence properties of MOF materials.

2.3.7 Hydrophobic properties

The attachment of water-repellent methyl and phenyl groups to the organic ligands is expected to impart various extents of hydrophobicity in the resulting MOFs. The degree of hydrophobicity of the ligands increases in the order: H_2TDC < H_2DMTDC < H_2MPTDC < H_2DPTDC. For examining the hydrophobicity of the MOF materials, initially water contact angle measurements were performed. With the increase in the degree of hydrophobicity of the ligands, a regular increment in water contact angle (Table 2.3) was observed, as expected. The MOF material incorporating the un-functionalized ligand (**1′**) showed the lowest contact angle (~136°). On the other hand, the diphenyl-functionalized material (**4′**) exhibited the highest contact angle (~157°). These results confirm that the attachment of methyl and phenyl groups to the organic ligands introduces different extents of hydrophobicity in the MOF compounds.

Table 2.3 Contact angles and water uptake capacities of the MOF compounds.

MOF	Contact Angle	Water Loading (g/g)	
		at p/p_0 = 0.5	at p/p_0 = 0.9
1'	136°	0.30	0.39
2'	148°	0.21	0.35
3'	155°	0.06	0.31
4'	157°	0.04	0.16

The hydrophobic nature of the MOF materials was further confirmed by water sorption experiments. The water uptake capacities of the compounds at p/p_0 = 0.9 are comparable to the maximum water uptake capacities of several well-known MOFs such as MIL-100(Al) (0.5 g g^{-1}), MIL 100(Fe) (0.65-0.75 g g^{-1}),[66,67] Al-fumarate (0.45 g g^{-1}),[68] CAU-10-H (0.33-0.34 g g^{-1}),[69,70] MIL-101(Cr) (1.0-1.5 g g^{-1}),[71,72] pp-MIL-101(Cr) @HIPE (0.29 g g^{-1}; composite with 59 wt% MOF),[73] MIL-100 (Cr) (0.6-0.7 g g^{-1}),[74] and MIL-100(Fe,Cr)@xerogel (0.33 g g^{-1}, composite with 50 wt% MOF; 0.28 g g^{-1}, composite with 51 wt% MOF),[75] and covalent triazine-based frameworks such as Ad2L1 (0.15 g g^{-1}) to Ad4L3 (0.68 g g^{-1}).[76] The water sorption isotherms of the presented MOF compounds (Figure 2.20) indicate a water uptake above the threshold of 0.3 g g^{-1}, however only at higher relative pressures (above a p/p_0 of 0.5). Other known MOFs, which are already considered hydrophobic like MIL-101(Cr)[71,75,77-79] or fluorinated MIL-53(Al) and MIL-47,[80] exhibit the major water uptake in the p/p_0 range of 0.4-0.5.[76] Water sorption results indicate that the MOF materials are hydrophobic in nature. The hydrophobicity of the MOF compounds is in agreement with that obtained from the water contact angle measurements. Thus, **4′** is the most hydrophobic MOF in the series.

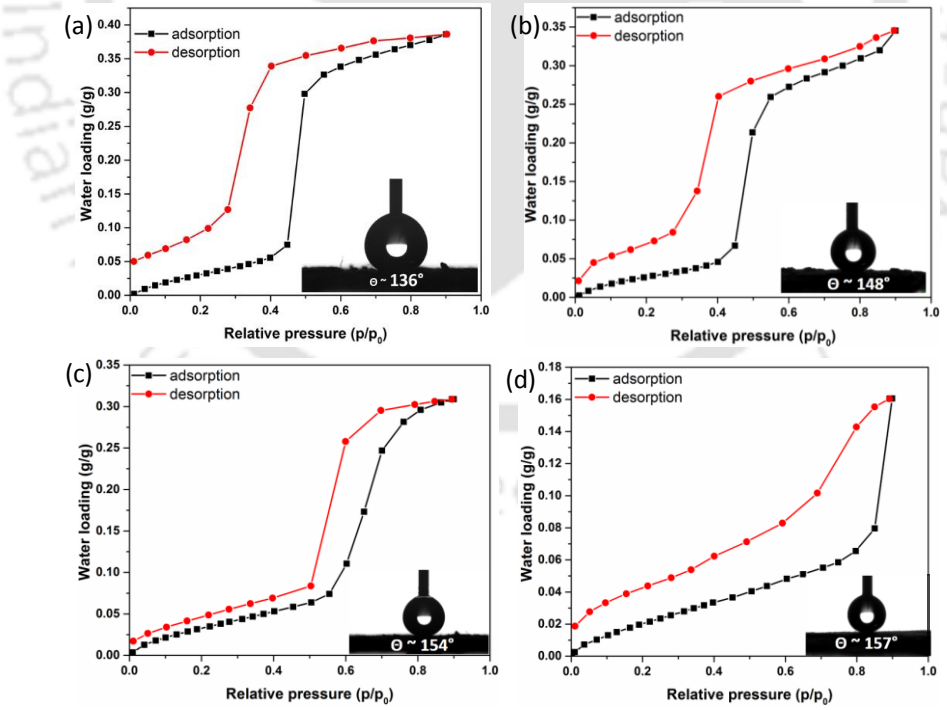

Figure 2.20 Water sorption isotherm of **1′** (a), **2′** (b) **3′** (c) and **4′** (d) at 20 °C. Inset shows corresponding advancing water contact angle.

2.3.8 Metal ion sensing behavior

The strong photoluminescence features of the compounds in the solid-state as well as in aqueous medium have encouraged us to investigate their application potential as luminescent probes for the selective, rapid and sensitive sensing of metal ions. In order to serve this purpose, fluorescence titration measurements were performed. 10 mM aqueous solutions of the nitrate salts of various cations (Na^{+}, K^{+}, Cd^{2+}, Co^{2+}, Cu^{2+}, Hg^{2+}, Mn^{2+}, Ni^{2+}, Fe^{2+}, Pb^{2+}, Zn^{2+}, Al^{3+}, Cr^{3+} and Fe^{3+}) were gradually added to the well-dispersed aqueous suspensions of all the materials and the fluorescence emission intensities of the compounds were monitored upon excitation at 330 nm at room temperature. Among the 14 metal ions examined, only Fe^{3+} displayed rapid quenching of the fluorescence intensities of all the compounds (Figure 2.21). For the remaining metal ions, the changes in their fluorescence intensities were almost negligible. The highest quenching efficiency was observed for **4′**. The quenching efficiencies of the materials towards Fe^{3+} ions decreased in the order: **4′** (98%) > **3′** (96%) > **2′** (91%) > **1′** (86%). This trend in the quenching efficiency of the compounds can be correlated with the electron density available in their frameworks. Thus, the quenching efficiencies of the materials for Fe^{3+} ions decreased with the decrease in the electron density in the framework compounds.

In order to check the selectivity of all the MOF materials towards Fe^{3+} ions in the presence of other potentially competing metal ions, competitive fluorescence titration experiments were performed. In these competitive titration measurements, fluorescence emission spectra were recorded upon the incremental addition of Fe^{3+} solution to the stable aqueous suspensions of the MOF compounds containing the potentially intrusive metal ions. The changes in the luminescence intensity of **1′**, **2′**, **3′** and **4′** upon the addition of Fe^{3+} solution in the absence and presence of other competing metal ions are presented in Figure 2.22. The results of these competitive fluorescence quenching experiments demonstrate that the thienothiophene-based MOF materials are highly selective towards Fe^{3+} ions, even in the presence of other potentially interfering metal ions.

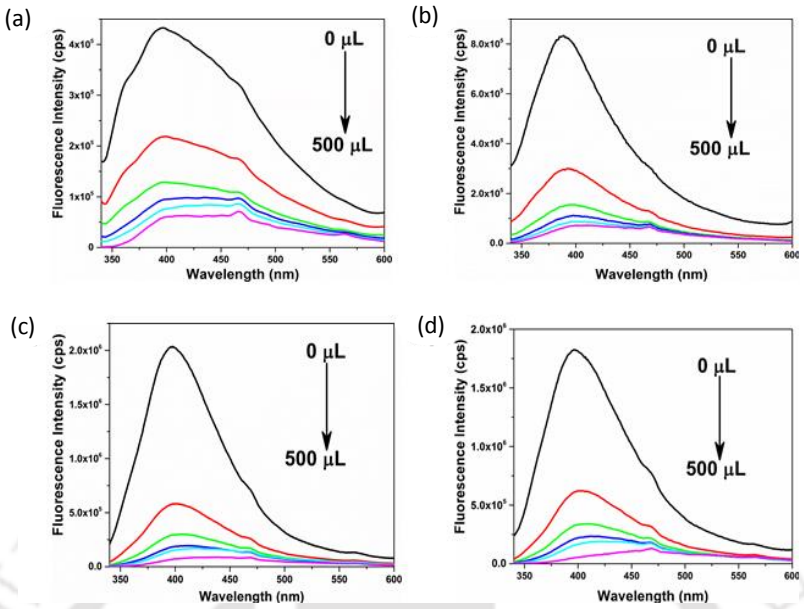

Figure 2.21 Quenching of fluorescence intensity with gradual addition of Fe^{3+} solution to a 3 mL aqueous suspension of **1′** (a), **2′** (b), **3′** (c) and **4′** (d).

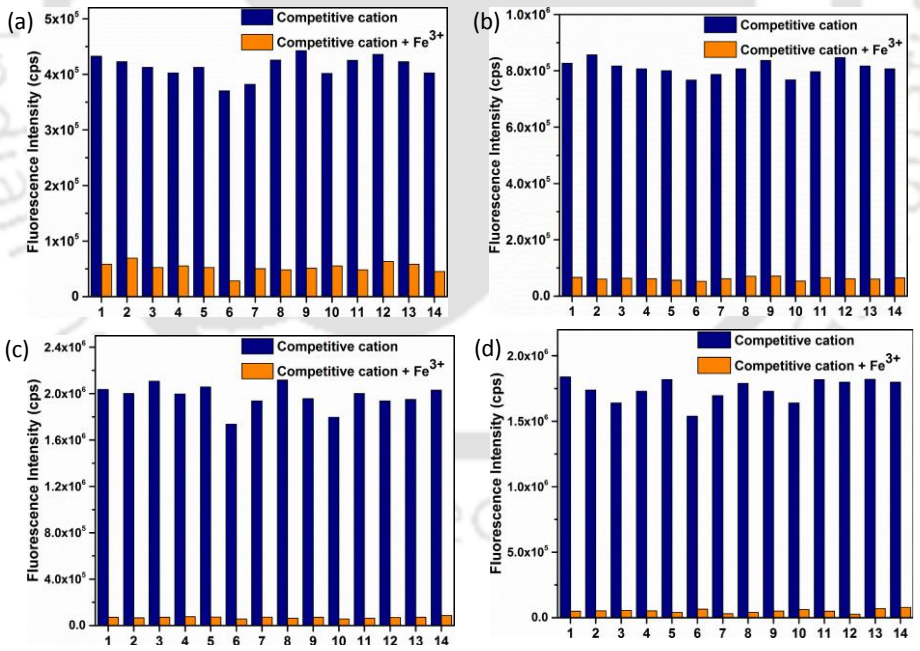

Figure 2.22 Change in the fluorescence intensity of **1′** (a), **2′** (b), **3′** (c) and **4′** (d) upon addition of 500 µL of Fe^{3+} solution in the absence and presence of blank (1), Na^{+} (2), K^{+} (3), Cd^{2+} (4), Co^{2+} (5), Cu^{2+} (6), Hg^{2+} (7), Mn^{2+} (8), Ni^{2+} (9), Fe^{2+} (10), Pb^{2+} (11), Zn^{2+} (12), Al^{3+} (13) and Cr^{3+} (14) ion.

Stern-Volmer (S-V) quenching constants were calculated by using the following equation:

$$(I_0/I) = K_{sv}[A] + 1$$

where I_0 and I represent the fluorescence intensity of the MOF compound before and after the addition of the analyte, respectively; K_{sv} denotes the quenching constant (expressed in M^{-1}) and [A] symbolizes the molar concentration of the analyte. The K_{sv} values for **1′**, **2′**, **3′** and **4′** were estimated to be 4.41×10^3, 8.81×10^3, 10.79×10^3 and 9.10×10^3 M^{-1}, respectively, after excluding the dilution effect. For the estimation of the limit of detection (LOD) of the thienothiophene-based MOF materials towards the sensing of Fe^{3+} ions, we gradually added very low concentrations of Fe^{3+} solution to the suspension of the compounds in water and then monitored their fluorescence intensities. The LOD values were determined by employing the following equation: LOD = $3\sigma/K$.[81] Here, K stands for the slope of the curves and σ represents the standard deviation of the preliminary fluorescence intensity of MOF materials in the absence of Fe^{3+} solution. The calculated LOD values of **1′**, **2′**, **3′** and **4′** for the sensing of Fe^{3+} ions are 1.26×10^{-6}, 8.57×10^{-7}, 9.33×10^{-7} and 3.4×10^{-7} M, respectively.

The reusability of the fluorescence sensing performances of the MOF probes towards Fe^{3+} ions was examined up to five cycles. For checking their recyclability, the MOF compounds were filtered off after each fluorescence titration experiment. The filtered materials were washed with water repeatedly and then dried in an oven. All the probes showed outstanding recovery of their initial fluorescence intensities, even after five consecutive cycles of fluorescence sensing experiments (Figure 2.23)All the probes showed outstanding recovery of their initial fluorescence intensities, even after five consecutive cycles of fluorescence sensing experiments. As verified by the XRPD experiments (Figure 2.24), all the MOF materials retained most of their initial crystallinity (thus structural robustness) after five successive cycles of fluorescence titration experiments. Additionally, we checked the effect of pH on the quenching. Fe^{3+} sensing experiments were carried out with solutions having pH values of 2 and 10. The quenching results suggest that a large change in the pH of the sensing medium hardly affects the quenching percentages (Figure 2.25). These results verify the reusability and high photostability of the MOF probes, which endow them with great potential for the long-term practical sensing of Fe^{3+} ions.

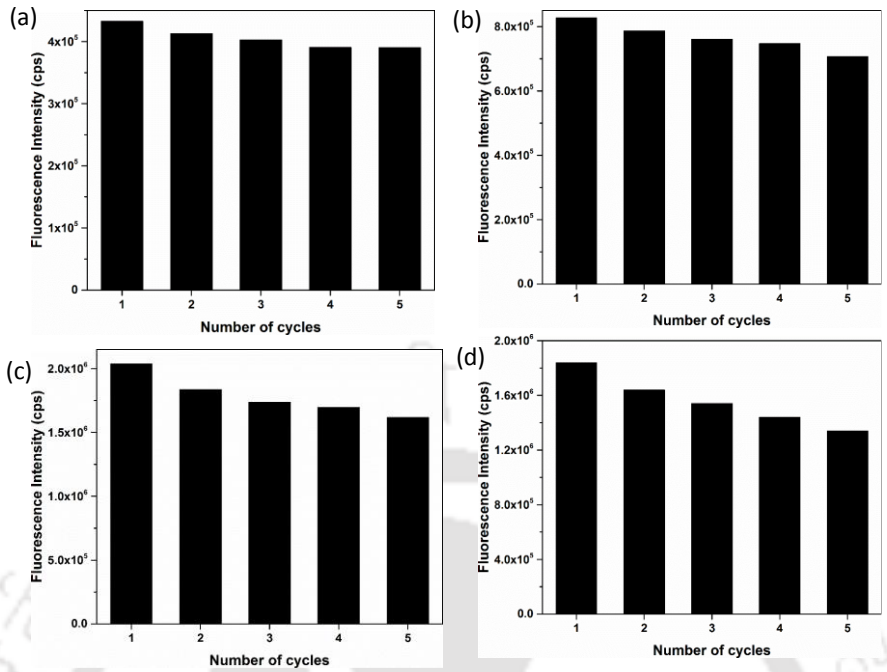

Figure 2.23 Reproducibility of the quenching efficiency of the aqueous suspension of **1′** (a), **2′** (b), **3′** (c) and **4′** (d) in aqueous solution towards 10 mM Fe^{3+} solution.

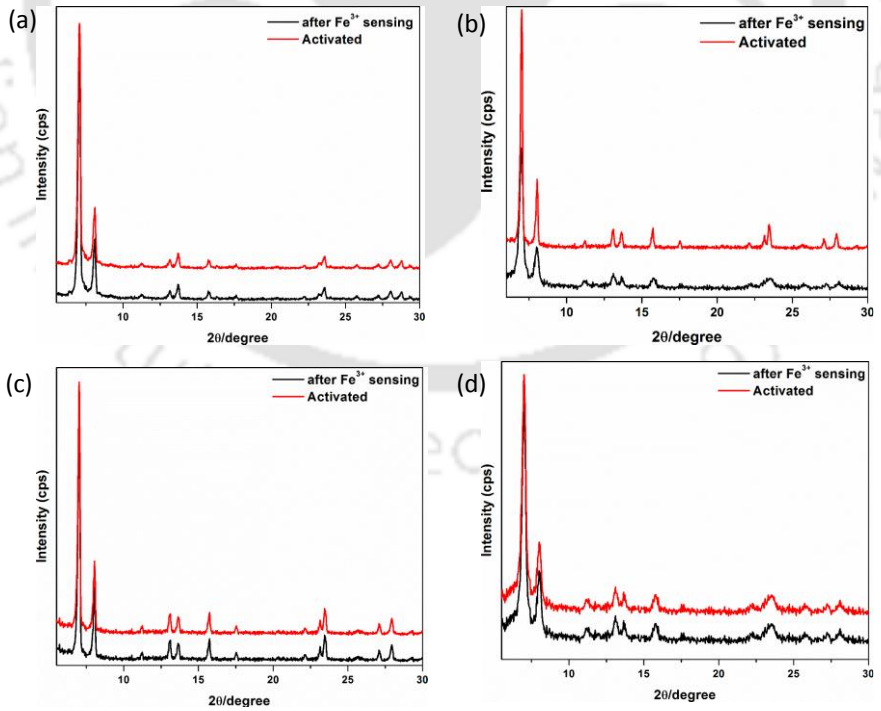

Figure 2.24 XRPD patterns of **1′** (a), **2′** (b), **3′** (c) and **4′** (d) before and after the Fe^{3+} sensing experiment.

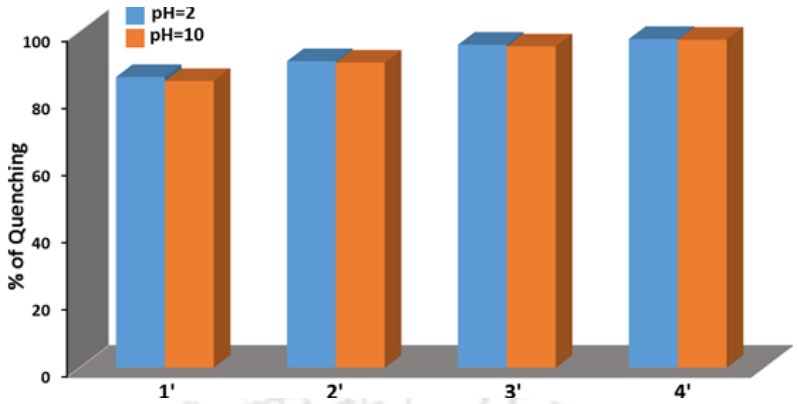

Figure 2.25. Effect of pH on fluorescence quenching for different MOFs.

2.3.9 Mechanisms for the detection of Fe^{3+} ions

Three mechanisms have been proposed in the literature for the sensing of Fe^{3+} ions employing MOF materials. They include: (1) collapse of the framework structure,[29] (2) exchange of the framework metal ions by externally added Fe^{3+} ions,[28] and (3) interactions of the Fe^{3+} ions with the coordinated organic ligand.[24] The XRPD patterns (Figure 2.24) of the MOF materials treated with Fe^{3+} ions were very similar to those of the untreated compounds. The retention of the structural integrity of the MOF compounds after the treatment with Fe^{3+} ions excludes the possibility of the first sensing mechanism. In order to check the possibility of the ion-exchange mechanism, energy-dispersive X-ray (EDX) experiments were accomplished with the MOF materials recovered after the fluorescence sensing experiments. The EDX spectra (Figure 2.26) reveal that either no Fe^{3+} ions or almost negligible amounts (~0.2 wt%) of Fe^{3+} ions are present in the MOF materials. The insignificant amounts of Fe^{3+} ions might correspond to the Fe^{3+} ions adsorbed in the pores during the fluorescence titration measurements. Therefore, the possibility of the second sensing mechanism can also be ruled out. The third sensing mechanism involving the electronic interactions between the Fe^{3+} ions and framework ligands might be operative in the presented MOF systems. The half-filled 3d ($3d^5\ 4s^0$) orbital of Fe^{3+} ions possesses a high charge density, and thus strong electron-withdrawing character compared to other metal ions.[82] The quenching of the fluorophore moiety by Fe^{3+} ions *via* the electron transfer mechanism has been well-documented for other nanomaterials including MOFs.[83-85] Therefore, we can presume that the electron transfer process from the electron-rich thienothiophene-based ligands to the Fe^{3+} ions might be responsible for the observed fluorescence quenching. The slightly red-shifted

fluorescence spectra upon Fe^{3+} addition also support the electron transfer mechansim.[86] For validating the existence of the electron transfer process, the aqueous suspensions of all the MOF materials were treated with the very well-known electron acceptor methyl viologen (MV^{2+}) dications. The fluorescence quenching profiles of the MOF compounds treated with the MV^{2+} dications are very similar to those treated with the Fe^{3+} ions (Figure 2.27). Since the viologen compounds are very good electron acceptors, [87] the fluorescence quenching can be proposed to occur through the electron transfer process from the electron-rich frameworks to the electron-deficient MV^{2+} dications. The similarity between the florescence quenching profiles obtained with MV^{2+} and Fe^{3+} ions points out that the electron transfer process from the electron-rich frameworks to the electron deficient Fe^{3+} ions can also be attributed to the luminescence quenching. The fluorescence quenching efficiencies of the MV^{2+} ions follow the order: **1′** (76%) > **2′** (71%) > **3′** (60%) > **4′** (43%). The reverse (i.e., **4′** (98%) > **3′** (96%) > **2′** (91%) > **1′** (86%)) of this trend is found for the quenching with the Fe^{3+} ions. For MV^{2+} dications (which are relatively larger than Fe^{3+} ions), the increase in steric hindrance and hydrophobicity inside the frameworks owing to the attached functional groups restricts their rates of diffusion through the porous channels, resulting in less interactions with the frameworks, and hence a decrease in the quenching efficiencies. On the other hand, the Fe^{3+} ions are small enough to diffuse rapidly through the porous channels of the MOF compounds, leading to greater interactions with the electron-rich frameworks. As a result, the quenching efficiencies of the Fe^{3+} ions increase with the increasing electron density in the framework materials. Therefore, both steric and electronic factors might be hypothesized to play major roles during the quenching of the fluorescence in these MOF systems. For realizing the excited-state interactions between the MOF materials and analyte (Fe^{3+} or MV^{2+} ions), time-resolved fluorescence decay experiments were conducted. Upon the addition of Fe^{3+} or MV^{2+} ions, the aqueous suspensions of all the MOF compounds exhibit tri-exponential fluorescence decays with the decrease in the average excited-state lifetime values (Tables 2.4-2.7). The decrease in the lifetime values of the MOF compounds in the presence of Fe^{3+} or MV^{2+} ions indicates that the fluorescence quenching mechanisms in these systems are dynamic in nature.

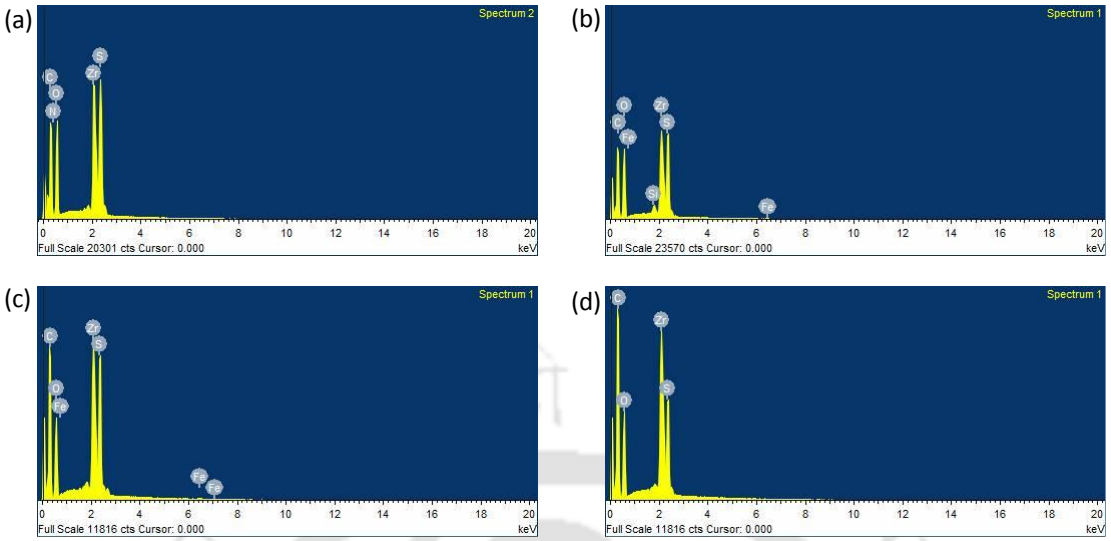

Figure 2.26 EDX spectrum of **1′** (a), **2′** (b), **3′** (c) and **4′** (d) recovered after the Fe^{3+} sensing experiment.

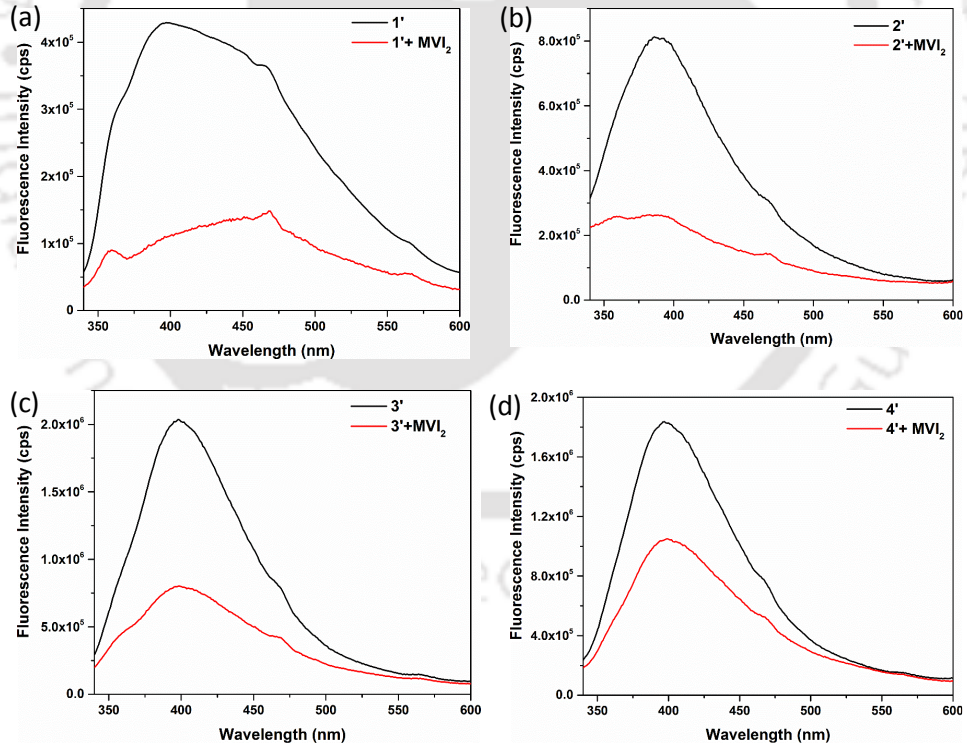

Figure 2.27 Change in the fluorescence intensity of **1′** (a), **2′** (b), **3′** (c) and **4′** (d) in presence of MVI_2.

Table 2.4. Excited-state lifetime analysis of **1′** in presence of Fe^{3+} aqueous solution (λ_{ex} = 290 nm, λ_{em} = 400 nm).

Volume of analyte added	τ (ns)			a			Average lifetime (ns) $\langle\tau\rangle$*	χ^2
	τ_1 (ns)	τ_2 (ns)	τ_3 (ns)	a_1	a_2	a_3		
0	16.56	1.72	0.13	0.35	0.09	0.55	6.02	1.03
400 µL (Fe^{3+})	13.06	2.16	0.059	0.21	0.12	0.67	3.03	1.09
400 µL (MVI_2)	10.21	1.79	0.010	0.16	0.11	0.73	1.83	1.05

Table 2.5 Excited-state lifetime analysis of **2′** in presence of Fe^{3+} aqueous solution (λ_{ex} = 290 nm, λ_{em} = 400 nm).

Volume of analyte added	τ (ns)			a			Average lifetime (ns) $\langle\tau\rangle$*	χ^2
	τ_1 (ns)	τ_2 (ns)	τ_3 (ns)	a_1	a_2	a_3		
0	15.44	4.73	0.69	0.50	0.17	0.33	8.77	1.11
400 µL (Fe^{3+})	9.92	0.93	0.06	0.30	0.12	0.58	3.17	1.04
400 µL (MVI_2)	10.31	1.87	0.14	0.16	0.11	0.73	1.94	1.01

Table 2.6 Excited-state lifetime analysis of **3′** in presence of different analyte in aqueous solution (λ_{ex} = 290 nm, λ_{em} = 400 nm).

Volume of analyte added (400 µL)	τ (ns)			a			Average lifetime (ns) $\langle\tau\rangle$*	χ^2
	τ_1 (ns)	τ_2 (ns)	τ_3 (ns)	a_1	a_2	a_3		
0	15.95	1.79	0.12	0.37	0.07	0.56	6.10	1.08
400 µL (Fe^{3+})	15.59	1.95	0.105	0.14	0.05	0.81	2.35	1.03
400 µL (MVI_2)	14.95	1.88	0.10	0.28	0.04	0.68	4.32	1.01

Table 2.7 Excited-state lifetime analysis of **4′** in presence of different analyte in aqueous solution (λ_{ex} = 290 nm, λ_{em} = 400 nm).

Volume of analyte added	τ (ns)			a			Average lifetime (ns) <τ>*	χ^2
	τ_1 (ns)	τ_2 (ns)	τ_3 (ns)	a_1	a_2	a_3		
0	16.71	1.95	0.12	0.33	0.10	0.57	5.8	1.04
400 µL (Fe^{3+})	13.59	1.96	0.10	0.19	0.08	0.73	2.84	1.07
400 µL (MVI_2)	11.37	1.79	0.10	0.25	0.07	0.68	2.99	1.09

*$\langle\tau\rangle = a_1\tau_1 + a_2\tau_2 + a_2\tau_2 + a_3\tau_3$

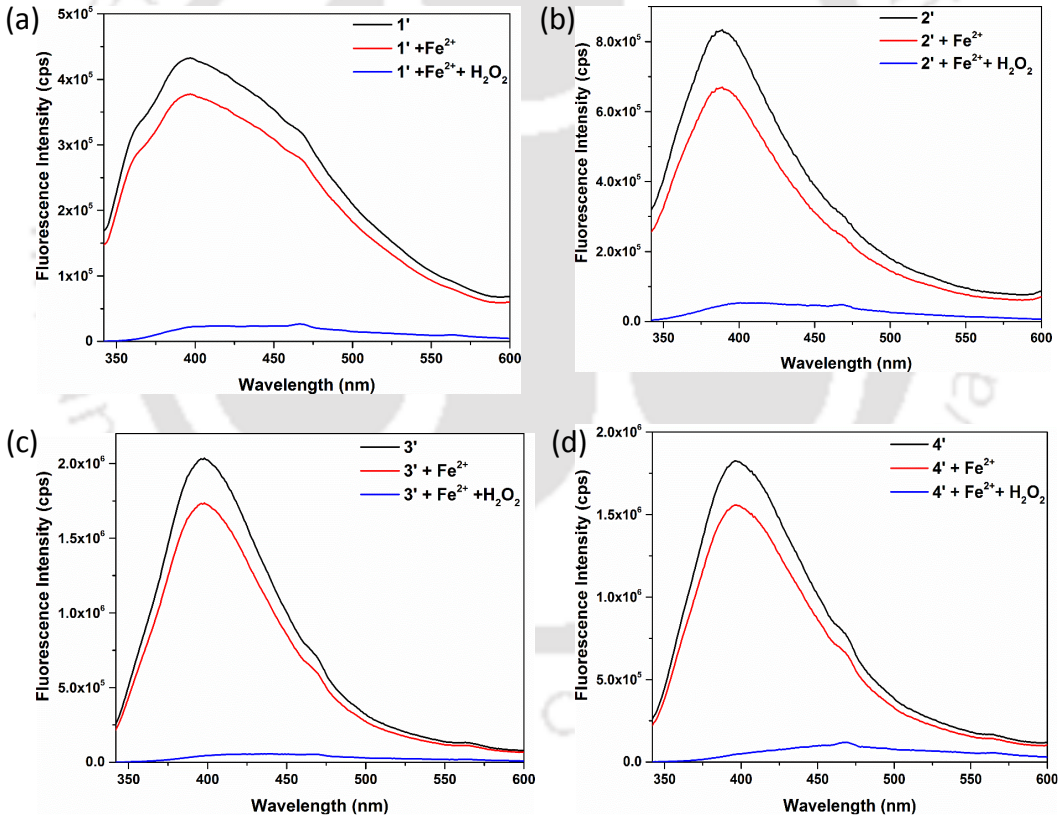

Figure 2.28 Change in the fluorescence intensity of **1′** (a), **2′** (b), **3′** (c) and **4′** (d) upon addition of H_2O_2 solution (1 mM) in presence of Fe^{2+} ion (500 µL).

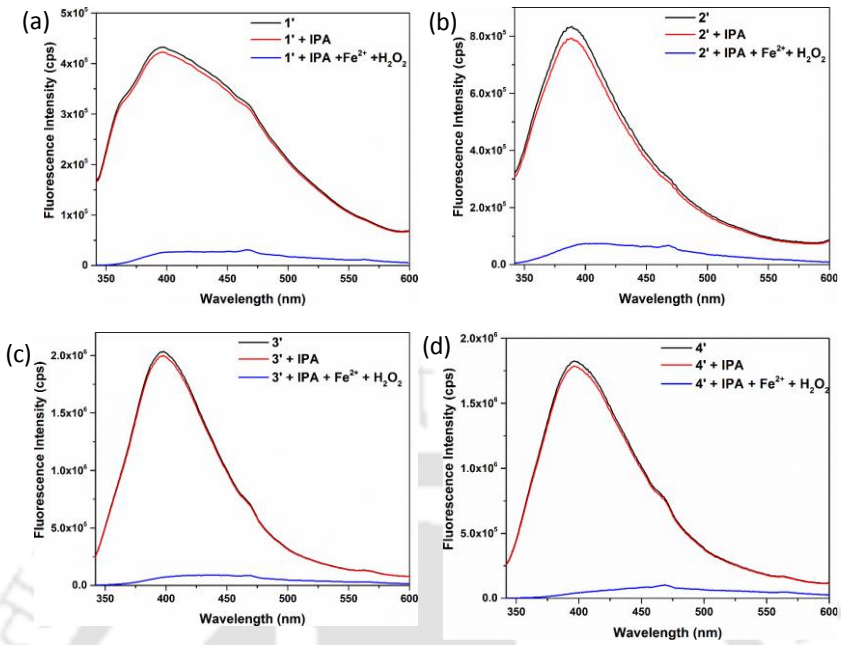

Figure 2.29 Change in the fluorescence intensity of **1′** (a), **2′** (b), **3′** (c) and **4′** (d) upon addition of Fe^{2+}-H_2O_2 solution in presence of IPA (300 µL).

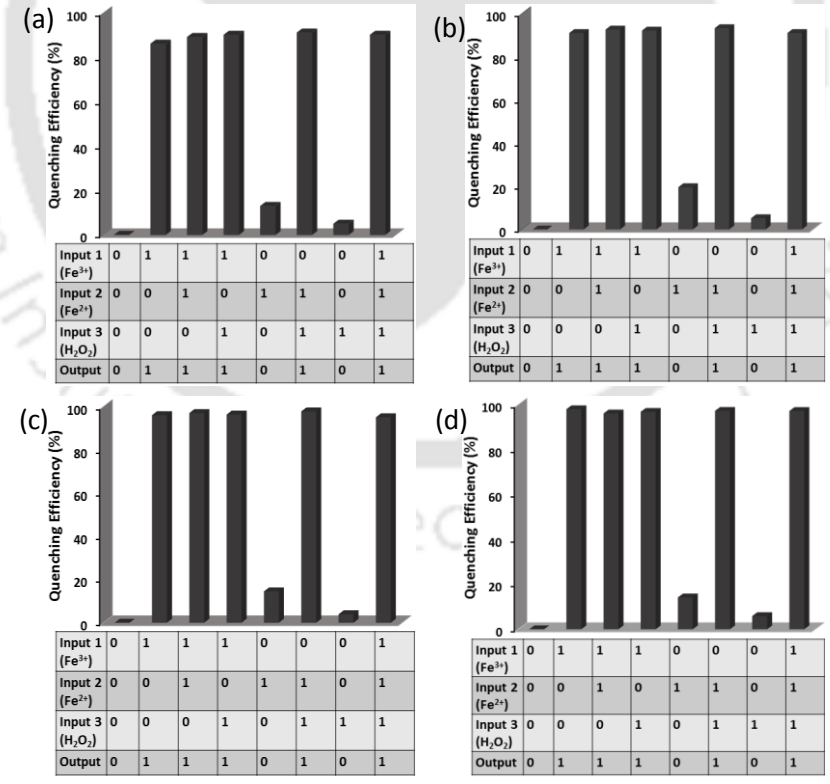

Figure 2.30 The fluorescence quenching efficiency of **1′** (a), **2′** (b), **3′** (c) and **4′** (d) in presence of different input and its corresponding truth table for logic gate construction.

2.3.10 Construction of molecular logic gates

We observed that all the MOFs showed selective sensing properties towards Fe^{3+} ions over other ions including Fe^{2+}, even in the presence of intrusive ions. We further investigated the fluorescence quenching efficiencies of the Fe^{3+} and Fe^{2+}/H_2O_2 systems. The well-known Fenton reaction occurs between Fe^{2+} ions and H_2O_2, which produces Fe^{3+} ions and the hydroxyl radical ($OH^{\bullet}$). The mixture of Fe^{2+} and H_2O_2 showed a rapid quenching of the fluorescence of all the MOF materials (Figure 2.28). The strongly oxidizing $OH^{\bullet}$ has the ability to capture electrons and can also act as a fluorescence quencher.[88,89] Therefore, $OH^{\bullet}$ can be expected to interfere with the quenching process. To check the effect of $OH^{\bullet}$ on the fluorescence quenching efficiency, we conducted similar fluorescence experiments in the presence of a large excess of isopropyl alcohol (IPA), which is a $OH^{\bullet}$ scavenger.[90] The results of these experiments disclosed that the fluorescence quenching efficiencies are negligibly influenced by the presence of IPA (Figure 2.29). The subsequent addition of the Fe^{2+}/H_2O_2 mixture to the suspensions of MOFs containing IPA triggered rapid fluorescence quenching. Therefore, it can be concluded that the Fe^{3+} ion is solely responsible for the fluorescence quenching. Silva and coworkers demonstrated the first example of a molecular logic gate based on fluorescence signalling.[91] Since their inception in 1993, a large number of molecular logic gates have been described in the literature until now.[92-94] Based on logic operations, the discriminative detection of different analytes has also been reported recently.[95-99] On the other hand, the reports on the construction of MOF-based logic gates are still (MV^{2+}) scarce.[100,101.] Based on the selective quenching behaviour of the MOFs towards Fe^{3+} and Fe^{2+}/H_2O_2 systems over Fe^{2+} ions, we have designed a molecular logic gate system (Figure 2.31), where Fe^{2+}, Fe^{3+} and H_2O_2 were used as three inputs. The presence and absence of the inputs were defined as '1' and '0', respectively. The quenched and unquenched fluorescence were used as the outputs. The quenched fluorescence was defined as output '1' and the unquenched fluorescence was defined as output '0'. The combination of Fe^{2+} and H_2O_2 was used in the formation of an AND logic gate. On the other hand, Fe^{3+} and the above-described AND logic gate were used in the formation of an OR logic gate. The logic operations were monitored in all eight possible input combinations. It becomes obvious from Figure 2.30 that among the eight possible inputs, five inputs [(011), (100), (101), (110) and (111)] showed fluorescence quenching (i.e. output 1). The other three inputs [(000), (010) and (001)] exhibited negligible changes in the fluorescence intensity (i.e. output 0).

(a)

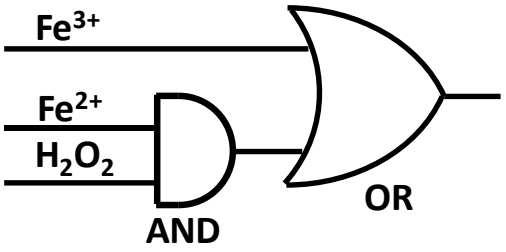

(b)

Input 1 (Fe^{3+})	Input 2 (Fe^{2+})	Input 3 (H_2O_2)	Output (Fluorescence Quenching)
0	0	0	0
1	0	0	1
1	1	0	1
1	0	1	1
0	1	0	0
0	1	1	1
0	0	1	0
1	1	1	1

Figure 2.31 (a) Logic gate circuit for AND and OR gates constructed from three-input system and the corresponding truth table (b).

2.4 Conclusions

We have successively synthesized four isoreticular thienothiophene-based Zr(IV) MOF materials under solvothermal conditions. The hydrophobicity and fluorescence properties of all the MOF compounds have been tuned in a systematic fashion by attaching methyl and phenyl groups to the thienothiophene-based ligands. XRPD experiments reveal that the MOF materials retain their structural robustness upon treatment with water, acetic acid, NaOH (pH = 11) and 1 M HCl solutions. Based on the thermogravimetric analyses, the MOF compounds possess moderate to high thermal stability. A combination of contact angle measurements and water sorption analyses confirms that the attachment of water-repellent methyl and phenyl groups to the ligands imparts different extents of hydrophobicity to the MOF materials. As verified by the fluorescence titration experiments, all the MOF materials featured selective, fast, and sensitive sensing of Fe^{3+} ions in water through the fluorescence quenching mechanism. Thorough experimental studies indicate that the transfer of electrons from the π-conjugated, electron-rich thienothiophene-based frameworks to the half-filled 3d orbitals of Fe^{3+} ions accounts for the

fluorescence quenching of MOF compounds. In contrast to the Fe^{3+} ions, the electron acceptor methyl viologen (MV^{2+}) dications displayed a completely reverse trend in the fluorescence quenching efficiencies of the MOF materials. During the elucidation of the reasons for this reverse trend in the quenching efficiency with the MV^{2+} ions, it has been observed that both the steric and electronic effects of the attached functional groups play decisive roles in the luminescence quenching mechanism. In addition, molecular logic gates could be designed by employing the MOFs for distinguishing between Fe^{3+} and Fe^{2+} ions. Overall, high photostability and reusability in Fe^{3+} sensing as well as the ability to discriminate between Fe^{3+} and Fe^{2+} ions through logic operations make the MOFs suitable for real-life applications. We believe that the results of this systematic investigation will provide fruitful insights for understanding the photophysical behavior of other MOFs and their interactions with different analytes.

2.5 References

1. K. P. Carter, A. M. Young and A. E. Palmer, *Chem. Rev.*, 2014, **114**, 4564-4601.
2. N. Stock and S. Biswas, *Chem. Rev.*, 2012, **112**, 933-969.
3. B. Chen, C. Liang, J. Yang, D. S. Contreras, Y. L. Clancy, E. B. Lobkovsky, O. M. Yaghi and S. Dai, *Angew. Chem.*, 2006, **118**, 1418-1421.
4. O. K. Farha, A. Ö. Yazaydın, I. Eryazici, C. D. Malliakas, G. Hauser, M. G. Kanatzidis, S. T. Nguyen, R. Q. Snurr and J. T. Hupp, *Nat. Chem.*, 2010, **2**, 944-948.
5. C. D. Wu, A. Hu, L. Zhang and W. Lin, *J. Am. Chem. Soc.*, 2005, **127**, 8940-8941.
6. T. Ishiwata, Y. Furukawa, K. Sugikawa, K. Kokado and K. Sada, *J. Am. Chem. Soc.*, 2013, **135**, 5427-5432.
7. M.-X. Wu and Y.-W. Yang, Adv. Mater., 2017, doi: 10.1002/adma.201606134.
8. L. E. Kreno, K. Leong, O. K. Farha, M. Allendorf, R. P. V. Duyne and J. T. Hupp, *Chem. Rev.*, 2011, **112**, 1105-1125.
9. X. Feng, L. Zeng, D. Zou, Z. Zhang, G. Zhong, S. Peng, L. Liu, L. Chen and J. Zhang, *RSC Adv.*, 2017, **7**, 37194-37199.
10. C. Y. Lee, O. K. Farha, B. J. Hong, A. A. Sarjeant, S. T. Nguyen and J. T. Hupp, *J. Am. Chem. Soc.*, 2011, **133**, 15858-15861.
11. B. Chen, L. Wang, Y. Xiao, F. R. Fronczek, M. Xue, Y. Cui and G. Qian, *Angew. Chem. Int. Ed.*, 2009, **48**, 500-503.
12. K. Müller-Buschbaum, F. Beuerle and C. Feldmann, *Microporous Mesoporous Mater.*, 2015, **216**, 171-199.

13. N. B. Shustova, A. F. Cozzolino, S. Reineke, M. Baldo and M. Dincă, *J. Am. Chem. Soc.*, 2013, **135**, 13326-13329.

14. K. A. Magnus, H. Ton-That and J. E. Carpenter, *Chem. Rev.*, 1994, **94**, 727-735.

15. C. Hsiao, I.-C. Chou, C. D. Okafor, J. C. Bowman, E. B. O'Neill, S. S. Athavale, A. S. Petrov, N. V. Hud, R. M. Wartell and S. C. Harvey, *Nat. Chem.*, 2013, **5**, 525-528.

16. http://www.who.int/water_sanitation_health/dwq/chemicals/iron.pdf.

17. R. R. Crichton, S. Wilmet, R. Legssyer and R. J. Ward, *J. Inorg. Biochem.*, 2002, **91**, 9-18.

18. G. Papanikolaou and K. Pantopoulos, *Toxicol. Appl. Pharmacol.*, 2005, **202**, 199-211.

19. S. J. Dixon and B. R. Stockwell, *Nat. Chem. Biol.*, 2014, **10**, 9-17.

20. L. Zecca, M. B. H. Youdim, P. Riederer, J. R. Connor and R. R. Crichton, *Nat. Rev. Neurosci.*, 2004, **5**, 863-873.

21. B. Wang, Q. Yang, C. Guo, Y. Sun, L.-H. Xie and J.-R. Li, *ACS Appl. Mater. Interfaces*, 2017, **9**, 10286-10295.

22. Y. Dong, H. Zhang, F. Lei, M. Liang, X. Qian, P. Shen, H. Xu, Z. Chen, J. Gao and J. Yao, *J. Solid State Chem.*, 2017, **245**, 160-163.

23. Q. Tang, S. Liu, Y. Liu, J. Miao, S. Li, L. Zhang, Z. Shi and Z. Zheng, *Inorg. Chem.*, 2013, **52**, 2799-2801.

24. X. Y. Dong, R. Wang, J. Z. Wang, S. Q. Zang and T. C. Mak, *J. Mater. Chem. A*, 2015, **3**, 641-647.

25. L. H. Cao, F. Shi, W. M. Zhang, S. Q. Zang and T. C. Mak, *Chem. Eur. J.*, 2015, **21**, 15705-15712.

26. S. Xing, Q. Bing, L. Song, G. Li, J. Liu, Z. Shi, S. Feng and R. Xu, Chem. Eur. J., 2016.

27. R. Wang, X. Liu, A. Huang, W. Wang, Z. Xiao, L. Zhang, F. Dai and D. Sun, *Inorg. Chem.*, 2016, **55**, 1782-1787.

28. C. X. Yang, H. B. Ren and X. P. Yan, *Anal. Chem.*, 2013, **85**, 7441-7446.

29. S. Dang, E. Ma, Z. M. Sun and H. Zhang, *J. Mater. Chem.*, 2012, **22**, 16920-16926.

30. Y. Zhou, H. H. Chen and B. Yan, *J. Mater. Chem. A*, 2014, **2**, 13691-13697.

31. Z. Xiang, C. Fang, S. Leng and D. Cao, *J. Mater. Chem. A*, 2014, **2**, 7662-7665.

32. D. Feng, Z. Y. Gu, J. R. Li, H. L. Jiang, Z. Wei and H. C. Zhou, *Angew. Chem.*, 2012, **124**, 10453-10456.

33. C. G. Silva, I. Luz, F. X. Llabrs i Xamena, A. Corma and H. García, *Chem. Eur. J.*, 2010, **16**, 11133-11138.

34. Y. Li, S. P. Singh and P. Sonar, *Adv. Mater.*, 2010, **22**, 4862-4866.

35. I. B. Kim, D. Khim, S. Y. Jang, J. Kim, B. K. Yu, Y. A. Kim and D. Y. Kim, *Org. Electron.*, 2015, **26**, 251-259.

36. N. Kleinhenz, L. Yang, H. Zhou, S. C. Price and W. You, *Macromolecules*, 2011, **44**, 872-877.

37. M. SK, M. Grzywa, D. Volkmer and S. Biswas, *J. Solid State Chem.*, 2015, **232**, 221-227.

38. W. W. He, G. S. Yang, Y. J. Tang, S. L. Li, S. R. Zhang, Z. M. Su and Y. Q. Lan, *Chem. Eur. J.*, 2015, **21**, 9784-9789.

39. R. Dalapati and S. Biswas, *Sens. Actuators, B.*, 2017, **239**, 759-767.

40. R. Dalapati, B. Sakthivel, A. Dhakshinamoorthy, A. Buragohain, A. Bhunia, C. Janiak and S. Biswas, *CrystEngComm*, 2016, **18**, 7855-7864.

41. A. Das and S. Biswas, *Sens. Actuators, B.*, 2017, **250**, 121-131.

42. L. Ge, W. Zhou, V. Rudolph and Z. Zhu, *J. Mater. Chem. A*, 2013, **1**, 6350-6358.

43. K. Wang, H. Huang, W. Xue, D. Liu, X. Zhao, Y. Xiao, Z. Li, Q. Yang, L. Wang and C. Zhong, *CrystEngComm*, 2015, **17**, 3586-3590.

44. T.-H. Chen, A. Schneemann, R. A. Fischer and S. M. Cohen, *Dalton Trans.*, 2016, **45**, 3063-3069.

45. J.-C. Tan, B. Civalleri, C.-C. Lin, L. Valenzano, R. Galvelis, P.-F. Chen, T. D. Bennett, C. M. Draznieks, C. M. Zicovich-Wilson and A. K. Cheetham, *Phys. Rev. Lett.*, 2012, **108**, 095502.

46. T. D. Bennett and A. K. Cheetham, *Acc. Chem. Res.*, 2014, **47**, 1555-1562.

47. J. H. Cavka, S. Jakobsen, U. Olsbye, N. Guillou, C. Lamberti, S. Bordiga and K. P. Lillerud, *J. Am. Chem. Soc.*, 2008, **130**, 13850-13851.

48. M. H. Beyzavi, R. C. Klet, S. Tussupbayev, J. Borycz, N. A. Vermeulen, C. J. Cramer, J. F. Stoddart, J. T. Hupp and O. K. Farha, *J. Am. Chem. Soc.*, 2014, **136**, 15861-15864.

49. M. Lammert, M. T. Wharmby, S. Smolders, B. Bueken, A. Lieb, K. A. Lomachenko, D. D. Vos and N. Stock, *Chem. Commun.*, 2015, **51**, 12578-12581.

50. Y. Bai, Y. Dou, L.-H. Xie, W. Rutledge, J.-R. Li and H.-C. Zhou, *Chem. Soc. Rev.*, 2016, **45**, 2327-2367.

51. M. SK and S. Biswas, *CrystEngComm*, 2016, **18**, 3104-3113.

52. S. Wang, T. Cao, H. Yan, Y. Li, J. Lu, R. Ma, D. Li, J. Dou and J. Bai, *Inorg. Chem.*, 2016, **55**, 5139-5151.

53. F. Zhang, Y. Wang, T. Chu, Z. Wang, W. Lia and Y. Yang, *Analyst*, 2016, **141**, 4502-4510.

54. Y. Q. Wang, Q. H. Tan, H. T. Liu and Z. L. Liu, *RSC Adv.*, 2015, **5**, 86614-86619.

55. W. Cao, M. Fang, Z. Chai, H. Xu, T. Duan, Z. Li, X. Chen, J. Qin and H. Han, *RSC Adv.*, 2015, **5**, 32967-32975.

56. D. Wang, Q. Guo, H. Gao, Z. Yang, H. Cao, W. He and H. Wang, *RSC Adv.*, 2016, **6**, 59327-59332.

57. M. D. Allendorf, C. A. Bauer, R. K. Bhakta and R. J. T. Houk, *Chem. Soc. Rev.*, 2009, **38**, 1330-1352.

58. M. Usman, S. Mendiratta, S. Batjargal, G. Haider, M. Hayashi, N. R. Gade, J. W. Chen, Y. F. Chen and K. L. Lu, *ACS Appl. Mater. Interfaces*, 2015, **7**, 22767-22774.

59. H. Q. Xu, J. Hu, D. Wang, Z. Li, Q. Zhang, Y. Luo, S. H. Yu and H. L. Jiang, *J. Am. Chem. Soc.*, 2015, **137**, 13440-13443.

60. E. F. Larsen, A. Røyset, J. H. Cavka and K. Thorshaug, *J. Phys. Chem. C*, 2013, **117**, 20610-20616.

61. L. Valenzano, B. Civalleri, S. Chavan, S. Bordiga, M. H. Nilsen, S. Jakobsen, K. P. Lillerud and C. Lamberti, *Chem. Mater.*, 2011, **23**, 1700-1718.

62. L. Zhai, W. W. Zhang, J. L. Zuob and X. M. Ren, *Dalton Trans.*, 2016, **45**, 11935-11938.

63. C.-K. Lin, D. Zhao, W.-Y. Gao, Z. Yang, J. Ye, T. Xu, Q. Ge, S. Ma and D.-J. Liu, *Inorg. Chem.*, 2012, **51**, 9039-9044.

64. T. Musho, J. Li and N. Wu, *Phys. Chem. Chem. Phys.*, 2014, **16**, 23646-23653.

65. T. P. Kaloni, G. Schreckenbach and M. S. Freund, *Sci. Rep.*, 2016, **6**, 36554.

66. F. Jeremias, A. Khutia, S. K. Henninger and C. Janiak, *J. Mater. Chem.*, 2012, **22**, 10148-10151.

67. F. Jeremias, D. Fröhlich, C. Janiak and S. K. Henninger, *New J. Chem.*, 2014, **38**, 1846-1852.

68. F. Jeremias, D. Fröhlich, C. Janiak and S. K. Henninger, *RSC Adv.*, 2014, **4**, 24073-24082.

69. D. Fröhlich, S. K. Henninger and C. Janiak, *Dalton Trans.*, 2014, **43**, 15300-15304.

70. D. Fröhlich, E. Pantatosaki, P. D. Kolokathis, K. Markey, H. Reinsch, M. Baumgartner, M. A. V. D. Veen, D. E. D. Vos, N. Stock and G. K. Papadopoulos, *J. Mater. Chem. A*, 2016, **4**, 11859-11869.

71. J. Ehrenmann, S. K. Henninger and C. Janiak, *Eur. J. Inorg. Chem.*, 2011, **2011**, 471-474.

72. S. K. Henninger, F. Jeremias, H. Kummer and C. Janiak, *Eur. J. Inorg. Chem.*, 2012, **2012**, 2625-2634.

73. M. Wickenheisser and C. Janiak, *Microporous Mesoporous Mater.*, 2015, **204**, 242-250.

74. G. Akiyama, R. Matsuda and S. Kitagawa, *Chem. Lett.*, 2010, **39**, 360-361.

75. M. Wickenheissera, A. Herbsta, R. Tannertb, B.Milowb and C. Janiak, *Microporous Mesoporous Mater.*, 2015, **215**, 143-153.

76. S. Dey, A. Bhunia, I. Boldog and C. Janiak, *Microporous Mesoporous Mater.*, 2016, **241**, 303-315.

77. A. Khutia, H. U. Rammelberg, T. Schmidt, S. Henninger and C. Janiak, *Chem. Mater.*, 2013, **25**, 790-798.

78. M. Wickenheisser, T. Paul and C. Janiak, *Microporous Mesoporous Mater.*, 2016, **220**, 258-269.

79. M. Wickenheisser, F. Jeremias, S. K. Henninger and C. Janiak, *Inorg. Chim. Acta*, 2013, **407**, 145-152.

80. S. Biswas, S. Couck, D. Denysenko, A. Bhunia, M. Grzywa, J. F. Denayer, D. Volkmer, C. Janiak and P. Van Der Voort, *Microporous Mesoporous Mater.*, 2013, **181**, 175-181.

81. A. Buragohain, M. Yousufuddin, M. Sarma and S. Biswas, *Cryst. Growth Des.*, 2016, **16**, 842-851.

82. H. Huang, H. Li, J.-J. Feng, H. Feng, A.-J. Wang and Z. Qian, *Sens. Actuators, B*, 2017, **241**, 292-297.

83. X. Luo, X. Zhang, Y. Duan, X. Wang and J. Zhao, *Dalton Trans.*, 2017, **46**, 6303-6311.

84. M. A. Cardona, C. J. Mallia, U. Baisch and D. C. Magri, *RSC Adv.*, 2016, **6**, 3783-3791.

85. P. Cheng, K.-x. Xu, W. Yao, E. Xie and J. Liu, *J. Lumin.*, 2013, **143**, 583-586.

86. Z. Zhang, F. Li, C. He, H. Ma, Y. Feng, Y. Zhang and M. Zhang, Sens. Actuators, B, 2017.

87. M. Porel, C. H. Chuang, C. Burda and V. Ramamurthy, *J. Am. Chem. Soc.*, 2012, **134**, 14718-14721.

88. Q. Mei, C. Jiang, G. Guan, K. Zhang, B. Liu, R. Liua and Z. Zhang, *Chem. Commun.*, 2012, **48**, 7468–7470.

89. Y. Song, S. Zhu, S. Xiang, X. Zhao, J. Zhang, H. Zhang, Y. Fu and B. Yang, *Nanoscale*, 2014, **6**, 4676-4682.

90. M. Humayun, Y. Qu, F. Raziq, R. Yan, Z. Li, X. Zhang and L. Jing, *Environ. Sci. Technol.*, 2016, **50**, 13600–13610.

91. P. A. d. Silva, N. H. Q. Gunaratne and C. P. McCoy, *Nature*, 1993, **364**, 42-44.

92. R. Freeman, T. Finder and I. Willner, *Angew. Chem., Int. Ed.*, 2009, **48**, 7818-7821.

93. J. Andreasson and U. Pischel, *Chem. Soc. Rev.*, 2010, **39**, 174-188.

94. W. Lu, Y. Gao, Y. Jiao, S. Shuang, C. Li and C. Dong, *Nanoscale*, 2017, **9**, 11545-11552.

95. A. Rai, A. K. Singh, A. K. Sonkar, A. Prakash, J. K. Roy, R. Nagarajan and L. Mishra, *Dalton Trans.*, 2016, **45**, 8272-8277.

96. N. Sharma, S. I. Reja, V. Bhalla and M. Kumar, *Dalton Trans.*, 2015, **44**, 6062-6068.

97. X. Chai, Y.-X. Fu, T. D. James, J. Zhang, X.-P. He and H. Tian, *Chem. Commun.*, 2017, **53**, 9494-9497.

98. D. Fan, C. Shang, W. Gu, E. Wang and S. Dong, *ACS Appl. Mater. Interfaces*, 2017, **9**, 25870-25877.

99. L. He, J. Li and J. H. Xin, *Biosens. Bioelectron.*, 2015, **70**, 69-73.

100. W. Li, X. Qi, C.-Y. Zhao, X.-F. Xu, A.-N. Tang and D.-M. Kong, 2017, **9**, 236-243.

101. J. M. Fang, P. F. Gao, X. L. Hu and Y. F. Li, *RSC Adv.*, 2014, **4**, 37349-37352.

Chapter 3

A cerium-based metal-organic framework having inherent oxidase-like activity applicable for colorimetric sensing of biothiols and aerobic oxidation of thiols

This chapter describes the solvothermal synthesis and characterization of a Ce(IV)-based MOF material incorporating 3,4-dimethyl thieno[2,3-b]thiophene-2,5-dicarboxylic acid. The XPS study reveals the presence of both Ce(III) and Ce(IV) ions in the framework. The cubic framework structure of the compound contains hexanuclear cluster cores having a $[Ce_6O_4(OH)_4]^{12+}$ *composition with UiO (UiO = University of Oslo) framework topology. The activated compound mimics the catalytic activity of biological oxidase enzymes and oxidize the chromogenic peroxidase substrates: TMB and AzBTS. Based on the oxidase-mimicking activity of MOF, a colorimetric sensing platform for biothiols was established. A significant heterogeneous catalytic performance of the MOF was also observed in the oxidation of thiol compounds using molecular oxygen.*

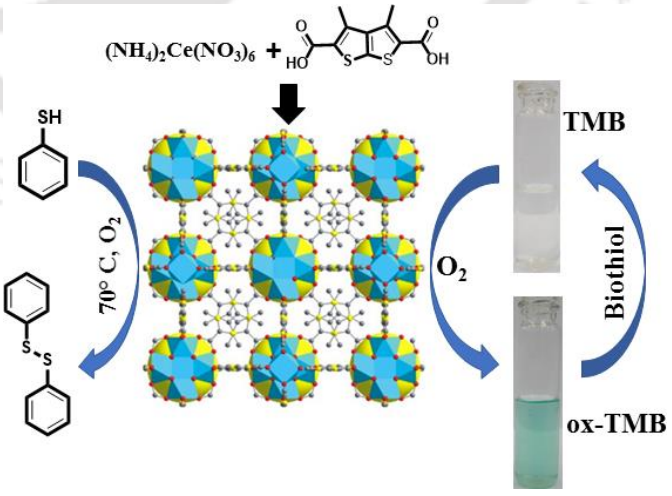

CrystEngComm

R. Dalapati, B. Sakthivel, M. K. Ghosalya, A. Dhakshinamoorthy and S. Biswas, *CrystEngComm*, 2017, **19**, 5915.

3.1 Introduction

The colorimetric sensing technique has gained immense attention in biology and analytical chemistry owing to its easy visual readout and rapid visual determination with naked eyes or low cost portable instruments.[1] Colorimetric biosensors are capable of showing response towards target biomolecules (cysteine, glutathione, homocysteine, thiamine, glucose, ascorbic acid, etc.) through a change in color.[2] Detection of these species is highly desirable, since they play vital roles in different physiological processes such as metabolism, protein synthesis, detoxification and reversible redox reactions.[3] For the sensing of biomolecules, optical,[4] electrochemical[5] and bio-electrochemical[6] sensing techniques are extensively employed. However, these methods have considerable disadvantages like the absence of rapidity, selectivity and sensitivity. Moreover, the bio-enzymes easily undergo denaturation or chemical changes upon heating. In addition, the preparation, storage and purification of enzymes require too much time.[7,8] Hence, numerous analogous materials such as Fe_3O_4,[9] Au nanoparticles,[10] graphene oxide[11] and carbon dots[12] have been investigated. Since the catalytic performances of these materials are analogous to those of natural enzymes, their enzyme-mimicking characteristics have been utilized for the sensing of biological analytes. The major advantages of these analogous materials include facile and controlled synthesis with high yields, a lower cost, adjustable catalytic performances, and tunable structures and compositions.[13] Because of these benefits, enzyme-mimetic nanomaterials have attracted widespread attention. These materials exhibit similar catalytic activity to natural oxidases or peroxidases and hence they have been efficiently utilized as biosensors for applications in environmental monitoring and biomedical diagnosis.[2]

The oxidation of thiols to disulfides has drawn immense interest since disulfides play vital roles in many biochemical and industrial processes.[14] In industry, disulfides are used in the synthesis of pharmaceuticals and agrochemicals and vulcanization of rubber.[15] Furthermore, the protection of thiols can be easily achieved through the formation of disulfides and conversely the cleavage of disulfide bonds leads to the formation of thiols.[16] The oxidation of thiol compounds is an effective method for the industrial production of disulfides because of the commercial availability of many thiols and their convenient preparation procedures. However, many over-oxygenated by-products such as sulfoxides and sulfones can be produced during the oxidation of thiols. On the other hand, the selective oxidation of thiols to disulfides has been achieved so far through the employment of a variety of reagents such as Ce(IV) salts, permanganates, peroxides,

air along with transition-metal oxides, sodium chlorite, sodium perborate, halogens, nitric oxide and ferric chloride.[17] MOFs have received tremendous attention in the last two decades since they have shown application potential in chemical sensing, gas adsorption and separation, heterogeneous catalysis and drug delivery.[18-20] Until today, few Fe(III)-containing MOFs such as MIL-53, MIL-88A, MIL-68, MIL-100, MIL-88-NH_2 and MIL-101 have been reported, which have exhibited inherent peroxidase-like catalytic behaviour applicable for colorimetric biosensing.[21-28] These examples also include two Zr(IV)-based MOFs having Fe(III)-metalated porphyrin ligands.[29-31] However, only two M(IV)-based (M = Zr, Ce) single-metal MOFs have been employed so far, demonstrating oxidase-like activity for biosensing. These MOFs include a mixed-valence (Ce^{3+}/Ce^{4+}) Ce-MOF (called MVCM)[32] and Zr(IV)-based MOF UiO-66-NH_2.[33] Among the various MOFs that have displayed either oxidase- or peroxidase-like activity, only Fe-MIL-88- NH_2,[31] MVCM and Zr-UiO-66-NH_2 have been applied for the facile colorimetric sensing of biothiols. On the other hand, only two MOFs, namely, Fe(BTC) and Fe-MIL-100, have been demonstrated to achieve oxidation catalysis of thiols to disulphides using molecular oxygen.[18,34] Cerium oxide nanoparticles (nanoceria) occur as mixed valence state oxides of Ce^{3+} and Ce^{4+} and are able to reversibly switch between the two oxidation states.[35] Due to this phenomenon, nanoceria has featured oxidase-mimicking characteristics beneficial for colorimetric biosensing.[36-38] Furthermore, the MVCM material has been recently reported to sense biothiols colorimetrically due to its oxidase-mimicking features.[32] On the other hand, few Ce(IV) complexes have been employed to achieve the oxidation of thiol compounds to disulphides in the homogeneous phase using molecular oxygen.[39] In addition, the ability of cerium(IV) ammonium nitrate (CAN) to act as a homogeneous oxidation catalyst has been demonstrated in various substrates including alcohols, thioethers, epoxides, alkylbenzenes and active methylene compounds.[40] Encouraged by the usefulness of cerium chemistry in colorimetric sensing and oxidation catalysis, we have synthesized a Ce-based MOF (**5**) incorporating H_2DMTDC as a ligand. The presence of both Ce(III) and Ce(IV) ions in the framework was confirmed by XPS analysis. The activated MOF (**5′**) features an inherent oxidase-mimicking behaviour in NaAc buffer at acidic pH, since it is capable of performing rapid oxidation of chromogenic peroxidase substrates like 3,3′,5,5′-tetramethylbenzidine (TMB) or 2,2′-azinobis(3-ethylbenzothizoline-6-sulfonic acid) (AzBTS) without the need of any external oxidizing agents (e.g. H_2O_2). On the basis of these outcomes, we have established a colorimetric sensing platform for biothiols in NaAc buffer (pH = 4.0) as well

as in human blood plasma. Moreover, the heterogeneous catalytic activity of **5′** for the oxidation catalysis of thiol compounds to disulphides using molecular oxygen has been thoroughly investigated.

3.2 Experimental

3.2.1 Materials and synthetic procedures

The synthesis of the H_2DMTDC ligand was carried out by following a previously documented protocol.[41] All the other reagents were procured from commercial vendors. The infrared (IR) spectra in the range 440-4000 cm^{-1} were collected using a Perkin Elmer Spectrum Two spectrometer. To describe absorption bands, the following notations were used: broad (br), shoulder (sh), weak (w), strong (s), medium (m) and very strong (vs). Thermogravimetric analyses (TGA) were carried out using a Mettler-Toledo TGA/SDTA 851e thermogravimetric instrument in the temperature range 25-700 °C with a heating rate of 5 °C min^{-1} in air atmosphere. X-Ray powder diffraction (XRPD) measurements were performed with a Bruker D2 PHASER X-ray diffractometer (10 mA, 30 kV) utilizing Cu-Kα (λ = 1.5406 Å) radiation. X-ray photoelectron spectroscopy (XPS) measurement was carried out at room temperature using a custom-built near-ambient pressure photoelectron spectrometer (Prevac, Poland) and the full details are available in ref. 18 and 19. It is equipped with an R3000HP analyser (Scienta) with a twin-anode source and a monochromatic (Al-Kα) X-ray source. However, the experiment was carried out with the Mg-Kα (hν = 1253.6 eV) source. The base pressure in the analysis chamber was kept in the 3 to 6 × 10^{-10} mbar range. The energy resolution of the spectrometer was set at 0.7 eV with Mg-Kα radiation at a pass energy of 20 eV. The calibration for the binding energy (BE) was carried out with the Au($4f_{7/2}$) core level at 84.0 eV. Field emission-scanning electron microscopy (FE-SEM) images were collected using a Zeiss (Zemini) scanning electron microscope. UV-vis spectra in the region 250-800 nm were recorded using a Perkin Elmer Lambda 25 UV-vis spectrometer. All solutions for the UV-vis measurements were prepared by using Milli-Q water. The nitrogen adsorption experiments at −196 °C were carried out employing a Quantachrome Autosorb iQ-MP volumetric gas adsorption equipment. Before the adsorption measurement, degassing of the sample was accomplished by heating at 80 °C overnight under high vacuum. The conversion and selectivity were determined using an Agilent 7820 gas chromatography system with FID. To identify the

products, gas chromatography-mass spectrometry (GC-MS) measurements were performed using a Perkin Elmer Clarius 500 spectrometer.

3.2.2 Synthesis of $[Ce_6O_4(OH)_4(DMTDC)_6]\cdot 2DMF\cdot 22H_2O$ (5)

A mixture of H_2DMTDC (40 mg, 0.16 mmol) in 2 mL of *N*,*N*-dimethylformamide (DMF) was sonicated until it dissolved completely. Consequently, ceric ammonium nitrate (CAN) was added as an aqueous solution (400 μL, 0.533 M). The mixture was put inside a glass tube, which was sealed. This tube was heated at 100 °C for 3.5 h by means of a dry block heater. The mixture was cooled down to ambient temperature and the light yellow precipitate was filtered off. This precipitate was washed twice with DMF and once with acetone. The resulting solid was dried in an oven at 70 °C for 6 h and denoted as **5**. The yield of the compound was 48 mg (0.02 mmol, 46%) considering the Ce salt. Anal. calcd for $C_{66}H_{98}Ce_6N_2O_{56}S_{12}$ (3040.95 g mol^{-1}): C, 26.06 H, 3.24 N, 0.921. Found: C, 26.74 H, 3.18 N, 1.02%. FT-IR (KBr, cm^{-1}): 3430 (br), 2927 (w), 2852 (w), 1647 (s), 1605 (sh), 1495 (m), 1378 (vs), 1268 (w), 1158 (sh), 1103 (m), 1019 (w), 799 (sh), 772 (m), 662 (w), 558 (m), 469 (w).

3.2.3 Activation of as-synthesized 5

At first, the as-synthesized material (0.2 g) was stirred in methanol (20 mL) for 24 h at ambient temperature. Then, the yellow material was filtered off. The degassing of the solid was accomplished by heating at 70 °C for 16 h under high vacuum. In this way, the activated material (denoted as **5′**) was obtained.

3.2.4 Oxidase-like activity of 5′

For the UV-vis experiments, aqueous suspensions of **5′** (concentration: 1 mg mL^{-1}) were prepared by ultrasonic treatment for 30 min. To examine the oxidase-like activity, the catalytic oxidation of 3,3′,5,5′-tetramethylbenzidine (TMB) was investigated in presence of **5′** and a blue colored solution of ox-TMB was obtained. For this purpose, a 120 μL aqueous suspension of **5′** and 100 μL of TMB solution (0.04 mM) were added to 2780 μL of NaAc buffer (0.2 M, pH = 4.0). The influence of reaction time on the absorbance (λ_{max} = 652 nm) of ox-TMB was examined by measuring the UV-vis spectra of the resulting mixture at a regular time interval (2 min) until the

absorbance of ox-TMB became constant. For the investigation of the steady-state reaction mechanism, additional UV-vis measurements were carried out under similar conditions to those mentioned above, except that various concentrations of TMB solution were added to the suspension.

3.2.5 Detection of biothiols in NaAc buffer

The colorimetric method for the detection of biothiols involve the following steps: initially, 2680 μL of 0.2 M NaAc buffer (pH = 4.0), 120 μL of TMB solution (1 mM, ethanol solution) and a 100 μL aqueous suspension of **5′** (1.0 mg mL^{-1}) were mixed together to obtain a blue-colored solution of ox-TMB. After the absorbance of ox-TMB became constant, 100 μL of a biothiol solution (0.5 mM) was added and the UV-vis spectrum of the resulting mixture was recorded. Analogous experiments were also carried out by replacing the biothiols with the following possibly interfering biomolecules: aspartic acid, alanine, arginine, proline, glycine, isoleucine, lysine, histidine, leucine, phenylalanine, threonine, methionine, valine, tryptophan and serine. In order to determine the selectivity of **5′** towards biothiols co-existing with other biomolecules, the above-mentioned procedure was followed, except the sequential addition of two amino acid solutions (i.e. interfering biomolecules followed by biothiols) in the last step instead of one amino acid (i.e. biothiols) solution.

3.2.6 Detection of biothiols in human blood plasma

From the left arm vain, 5 mL of human blood was collected in a tube having ethylenediaminetetraacetic acid (EDTA) under aseptic conditions. For the separation of plasma, the blood was centrifuged at 3000 rpm for 5 min. Afterwards, the straw-colored supernatant human blood plasma (HBP) was collected and employed for further experiments. 160 μL of HBP was placed in four microcentrifuge tubes and different amounts of cysteine solutions were spiked. After that, incubation of the mixture was accomplished at 37 °C for 5 min. Later, 200 μL of 60% (v/v) acetonitrile was added to this mixture to precipitate the proteins. Then, the mixture was centrifuged at 6000 rpm for 5 min for the complete separation of the proteins. The resulting supernatant solution was used further for sensing cysteine in a similar method to the sensing of cysteine in NaAc buffer. A control experiment was also carried out without spiking cysteine.

3.2.7 Aerobic oxidation catalysis

A typical reaction was performed in which thiophenol (1 mmol) and 2 mL of methanol were poured in a 25 mL round-bottom flask and catalyst **5′** (20 mg) was added to the mixture. The reaction mixture was stirred at 70 °C in a preheated oil bath and oxygen from a balloon was purged into it. The progress of the reaction was regulated by GC through sampling aliquots at various time gaps. The heterogeneity of the catalytic reaction was investigated as indicated above, except that the catalyst was filtered off after 2 h from the reaction mixture using a 0.2 μm PTFE filter and then the reaction was continued up to 12 h in the absence of the catalyst. In addition, the stability of the catalyst was checked by performing reusability experiments under the optimized reaction conditions. After the reaction, **5′** was filtered off, washed twice with methanol and then washed thoroughly with acetone for the exclusion of all unreacted compounds from the catalyst. Afterwards, the material was dried at 80 °C for 16 h in a traditional oven. This dried compound (**5′**) was used as the catalyst in the subsequent catalytic runs.

3.3 Results and discussion

3.3.1 Preparation and activation procedure

Compound **5** was synthesized by heating a mixture of aqueous ammonium cerium(IV) nitrate and the 3,4-dimethylthieno[2,3-b]thiophene-2,5-dicarboxylic acid (H_2-DMTDC) ligand in *N*,*N*-dimethylformamide (DMF) at 100 °C for 3.5 h. In order to remove the occluded DMF molecules, the as-synthesized material was first stirred in methanol. Later, the methanol molecules were removed from the cages by heating the methanol-exchanged material under high vacuum at 80 °C for 12 h. In this way, the activated material (termed as **5′**) was obtained.

3.3.2 Structure description

The experimental XRPD pattern of the as-synthesized form of **5** matches closely with the theoretical XRPD pattern of its previously reported Zr(IV) analogue having a UiO-66 type of framework topology (Figure 3.1).[42,43] Therefore, both **5** and its Zr(IV) analogue have the same framework topology as UiO-66.[44] The XRPD pattern of the as-synthesized compound can be

successfully indexed in the cubic crystal system. The unit cell parameters of **5** (Table 3.1) are very similar to those of the isostructural Zr(IV)-containing material.[42,43]

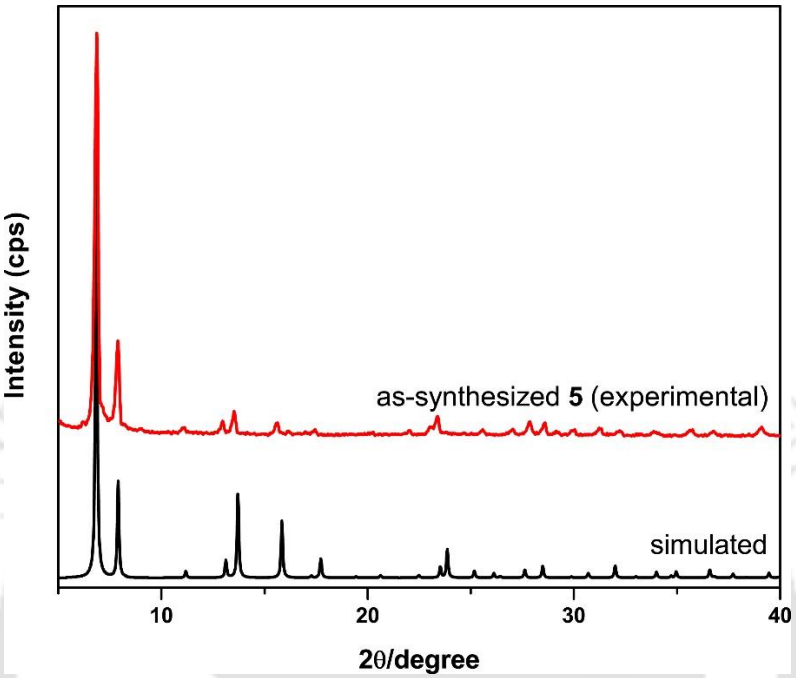

Figure 3.1 Simulated (black) and experimental (red) XRPD patterns of **5**.

Table 3.1 Refined unit cell parameters for as-synthesized **5** and isostructural Zr(IV)-based compound having cubic unit cells.

Compound	*a* (Å)	*V* (Å^3)
as-synthesized **5**	23.111(6)	12343.6(54)
$[Zr_6O_4(OH)_4(DMTDC)_6]\cdot 4.8DMF\cdot 10H_2O$[42]	23.0917(6)	12313.1(3)
Zr-DMTDC[43]	23.12	12358.43

The framework structure of the isostructural Zr(IV) material has been described previously by us.[42,43] Briefly, the cubic framework structure (Figure 3.2) of the title compound comprises hexanuclear cluster cores having a $[Ce_6O_4(OH)_4]^{12+}$ composition.[45] In these cluster cores, the six cerium atoms are situated at the corners of an octahedron. The eight faces of each octahedron are

bridged by the O atoms of μ_3-O and μ_3-OH groups, which are arranged in an alternating fashion. Eight O atoms are coordinated with each Ce atom. The latter has a square antiprismatic geometry in which the O atoms from the carboxylate, μ_3-O and μ_3-OH groups occupy the square faces. Each $[Ce_6O_4(OH)_4]^{12+}$ cluster core is linked with the carboxylate groups of twelve DMTDC ligands. The chemical structure of the H_2DMTDC ligand is shown in Figure 3.2e. The cubic, 3D framework of **5** is formed by the interconnection of the cluster cores with the carboxylate groups of adjacent ditopic DMTDC ligands. The structure incorporates two types of cages: larger octahedral and smaller tetrahedral. Eight tetrahedral cages surround each central octahedral cage. Both cage types are accessible to guest molecules via narrow triangular windows. The methyl groups attached with the DMTDC ligands are located at the triangular windows. These methyl groups project towards the inner side of the octahedral cages.

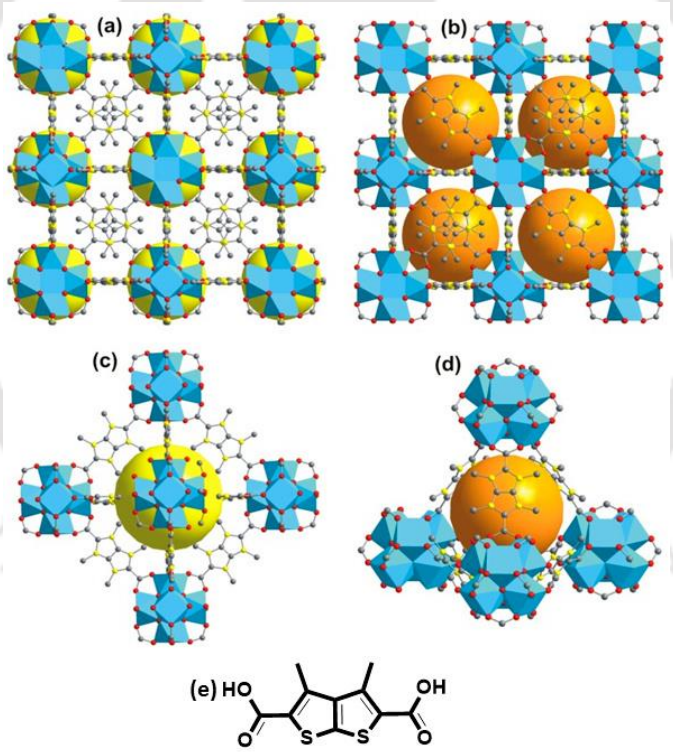

Figure 3.2 Cubic 3D framework structure of **5** in ball-and-stick representation. (a, b) Depiction of octahedral (yellow spheres) and tetrahedral (orange spheres) cages. (c, d) are the magnified views of (a, b), respectively. (e) Structure of the H_2DMTDC ligand. Color codes: Ce, blue polyhedra; C, grey; O, red; S, yellow.

3.3.3 Material characterization

The oxidation state of cerium in **5** was investigated by XPS analysis. The XPS study reveals that both Ce(III) and Ce(IV) ions are present in the framework of **5** (Figure 3.3).[46] The Ce 3d core level spectrum was analyzed to explore the oxidation state of Ce. The deconvolution of the Ce 3d core level spectrum suggests the presence of ten peaks. The six peaks at 883.1, 888.5, 898.4, 902.1, 907.5 and 916.8 eV correspond to the Ce(IV) state, whereas the Ce(III) state gives rise to four peaks at 880.6, 885.6, 900.0 and 904.8 eV.[46-48] The relative amount of Ce(III) ions present in **5** was determined to be 23.6% by utilizing the peak area of the deconvoluted core level spectrum.[49] The reducing ability of the DMF solvent with prolonged reaction time at high temperature might be responsible for the reduction of the Ce(IV) ions.[50]

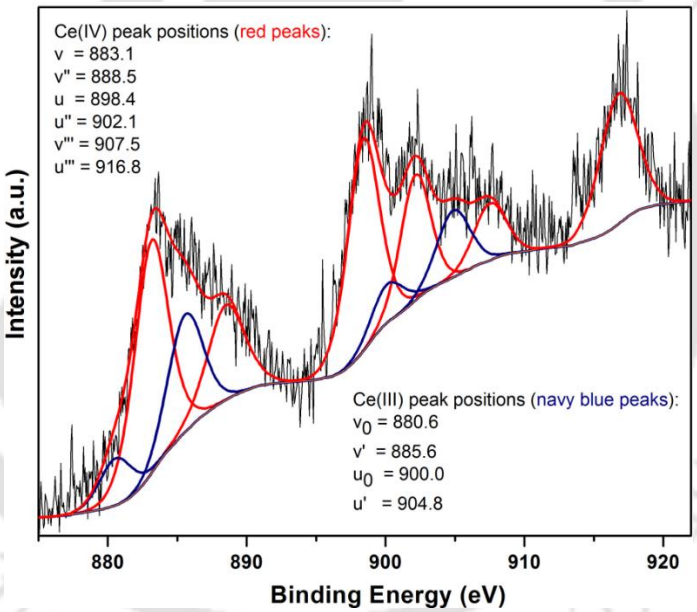

Figure 3.3 XPS spectrum of the as-synthesized form of **5** (Ce 3d core level).

In the IR spectra (Figure 3.4a) of as-synthesized and activated **5**, absorption peaks with high intensity are observed at around 1595 and 1385 cm^{-1}. These peaks occur due to the asymmetric and symmetric CO_2 stretching vibrations of the framework DMTDC ligands, respectively.[51,52] The IR spectrum of as-synthesized **5** contains a medium absorption peak at around 1650 cm^{-1}, which is attributable to the stretching vibrations for the carbonyl group of DMF molecules residing inside the pores. The IR spectrum of the activated compound does not contain

any absorption peaks for the occluded DMF molecules. The results from the FT-IR analysis confirm the complete activation of the compound.

In order to check the permanent porosity of activated **5′**, N_2 sorption experiments were conducted. In Figure 3.4b, the N_2 sorption isotherms of **5′** are displayed. The N_2 sorption isotherms follow a type-I behaviour according to the IUPAC classification. From the N_2 adsorption isotherm, the specific BET surface area and micropore volume (at $p/p_0 = 0.5$) of **5′** were calculated to be 1020 $m^2\ g^{-1}$ and 0.65 $cm^3\ g^{-1}$, respectively.

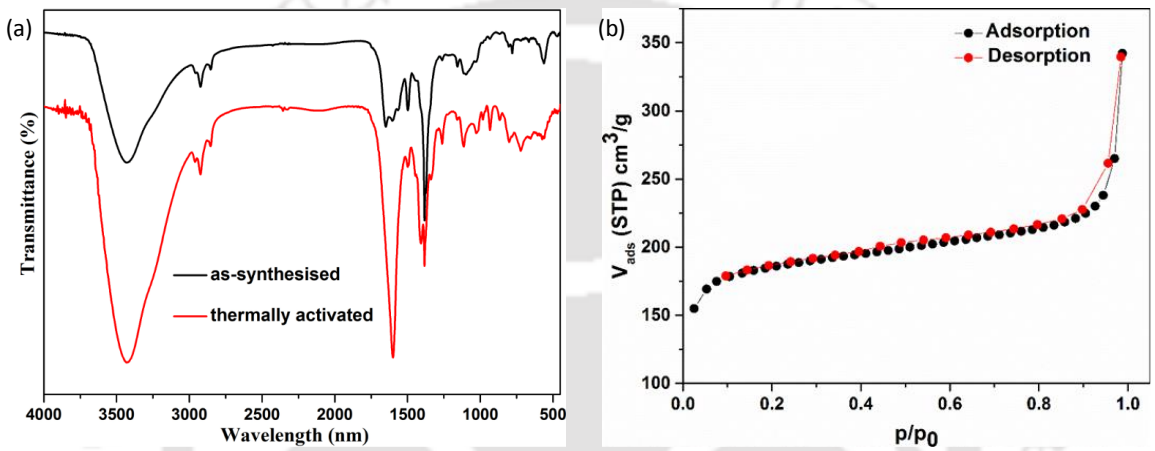

Figure 3.4 (a) FT-IR spectra of the as-synthesized (black) and thermally activated (red) forms of **5**, (b) N_2 sorption isotherms of **5′** collected at −196 °C.

To investigate the thermal stability of **5** and **5′**, thermogravimetric analyses were performed in the range 25-700 °C under air atmosphere. From the TG traces (Figure 3.5a), it can be concluded that the material is stable up to 300 °C. The first weight loss of 13.2 wt% (range: 40-150 °C) in the TG trace of as-synthesized **5** occurs because of the removal of 22 guest H_2O molecules per formula unit (calcd.: 13.0 wt%). In the range 150-210 °C, the second weight loss of 5.0 wt% takes place due to the removal of 2 occluded DMF molecules per formula unit (calcd.: 4.86 wt%). After 210 °C, the material starts to decompose on account of the loss of framework ligands. The TG trace of activated **5′** contains one weight loss stage below the decomposition temperature which is observed because of the removal of the adsorbed water molecules from the pores. The activated material adsorbs water (moisture) from air during storage under ambient conditions before the TG measurement.

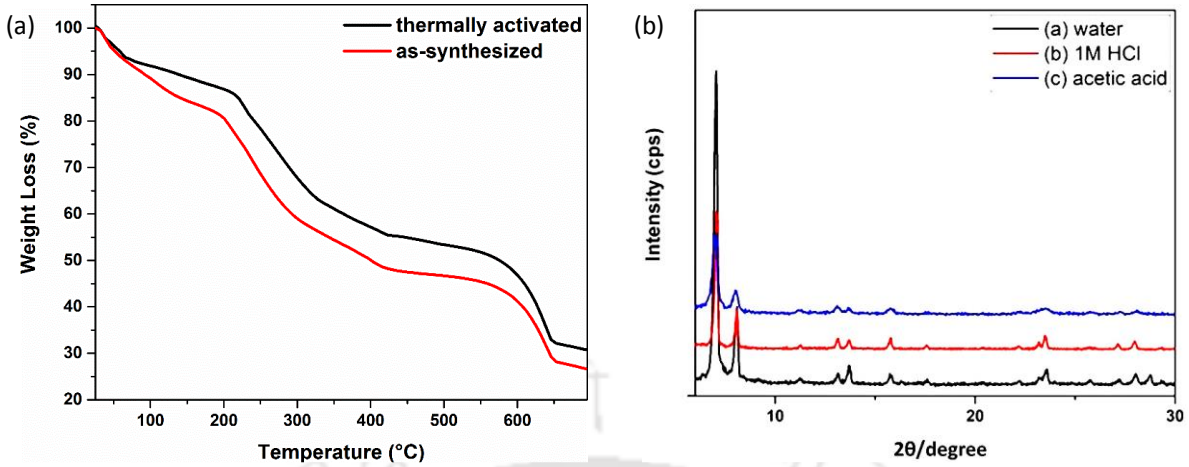

Figure 3.5 (a) TG curves of as-synthesized (red) and thermally activated (black) forms of **5** measured under air atmosphere in the range 25-700 ˚C at a heating rate of 5 °C min^{-1}. (b) XRPD patterns of **5′** after treatment with different liquids.

To check the chemical stability of activated **5′**, the samples (0.1 g) were stirred in various liquids such as water, 1 M HCl and acetic acid (15 mL for each liquid) at ambient temperature for 12 h. Then, the samples were filtered and XRPD experiments were carried out to check their crystallinity. Fortunately, the crystallinity of the compound did not change upon stirring in these liquids, which was obvious from the XRPD patterns (Figure 3.5b). The high stability of the material in both aqueous and acidic media encouraged us to investigate its oxidase-like catalytic activity in acidic medium. To check the phase purity and morphology of **5′**, FE-SEM images were collected. The FE-SEM images (Figure 3.6) confirm the homogeneous crystalline nature of **5′** and the absence of any impure phases.

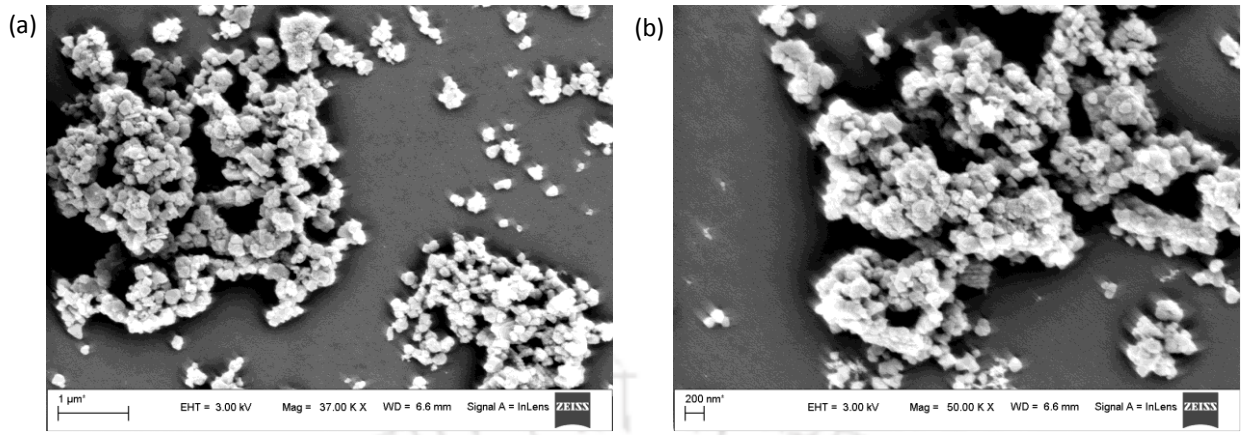

Figure 3.6 FE-SEM images of activated **5′**.

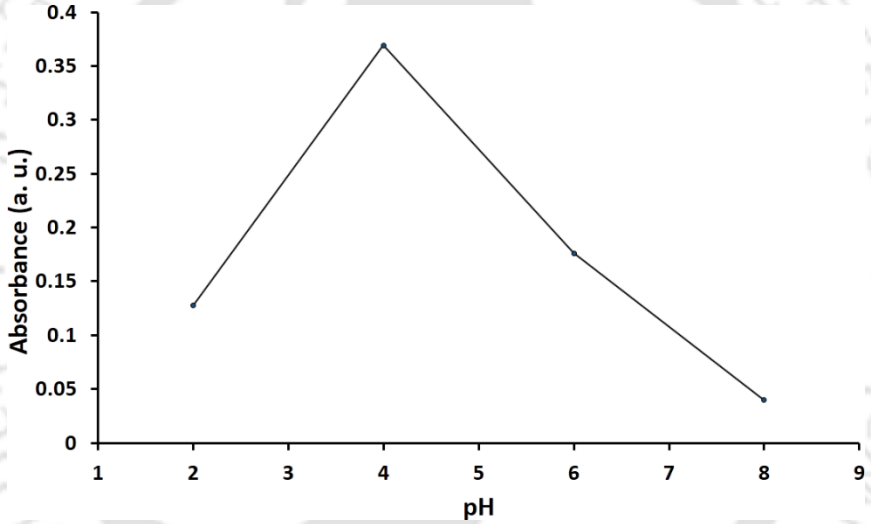

Figure 3.7 Effect of pH on the oxidase-like catalytic activity of **5′** towards TMB.

3.3.4 Oxidase-mimicking properties

At first, we have explored the ability of **5′** to oxidize peroxidase substrates in acidic medium. For this purpose, we have chosen two typical chromogenic peroxidase substrates, namely, 2,2-azinobis (3-ethylbenzothizoline-6-sulfonic acid) (AzBTS) and 3,3′,5,5′-tetramethylbenzidine (TMB). Either a blue (for ox-TMB) or green (for ox-AzBTS) color is produced when these substrates are oxidized in aqueous medium. These substrates have been previously employed for examining the peroxidase-like activity of several MOF materials[23,24,26,28,53-67] where H_2O_2 is employed as an oxidizing agent. On the other hand, the

present cerium-based **5′** is capable of oxidizing both AzBTS and TMB without any external oxidizing agents such as H_2O_2. These facts have been confirmed by the visual color changes of the dye molecules in NaAc buffer (pH = 4) in the presence of **5′** and the corresponding drastic changes in the UV-vis spectra. The pH dependent investigation disclosed that the optimal pH value for the oxidase-like activity of **5′** is ca. 4. The pH values higher or lower than 4 led to a decrease in the oxidase-mimicking activity of the MOF towards TMB (Figure 3.7). For TMB, the formation of a blue-colored solution having absorption maxima at 652 and 370 nm (Figure 3.8a) confirms the formation of the oxidized product (denoted as ox-TMB).[68] In the case of AzBTS, new absorption bands appeared at around 415 and 644 nm, which corroborates the generation of an $ABTS^{\cdot+}$ radical (Figure 3.8b).[69] The green color was developed within one minute, which indicates rapid oxidation of the dye molecule by **5′**. We have systematically studied the influence of catalyst amount on the catalytic activity of **5′**. The change in the absorbance (monitored at 652 nm) of TMB as a function of time upon addition of various amounts of **5′** is plotted in Figure 3.9. This figure reveals that the catalytic activity of **5′** increases when increasing amounts of its suspension are added to the reaction medium. Furthermore, the recyclability of **5′** towards the catalytic oxidation of TMB was investigated up to 4 cycles. The results confirmed that the MOF material is highly stable and reusable up to 4 cycles under the optimized reaction conditions (Figure 3.10).

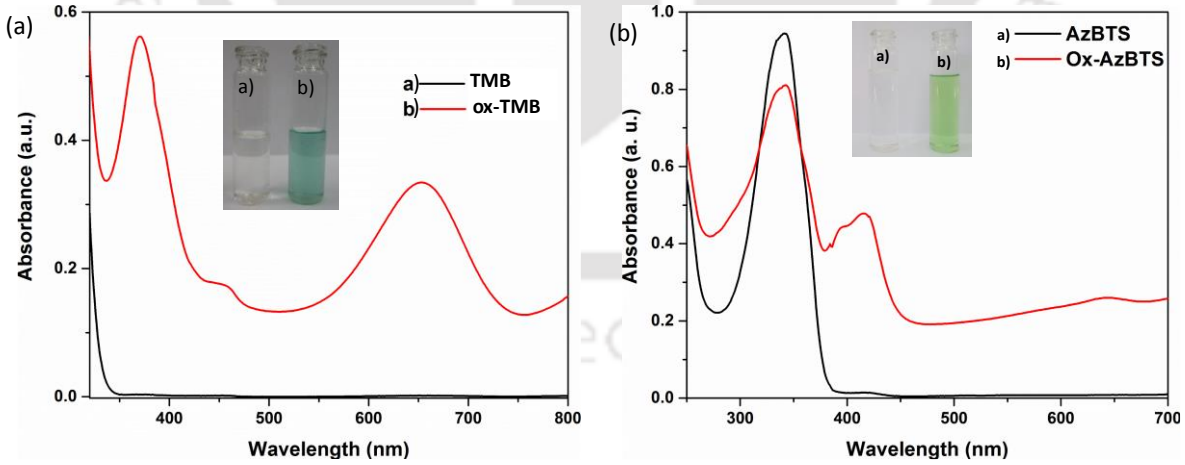

Figure 3.8 UV-vis spectra of (a) TMB and (b) AzBTS in the absence (black) and presence (red) of **5′** in NaAc buffer (0.2 M, pH = 4) at room temperature. Inset: corresponding chromogenic change of peroxidase substrates.

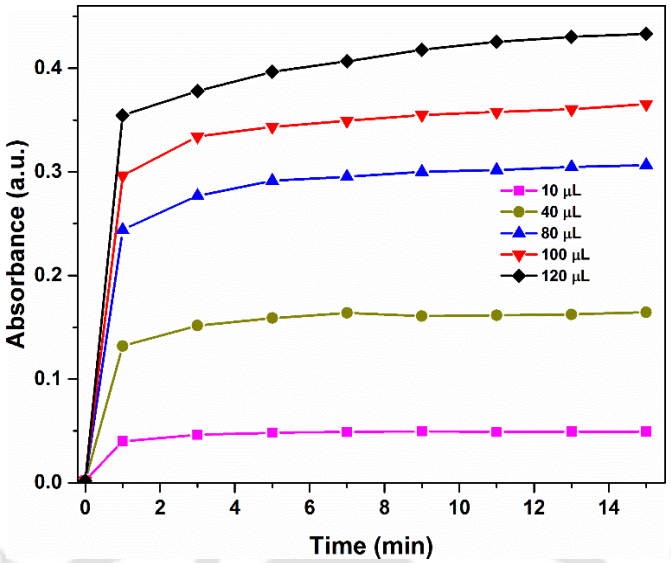

Figure 3.9 Time-dependent variation in the absorbance of TMB (monitored at 652 nm) upon addition of various amounts of **5′** in NaAc buffer (0.2 M, pH = 4).

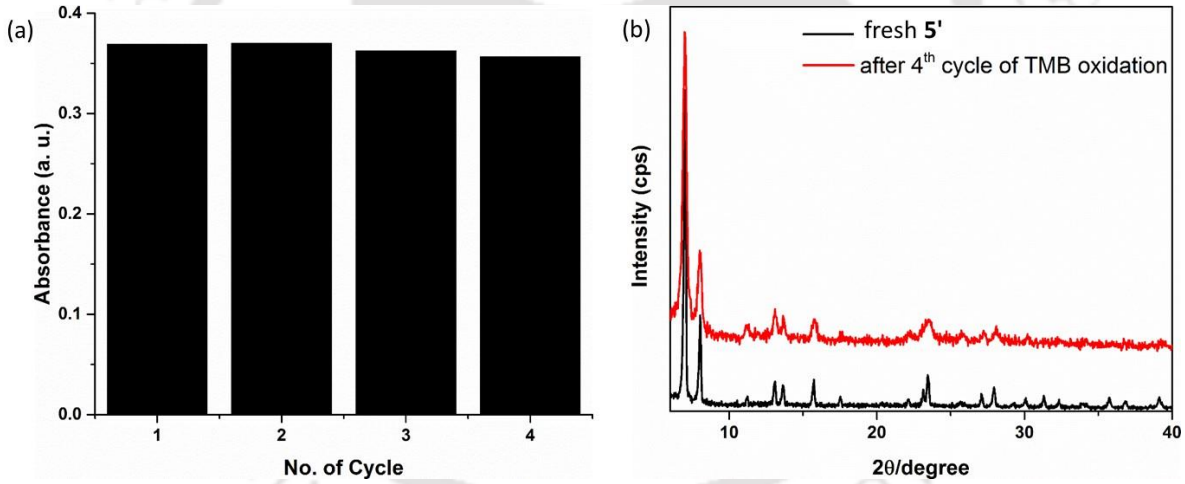

Figure 3.10 (a) Recyclability of the oxidase-like catalytic activity of **5′** towards TMB, (b) XRPD patterns of **5′** before and after oxidase-like catalytic activity towards TMB.

Since **5′** displayed oxidase-like activity, the apparent steady-state kinetic parameters were evaluated for the oxidation of TMB by **5′**. For this purpose, the concentration of TMB was varied. To analyze the kinetic parameters, a typical Michaelis-Menten equation was employed. A Lineweaver-Burk plot (Figure 3.11) was used in order to evaluate the maximum initial velocity (V_{max}) and Michaelis-Menten constant (K_m). From this plot, the values of K_m and V_{max} were estimated to be 88 μM and 0.11 μM s^{-1}, respectively. The K_m value for **5′** is lower than that for a

natural enzyme called horseradish peroxidase (HRP),[50] the recently reported Ce-MOF called MVCM[32] as well as nanoceria[36]. This K_m value suggests that the affinity of **5′** towards TMB molecules is higher as compared to HRP, MVCM as well as nanoceria.

The mechanism of the oxidase-like activity of cerium based **5′** towards TMB may be related to the $Ce^{4+} \leftrightarrow Ce^{3+}$ spontaneous electron shuttling through the framework system. [32] When TMB solution was added to the suspension of **5′** in NaAc buffer (0.2 M, pH = 4.0), the Ce^{4+} ions quickly oxidize TMB to form blue-colored ox-TMB. During this process, Ce^{4+} ions are reduced to Ce^{3+} ions. Then, the latter are naturally converted to Ce^{4+} ions.

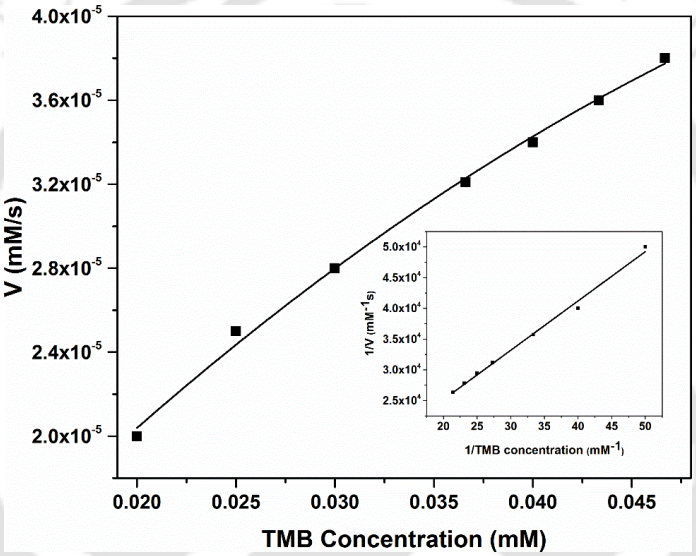

Figure 3.11 Steady-state kinetic assay of **1'** with TMB at pH = 4. Inset: Lineweaver–Burk plot of the double reciprocal of the Michaelis–Menten equation.

3.3.5 Detection of biothiols in NaAc buffer

It has been previously reported that biological thiols (biothiols) have the capability to reduce the blue-colored ox-TMB in aqueous medium, leading to the formation of colorless TMB.[31,32,70,51] Encouraged by this fact, we have developed a colorimetric protocol for the sensing of biothiols. The UV-vis spectra of ox-TMB comprising **5′** in NaAc buffer (0.2 M, pH = 4) were recorded with incremental addition of 0.5 mM solutions of various amino acids (including alanine, cysteine, aspartic acid, arginine, histidine, glycine, leucine, isoleucine, lysine, phenylalanine,

methionine, serine, proline, tryptophan threonine and valine) and other thiol-containing biomolecules (such as homocysteine and glutathione). Among the different amino acids and thiol-containing biomolecules added, rapid decolorization of ox-TMB was observed upon addition of biothiol compounds such as glutathione, cysteine and homocysteine. It can be seen from Figure 3.12-3.14 that the absorbance of ox-TMB decreased dramatically upon gradual addition of 0.5 mM solutions of cysteine, homocysteine and glutathione. In sharp contrast, a negligible change in the absorbance of ox-TMB was observed in the presence of other possibly interfering biomolecules. Even methionine, another sulphur-containing amino acid, resulted in a negligible change in the absorbance of ox-TMB under the presented conditions. These phenomena can be understood considering that after oxidation of TMB by the MOF catalyst to produce bluish colored ox-TMB, the biothiols reverse the process by reduction of ox-TMB back to colorless TMB. The results presented herein suggest that **5′** shows high selectivity towards the sensing of biothiols (glutathione, cysteine and homocysteine).

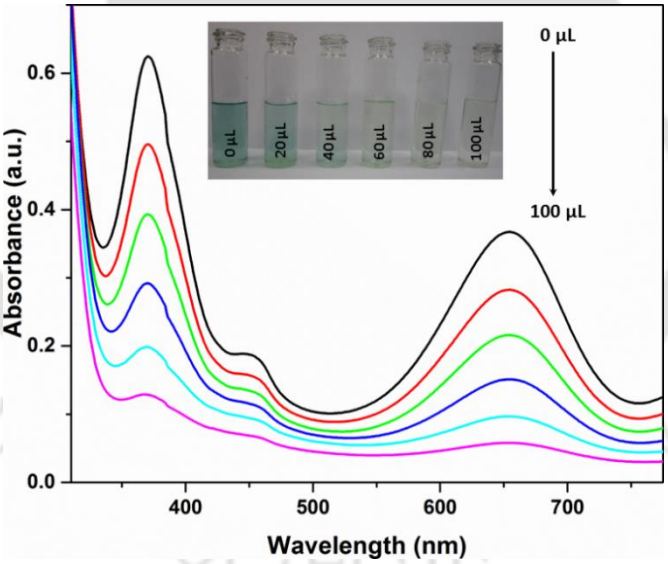

Figure 3.12 Change in the absorption spectrum of ox-TMB upon gradual addition of 0.5 mM cysteine solution in NaAc buffer (0.2 M, pH = 4). Inset: corresponding change in color of the ox-TMB solution.

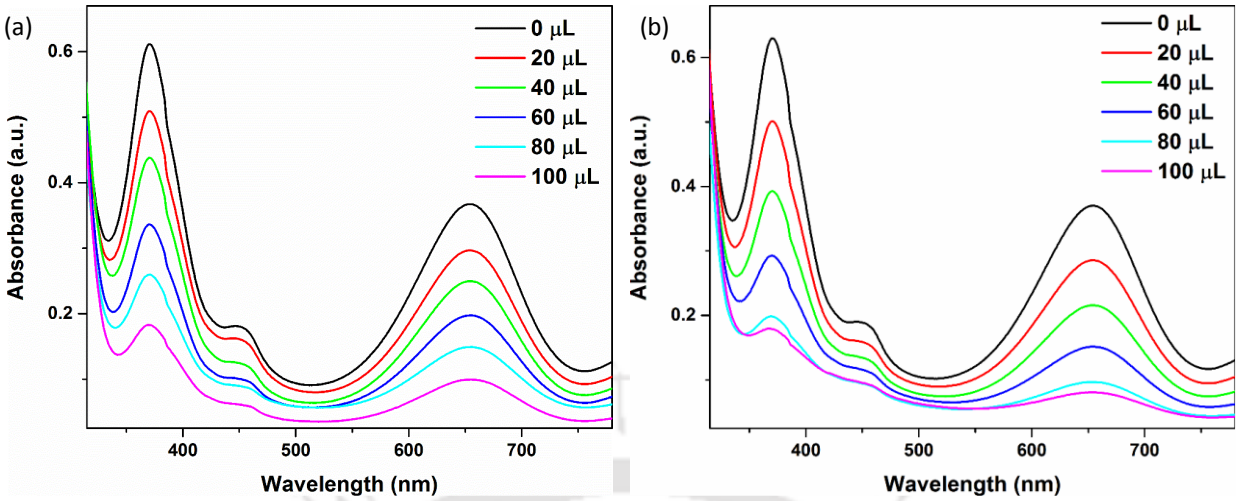

Figure 3.13 Absorbance spectra of ox-TMB in presence of glutathione (a) and homocysteine (b) at varying concentration.

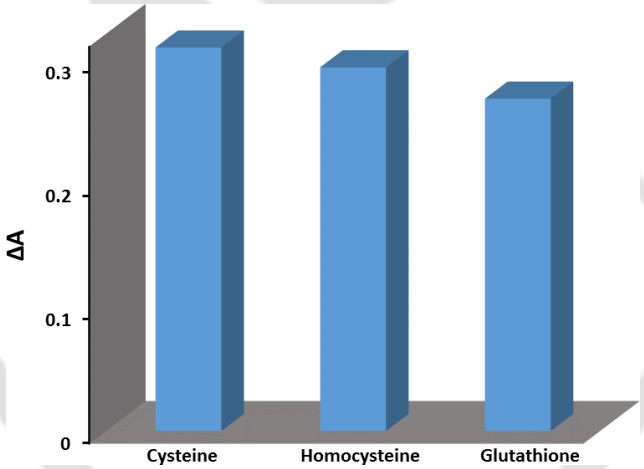

Figure 3.14. Change in the absorbance of ox-TMB in presence of different biothiols.

In order to investigate the selectivity of **5′** towards the sensing of biothiols, the UV-vis spectral response of the MOF system (i.e., **5′** containing ox-TMB in aqueous medium) was measured towards biothiols in the existence of several potentially interfering amino acids. It has been observed that the absorbance of the MOF system changed significantly only after the introduction of biothiols to the reaction medium, whereas the introduction of other amino acids caused negligible changes in the absorbance (Figure 3.15). Therefore, the selective colorimetric sensing of biothiols in the presence of other potentially competing amino acids can be achieved by

this method. The LOD values were estimated by employing the following equation: LOD = 3σ/K as previously reported.[50] The LOD values for cysteine, homocysteine and glutathione by this colorimetric biosensing technique were estimated to be 0.150, 0.132 and 0.125 μM, respectively. These LOD values are either similar or lower as compared to previously reported MOFs[31,33,72] exhibiting selective detection properties towards biothiols.

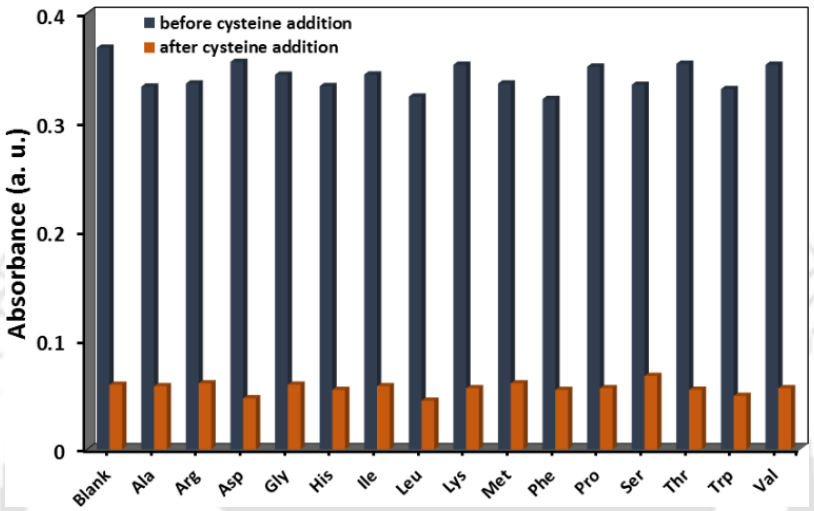

Figure 3.15 Absorbance of ox-TMB (monitored at 652 nm) upon addition of a potentially competing amino acid, followed by the addition of cysteine in NaAc buffer (0.2 M, pH = 4).

3.3.6 Detection of biothiols in human blood plasma

It is well known that human blood plasma contains high concentrations of cysteine (165-335 μM),[73] homocysteine (9-13 μM)[74] and glutathione (14-20 μM).[75] Therefore, the ability of **5′** to detect cysteine in human blood plasma (HBP) was evaluated. The concentration of cysteine in HBP samples was determined by utilizing the standard addition method. The recovery experiments were carried out with two HBP samples spiked with cysteine. As shown in Table 3.2, the recovery for cysteine measurement ranges from 98 to 102% with low RSD (n = 3) values. These results confirm the suitability of the developed protocol for the sensing of cysteine in HBP samples.

Table 3.2 Concentrations of cysteine found in diluted HBP samples determined by the standard addition technique.

HBP Sample	Without Spiking (μM)	Cysteine Added (μM)	Cysteine Found (μM)	Recovery (%)	RSD (%)
Sample 1	65.4	10	9.8	98	1.8
Sample 2	110.5	50	50.1	100.2	2.1
		10	0.1	101	1.6
		50	51.2	102.4	1.2

3.3.7 Catalytic oxidation of thiol compounds

MOFs are considered to be promising heterogeneous catalysts for organic transformations including oxidation reactions.[76,77] MOFs have previously served as heterogeneous catalysts in the aerobic oxidation of cycloalkanes, hydrocarbons, benzyl alcohol, thiols, amines and sulfides.[78] Recently, research interest in the construction of MOF-type heterogeneous catalysts for the aerobic oxidation of organic substrates has grown rapidly.[76] Inspired by these observations, we have investigated the catalytic activity of **5′** using thiophenol as a model substrate under an oxygen atmosphere, as shown in Scheme 3.1.

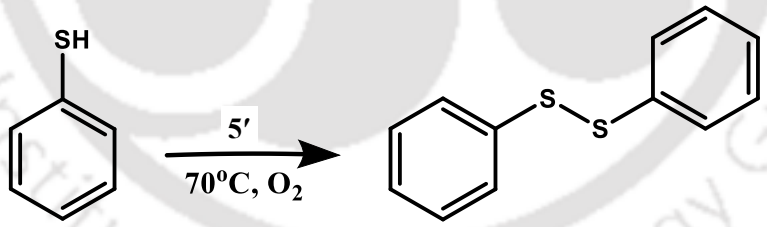

Scheme 3.1 Oxidation of thiophenol to 1,2-diphenyldisulfide in presence of catalyst **5′** and molecular oxygen.

Aerobic oxidation of thiophenol in the absence of **5′** exhibited only 9% conversion at 70 °C in methanol after 12 h (entry 1, Table 3.3). In sharp contrast, the oxidation of thiophenol with **5′** using tert-butylhydroperoxide (TBHP) as an oxidant resulted in 65% conversion after 12 h in acetonitrile (entry 2, Table 3.3). On the other hand, the oxidation of thiophenol using molecular oxygen afforded 22% conversion (entry 3, Table 3.3) in acetonitrile under the same conditions.

Interestingly, the aerobic oxidation of thiophenol afforded quantitative conversion to the corresponding 1,2-diphenyldisulfide in the presence of **5′** as a catalyst in methanol (entry 4, Table 3.3) after 12 h. The time-conversion curve for the oxidation of thiophenol by employing **5′** (catalyst) and molecular oxygen is shown in Figure 3.16. Under similar conditions, the oxidation of thiophenol using catalyst **5′** and molecular oxygen in the presence of pyridine significantly reduced the conversion of thiophenol to 27% (entry 5, Table 3.3). This experiment clearly demonstrates the negative role of pyridine by acting as a catalyst poison through coordination with the Lewis acid sites, thus inhibiting the coordination of thiophenol with cerium ions. It has already been reported that the ceric ammonium nitrate (CAN) ion is highly effective in the catalytic oxidation of thiols and thioethers utilizing molecular oxygen.[40] In this context, a control experiment in the presence of CAN was performed and the observed results are given in Table 3.3. It is clear from these data that the reaction proceeds in the presence of CAN; however, it could not reach completion because of the absence of adequate Ce(IV) ions in the reaction medium (entry 6, Table 3.3). In contrast, the reaction in the presence of **5′** resulted in complete conversion due to the presence of a sufficient amount of Ce(IV) ions as active sites in the framework, thus proving the merit of heterogeneity.

Table 3.3 Oxidation of thiophenol to 1,2-diphenyldisulfide in the presence of **5′** under various conditions.[a]

Sl. No.	Catalyst (mg)	Oxidant	Solvent	Conversion (%)
1	---	O_2	CH_3OH	9
2[b]	20	TBHP	CH_3CN	65
3	20	O_2	CH_3CN	22
4	20	O_2	CH_3OH	100
5[c]	20	O_2	CH_3OH	27
6[d]	27	O_2	CH_3OH	68
7	run-1	O_2	CH_3OH	100
8	run-2	O_2	CH_3OH	98
9	run-3	O_2	CH_3OH	97
10	run-4	O_2	CH_3OH	96

[a] Reaction conditions: thiophenol (1 mmol), solvent (2 mL), **5′** (20 mg), 70 °C, 12 h.

[b] with 1 mmol TBHP.

[c] with 1 mmol pyridine.

[d] with CAN.

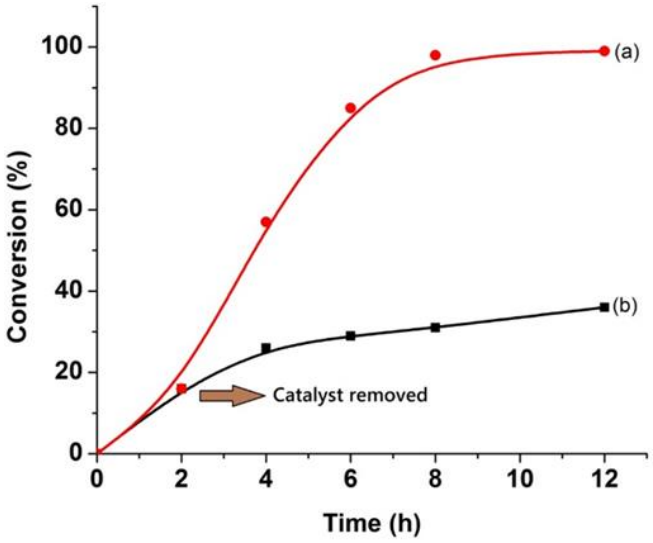

Figure 3.16 Hot filtration experiment for the aerobic oxidation of thiophenol (a) with and (b) without **5′**. Reaction conditions: thiophenol (1 mmol), CH_3OH (2 mL), **5′** (20 mg), 70 °C.

A hot filtration experiment was performed in order to verify the heterogeneity of the reaction. Therefore, the oxidation of thiophenol was carried out in the presence of **5′** and molecular oxygen under the optimum reaction conditions. The catalyst **5′** was filtered off after 2 h and the reaction was prolonged with the supernatant liquid for another 10 h. The results obtained from these experiments are shown in Figure 3.16. These results confirm the heterogeneity of the oxidation catalysis reaction. However, there was marginal enhancement in the conversion of thiophenol after removal of the catalyst, which is indicative of the contribution from the blank control. In addition, the recyclability of **5′** for the oxidation of thiophenol with molecular oxygen was examined under the optimized reaction conditions. The conversion of thiophenol observed in the 1st, 2nd, 3rd and 4th cycles after 12 h corresponded to 100%, 98%, 97% and 96%, respectively (entry 7-10, Table 3.3).

Table 3.4 Oxidation of various thiophenols in the presence of **5′** and molecular oxygen.[a]

Sl. No.	Thiol	Disulfide	Yield (%)[b]
1	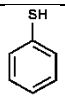	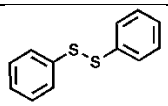	100
2	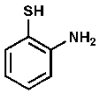	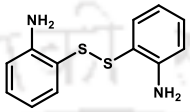	71
3	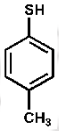	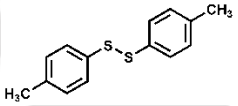	97
4	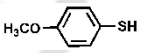	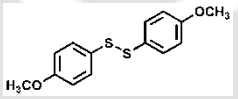	59
5		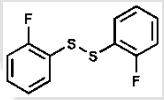	87
6	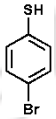	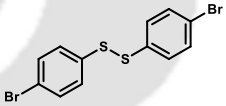	82
7	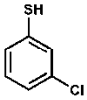	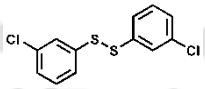	91
8	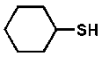	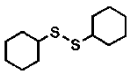	26

[a] Reaction conditions: Thiol (1 mmol), **5′** (20 mg), methanol (2 mL), 70 °C, 12 h, molecular oxygen.

[b] Deduced by GC employing external standard method.

The encouraging results concerning the aerobic oxidation of thiophenol using **5′** as a catalyst prompted us to explore the versatility of this catalyst with substituted thiophenols. The results of these experiments are summarized in Table 3.4. Thiophenols with electron donating substituents such as amino, methyl and methoxy at 2-, 4- and 4-positions exhibited the respective disulfides in 71, 97 and 59% yields after 12 h (entries 2-4, Table 3.4). On the other hand, thiophenols containing electron withdrawing groups like fluoro, chloro and bromo at 2, 3- and 4-positions resulted in 87, 91 and 82% yields of the corresponding disulfides (entries 5-7, Table 3.4). Similarly, cyclohexanethiol gave 26% yield of the corresponding disulfide under identical conditions (entry 8, Table 3.4). Furthermore, the crystallinity of the catalyst recovered after the 4th cycle was very similar to that of the fresh **5′**, as corroborated by the corresponding XRPD patterns (Figure 3.17). The structural robustness of the MOF catalyst during the catalytic cycles was confirmed by these experiments.

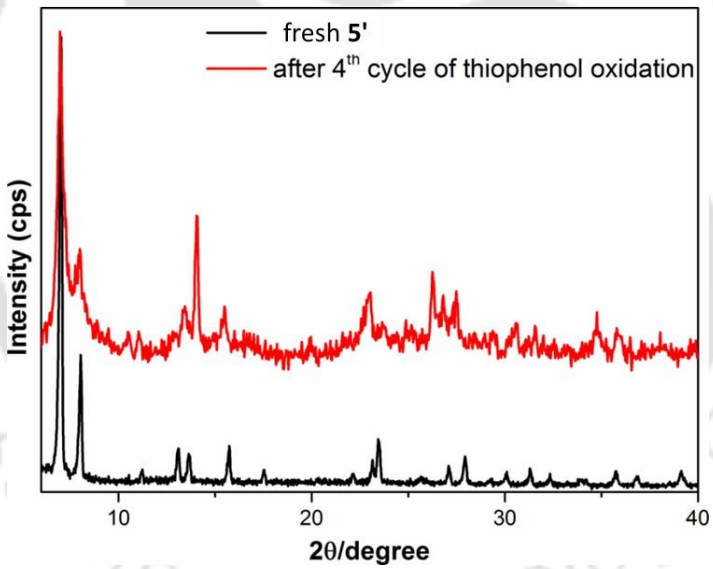

Figure 3.17 XRPD patterns of **5′** before and after catalytic oxidation of thiophenol.

3.4 Conclusions

We have successfully synthesized a cerium-based MOF material (**5**) incorporating 3,4-dimethylthieno[2,3-b]thiophene-2,5- dicarboxylic acid as a ligand under solvothermal conditions. To ensure the phase purity of the material, a comprehensive characterization study was carried out by employing methods like XRPD, XPS, FT-IR spectroscopy, TG and N_2 sorption experiments.

According to the N_2 sorption experiments, **5′** exhibited a large specific BET surface area (1020 $m^2 g^{-1}$). As gleaned from the XRPD measurements, the material displayed high structural robustness in water, 1 M HCl and acetic acid. Remarkably, the compound showed intrinsic oxidase-mimicking catalytic activity due to the existence of redox-active cerium atoms in the framework. The excellent oxidase-like catalytic properties of the material were demonstrated by employing typical chromogenic peroxidase substrates: TMB and AzBTS. The oxidase-mimicking activity of **5′** allowed us to establish a colorimetric sensing platform for biothiols in NaAc buffer (0.2 M, pH = 4). In addition, the MOF displayed a sensing ability towards cysteine in human blood plasma. Owing to the existence of framework Ce(III)/ Ce(IV) sites, significant heterogeneous catalytic performance of **5′** was observed in the oxidation of thiol compounds using molecular oxygen. The MOF material is reusable, both as a heterogeneous catalyst and a colorimetric biosensor. Moreover, the compound is highly stable, low-cost and recyclable. These features along with high biomimetic and heterogeneous catalytic activities make the present compound suitable for biological sample analysis, medical diagnostics as well as for industrial oxidation catalysis.

3.5 References

1. T. R. Lin, L. S. Zhong, L. Q. Guo, F. F. Fu and G. N. Chen, *Nanoscale*, 2014, **6**, 11856-11862.
2. Y. Song, W. Wei and X. Qu, *Adv. Mater.*, 2011, **23**, 4215-4236.
3. M. A. Mansoor, A. M. Svardal and P. M. Ueland, *Anal. Biochem.*, 1992, **200**, 218-229.
4. T. W. Kang, S.-J. Jeon, H.-I. Kim, J. H. Park, D. Yim, H.-R. Lee, J.-M. Ju, M.-J. Kim and J.-H. Kim, *ACS Nano*, 2016, **10**, 5346-5353.
5. H. Cahová, L. Havran, P. Brázdilová, H. Pivoňková, R. Pohl, M. Fojta and M. Hocek, *Angew. Chem.*, 2008, **120**, 2089-2092.
6. Y. Shao, J. Wang, H. Wu, J. Liu, I. A. Aksay and Y. Lin, *Electroanalysis*, 2010, **22**, 1027-1036.
7. V. L. Arcus, E. J. Prentice, J. K. Hobbs, A. J. Mulholland, M. W. Van der Kamp, C. R. Pudney, E. J. Parker and L. A. Schipper, *Biochemistry*, 2016, **55**, 1681-1688.
8. Y. Lin, J. Ren and X. Qu, *Acc. Chem. Res.*, 2014, **47**, 1097-1105.
9. M. Liang, K. Fan, Y. Pan, H. Jiang, F. Wang, D. Yang, D. Lu, J. Feng, J. Zhao and L. Yang, *Anal. Chem.*, 2012, **85**, 308-312.
10. J. Liu and Y. Lu, *J. Am. Chem. Soc.*, 2003, **125**, 6642-6643.

11. Y. Zhang, J. Zhang, X. Huang, X. Zhou, H. Wu and S. Guo, *Small*, 2012, **8**, 154-159.
12. H. Li, W. Kong, J. Liu, M. Yang, H. Huang, Y. Liu and Z. Kang, *J. Mater. Chem. B*, 2014, **2**, 5652-5658.
13. S. Song, Y. Qin, Y. He, Q. Huang, C. Fan and H.-Y. Chen, *Chem. Soc. Rev.*, 2010, **39**, 4234-4243.
14. A. Saxena, A. Kumar and S. Mozumdar, *J. Mol. Catal. A: Chem.*, 2007, **269**, 35-40.
15. H. P. Xiang, M. Z. Rong and M. Q. Zhang, *ACS Sustainable Chem. Eng.*, 2016, **4**, 2715-2724.
16. A. Ogawa, Y. Nishiyama, N. Kambe, S. Murai and N. Sonoda, *Tetrahedron Lett.*, 1987, **28**, 271-3274.
17. M. H. Ali and M. McDermott, *Tetrahedron Lett.*, 2005, **46**, 3583-3585.
18. Y.-B. Huang, J. Liang, X.-S. Wang and R. Cao, *Chem. Soc. Rev.*, 2017, **46**, 126-157.
19. F.-Y. Yi, D. Chen, M.-K. Wu, L. Han and H.-L. Jiang, *ChemPlusChem*, 2016, **81**, 675-690.
20. Z. Kang, L. Fan and D. Sun, *J. Mater. Chem. A*, 2017, **5**, 10073-10091.
21. J.-W. Zhang, H.-T. Zhang, Z.-Y. Du, X. Wang, S.-H. Yu and H.-L. Jiang, *Chem. Commun.*, 2014, **50**, 1092-1094.
22. D. Chen, B. Li, L. Jiang, D. Duan, Y. Li, J. Wang, J. He and Y. Zeng, *RSC Adv.*, 2015, **5**, 97910-97917.
23. F. Cui, Q. Deng and L. Sun, *RSC Adv.*, 2015, **5**, 98215-98221
24. L. Ai, L. Li, C. Zhang, J. Fu and J. Jiang, *Chem. Eur. J.*, 2013, **19**, 15105-15108.
25. Z. Yuan, F. Lu, M. Peng, C.-W. Wang, Y.-T. Tseng, Y. Du, N. Cai, C.-W. Lien, H.-T. Chang, Y. He and E. S. Yeung, *Anal. Chem.*, 2015, **87**, 7267-7273.
26. Y. L. Liu, X. J. Zhao, X. X. Yang and Y. F. Li, *Analyst*, 2013, **138**, 4526-4531.
27. Z. J. Sun, J. Z. Jiang and Y. F. Li, *Analyst*, 2015, **140**, 8201-8208.
28. Y. Wang, Y. Zhu, A. Binyam, M. Liu, Y. Wu and F. Li, *Biosens. Bioelectron.*, 2016, **86**, 432.
29. D. Feng, Z.-Y. Gu, J.-R. Li, H.-L. Jiang, Z. Wei and H.-C. Zhou, *Angew. Chem. Int. Ed.*, 2002, **51**, 10307-10310.
30. Y. Chen, T. Hoang and S. Ma, *Inorg. Chem.*, 2012, **51**, 12600-12602.
31. Z. W. Jiang, Y. Liu, X. Hu and Y. Li, *Anal. Methods*, 2014, **6**, 5647-5651.
32. Y. Xiong, S. Chen, F. Ye, L. Su, C. Zhang, S. Shen and S. Zhao, *Chem. Commun.*, 2015, **51**, 4635-4638.
33. Z. Hu, X. Jiang, F. Xu, J. Jia, Z. Long and X. Hou, *Talanta*, 2016, **158**, 276-282.

34. A. Dhakshinamoorthy, M. Alvaro and H. Garcia, *Chem. Commun.*, 2010, **46**, 6476-6478.

35. I. Celardo, J. Z. Pedersen, E. Traversa and L. Ghibelli, *Nanoscale*, 2011, **3**, 1411-1420.

36. A. Asati, S. Santra, C. Kaittanis, S. Nath and J. M. Perez, *Angew. Chem. Int. Ed.*, 2009, **48**, 2308-2312.

37. D. H. Kim, J. Hur, H. G. Park and M. I. Kim, *Biosens. Bioelectron.*, 2017, **93**, 226-233.

38. M. Ornatska, E. Sharpe, D. Andreescu and S. Andreescu, *Anal. Chem.*, 2011, **83**, 4273-4280.

39. H. Firouzabadi, N. Iranpoor, H. Parham, A. Sardarian and J. Toofan, *Synth. Commun.*, 1984, **14**, 717-723.

40. V. Sridharan and J. C. Menéndez, *Chem. Rev.*, 2010, **110**, 3805-3849.

41. S. H. Mashraqui, H. Hariharasubrahmanian and S. Kumar, *Synthesis*, 1999, 2030-2032.

42. S. Mostakim, M. Grzywa, D. Volkmer and S. Biswas, *J. Solid State Chem.*, 2015, **232**, 221-227.

43. K. Wang, H. Huang, W. Xue, D. Liu, X. Zhao, Y. Xiao, Z. Li, Q. Yang, L. Wang and C. Zhong, *CrystEngComm*, 2015, **17**, 3586-3590.

44. L. Valenzano, B. Civalleri, S. Chavan, S. Bordiga, M. H. Nilsen, S. Jakobsen, K. P. Lillerud and C. Lamberti, *Chem. Mater.*, 2011, **23**, 1700-1718.

45. C. Hennig, A. Ikeda-Ohno, W. Kraus, S. Weiss, P. Pattison, H. Emerich, P. M. Abdala and A. C. Scheinost, *Inorg. Chem.*, 2013, **52**, 11734-11743.

46. R. Jain, A. Dubey, M. K. Ghosalya and C. S. Gopinath, *Catal. Sci. Technol.*, 2016, **6**, 1746-1756.

47. E. Bêche, P. Charvin, D. Perarnau, S. Abanades and G. Flamant, *Surf. Interface Anal.*, 2008, **40**, 264-267.

48. G. Zhou, Y. Yao, X. Zhao, X. Liu, B. Sun and A. Zhou, *RSC Adv.*, 2016, **6**, 59370-59374.

49. M. S. P. Francisco, V. R. Mastelaro, P. A. P. Nascente and A. O. Florentino, *J. Phys. Chem. B*, 2001, **105**, 10515-10522.

50. S. Garain, K. Barman, T. K. Sinha, S. Jasimuddin, J. Haeberle, K. Henkel, D. Schmeisser and D. Mandal, *ACS Appl. Mater. Interfaces*, 2016, **8**, 21294-21301.

51. R. Dalapati and S. Biswas, *Sens. Actuators., B*, 2017, **239**, 759-767.

52. R. Dalapati, B. Sakthivel, A. Dhakshinamoorthy, A. Buragohain, A. Bhunia, C. Janiak and S. Biswas, *CrystEngComm*, 2016, **18**, 7855-7864.

53. F.-X. Qin, S.-Y. Jia, F.-F. Wang, S.-H. Wu, J. Song and Y. Liu, *Catal. Sci. Tech.*, 2013, **3**, 2761-2768.

54. Y. Chen, V. Lykourinou, T. Hoang, L.-J. Ming and S. Ma, *Inorg. Chem*, 2012, **51**, 9156-9158.

55. H. Tan, Q. Li, Z. Zhou, C. Ma, Y. Song, F. Xu and L. Wang, *Anal. Chim. Acta*, 2015, **856**, 90-95.

56. Y. L. Liu, W. L. Fu, C. M. Li, C. Z. Huang and Y. F. Li, *Anal. Chim. Acta*, 2015, **861**, 55-61.

57. Q. Zhu, Y. Chen, W. Wang, H. Zhang, C. Ren, H. Chen and X. Chen, *Sens. Actuators, B.*, 2015, **210**, 500-507.

58. F. Luo, Y. Lin, L. Zheng, X. Lin and Y. Chi, *ACS Appl. Mater. Interfaces*, 2015, **7**, 11322-11329.

59. J.-W. Zhang, H.-T. Zhang, Z.-Y. Du, X. Wang, S.-H. Yu and H.-L. Jiang, *Chem. Commun.*, 2014, **50**, 1092-1094.

60. D. Chen, B. Li, L. Jiang, D. Duan, Y. Li, J. Wang, J. He and Y. Zeng, *RSC Adv.*, 2015, **5**, 97910-97917.

61. L. Su, Y. Xiong, H. Yang, P. Zhang and F. Ye, *J. Mater. Chem. B*, 2016, **4**, 128-134.

62. Y. Chen, V. Lykourinou, T. Hoang, L.-J. Ming and S. Ma, *Inorg. Chem.*, 2012, **51**, 9156-9158.

63. Y. Chen, T. Hoang and S. Ma, *Inorg. Chem.*, 2012, **51**, 12600-12602.

64. D. Feng, Z.-Y. Gu, J.-R. Li, H.-L. Jiang, Z. Wei and H.-C. Zhou, *Angew. Chem. Int. Ed.*, 2012, **51**, 10307-10310

65. Y. Chen and S. Ma, *Dalton Trans.*, 2016, **45**, 9744-9753.

66. K. Müller-Buschbaum, F. Beuerle and C. Feldmann, *Microporous Mesoporous Mater.*, 2015, **216**, 171-199.

67. E.-L. Zhou, C. Qin, P. Huang, X.-L. Wang, W.-C. Chen, K.-Z. Shao and Z.-M. Su, *Chem. Eur. J.*, 2015, **21**, 11894-11898.

68. X. Zhang, X. Bi, W. Di and W. Qin, *Sens. Actuators, B.*, 2016, **231**, 714-722.

69. A. Garcia-Leis, D. Jancura, M. Antalik, J. Garcia-Ramos, S. Sanchez-Cortes and Z. Jurasekova, *Phys. Chem. Chem. Phys.*, 2016, **18**, 26562-26571.

70. Z. Hu, X. Jiang, F. Xu, J. Jia, Z. Long and X. Hou, *Talanta*, 2016, **158**, 276-282.

71. H. S. Jung, X. Chen, J. S. Kim and J. Yoon, *Chem. Soc. Rev.*, 2013, **42**, 6019-6031.

72. Y. Xiong, S. Chen, F. Ye, L. Su, C. Zhang, S. Shen and S. Zhao, *Chem. Commun.*, 2015, **51**, 4635-4638.

73. Y. Liu, X. Lv, M. Hou, Y. Shi and W. Guo, *Anal. Chem.*, 2015, **87**, 11475-11483.

74. R. S. Vasan, A. Beiser, R. B. D'Agostino, D. Levy, J. Selhub, P. F. Jacques, I. H. Rosenberg and P. W. F. Wilson, *JAMA*, 2003, **289(10)**, 1251-1257.

75. D. Ścibior, M. Skrzycki, M. Podsiad and H. Czeczot, *Clin. Biochem.*, 2008, **41**, 852-858.

76. A. Dhakshinamoorthy, A. M. Asiri and H. Garcia, *Chem. Eur. J.*, 2016, **22**, 8012-8024.

77. A. Dhakshinamoorthy, M. Alvaro and H. Garcia, *Catal. Sci. Technol.*, 2011, **1**, 856-867.

78. A. Dhakshinamoorthy, M. Alvaro and H. Garcia, *Chem. Commun.*, 2012, **48**, 11275-11288.

Chapter 4

A dinitro-functionalized Zr(IV)-based metal-organic framework as colorimetric and fluorogenic probe for highly selective detection of hydrogen sulphide

This chapter describes the synthesis, characterization of dinitro-functionalized Zr(IV)-based DUT-52-$(NO_2)_2$ MOF (DUT = Dresden University of Technology). The activated material acts as a colorimetric and fluorogenic turn-on probe for the sensing of H_2S under physiological conditions (HEPES buffer, pH = 7.4, temperature = 37 °C). The reduction of nitro functional group by H_2S to amine functional group is responsible for turn-on sensing. Remarkably, the compound exhibited visually detectable colorimetric and fluorogenic responses towards H_2S under day light as well as under UV irradiation. In addition, the probe could be used for the detection of H_2S in human blood plasma and as well as living cells.

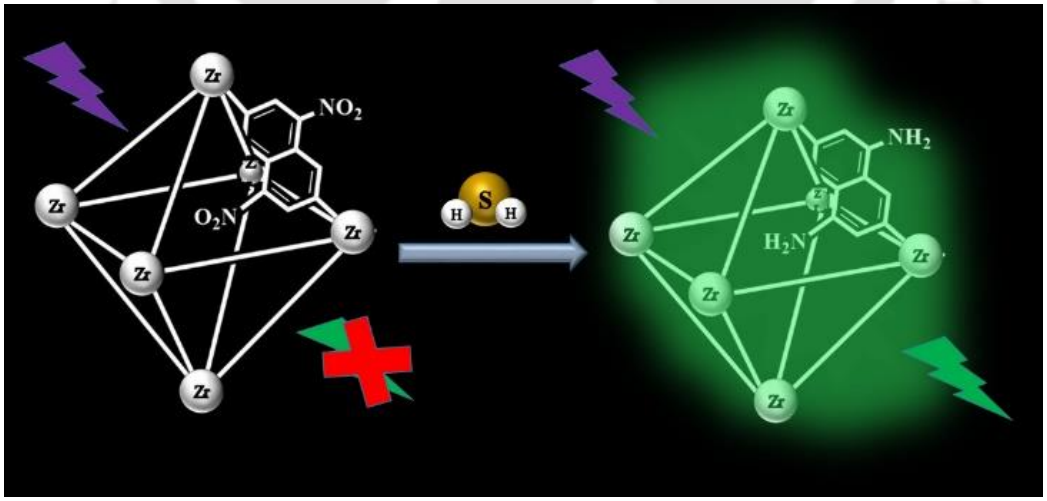

SENSORS and ACTUATORS B Chemical

R. Dalapati, S. N. Balaji, V. Trivedi, L. Khamari, S. Biswas, *Sens. Actuators, B.*, 2017, **245**, 1039.

4.1 Introduction

Hydrogen sulfide (H_2S) has a unpleasant rotten egg smell and is considered as a toxic gas.[1] It is released from geothermal, anthropogenic and biological sources and exerts harmful effects to both human beings and the environment.[2] It has been recently recognized as one of the three important biosynthetic gasotransmitters including nitric oxide (NO) and carbon monoxide (CO).[3-5] Thus, H_2S can function as a signal transmitter in living organisms.[6,7] This gas, which is endogenously generated by enzymes, is engaged in regulating a variety of important genes.[8-10] In various living organisms, H_2S is used for immune response, signal transduction and energy production.[11-15] It is also involved in various other physiological processes like regulation of blood pressure, neurotransmission, anti-inflammatory action, angiogenesis, anti-oxidation and apoptosis.[16-21] The H_2S concentration in biological systems varies from tens of nanomoles to hundreds of micromoles per liter.[22] The abnormal levels of produced H_2S in human body can cause numerous pathological processes such as Alzheimer's disease,[23] diabetic complications,[24] liver cirrhosis,[25] Down's syndrome[26] and cancer.[27] In the diagnosis and treatment of these diseases, H_2S is a potential target. Owing to its considerable role in biological systems, the detection as well as controlling the levels of H_2S in highly demanding for investigating and better understanding of its physiological and pathological functions.

Several conventional detection techniques such as gas chromatography,[22] high performance liquid chromatography,[28,29] electrochemical analysis,[30] colorimetry[31,32] and metal-induced sulphide precipitation[33] have been employed so far for detecting the H_2S level (Table 4.1). However, these detection methods are not suitable for the real-time detection because of the complicated instrumentation, lack of portability, highly reactive and diffusible characteristics of H_2S. The in-situ detection of H_2S in living biosamples by using these techniques requires post-mortem and destruction of tissues or cells,[34,35] which restricts their use. On the other hand, fluorescence based detection techniques provide several advantages over other methods due to their simplicity, high selectivity and sensitivity, short response time, non-destructive characteristics, great temporal and spatial sampling capability, real-time monitoring and easy sample processing.[36,37] Since the detection takes place relative to dark background, fluorescent turn-on probes are able to avoid incorrect response and enhance signal to noise ratio.[13] An ideal luminescent probe should feature turn-on behaviour, rapid response time, high sensitivity and excellent selectivity over competing biochemical species.[34,35]

Numerous fluorescent turn-on probes for the sensing of H_2S have been reported (Table 4.1) so far in the literature.[10,34,38-51] Nevertheless, combining all the above-mentioned advantages in one fluorescent probe has still remained a challenging task. Therefore, the design and synthesis of fluorescence probes for the detection of endogenous H_2S are attracting immense research interests in recent years.

Table 4.1 Comparison of the various existing materials and methods for the sensing of H_2S.

Sl. No.	Sensor Material	Type of Material	Method Used	Response Time (s)	Detection Limit	Analyte Used	Ref.
1	Zr-DUT-52-$(NO_2)_2$	MOF	fluorescence	3300	20.0 µM	Na_2S	this work
2	Ce-UiO-66-N_3	MOF	fluorescence	760	12.2 µM	NaHS	52
3	Ce-UiO-66-NO_2	MOF	fluorescence	760	34.84 µM	NaHS	53
4	Zr-UiO-66-N_3	MOF	fluorescence	180	176.7 µM	NaHS	54
5	Zr-UiO-66-NO_2	MOF	fluorescence	480	95.4 µM	NaHS	54
6	IRMOF-3-N_3	MOF	fluorescence	< 120	28.3 µM	NaHS	55
7	Zr-UiO-66-N_3	MOF	fluorescence	180	118 µM	Na_2S	56
8	Zr-UiO-66-NO_2	MOF	fluorescence	≈ 460	188 µM	Na_2S	56
9	Al-TCPP-Cu	MOF	fluorescence	-	-	NaHS	49
10	Al-MIL-101-N_3	MOF	fluorescence	-	100 µM (UV)	Na_2S	57
11	Eu^{3+}/Cu^{2+}@UiO-66-$(COOH)_2$	MOF	fluorescence	30	5.45 µM	NaHS	58
12	Fe-MIL-88-NH_2	MOF	fluorescence	≈ 360	10 µM	NaHS	59
13	$Zn_3(BTC)_2 \cdot 12 H_2O$, ZIF-8	MOF	cataluminescence	0.3, 0.1	4.4 ppm, 3.0 ppm	H_2S	60
14	fum-fcu-MOF	MOF	capacitance	-	5.4 ppb	H_2S	61
15	NHS1	organic molecule	fluorescence	4800	0.02 µM	NaHS	62
16	Cy-N_3	organic molecule	fluorescence	1200	0.08 µM	NaHS	63

17	SFP-1, SFP-2	organic molecule	fluorescence	7200, 14400	-	Na_2S	64
18	WSP5	organic molecule	fluorescence	-	0.047 µM	NaHS	65
19	SF4	organic molecule	fluorescence	-	0.125 µM	NaHS	11
20	SHS-M1, SHS-M2	organic molecule	fluorescence	-	0.2 µM, 0.4 µM	Na_2S	66
21	probe 1	organic molecule	fluorescence	≈ 3600	2.4 µM	NaHS	67
22	PSS-PA-Cu NC aggregates	Nanoclus-ter	fluorescence	-	0.65 µM	Na_2S	68
23	bare gold NPs	Nanopart-icles	UV-vis spectroscopy	-	0.08 µM	Na_2S	69
24	ZnO rods	Semicon-ducting oxide	conductivity impedance	-	50 ppb	H_2S	70
25	CuO-BSST	semiconducting oxide	conductivity impedance	10	4-10 ppb	H_2S	71
26	In_2O_3 whiskers	semiconducting oxide	conductivity impedance	120-210	200 ppb	H_2S	72
27	Nafion membrane (H_2SO_4 treated)	solid polymer electrolyte	amperometry	9	100 ppb	H_2S	73
28	polyaniline nanowires-gold nanoparticles	conducting polymer	conductivity impedance	<120	0.1 ppb	H_2S	74
29	polymer P1	semiconducting polymer	conductivity impedance	-	1 ppb	H_2S	75
30	WO_3 film on a single $LiNbO_3$ substrate	surface acoustic wave	oscillation frequency	100	<10 ppb	H_2S	76
31	QCM coated with PPy/TiO_2 film	quartz-crystal microbalance	frequency shift	-	10 ppm	H_2S	77

Metal-organic frameworks (MOFs)[78,79] have shown tremendous potentials in the field of fluorescence-based detection of various analytes[80] due to their outstanding chemical stability,

tuneable pore sizes and functionalities and possibility for pre/post-synthetic modification. Thus, MOF-based fluorescent sensor materials could be developed for the fast, cost-effective, selective and sensitive detection as well as real-time monitoring of H_2S in living biosystems. Until today, only a few MOF compounds have been reported (Table 4.1) to exhibit fluorescence turn-on properties towards H_2S.[10,39, 40, 49-51] Based on the sensing mechanisms, they can be categorized into four types: (i) H_2S-promoted reduction of azide/nitro functional groups into amines leads to fluorescence turn-on state from initial turn-off state[39,40,51,51] (ii) coordination of auxochromic H_2S molecules with central Pb(II) ions in two Pb(II)-based MOFs results in enhancement of the fluorescence intensity[81,82] (iii) Al-Cu mixed-metal MOF containing porphyrin-based ligand has shown fluorescence turn-on behaviour towards H_2S due to removal of Cu^{2+} ions as CuS with concomitant release of the fluorescent MOF,[49] and (iv) fluorescence turn-on response has been observed when the α,β-unsaturated malonitrile units in malonitrile-functionalized ZIF-90 have undergone cleavage of the double bonds in presence of thiol compounds.[10] Although mononitro-functionalized Zr(IV) and Ce(IV) based MOF materials have been previously employed[39,51] for the sensing of H_2S, the fluorescence turn-on behaviour of any dinitro-functionalized MOF towards H_2S has not been reported until now. Moreover, the visual detection of H_2S under ambient conditions has not been achieved so far by any MOF material. In this work, we have explored the potential of the dinitro-functionalized Zr(IV)-based MOF compound called DUT-52-$(NO_2)_2$ (**6**, DUT = Dresden University of Technology) as colorimetric and fluorogenic probe for the detection of H_2S (Scheme 4.1) under physiological conditions (HEPES buffer, pH = 7.4, temperature = 37 °C). We have used Na_2S as the source of H_2S in the present investigation. It is noteworthy that the CO_2 sorption and separation ability of the DUT-52-$(NO_2)_2$ material has been very recently reported[81] but its H_2S sensing properties have not been examined. We have prepared this compound by a completely different procedure and thoroughly investigated its luminescence turn-on behaviour towards H_2S.

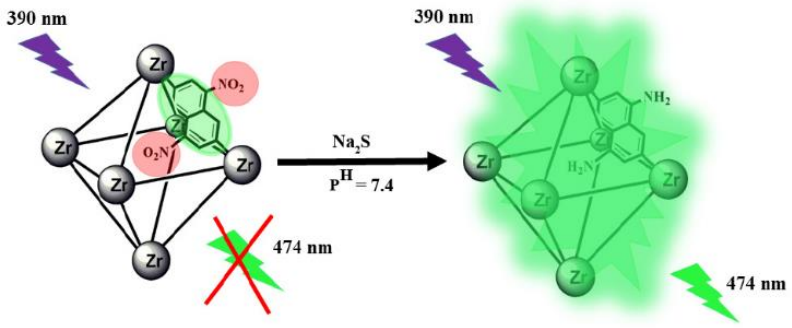

Scheme 4.1 Sensing of H_2S sensing by **6′** under physiological conditions (HEPES buffer, pH = 7.4, temperature = 37 °C) through fluorescence turn-on mechanism.

4.2 Experimental

4.2.1 Materials and physical measurements

The $H_2NDC\text{-}(NO_2)_2$ ligand was synthesized as described previously.[82] All other starting materials were of reagent grade and used as received from the commercial suppliers. Fourier transform infrared (FT-IR) spectra were recorded in the region of 440-4000 cm^{-1} with a Perkin Elmer Spectrum Two FT-IR spectrometer. The following indications are used to characterize absorption bands: very strong (vs), strong (s), medium (m), weak(w), shoulder (sh) and broad (br). Elemental analyses (C, H, N) were performed on a Thermo Scientific Flash 2000 CHNS-O analyzer equipped with a TCD detector. Thermogravimetric analysis (TGA) was carried out with a Netzsch STA-409CD thermal analyzer in a temperature range of 25-600 °C under air atmosphere ata heating rate of 5 °C min^{-1}. Ambient temperature X-Ray powder diffraction (XRPD) patterns were recorded on a Bruker D2 Phaser X-ray diffractometer (30 kV, 10 mA) using Cu-Kα (λ = 1.5406 Å) radiation. Fluorescence emission investigations were performed with a HORIBA JOBIN YVON Fluoromax-4 spectrofluorometer. The nitrogen sorption isotherms up to 1 bar were measured using a Quantachrome Autosorb iQ-MP gas sorption analyzer at −196 °C. The compound was degassed at 190 °C under vacuum for 8 h before the sorption measurement.

4.2.2 Synthesis of $[Zr_6O_4(OH)_4(NDC\text{-}(NO_2)_2)_6]\cdot 6H_2O\cdot 6DMF$(DUT-52-$(NO_2)_2$) (6)

A mixture of $ZrCl_4$ (50 mg, 0.22 mmol) and $H_2NDC\text{-}(NO_2)_2$ ligand (66 mg, 0.22 mmol) was placed in a glass tube. The mixture was dissolved in 3 mL of DMF by sonication inside the

tube and then acetic acid (386 µL, 6.45 mmol) was added to it. The tube containing the reaction mixture was tightly sealed and heated in a block heater at 130 °C for 24 h. After cooling down to room temperature, the precipitate was collected by filtration, washed several times with acetone and dried at 60 °C in an oven. The yield was 90 mg (0.03 mmol, 82%). Elemental analysis calcd. for $C_{90}H_{82}N_{18}O_{68}Zr_6$ (3051.03 g mol^{-1}): C 35.42, H 2.70, N 8.26; found: C 35.31, H 2.45,N 8.37%. FT-IR (KBr, cm^{-1}): 3401 (br), 3079 (w), 2926 (w), 1662 (m),1627 (sh), 1592 (s), 1530 (s), 1417 (vs), 1355 (s), 1208 (w), 1104 (w),1020 (w), 922 (w), 894 (w), 782 (m), 748 (sh), 720 (m), 656 (s), 468(m).

4.2.3 Activation of the as-synthesized 6

For the removal of the guest molecules encapsulated within the pores, the as-synthesized form of **6** was directly heated at 190 °C under dynamic vacuum for 8 h. The thermally activated form of the compound is denoted as **6′** hereafter.

4.2.4 Preparation of the medium for fluorescence sensing experiments in HEPES buffer

All the fluorescence titration experiments were carried out under physiological conditions (HEPES buffer, pH = 7.4). HEPES (0.24 g) was dissolved in 100 mL of deionized water. Then, an appropriate amount of 0.5 (N) NaOH solution was added to this solution in order to maintain a pH of 7.4.

4.2.5 Fluorescence sensing experiments in HEPES buffer

For all the fluorescence titration measurements, 0.5 mg of **6′** (1.24 µM for two -NO_2 groups) was suspended in 2 mL of HEPES buffer (pH = 7.4) in a quartz cuvette and the temperature of the cuvette was maintained at 37 °C. Fluorescence emission was monitored at 474 nm, using an excitation wavelength of 390 nm. For time-dependent fluorescence titration experiments, 24 mmol of Na_2S (10 equiv. per NO_2group) was added to the suspension of **6′** and fluorescence spectra were recorded at a regular time interval of 5 min up to 90 min. In case of concentration-dependent fluorescence titration measurements, 0 to 12 mmol of Na_2S were added to the suspension of **6′** and fluorescence spectra were measured. Similar experiments were carried out by replacing Na_2S with other competing analytes like alanine, cysteine, serine, glutathione, NaCl, NaBr, NaI, $NaNO_2$ and

$NaNO_3$. Another set of fluorescence titration experiments were performed by adding 24 mmol of Na_2S to the suspension of **6′** containing the competing analytes.

4.2.6 Fluorescence sensing experiments in human blood plasma

Human blood (5 mL) was collected from the left arm vain under aseptic conditions in a tube containing ethylenediaaminetetraacetic acid (EDTA). The blood was then centrifuged at 3000 rpm for 5 min to separate the plasma. The supernatant plasma was collected and used for the subsequent experiments. The detection of H_2S in human blood plasma (HBP) was carried out by using Na_2S as an internal standard. In four micro centrifuge tubes, 160 µL of HBP and 20 µL of $ZnCl_2$ (final concentration = 1 mM) were added, and 20 µL of Na_2S (final concentrations of 0.0, 0.5, 5.0, 50.0 µM) was spiked. Then, the mixture was incubated at 37 °C for 5 min. After the incubation, 200 µL of 60% (v/v) acetonitrile was added to this mixture to precipitate the proteins. Afterwards, the mixture was centrifuged at 6000 rpm for 5 min to separate the proteins. The supenatent solution was used further for the detection of H_2S in HEPES buffer. 100 µL of HBP was added to suspension of **6′** (final concentration = 150 µg/mL) in HEPES buffer. This mixture was incubated at 37 °C for 1 h. After the incubation, fluorescence emission spectra were recorded (λ_{ex} = 390 nm, λ_{em} = 474 nm).

4.2.7 Macrophage cell culture

Mouse macrophage J774A.1 cells were cultured in Dulbecco's modified eagle's medium (DMEM) supplemented with 10% fetal bovine serum (FBS) and 1% penicillin-streptomycin antibiotic (100 units/ml penicillin and 100 µg/ml streptomycin sulfate) in 100 mm^2 cell culture dish and maintained as described previously.[83]

4.2.8 Testing toxicity of 6′ in proliferating cells

Toxicity of **6′** was assessed in proliferating macrophage J774A.1cells as described earlier.[83] Briefly, macrophage J774A.1 cells were treated with different concentrations of **6′** (0-30 µM) for 12 hat 37 °C in DMEM-high glucose (DMEM-HG) complete media. Cells were washed gently with phosphate buffer saline (PBS) and MTT reduction assay was used to measure the cell viability.[84] Untreated macrophage cells were considered as 100% viable.

4.2.9 Cell imaging experiments

Twenty thousand macrophage J774A.1 cells were incubated with 20 μM probe for 12 h at 37 °C in a 96-well cell culture dish. Cells were gently washed to remove the excess probe present in the media, and then treated with Na_2S (5 μM) and $ZnCl_2$ (1 mM) for12 h to generate H_2S gas inside the cells. Post treatment, incomplete media was replaced with PBS and cells were observed with Cytell cell imaging system (GE healthcare) in blue channel (λ_{ex} = 385 nm; λ_{em} = 431 nm) and bright light. A total of 10 random fields were selected and captured.

4.3 Results and discussion

4.3.1 Synthesis and characterization

6 was synthesized under solvothermal conditions (130 °C, 24 h) by using $ZrCl_4$ as the metal source and acetic acid as the modulator in DMF. The $ZrCl_4/H_2NDC\text{-}(NO_2)_2$ ligand/acetic acid molar ratio was maintained at 1:1:30. It is worthy to note that the reported Zr-NDC-$2NO_2$ materials was prepared by heating a mixture of $ZrCl_4$, $H_2NDC\text{-}(NO_2)_2$ ligand and benzoic acid (molar ratio = 1:1:15) in DMF at 120 °C for 48 h.[81] Under the reported synthesis conditions, we obtained the material having slightly lower crystallinity than that of **6**. In order to check the reproducibility in the synthesis of the MOF, reactions were performed in five different batch using the optimum synthesis conditions. The XRPD patterns (Figure 4.1a) of the materials from all the batches were very similar and revealed that all the samples were highly crystalline in nature. These results confirmed the reproducibility of the optimum synthesis conditions for the MOF. Moreover, the storage of the material under ambient conditions for two weeks did not affect its crystallinity and hence structural integrity. The as-synthesized sample of **6** encapsulates occluded H_2O and DMF molecules inside the pores. These guest molecules were removed by heating the as-synthesized compound directly under vacuum at 190 °C for 8 h. Both the as-synthesized and thermally activated form of the material exhibit similar XRPD patterns (Figure 4.1b) thus confirming the structural integrity of the compound after the thermal activation process.

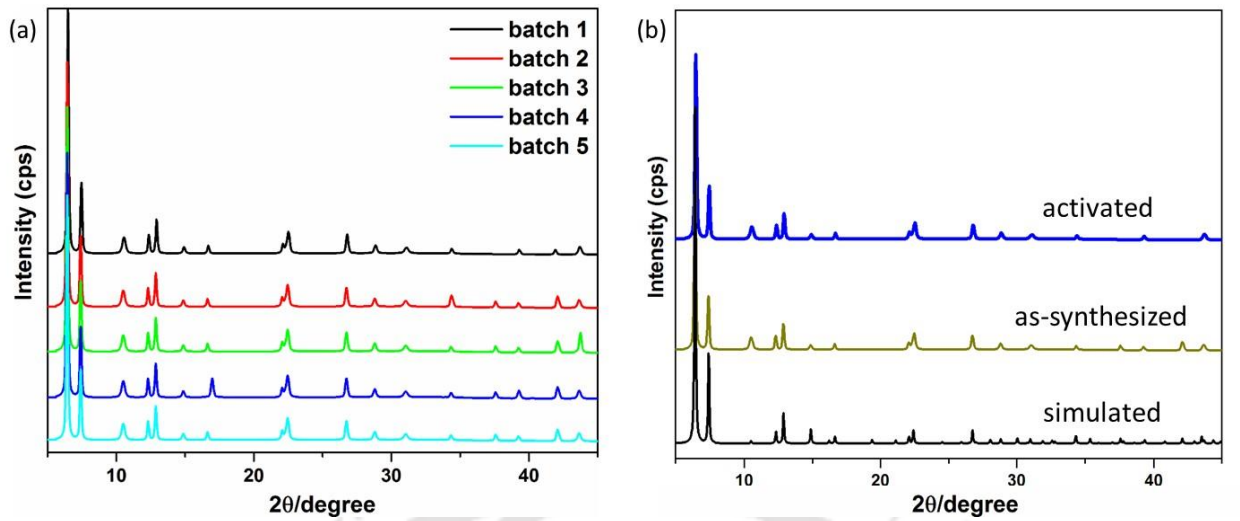

Figure 4.1 (a) XRPD patterns of **6′** showing batch-to-batch reproducibility of its optimum synthesis conditions. (b) Calculated XRPD pattern of DUT-52 and experimental XRPD pattern of as-synthesized and activated **6**.

The FT-IR spectra (Figure 4.2) of the as-synthesized and thermally activated sample of **6** display strong absorption bands in the regions 1590-1620 and 1415-1425 cm^{-1}, which can be assigned to the asymmetric and symmetric CO_2 stretching vibrations of the coordinated NDC-$(NO_2)_2$ ligands, respectively.[51,85-93] In both the FT-IR spectra, the strong absorption band at around 1530 cm^{-1}can be attributed to the asymmetric N=O stretching vibration of the NO_2 groups attached with the coordinated ligands.[94] The carbonyl stretching vibration of the occluded DMF molecules gives rise to medium absorption band at 1655 cm^{-1} in the IR spectrum of as-synthesized **6**. This absorption band is absent in the IR spectrum of thermally activated **6′**, indicating complete activation of the compound.

The experimental XRPD pattern of the as-synthesized sample of **6** is very similar with the simulated XRPD pattern of parent DUT-52 compound (Figure 4.2b). This similarity in XRPD patterns suggests that the framework structure of **6** is analogous with the unfunctionalized DUT-52[95] and structurally related materials.[96,97] Thus, **6** bears a cubic framework structure. The structure of DUT-52 has been formerly described by Kaskel and co-workers.[95] Similar as DUT-52, the cubic framework of the presented compound is composed of hexanuclear $[Zr_6O_4(OH)_4]^{12+}$ building units. These inorganic building blocks are further interconnected by the carboxylate groups of twelve NDC-$(NO_2)_2$ ligands, resulting in the formation of a 3D, cubic, microporous framework. The

network has larger octahedral (free diameter ~9.3 Å) and smaller tetrahedral (free diameter ~7.5 Å) cages. The two types of cages are interconnected by narrow triangular windows (free diameter ~4.4 Å).

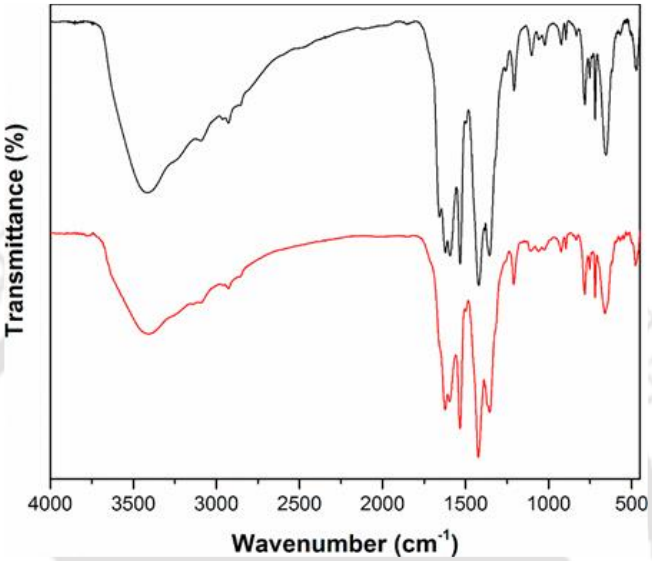

Figure 4.2 FT-IR spectra of as-synthesized **6** (black) and activated (red) **6′**.

In order to prove the permanent microporosity, N_2 adsorption experiment was carried out with the thermally activated **6′**.The material displayed N_2 adsorption isotherms of type-I (Figure 4.3), which is a characteristic of microporous materials. The specific BET surface area and micropore volume of **6′**, which were determined from the N_2 adsorption isotherms, correspond to 330 m^2g^{-1} and 0.87 cm^3g^{-1} (at $p/p_0 = 0.99$), respectively. It is noteworthy that **6′** possesses lower specific BET surface area as compared to that of the reported Zr-NDC-2NO_2 compound (812 m^2g^{-1}).[47]

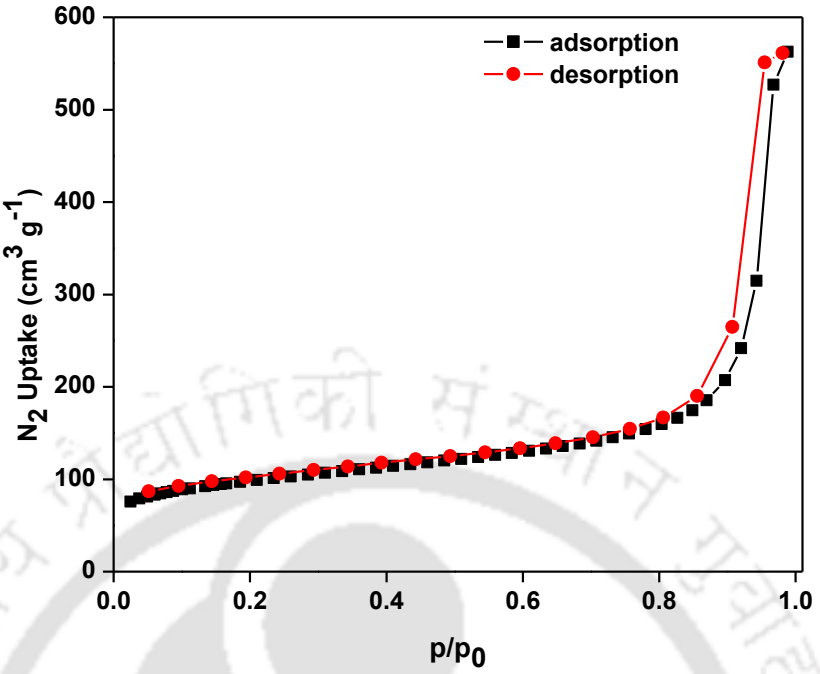

Figure 4.3 N_2 adsorption and desorption isotherms of thermally activated **6′** recorded at –196 °C.

4.3.2 Thermal and chemical stability

For investigation of the thermal stability of **6** and **6′**, thermogravimetric analyses were performed in an air atmosphere in the temperature range 25-600 °C. From the TG traces (Figure 4.4a), it can be concluded that both **6** and **6′** are highly stable up to 340 °C. However, **6** possesses lower thermal stability as compared to un-functionalized DUT-52[81] and structurally related materials.[96,97] In the TG curve of **6**, the first weight loss of 3.5 wt% in temperature range 25-140 °C can be assigned to the removal of 6 occluded water molecules per formula unit (cald.: 3.5 wt%). The second weight loss of 17.8 wt% in temperature range 140-340 °C can be assigned to the removal of 6 guest DMF molecules per formula unit (cald.: 17.9 wt%). After 340 °C, the compound starts to decompose due to the removal of organic ligands from the framework. For checking the chemical stability of **6′**, samples were stirred at room temperature for 4 h in different liquids such as water, 1M HCl and acetic acid. Then, the materials were collected by filtration and the crystallinity of the filtered solids was examined by XRPD experiments (Figure 4.4b). The crystallinity of **6′** remains unchanged after treatment with water, 1M HCl and acetic acid. Thus, **6′** retains its structural integrity when exposed to these liquids. Inspired by the considerable stability

of **6′** in water, HEPES buffer (pH = 7.4) was chosen as the medium for the H_2S sensing experiments.

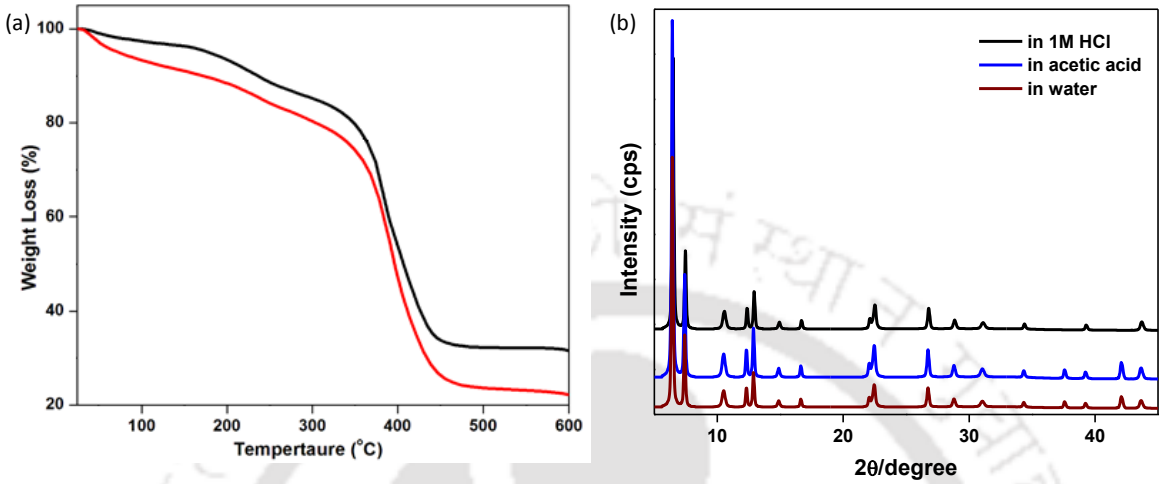

Figure 4.4 (a) TG curves of as-synthesized **6** and activated **6′** recorded in an air atmosphere in the temperature range of 25-600 °C with a heating rate of 5 °C min^{-1}. (b) XRPD patterns of **6′** compound after treatment with water, acetic acid and 1M HCl.

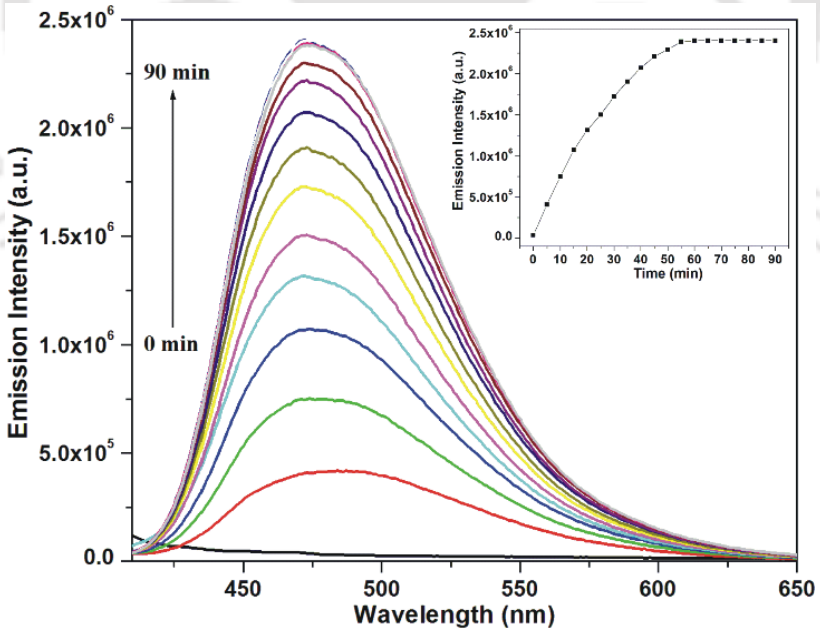

Figure 4.5 Fluorescence turn-on response of **6′** towards addition of Na_2S at a regular time interval of 5 min up to 90 min. Time-dependence of the emission intensity (monitored at 474 nm) is shown in the inset.

4.3.3 Detection of H_2S in HEPES buffer

Owing to their non-toxicity and biocompatibility, the Zr-based MOF called UiO-66 have been formerly employed as a potential platform for drug delivery and imaging.[98,99] Moreover, the rapid and selective H_2S sensing ability of the mononitro-functionalized Zr-UiO-66-NO_2 compound under physiological conditions has been documented in the literature.[39] The presence of two nitro functional groups per H_2NDC-$(NO_2)_2$ ligand completely quench the fluorescence of the naphthalene moiety in dinitro-functionalized Zr-based DUT-52 (Figure 4.5). The corresponding diamino-functionalized MOF compound, formed through H_2S-mediated reduction, is expected to be more fluorescent than the dinitro-functionalized material. In this work, the potentiality of the dinitro-functionalized Zr-based DUT-52 compound has been examined as a turn-on fluorescence probe for the detection of H_2S under physiological conditions (HEPES buffer, pH = 7.4, temperature = 37 °C).

The detection capability of **6′** for H_2S was investigated by performing fluorescence turn-on experiments under physiological conditions. Na_2S was used as a source of H_2S in these experiments.[100,101] The existence of two electron-withdrawing NO_2 groups attached with each H_2NDC-$(NO_2)_2$ ligand molecule results in weak fluorescence emissions for **6′**, which remains in the fluorescence turn-off state before the addition of Na_2S. Upon exposure of **6′** towards H_2S, the electron-withdrawing NO_2 groups are post-synthetically reduced to electron-donating amines. During the reaction-based sensing of H_2S, the structural integrity of the framework of the material is retained. The fluorescence turn-on behaviour of **6′** upon excitation at 390 nm can be attributed to the formation of the strongly fluorescent amine-functionalized MOF compound. The electron-donating amine groups push the electron density towards the naphthalene ring of the ligand molecule and thus **6′** is converted to the fluorescence turn-on state after treatment with Na_2S.[102,103]

In order to investigate the fluorescence turn-on response of **6′** towards H_2S, the fluorescence spectra were measured at a regular time interval of 5 min after addition of 24 mM of Na_2S to the suspension of the material in HEPES buffer (10 mM, pH = 7.4) at 37 °C. Upon the addition of Na_2S, the fluorescence emission (monitored at 474 nm) intensity increased nearly 12-fold after 5 min (Figure 4.5). The fluorescence emission intensity of **6′** became saturated after 55 min of addition of Na_2S with 68-fold increment in fluorescence intensity and development of a brownish color. The results of the time-dependent fluorescence titration experiments demonstrate

that **6′** is a promising luminescent sensor material for the real-time detection of H_2S. Note worthily, the response time of **6′** towards H_2S is much slower as compared to those of the formerly documented MOF-based H_2S sensor probes.[10,39,4049,50] Nevertheless, the fold increment of the fluorescence emission intensity of the presented material upon addition of H_2S is significantly higher as compared to the known MOF-based H_2S sensor compounds.

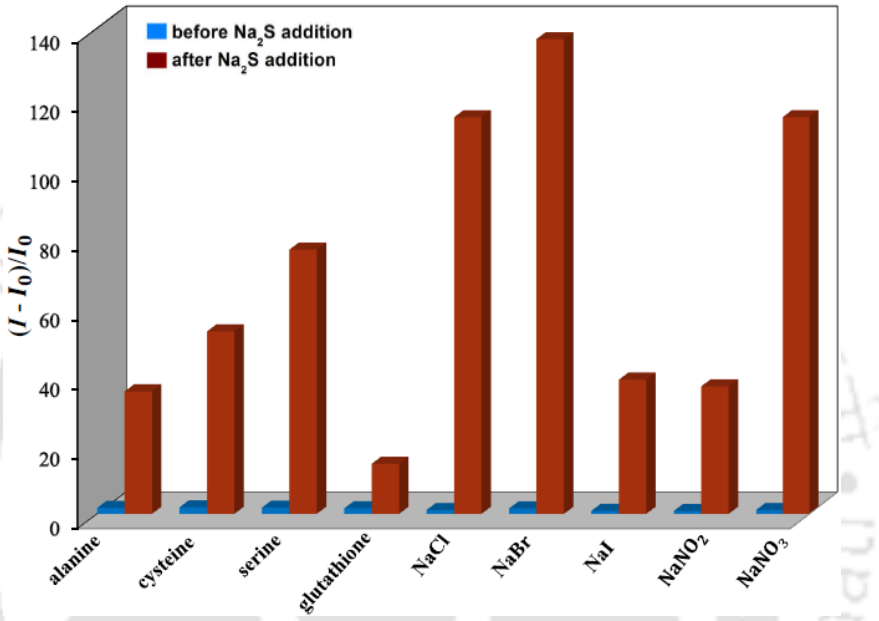

Figure 4.6 Fluorescence turn-on response of **6′** (0.04 M) monitored at 474 nm in presence of a competing analyte, followed by addition of 12 mM Na_2S solution to the solution containing the analyte (HEPES buffer, pH = 7.4, temperature = 37 °C). The emission intensities were recorded after 60 min of analyte addition.

The real-world application of a fluorescence turn-on probe in biological systems requires high selectivity towards the target analyte molecule over other potentially competing biomolecules. For evaluating the selectivity of **6′** towards H_2S over other possibly interfering biomolecules commonly present in biological system (like alanine, serine, cysteine and glutathione) and few common biological anions (like NaCl, NaBr, NaI, $NaNO_2$ and $NaNO_3$), the fluorescence responses of the probe were recorded in presence of these potentially competing biological species under physiological conditions (HEPES buffer, pH = 7.4, temperature = 37 °C). The inorganic salts and organic compounds were chosen based of the facts that they have

physiological significance and can be found in complex biological systems along with sulphide ion. It was observed that the fluorescence emission intensity of **6′** was affected negligibly by the addition of the potentially competing biological molecules and anions to the suspension of the compound. The results of these experiments revealed that the probe is highly selective towards H_2S over common reducing biological anions and biomolecules.

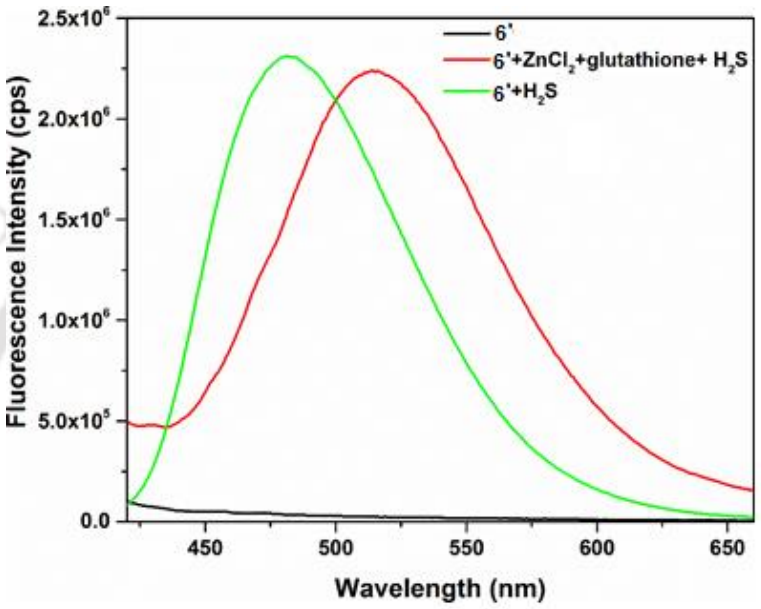

Figure 4.7 Fluorescence response of **6′** towards H_2S in presence of glutathione and $ZnCl_2$.

The effective detection of H_2S in complicated biological systems necessitates an efficient fluorescence turn-on response of the sensor probe in presence of other potentially interfering biochemical species. Hence, we have investigated the selective fluorescence turn-on response of **6′** towards H_2S in presence of other possibly competing analytes. For this purpose, 24 mM Na_2S was first added to the suspension of **6′** in HEPES buffer (10 mM, pH = 7.4), which also contained the interfering analyte. After 60 min of the addition of Na_2S, the fluorescence emission spectra were measured. Even in the existence of other possibly competing biomolecules, the observed fluorescence turn-on response of **6′** towards H_2S was considerably high (Figure 4.6). Among the potentially interfering analytes, glutathione, iodide and nitrite exhibited noticeable interferences in the detection of H_2S. The lowest luminescence turn-on response of **6′** towards H_2S was noticed in the presence of glutathione, which exerted a negative effect on the fluorescence response of the sensor probe for H_2S. It is known that glutathione has strong reducing behavior and can react with

nitro functional groups.[104-106] For example, the aristolochic acid undergoes hydrogenolysis reaction in presence of glutathione, where the aromatic nitro group is replaced by a hydrogen atom.[107] Since **6′** contains nitro functional groups, glutathione can be expected to react with these functional groups. This probable reaction can be accounted for the lower fluorescence turn-on response of **6′** towards Na_2S in presence of glutathione. To minimize the interference of glutathione, **6′** was treated with glutathione in presence of equivalent amount of $ZnCl_2$. Since Zn^{2+} ion has affinity to bind with glutathione by soft-soft interactions,[108,109] it is expected that Zn^{2+} ion will bind with the free thiol group of glutathione and thus prevent interactions with the nitro groups of **6′**. Interestingly, in presence of $ZnCl_2$, glutathione showed a negligible interference in the H_2S sensing ability of **6′** (Figure 4.7). The iodide ion also showed considerable interference in fluorescence turn-on behavior of **6′** towards H_2S, which can be attributed to the fact that it is a well-known fluorescence quencher.[110] Along the same line, the probe suffered strong interference from the nitrite ion during the H_2S sensing experiment. A large number of studies have disclosed that nitrite can be reduced in vivo, either non-enzymatically or enzymatically, which is catalyzed in presence of sulphide.[111] For this reason, nitrite is used as an antidote for H_2S poisoning.[112] Therefore, the consumption of sulphide by nitrite may occur during the long incubation period, which may exert detrimental effect during the H_2S sensing event.

In order to quantify the fluorescence turn-on responses of **6′** towards H_2S, fluorescence titration experiments were performed with various concentrations of Na_2S (0-12 mM). The fluorescence emission intensity (Figure 4.8a) of the material increased progressively as a result of the gradual addition of Na_2S. The corresponding naked-eye colorimetric responses of **6′** towards H_2S under daylight and under UV radiation are shown in Figure 4.8b and 4.8c, respectively. These visually detectable responses demonstrate that **6′** is an excellent colorimetric and fluorogenic probe for the highly selective sensing of H_2S under physiological conditions. Remarkably, the structural integrity of the compound is retained after the H_2S sensing experiments.[10] This fact has been verified by the XRPD experiments (Figure 4.9).

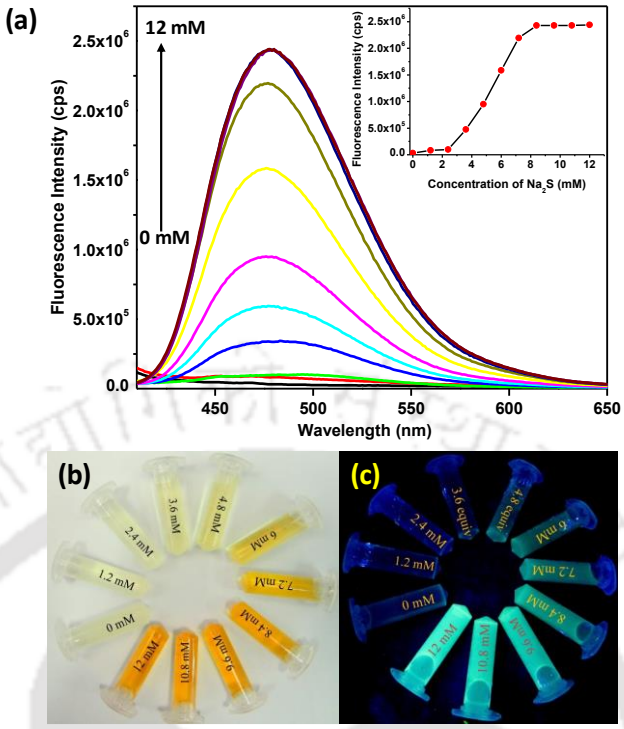

Figure 4.8 (a) Fluorescence turn-on response of **6′** (0.04 M) with increasing concentrations of Na_2S. Concentration-dependence of the emission intensity (monitored at 474 nm) is shown in the inset. The corresponding naked-eye colorimetric responses of **6′** towards H_2S under (b) day light and (c) UV light are also displayed.

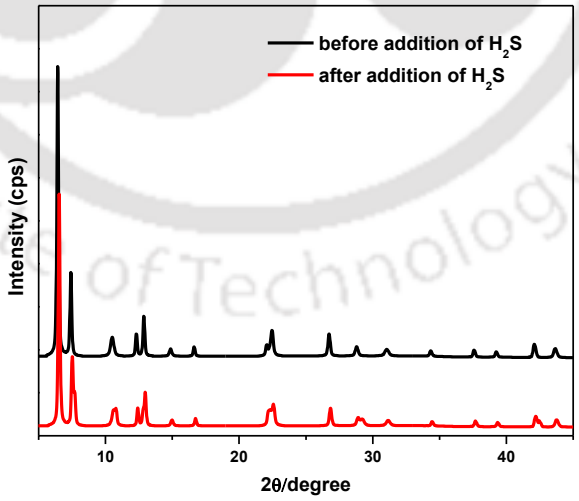

Figure 4.9 XRPD patterns of **6′** before (a) and after (b) the H_2S sensing experiments.

4.3.4 Validation of the analytical method for the detection of H_2S in HEPES buffer

Table 4.2 Analytical parameters for the fluorimetric detection of H_2S by **6′**.

Concen-tration range (μM)	Regression equation	Correlation Coefficient (R^2)	RSS[a]	$S_{y/x}$[b]	Slope	LOD[c] (μM)	LOQ[d] (μM)	Intraday Precision		Interday Precision	
								Found[e] (Mean ± RSD)	Recovery[f] (%)	Found[e] (Mean ± RS)	Recovery[f] (%)
100-700	1.74x+6.29 $\times10^6$	0.9949	3.59 $\times10^7$	119 8.33	1.75 $\times10^8$	20.0	68.9	200.6 ± 2.07	100.3	195.2 ± 6.5	97.5

[a] Residual sum of squares

[b] Standard deviation of the residuals

[c] Limit of detection, 3RSD/slope

[d] Limit of quantification, 10RSD/slope

[e] Spiked concentration (200 μM)

[f] (Mean measured concentration/spiked concentration) ×100

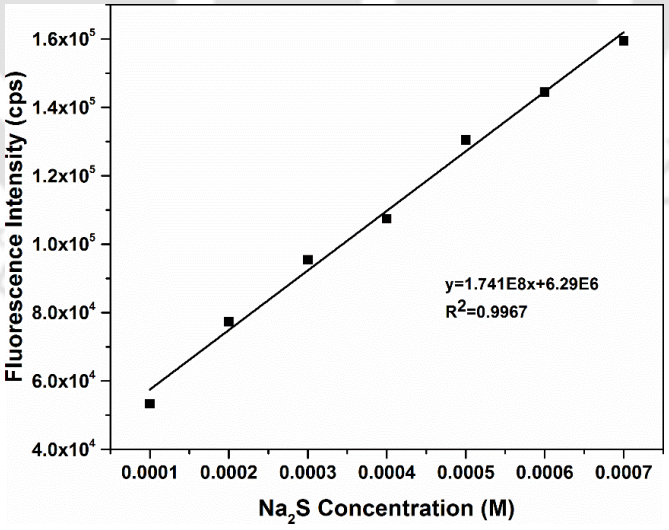

Figure 4.10 Change in the fluorescence intensity of **6′** in HEPES buffer as a function of Na_2S concentration.

The presented analytical method for the H_2S sensing was validated in terms of linearity, limits of detection (LOD) and limits of quantification (LOQ). The calibration curve was obtained by plotting the fluorescence intensity of **6′** as a function of different concentrations (in the range of 100-700 µM) of Na_2S under the optimum conditions. The plot of the fluorescence intensity of **6′** versus the concentration of Na_2S disclosed a linear relationship (Figure 4.10). The analytical parameters related to this plot are summarized in Table 4.2. The LODs and LOQs for the detection of H_2S were calculated at a signal-to-noise (S/N) ratio of 3 and 10. The LOD of **6′** towards H_2S has been estimated to be 20 µM. The calculated LOD of the material for H_2S lies within the range of H_2S concentration observed in the biological systems.[13,15] The LOD of **6′** is in agreement with those of the existing MOF-based H_2S sensor probes.[10,39,59-61] Quantitative analysis was carried out by the external standard method. The accuracy of the method was estimated by the recovery experiment, which was performed by adding a known amount of analyte solution to the probe. For determining the reproducibility and precision of the developed method, spiked samples were analyzed and the results were expressed in terms of relative standard deviation (RSD). Intra-day precision was determined by measuring a sample with spiked standard of 200 µM with five replicates in the same day, and inter-day precision was obtained by analyzing the sample in five different days.

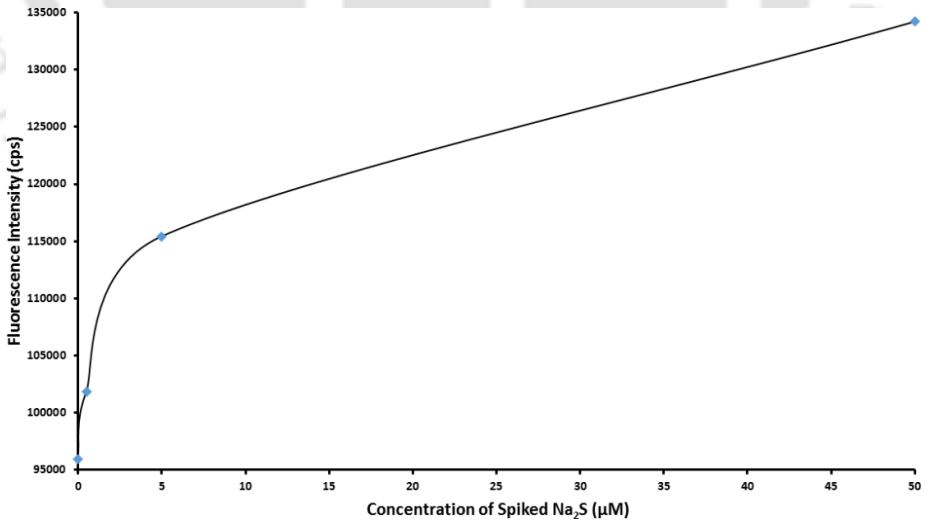

Figure 4.11 Change in the fluorescence intensity of **6′** in presence of human blood plasma, where Na_2S was spiked as an internal standard.

4.3.5 Detection of H_2S in human blood plasma

In order to establish the utility of **6′** in biological systems, the H_2S sensing experiments were performed in presence of human blood plasma (HBP). Na_2S was spiked as an internal standard.[113] **6′** was treated with four different concentrations of Na_2S (0.0, 0.5, 5.0, 50.0 μM) and the fluorescence emission intensity were recorded. The plot of emission intensity of **6′** versus sulphide concentration (Figure 4.11) revealed that a slight increment in the sulphide concentration (0.5 μM) in HBP can be detected by **6′**.

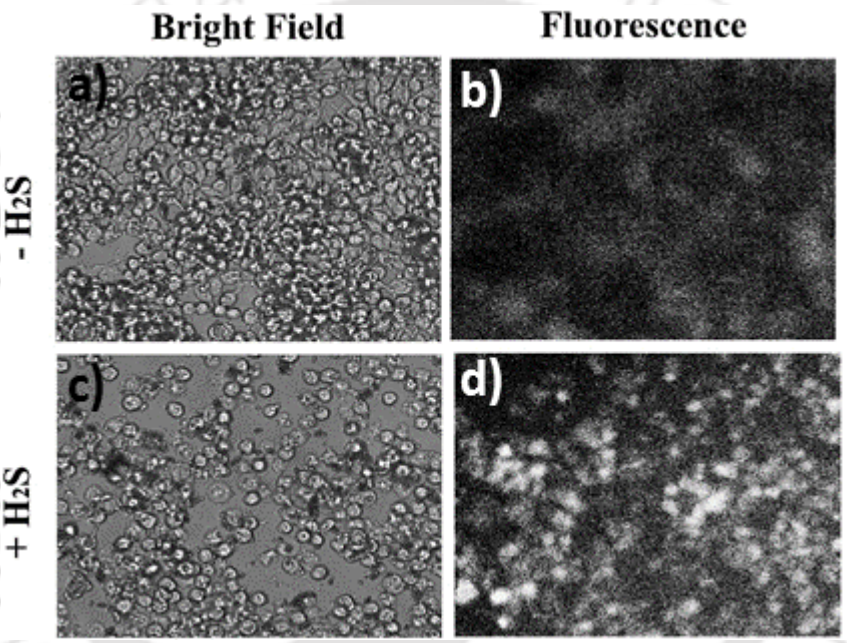

Figure 4.12 Sensing of intracellular H_2S by **6′** in macrophage J774A.1 cells. Macrophage J774A.1 cells were loaded with **6′** and then cells were treated with $Na_2S/ZnCl_2$ (5 μM) at 37 °C for 12 h and observed with Cytell cell imaging system (GE-healthcare). Images of untreated macrophage J774A.1 cells: (a) bright-field image of cells in presence of 30 μM **6′**; (b) observation of (a) in blue fluorescence channel; or Images of $Na_2S/ZnCl_2$ treated macrophage J774A.1 cells: (c) bright-field image of cells after treatment with Na_2S; (d) observation of (c) in blue fluorescence channel. The treated cells are exhibiting bright fluorescence.

4.3.6 Detection of H_2S in living cells

For demonstrating the sensing ability of **6′** in biological media, cytotoxicity and cell imaging experiments were performed employing J774A.1 macrophage cell line. The macrophage J774A.1 is a rapid proliferating cells and treatment of these cells with different concentrations of **6′** indicate that there is no significant loss of viability of cells. At 30 μM concentration of **6′**, the cells exhibited 69.5 ± 2.9 viability. The cellular morphology is intact with no visible sign of cellular damage or membrane blebbing pattern (Figure 4.12a).

For checking the ability of the probe to detect H_2S in biological systems, cell imaging investigations were carried out using J774A.1 macrophage cell line. The macrophage cells were loaded with 30 μM **6′** and then intracellular H_2S was generated by incubating the cells with a combination of Na_2S and $ZnCl_2$.[114] The cells loaded with the probe alone showed good morphology but did not exhibit any fluorescence (Figure 4.12a–b). Compared to this, the cells treated with a combination of Na_2S and $ZnCl_2$ exhibited good morphology and bright fluorescence (Figure 4.12b–c). The current experiment proves the utility of **6′** in detecting H_2S inside the cells.

4.4 Conclusions

We have successfully employed the dinitro-functionalized Zr(IV)-based DUT-52-$(NO_2)_2$ MOF material as a colorimetric and fluorogenic turn-on probe for the sensing of H_2S under physiological conditions (HEPES buffer, pH = 7.4, temperature = 37 °C). As confirmed by the steady-state fluorescence titration experiments, the MOF compound features significant capabilities for the highly selective and sensitive (detection limit: 20 μM) detection of H_2S. In terms of fold-increase (68-fold at saturation) of the fluorescence emission intensity, the detection performance of the presented MOF material towards H_2S is significantly higher as compared to the previously reported MOF-based H_2S sensor probes. Remarkably, the compound exhibited visually detectable colorimetric and fluorogenic responses towards H_2S under day light as well as under UV irradiation. In addition, the probe could be used for the detection of H_2S in human blood plasma and as well as living cells. The unprecedented selectivity for detection of H_2S even in the existence of other potentially competing biomolecules and anions in biological system makes the presented compound a potential candidate for the real-time monitoring of H_2S in biological systems.

4.5 References

1. C. Szabo, C. Ransy, K. Módis, M. Andriamihaja, B. Murghes, C. Coletta, G. Olah, K. Yanagi and F. Bouillaud, *J. Pharmacol.*, 2014, **171**, 2099-2122.
2. R. J. Reiffenstein, W. C. Hulbert and S. H. Roth, *Annu. Rev. Pharmacol. Toxicol.*, 1999, **32**, 109-134.
3. C. Szabo, *Nat. Rev. Drug Discov.*, 2007, **6**, 917-935.
4. D. Boehning and S. H. Synder, *Annu. Rev. Nurosci.*, 2003, **26**, 105-131.
5. T. S. Bailey and M. D. Pluth, *J. Am. Chem. Soc.*, 2013, **135**, 16697-16704.
6. R. Wang, *FASEB J.*, 2002, **16**, 1792-1798.
7. Y. Han, J. Qin, X. Chang, Z. Yang and J. Du, *Cell. Mol. Neurobiol.*, 2006, **26**, 101-107.
8. M. H. Stipanuk and I. Ueki, *J. Inherit. Metab. Dis.*, 2011, **34**, 17-32.
9. H. Kimura, *Amino Acids*, 2011, **41**, 113-121.
10. H. Li, X. Feng, Y. Guo, D. Chen, R. Li, X. Ren, X. Jiang, Y. Dong and B. Wang, *Sci. Rep.*, 2014, **4**, 4366-4370.
11. V. S. Lin, A. R. Lippert and C. J. Chang, *Proc. Natl. Acad. Sci. U.S.A.*, 2013, **110**, 7131-7135.
12. G. Yang, L. Wu, B. Jiang, W. Yang, J. Qi, K. Cao, Q. Meng, A. K. Mustafa, W. Mu, S. Zhang, S. H. Snyder and R. Wang, *Science*, 2008, **322**, 587-590.
13. L. Li, P. Rose and P. K. Moore, *Annu. Rev. Pharmacol. Toxicol.*, 2011, **51**, 169-187.
14. J. Liu, Y.-Q. Sun, J. Zhang, T. Yang, J. Cao, L. Zhang and W. Guo, *Chem. Eur. J.*, 2013, **19**, 4717-4722.
15. P. Wu, J. Zhang, S. Wang, A. Zhu and X. Hou, *Chem. Eur. J.*, 2014, **20**, 952-956.
16. G. Yang, L. Wu, B. Jiang, B. Yang, J. Qi, K. Cao, Q. Meng, A. K. Mustafa, W. Mu, S. Zhang, S. H. Snyder and R. Wang, *Science*, 2008, **322**, 587-590.
17. K. Abe and H. J. Kimura, *J. Neurosci.*, 1996, **16**, 1066-1071.
18. L. Li, M. Bhatia, Y. Z. Zhu, Y. C. Zhu, R. D. Ramnath, Z. J. Wang, F. B. Anuar, M. Whiteman, M. Salto-Tellez and P. K. Moore, *FASEB J.*, 2005, **19**, 1196-1198.
19. A. Papapetropoulos, A. Pyriochou, Z. Altaany, G. Yang, A. Marazioti, Z. Zhou, M. G. Jeschke, L. K. Branski, D. N. Herndon, R. Wang and C. Szabó, *Proc. Natl. Acad. Sci. U.S.A.*, 2009, **106**, 21972-21977.

20. J. W. Calvert, S. Jha, S. Gundewar, W. J. Elrod, A. Ramachandran, C. B. Pattillo, C. G. Kevil and D. J. Lefer, *Circ. Res.*, 2009, **105**, 365-374.
21. G. Yang, L. Wu and R. Wang, *FASEB J.*, 2006, **20**, 553-555.
22. J. Furne, A. Saeed and M. D. Levitt, *Am. J. Physiol. Regul. Integr. Comp. Physiol.*, 2008, **295**, R1479-R1485.
23. K. Eto, T. Asada, K. Arima, T. Makifuchi and H. Kimura, *Biochem. Biophys. Res. Commun.*, 2002, **293**, 1485-1488.
24. P. Kamoun, M. C. Belardinelli, A. Chabli, K. Lallouchi and B. Chadefaux-Vekemans, *Am. J. Med. Genet. Sect. A.*, 2003, **116**, 310-311.
25. S. Fiorucci, E. Antonelli, A. Mencarelli, S. Orlandi, B. Renga, G. Rizzo, E. Distrutti, V. Shah and A. Morelli, *Hepatology*, 2005, **42**, 539-548.
26. W. Yang, G. Yang, X. Jia, L. Wu and R. Wang, *J. Physiol.*, 2005, **569**, 519-531.
27. C. Szabo, C. Coletta, C. Chao, K. Modis, B. Szczesny, A. Papapetropoulos and M. R. Hellmich, *Proc. Natl. Acad. Sci. USA*, 2013, **110**, 12474-12479.
28. A. R. Ivanov, I. V. Nazimov and L. A. Baratova, *J. Chromatogr., A*, 2000, **870**, 433-442.
29. Y. V. Tcherkas and A. D. Denisenko, *J. Chromatogr., A*, 2001, **913**, 309-313.
30. N. S. Lawrence, J. Davis, L. Jiang, T. G. J. Jones, S. N. Davies and R. G. Compton, *Electroanal.*, 2000, **12**, 1453-1460.
31. M. G. Choi, S. Cha, H. Lee, H. L. Jeon and S. K. Chang, *Chem. Commun.*, 2009, 7390-7392.
32. M. M. F. Choi, *Analyst*, 1998, **123**, 1631-1634.
33. M. Ishigami, K. Hiraki, K. Umemura, Y. Ogasawara, K. Ishii and H. Kimura, *Antioxid. Redox Signal.*, 2009, **11**, 205-214.
34. G.-J. Mao, T.-T. Wei, X. X. Wang, S. Huan, D.-Q. Lu, J. Zhang, X.-B. Zhang, W. Tan, G.-L. Shen and R.-Q. Yu, *Anal. Chem.*, 2013, **85**, 7875-7881.
35. H. Peng, W. Chen, S. Burroughs and B. Wang, *Curr. Org. Chem.*, 2013, **17**, 641-653.
36. F. Yu, X. Han and L. Chen, *Chem. Commun.*, 2014, **50**, 12234-12249.
37. C. Liu, J. Pan, S. Li, Y. Zhao, L. Y. Wu, C. E. Berkman, A. R. Whorton and M. Xian, *Angew. Chem. Int. Ed.*, 2011, **50**, 10327-10329.
38. B. Ke, W. Wu, W. Liu, H. Liang, D. Gong, X. Hu and M. Li, *Anal. Chem.*, 2016, **88**, 592-595.

39. S. S. Nagarkar, A. V. Desai and S. K. Ghosh, *Chem. Eur. J.*, 2015, **21**, 9994-9997.
40. X. Zhang, J. Zhang, Q. Hu, Y. Cui, Y. Yang and G. Qian, *Appl. Surf. Sci.*, 2015, **355**, 814-819.
41. A. R. Lippert, E. J. New and C. J. Chang, *J. Am. Chem. Soc.*, 2011, **133**, 10078-10080.
42. L. A. Montoya and M. D. Pluth, *Chem. Commun.*, 2012, **48**, 4767-4769.
43. S. Chen, Z.-j. Chen, W. Ren and H.-w. Ai, *J. Am. Chem. Soc.*, 2012, **134**, 9589-9592.
44. S. K. Das, C. S. Lim, S. Y. Yang, J. H. Han and B. R. Cho, *Chem. Commun.*, 2012, **48**, 8395-8397.
45. Q. Wan, Y. Song, Z. Li, X. Gao and H. Ma, *Chem. Commun.*, 2013, **49**, 502-504.
46. Z. Wu, Z. Li, L. Yang, J. Han and S. Han, *Chem. Commun.*, 2012, **48**, 10120-10122.
47. Y. Jiang, Q. Wu and X. Chang, *Talanta*, 2014, **121**, 122-126.
48. H. Peng, Y. Cheng, C. Dai, A. L. King, B. L. Predmore, D. J. Lefer and B. Wang, *Angew. Chem. Int. Ed.*, 2011, **50**, 9672-9675.
49. Y. Ma, H. Su, X. Kuang, X. Li, T. Zhang and B. Tang, *Anal. Chem.*, 2014, **86**, 11459-11463.
50. S. S. Nagarkar, T. Saha, A. V. Desai, P. Talukdar and S. K. Ghosh, *Sci. Rep.*, 2014, **4**, 7053-7058.
51. M. SK and S. Biswas, *CrystEngComm*, 2016, **18**, 3104-3113.
52. A. Buragohain and S. Biswas, *CrystEngComm*, 2016, **18**, 4374-4381.
53. S. S. Nagarkar, T. Saha, A. V. Desai, P. Talukdar and S. K. Ghosh, *Scientific reports*, 2014, **4**.
54. X. Zhang, J. Zhang, Q. Hu, Y. Cui, Y. Yang and G. Qian, *Appl. Surf. Sci.*, 2015, **355**, 814.
55. A. Legrand, A. Pastushenko, V. Lysenko, A. Geloen, E. A. Quadrelli, J. Canivet and D. Farrusseng, *ChemNanoMat*, 2016, **2**, 866-872.
56. X. Zhang, Q. Hu, T. Xia, J. Zhang, Y. Yang, Y. Cui, B. Chen and G. Qian, *ACS Appl. Mater. Interfaces*, 2016, **8**, 32259-32265.
57. Y.-Y. Cao, X.-F. Guo and H. Wang, *Sens. Actuators, B*, 2017, **243**, 8-13.
58. X. Wan, L. Wu, L. Zhang, H. Song and Y. Lv, *Sens. Actuator, B*, 2015, **220**, 614-621.
59. O. Yassine, O. Shekhah, A. H. Assen, Y. Belmabkhout, K. N. Salama and M. Eddaoudi, *Angew. Chem. Int. Ed.*, 2016, **55**, 15879-15883.

60. G.-J. Mao, T.-T. Wei, X.-X. Wang, S.-y. Huan, D.-Q. Lu, J. Zhang, X.-B. Zhang, W. Tan, G.-L. Shen and R.-Q. Yu, *Analytical chemistry*, 2013, **85**, 7875-7881.
61. F. Yu, P. Li, P. Song, B. Wang, J. Zhao and K. Han, *Chemical communications*, 2012, **48**, 2852-2854.
62. Y. Qian, J. Karpus, O. Kabil, S.-Y. Zhang, H.-L. Zhu, R. Banerjee, J. Zhao and C. He, *Nature communications*, 2011, **2**, 495.
63. B. Peng, W. Chen, C. Liu, E. W. Rosser, A. Pacheco, Y. Zhao, H. C. Aguilar and M. Xian, *Chem. Eur. J.*, 2013, **20**, 1010-1016.
64. S. K. Bae, C. H. Heo, D. J. Choi, D. Sen, E.-H. Joe, B. R. Cho and H. M. Kim, *J. Am. Chem. Soc.*, 2013, **135**, 9915-9923.
65. Y. Jiang, Q. Wu and X. Chang, *Talanta*, 2014, **121**, 122-126.
66. P.-C. Chen, Y.-C. Li, J.-Y. Ma, J.-Y. Huang, C.-F. Chen and H.-T. Chang, *Sci. Rep.*, 2016, **6**, 24882-24890.
67. H.-H. Deng, S.-H. Weng, S.-L. Huang, L.-N. Zhang, A.-L. Liu, X.-H. Lin and W. Chen, *Anal. Chim. Acta*, 2014, **852**, 218-222.
68. C. n. Wang, X. n. Chu and M. W. Wu, *Sens. Actuators, B*, 2006, **113**, 320-323.
69. G. H. Jain and L. A. Patil, *Sens. Actuators, B*, 2007, **123**, 246-253.
70. M. Kaur, N. Jain, K. Sharma, S. Bhattacharya, M. Roy, A. K. Tyagi, S. K. Gupta and J. V. Yakhmi, *Sens. Actuator, B*, 2008, **133**, 456-461.
71. C. Yu, Y. Wang, K. Hu, W. Xing and T. Lu, *Sens. Actuators, B*, 2002, **96**, 259-265.
72. M. D. Shirsat, M. A. Bangar, M. A. Deshusses, N. V. Myung and A. Mulchandani, *Appl. Phys. Lett.*, 2009, **94**, 083502-083504.
73. A. Lv, M. Wang, Y. Wang, Z. Bo and L. Chi, *Chem. Eur. J.*, 2016, **22**, 3654-3659
74. J. F. Vetelino, R. K. Lade and R. S. Falconer, *IEEE Trans. Ultrason. Ferroelectr. Frequ. Control*, 1987, **34**, 156-161.
75. S. Cui, L. Yang, J. Wang and X. Wang, *Sens. Actuator B-Chem.*, 2016, **233**, 337-346.
76. Special issue of MOFs, *Chem. Rev.*, 2012, **112**, 673-1268.
77. Themed issue of MOFs, *Chem. Soc. Rev.*, 2009, **38**, 1201-1508.
78. K. Müller-Buschbaum, F. Beuerle and C. Feldmann, *Microporous Mesoporous Mater.*, 2015, **216**, 171-199.

79. X. Xin, J. Wang, C. Gong, H. Xu, R. Wang, S. Ji, H. Dong, Q. Meng, L. Zhang, F. Dai and D. Sun, *Sci. Rep.*, 2016, **6**, 21951-21959.
80. J. Cui, Y.-L. Wong, M. Zeller, A. D. Hunter and Z. Xu, *Angew. Chem. Int. Ed.*, 2014, **53**, 14438-14442.
81. H. Huang, W. Zhang, F. Yang, B. Wang, Q. Yang, Y. Xie, C. Zhong and J.-R. Li, *Chem. Eng. J.*, 2016, **289**, 247-253.
82. A. T. Nielsen, A. A. DeFusco and T. E. Browne, *J. Org. Chem.*, 1985, **50**, 4211-4218.
83. R. Deshmukh and V. Trivedi, *PLoS One*, 2014, **9**, e103706-e103718.
84. R. Deshmukh and V. Trivedi, *Toxicol. In Vitro*, 2013, **27**, 16-23.
85. S. Biswas, J. Zhang, Z. Li, Y.-Y. Liu, M. Grzywa, L. Sun, D. Volkmer and P. V. D. Voort, *Dalton Trans.*, 2013, **42**, 4730-4737.
86. S. Biswas and P. V. D. Voort, *Eur. J. Inorg. Chem.*, 2013, **2013**, 2154-2160.
87. M. SK, S. Bhowal and S. Biswas, *Eur. J. Inorg. Chem.*, 2015, **2015**, 3317-3322.
88. S. Biswas, T. Ahnfeldt and N. Stock, *Inorg. Chem.*, 2011, **50**, 9518-9526.
89. S. Biswas, D. E. P. Vanpoucke, T. Verstraelen, M. Vandichel, S. Couck, K. Leus, Y.-Y. Liu, M. Waroquier, V. V. Speybroeck, J. F. M. Denayer and P. V. D. Voort, *J. Phys. Chem. C*, 2013, **117**, 22784-22796.
90. A. Buragohain, S. Couck, P. V. D. Voort, J. F. M. Denayer and S. Biswas, *J. Solid State Chem.*, 2016, **238**, 195-202.
91. M. SK, M. Grzywa, D. Volkmer and S. Biswas, *J. Solid State Chem.*, 2015, **232**, 221-227.
92. A. Buragohain, P. V. D. Voort and S. Biswas, *Microporous Mesoporous Mater.*, 2015, **215**, 91-97.
93. A. Buragohain and S. Biswas, *Eur. J. Inorg. Chem.*, 2015, **2015**, 2463-2468.
94. D. L. Pavia, G. M. Lampman, G. S. Kriz and J. A. Vyvyan, *Introduction to Spectroscopy*, Thomson Brooks/Cole Stamford, USA, 5th edn., 2015.
95. V. Bon, I. Senkovska, M. S. Weiss and S. Kaskel, *CrystEngComm*, 2013, **15**, 9572-9577.
96. W. Zhang, H. Huang, D. Liu, Q. Yang, Y. Xiao, Q. Ma and C. Zhong, *Microporous Mesoporous Mater.*, 2013, **171**, 118-124.
97. V. Guillerm, F. Ragon, M. Dan-Hardi, T. Devic, M. Vishnuvarthan, B. Campo, A. Vimont, G. Clet, Q. Yang, G. Maurin, G. Férey, A. Vittadini, S. Gross and C. Serre, *Angew. Chem. Int. Ed.*, 2012, **51**, 9267-9271.

98. P. Horcajada, R. Gref, T. Baati, P. K. Allan, G. Maurine, P. Couvreur, G. Ferey, R. Morris and C. Serre, *Chem. Rev.*, 2012, **112**, 1232-1268.

99. D. Cunha, M. B. Yahia, S. Hall, S. R. Miller, H. Chevreau, E. Elkaïm, G. Maurin, P. Horcajada and C. Serre, *Chem. Mater.*, 2013, **25**, 2767-2776.

100. Y. Qian, B. Yang, Y. Shen, Q. Du, L. Lin, J. Lin and H. Zhu, *Sens. Actuator B-Chem.*, 2013, **182**, 498-503.

101. M. Ren, B. Deng, X. Kong, K. Zhou, K. Liu, G. Xu and W. Lin, *Chem. Commun*, 2016, **52**, 6415-6418.

102. N. Kumar, V. Bhalla and M. Kumar, *Coord. Chem. Rev.*, 2013, **257**, 2335-2347.

103. H. A. Henthorn and M. D. Pluth, *J. Am. Chem. Soc.*, 2015, **137**, 15330-15336.

104. S. Al-Kassab, E. Boyland and K. Williams, *Biochem. J.*, 1963, **87**, 4.

105. L. M. Baker, P. R. Baker, F. Golin-Bisello, F. J. Schopfer, M. Fink, S. R. Woodcock, B. P. Branchaud, R. Radi and B. A. Freeman, *J. Biol. Chem.*, 2007, **282**, 31085-31093.

106. C. Appenzeller-Herzog, *J. Cell Sci.*, 2011, **124**, 847-855.

107. H. A. Priestap and M. A. Barbieri, *J. Nat. Prod.*, 2013, **76**, 965-968.

108. M. A. C. Morelli, A. Ostuni, G. Matassi, C. Minichino, A. Flagiello, P. Pucci and A. Bavoso, *Inorg. Chim. Acta*, 2016, **453**, 330-338.

109. N. J. Pace and E. Weerapana, *ACS Chem. Biol.*, 2013, **9**, 258-265.

110. A. Chmyrov, T. Sandén and J. Widengren, *J. Phys. Chem. B*, 2010, **114**, 11282-11291.

111. G. Percheron, S. Michaud, N. Bernet and R. Moletta, *J. Chem. Technol. Biotechnol.*, 1998, **72**, 213-220.

112. J. L. Miljkovic, I. Kenkel, I. Ivanović-Burmazović and M. R. Filipovic, *Angew. Chem. Int. Ed.*, 2013, **52**, 12061-12064.

113. S. Sreejith, K. P. Divya and A. Ajayaghosh, *Angew. Chem. Int. Ed.*, 2008, **120**, 8001-8005.

114. L. Zhang, W.-q. Meng, L. Lu, Y.-S. Xue, C. Li, F. Zou, Y. Liu and J. Zhao, *Sci. Rep.*, 2014, **4**, 5870-5878.

Chapter 5

Fluorogenic naked-eye sensing and live-cell imaging of cyanide by a hydrazine-functionalized CAU-10 metal-organic framework

This chapter describes the synthesis and systematic characterization of a hydrazine-functionalized Al(III) MOF namely CAU-10-N_2H_3 (CAU = Christian-Albrechts-University). The activated MOF material is capable of sensing CN^- ions even in the presence of other competitive anions present in water. The appearance of green fluorescence under UV light upon cyanide addition makes this material a naked-eye fluorescent sensor for CN^- ions in aqueous medium. The live cell imaging experiments with non-toxic Al(III) MOF also establish that the MOF is capable of intracellular CN^- ions

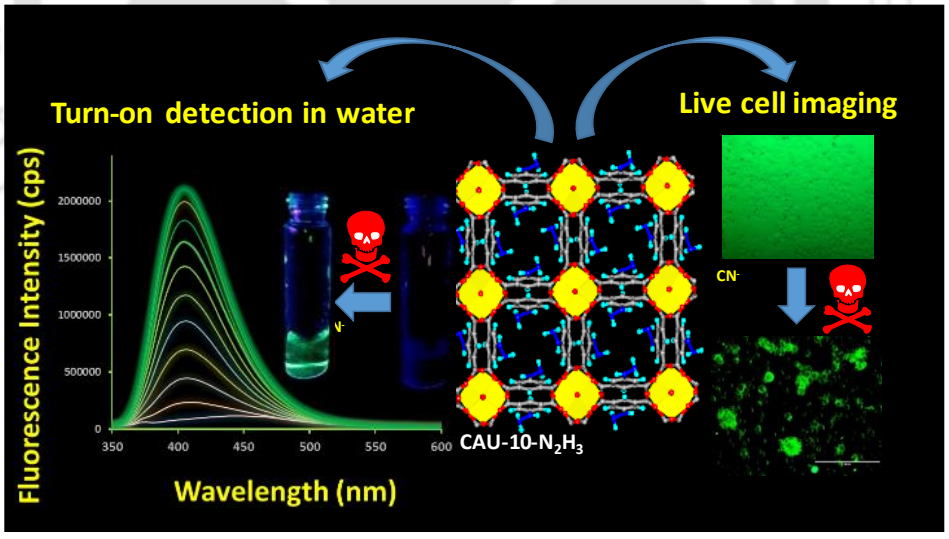

CrystEngComm

R. Dalapati, S. Nandi, H. Reinsch, B. K. Bhunia, B. B. Mandal, N. Stock, S. Biswas, *CrystEngComm*, 2018, **20**, 4194 - 4201.

5.1 Introduction

A large variety of fluorescent probes has been developed during the last twenty years for the sensing of anions. Among the common anions present in biological systems, the cyanide (CN^-) anion is deadly towards living organisms.[1] Cyanide induced inhibition of respiration, which is caused by strong cyanide binding at the heme unit of cytochrome c in its active site, leads to cytotoxic hypoxia and cellular asphyxiation.[2] The WHO (World Health Organization) recommended that the tolerable concentration of cyanide for drinking water is only 1.9 μM.[3,4] Though a large number of fluorescent sensor materials have been investigated so far,[5] their applications for real biological or medical purposes require the use of a pure aqueous medium. Unfortunately, the majority of conventional organic fluorescent molecules work in a mixed-organic medium, which restricts their real-life applications.[6,7] The detection of cyanide by fluorescent sensors in 100% aqueous medium is still rare.[8,9] Hence, the development of new fluorescent sensors for CN^- ions, which can work in a pure aqueous system, is still a challenging work for environmental or medical applications.

A large number of inorganic and organic fluorescent compounds have been developed to date for detecting different types of species.[10,11] The combination of both inorganic and organic constituents makes the metal-organic framework (MOF) materials exceptional candidates in the area of fluorescence-based detection. Based on the great advantages of MOF materials, a large number of MOF materials have been examined as fluorescence-based sensors for gaseous, liquid and solid species.[12-15] The main challenge of MOF materials for fluorescence sensing in an aqueous environment is their relatively low hydrolytic stability. Therefore, the smart design of water-stable MOFs is always desirable. Very recently, Ghosh *et al.* have reported fluorescence-based cyanide sensing in aqueous medium by two MOF materials.[16,17] Unfortunately, for these systems, either post-synthetic modification of the ligand or encapsulation of a reactive fluorescent probe is required for the cyanide sensing. A simple, single-step synthesis procedure would be desirable over a multi-step method for the synthesis of the target MOF probe.[18] Taking into account the above-mentioned concerns, in this work we present the preparation of a hydrazine-functionalized Al(III) MOF with CAU-10 (CAU = Christian-Albrechts-University) topology[19,20] called CAU-10-N_2H_3 (**7**). The activated (**7′**) material was employed for the fluorometric detection of lethal CN^- ions in pure aqueous medium. The MOF material shows fast response, good selectivity and sensitivity towards the detection of CN^- ions with naked-eye

visualization of the green fluorescence under a UV lamp. The probe can also detect CN^- ions in water samples as well as in living cells.

5.2 Experimental

5.2.1 Materials and physical measurements

All the reagent grade starting materials were obtained from commercial suppliers. Milli-Q water was used as a medium in all the fluorescence titration experiments. A Perkin Elmer Spectrum Two FT-IR spectrometer was used to record Fourier transform infrared spectra in the range of 440-4000 cm^{-1}. The following standard classifications were used to describe the FT-IR absorption bands: strong (s), medium (m), very strong (vs), broad (br), shoulder (sh) and weak (w). A Bruker D2 Phaser X-ray diffractometer working at 30 kV and 10 mA was utilized for the collection of X-ray powder diffraction (XRPD) patterns using Cu-Kα (λ = 1.5406 Å) radiation. A Mettler-Toledo TGA/SDTA 851e thermogravimetric analyzer was used to conduct thermogravimetric analyses in the temperature range of 25-600 °C with a heating rate of 5 °C min^{-1} under an air atmosphere. By employing a Quantachrome Autosorb iQMP gas sorption analyser, the nitrogen sorption experiments were accomplished at −196 °C, up to 1 bar. A Quantachrome iSorb-HP volumetric gas sorption analyser was applied for collecting the CO_2 adsorption isotherms (up to 1 bar) at 25 °C. Before the sorption analyses, the compounds were degassed at 100 °C overnight under dynamic vacuum. A HORIBA Jobin Yvon Fluoromax-4 spectrofluorometer was used to collect all the fluorescence emission spectra. To perform fluorescence lifetime measurements, an Edinburgh Instruments Life-Spec II instrument was employed, which utilizes the time-correlated single-photon counting method. The FAST software of Edinburgh Instruments was used for the fluorescence decay analysis by a reconvolution method.

5.2.2 Synthesis of the $H_2IPA\text{-}N_2H_3$ ligand

5-Aminoisophthalic acid (3.0 g, 0.016 mole) was suspended in 30 mL water/conc. HCl (2:1, v/v) mixture at 0 °C. An ice-cold solution (10 mL) of $NaNO_2$ (0.69 g, 0.01 mole) was added to it and the mixture was stirred for 30 min. Then, a solution of $SnCl_2{\cdot}2H_2O$ (6.77 g, 0.03 mole) in conc. HCl (20 mL) was added slowly with vigorous stirring and the reaction mixture was

allowed to stir for an extra hour. The precipitate was filtered off, thoroughly washed with an excess amount of water and then dried at 60 °C in an oven for 6 h. The purification of the ligand was completed by column chromatography employing ethyl acetate as the eluent. Yield: 3.02 g (0.015 mole, 93%). ^{1}H NMR (δ, ppm, 600 MHz, DMSO-d_6): 8.76 (s, 1H, -NH), 8.05 (s, 1H, Ar-H), 7.77 (s, 2H, Ar-H). ^{13}C NMR (δ, ppm, 150 MHz, DMSO-d_6): 166.87, 146.70, 132.46, 123.06, 119.14. ESI-MS (m/z): 197.06 for $[M + H]^+$.

5.2.3 Synthesis of [Al(OH)(IPA-N_2H_3)]·3.4H_2O·0.5DMF (CAU-10-N_2H_3, 7) and activation.

For the synthesis of **7**, the H_2IPA-N_2H_3 ligand (0.20 g, 1.02 mmol), 2 M aqueous solution of $AlCl_3·6H_2O$ (0.50 mL, 1.02 mmol), DMF (0.55 mL) and H_2O (1.75 mL) were mixed in a Teflon-liner and heated in a stainless steel autoclave at 120 °C for 12 h. The microcrystalline powder was filtered off and washed repeatedly with acetone (5 mL). Then, the solid was dispersed in water by sonication for 30 min. The dispersion was filtered and the light orange colored solid was dried in an air oven at 80 °C for 6 h. Yield: 184 mg (0.77 mmol, 76%) based on the Al salt. Anal. cald. for $C_{9.5}H_{17.3}AlN_{2.5}O_{8.9}$ (335.93 g mol^{-1}): C, 33.96 H, 5.19 N, 10.42%. Found: C, 34.1 H, 4.9 N, 10.56%. FT-IR (KBr, cm^{-1}): 3419 (br), 3079 (w), 2923 (w), 2214 (w), 1684 (s), 1635 (s), 1577 (vs), 1434 (s), 1407 (vs), 1112 (m), 1004 (w), 785 (s), 727 (s), 607 (s), 526 (m).

We activated the as-synthesized CAU-10-N_2H_3 material in two steps. The stirring of the as-synthesized compound (200 mg) was conducted in methanol (50 mL) at ambient temperature for 24 h. Then, the solvent-exchanged compound was filtered off and degassed at 100 °C for 24 h under high vacuum. The activated form of **7** was denoted as **7′**.

5.2.4 Pawley refinement

The cell parameters were deduced by Pawley refinement using TOPAS software.[21] The model of CAU-10-N_2H_3 (activated form) was generated by force field optimization using the universal force field implemented in Materials Studio.[22] The structure of the structurally related compound CAU-10- N_3 was utilized as a preliminary model.[23] The cell parameters were changed to the ones observed for CAU-10-N_2H_3 (activated form) and the fractional position of the metal ions was fixed. The protons were generated using the implemented tool and the structural model

was energetically optimized. However, no Rietveld refinement was possible which we attribute to the existence of solvent molecules within the pores and severe disorder in the structure induced by the bulky protic groups.

5.2.5 Fluorescence titration experiments

Initially, suspensions of **7′** in water having a concentration of 2 mg mL^{-1} were prepared by sonication to perform fluorescence titration measurements. Then, 100 μL of the suspension was diluted with 2900 μL of water (final concentration = 66.6 μg mL^{-1}) in a quartz cuvette and the solutions of different anions (concentration = 4 mM) were added in an incremental way.

5.2.6 Culture and maintenance of the RAW 264.7 (macrophage) cell line

RAW 264.7 macrophages (acquired from the National Centre for Cell Science, Pune, India) were cultured in high glucose Dulbecco's Modified Eagle's Medium (DMEM; Gibco, Life Technologies, U.S.A.) supplemented with 10% fetal bovine serum (FBS; Gibco, Life Technologies, U.S.A.) and 1% streptomycin-penicillin. Cells were seeded in a tissue culture flask and maintained at 37 °C in a humidified incubator with 5% CO_2. The medium was changed on every alternate day.

5.2.7 Cytocompatibility assay

Cytocompatibility of probe **7′** was checked by the MTT [3-(4,5- dimethylthiazol-2-yl)-2,5-diphenyltetrasodium bromide] (Sigma, U.S.A.) assay following a previously described protocol.[24] In brief, RAW 264.7 macrophages (5 × 103 cells in 180 μL) were plated in each well of a 96-well plate followed by the addition of 20 μL of different concentrations of probe **7′** (0-100 μM). The plates were kept for 72 h at 37 °C in a humidified incubator with 5% CO_2. After incubation, wells were replenished with fresh medium and 20 μL of MTT (prepared in a concentration of 5 mg ml^{-1} in phosphate buffered saline; PBS, pH = 7.4) was added in each well. 4 h of post incubation, 200 μL of dimethyl sulfoxide (DMSO; Sigma, U.S.A.) was added to solubilize the formazan crystals. Absorbance was recorded at 570 nm using a multiplate reader (Tecan Infinite 200 Pro, Switzerland).

5.2.8 Live cell imaging

For live cell imaging, RAW 264.7 macrophages (1 × 104 cells per well) were seeded in a 96-well plate and incubated at 37 °C in a humidified incubator with 5% CO_2. After 24 h, 25 μM of probe **7′** (prepared in the same cell culture media) was added and kept for 8 h. Post incubation, cells were washed with PBS (pH = 7.4) to remove surplus probe molecules from the surface of cells. Prior to live cell imaging, 15 μM of NaCN (prepared in PBS, pH = 7.4) was added to the wells and incubated for 15 min. However, few wells were left without addition of NaCN to understand the effect of only probe **7′**. Images were captured using a fluorescence microscope (EVOS FL, Life Technologies, U.S.A.).

5.3 Results and discussion

5.3.1 Synthesis and activation

The new hydrazine-functionalized MOF, CAU-10-N_2H_3 (**7**) was synthesized by following previous synthesis procedures documented for CAU-10-X (X = -H, -OCH_3, -CH_3, -NH_2, -NO_2, -OH) materials.[19,23] Briefly, a solvothermal reaction was conducted at 120 °C for 12 h between $AlCl_3 \cdot 6H_2O$ and the H_2IPA-N_2H_3 ligand with a 1 : 1 molar ratio using a mixed solvent system of *N*,*N*-dimethylformamide (DMF) and water. After the reaction, the microcrystalline powder material (**7**) was collected by filtration.

The solvent molecules entrapped in the pores of the as-synthesized compound (**7**) were first exchanged with methanol (having low boiling point and thus easily removable) molecules. Then, the solvent-exchanged **7** was heated under dynamic vacuum at 100 °C overnight to remove the guest solvent molecules. The solvent-exchange of the compound followed by thermal activation did not alter the XRPD pattern (Figure 5.1), which suggests that the compound retained its structural integrity throughout the activation process.

5.3.2 FT-IR spectroscopy

Both the as-synthesized and activated materials show very strong absorption bands around 1580 and 1405 cm^{-1} in their FT-IR spectra (Figure 5.2). These two absorption bands arise owing to the asymmetric and symmetric carboxylate stretching vibration of the framework IPA-

N_2H_3 ligands, respectively. [25] In both IR spectra, the two sharp absorption bands around 785 and 725 cm^{-1} arise from the C-H out-of-plane vibrations of the hydrazine-functionalized ligand present in the framework structure.[26]

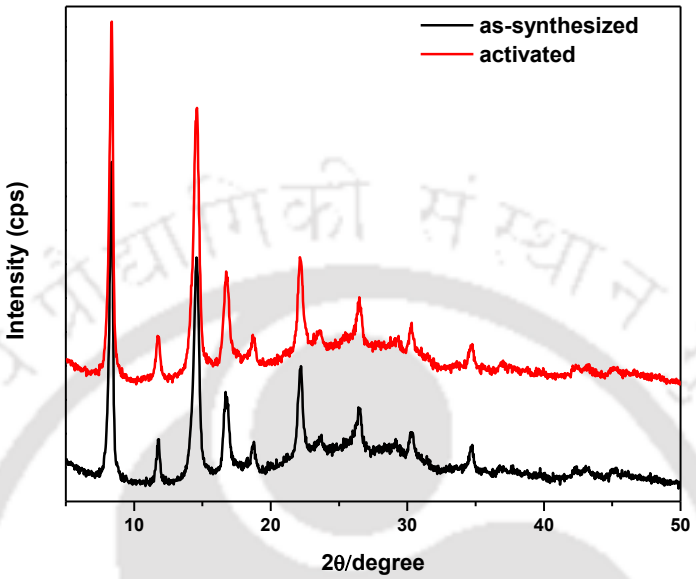

Figure 5.1 XRPD patterns of as-synthesized **7** and thermally activated **7′**.

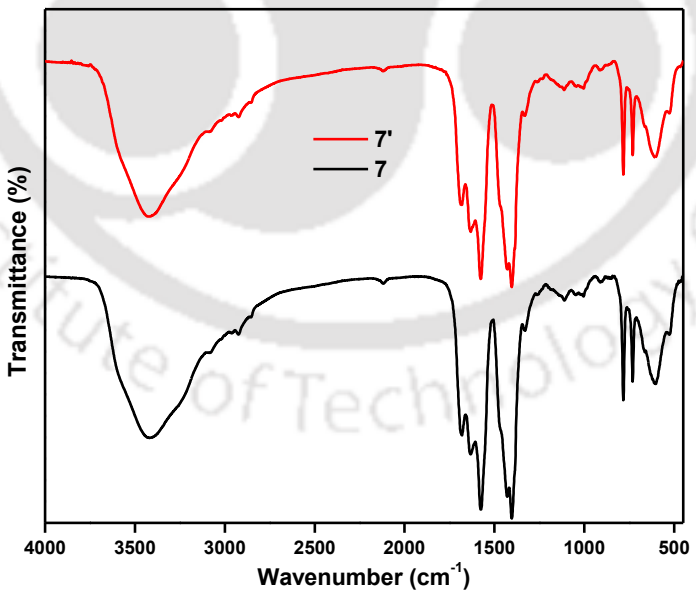

Figure 5.2 FT-IR spectra of as-synthesized **7** and thermally activated **7′**.

5.3.3 Structure description

The XRPD patterns of the as-synthesized and thermally activated samples of compound **7** were successfully indexed, which suggests that the compound crystallizes in the tetragonal crystal system possessing a space group of $I4_1/a$ (Table 5.1). The Pawley refinement unveiled a good agreement between the assumed space group and the experimental XRPD patterns of **7** (Figure 5.3). The isotypic crystal structure of CAU-10-N_3 was used as a preliminary model for the structural simulation by force-field calculation (for details, see Experimental section).[23] The framework structure of **7** is presented in Figure 5.4. As revealed from the figure, the framework of CAU-10-N_2H_3 is formed by the interconnection of cis-corner sharing [AlO_6] octahedral with the hydrazine-functionalized isophthalate ligand molecules. This structural connectivity leads to the formation of helical chains (Figure 5.4b). Each helix is connected with four nearby inorganic building units having an alternating rotational arrangement through the coordinated isophthalate (IPA) ligands. Two adjacent helices are related by a mirror plane. This distinct arrangement of the inorganic building units and ligand molecules leads to the formation of square shaped one-dimensional channels. The hydrazine groups protrude towards the inner side of the channels.

Table 5.1 Pawley refinement parameters for **7** and **7′**.

Compound	**7**	**7′**
space group	$I4_1/a$	$I4_1/a$
$a = b$ [Å]	21.379(16)	21.395(12)
c [Å]	11.346(8)	11.223(6)
$\alpha = \beta = \gamma$ [°]	90	90
R_{WP} [%]	3.3	3.6
GoF	2.2	2.4

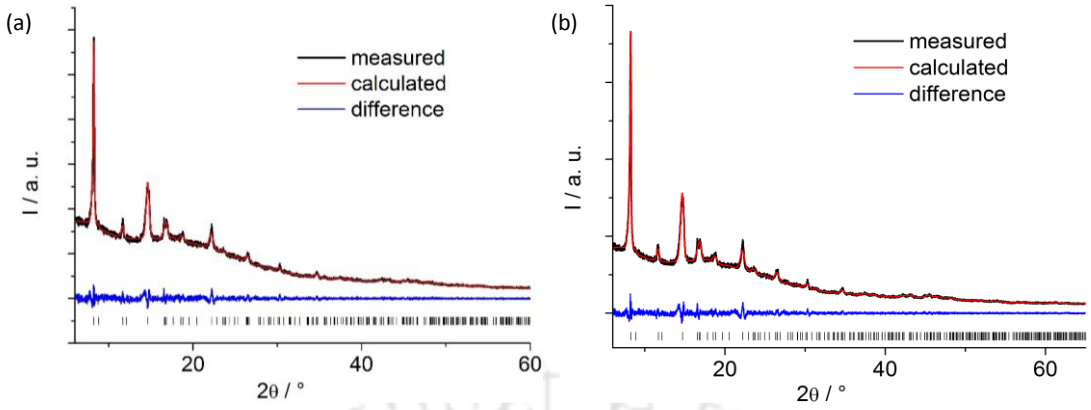

Figure 5.3 Final Pawley refinement plot for as-synthesized (a) and activated (b) form of **7**. The black and red curves denote the measured and calculated XRPD patterns, respectively. The difference between the experimental and theoretical data is indicated by the blue curve, whereas the allowed Bragg reflection positions are represented by the vertical bars.

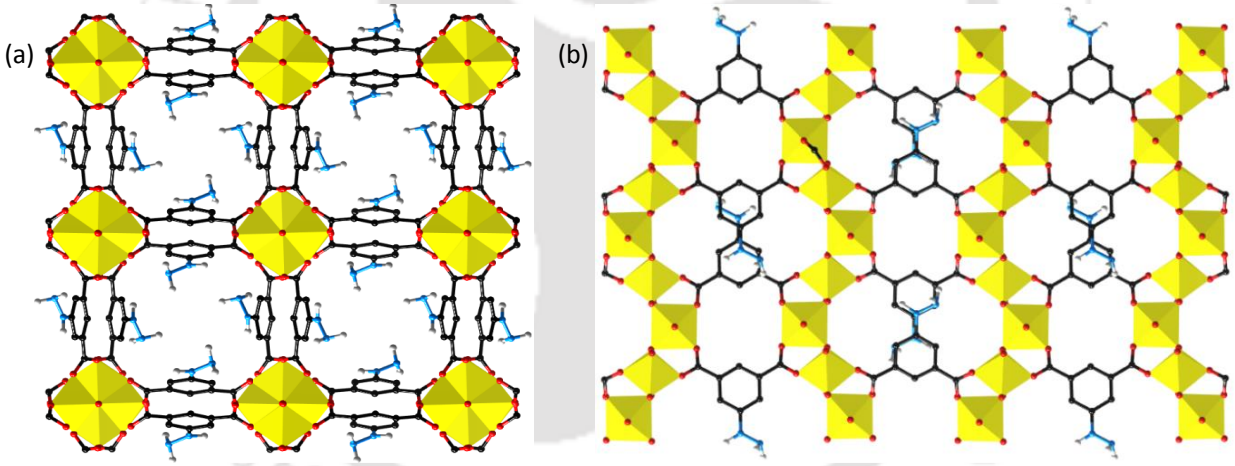

Figure 5.4 The simulated structure of the framework of CAU-10-N_2H_3 (**7**) compound (a). Hydrogen atoms have been omitted from phenyl ring of the structural diagram for clarity. Helical arrangement of [AlO_6] octahedra in the framework of CAU-10-N_2H_3 as seen along the b-axis (b). Color codes: C, black; O, red; N, blue; Al, yellow polyhedra; H, white.

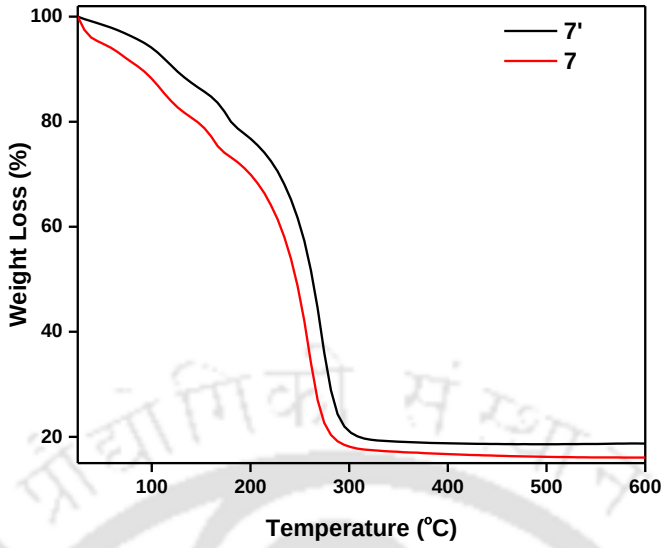

Figure 5.5 TG curves of **7** and **7′** recorded in an air atmosphere in the temperature range of 25-600 °C with a heating rate of 5 °C min^{-1}.

5.3.4 Thermal stability

Thermogravimetric analyses were carried out to check the thermal stability of the as-synthesized and activated materials under an air atmosphere in the temperature range of 25-600 °C. TG curves of both forms of the material (Figure 5.5) reveal that the compound exhibits thermal stability only up to 250 °C. The structural collapse of the material occurs after this temperature due to the elimination of the coordinated IPA-N_2H_3 ligands from the framework.

The first weight loss of 18.4% in the TG curve of the as-synthesized compound in the range of 30-120 °C can be assigned to the elimination of 3.4 guest water molecules (calcd.: 18.2 wt%) per formula unit. In the second step, a weight loss of 10.6% in the temperature range of 130-190 °C can be ascribed to the removal of 0.5 DMF molecules per formula unit (calcd.: 10.8 wt%). The results of thermogravimetric and elemental analyses were utilized to determine the chemical formula of the CAU-10-N_2H_3 compound.

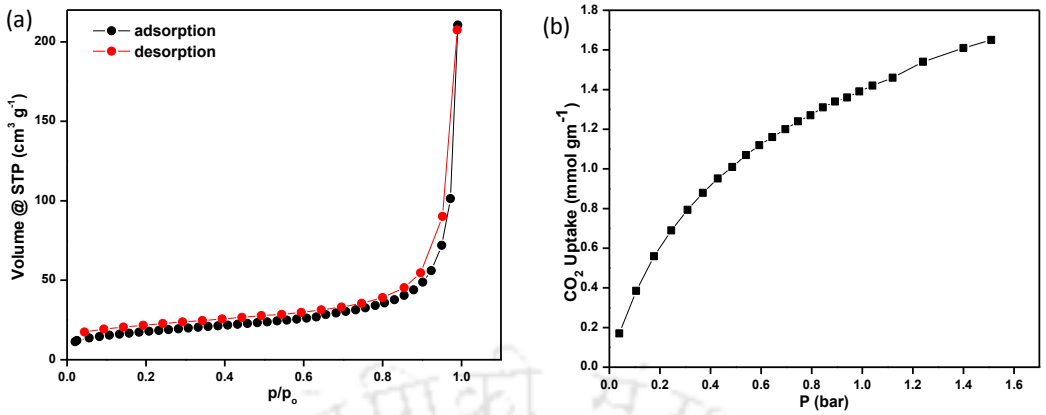

Figure 5.6 (a) N_2 adsorption (black circles) and desorption (red circles) isotherms of **7′** recorded at –196 °C. (b) CO_2 adsorption of **7′** recorded at 25 °C.

5.3.5 Gas sorption properties

The permanent porosity of the activated CAU-10-N_2H_3 material was checked by N_2 sorption analysis (Figure 5.6a). The specific surface area (S_{BET}) of **7′** was calculated as 61 $m^2\ g^{-1}$ from the N_2 adsorption isotherm. Thus, the compound showed almost no porosity towards N_2, which contrasts with previously reported CAU-10-H (S_{BET} = 635 $m^2\ g^{-1}$) and CAU-10-NO_2 (S_{BET} = 440 $m^2\ g^{-1}$) materials.[27] We assume that the bulky hydrazine functional groups prohibit the free diffusion of N_2 molecules through the narrow channels.

A CO_2 adsorption experiment was additionally carried out to check the permanent porosity of **7′**. The low-pressure CO_2 adsorption measurement showed that the adsorption capacity reached up to 1.4 mmol g^{-1} (Figure 5.6b) at 1 bar and 25 °C. Thus, the CO_2 adsorption experiment unambiguously verifies the permanent microporosity of activated **7**. The CO_2 adsorption capacity of **7′** is comparable with those of the existing structurally related CAU-10-X (X = -H, -OCH_3, -CH_3, -NH_2, -NO_2, -OH) compounds.[19]

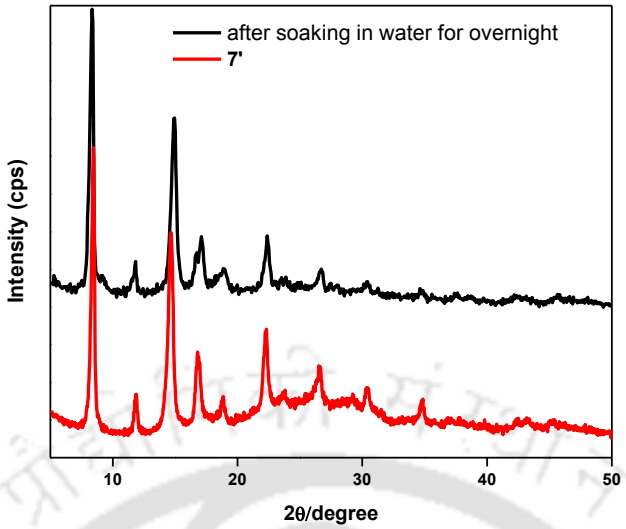

Figure 5.7 Hydrolytic stability of **7′**.

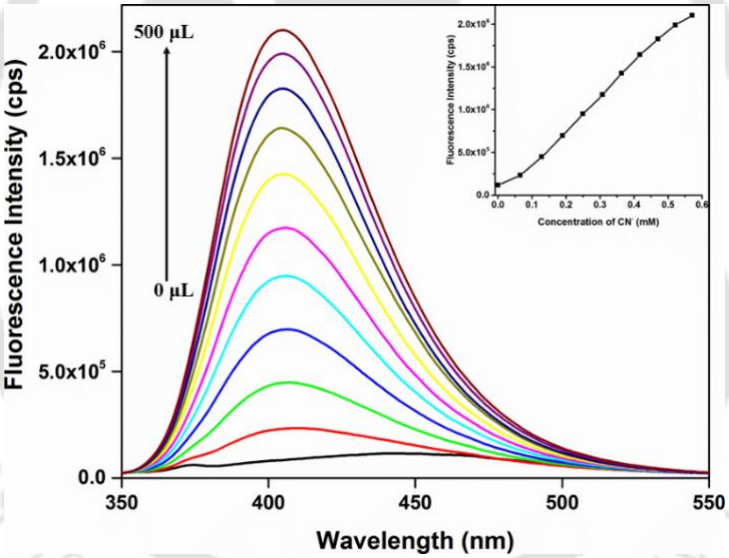

Figure 5.8 Change in the fluorescence signal of **7′** with increasing addition of 4 mM CN^- solution. Inset: concentration-dependent fluorescence signal enhancement of **7′** monitored at 405 nm.

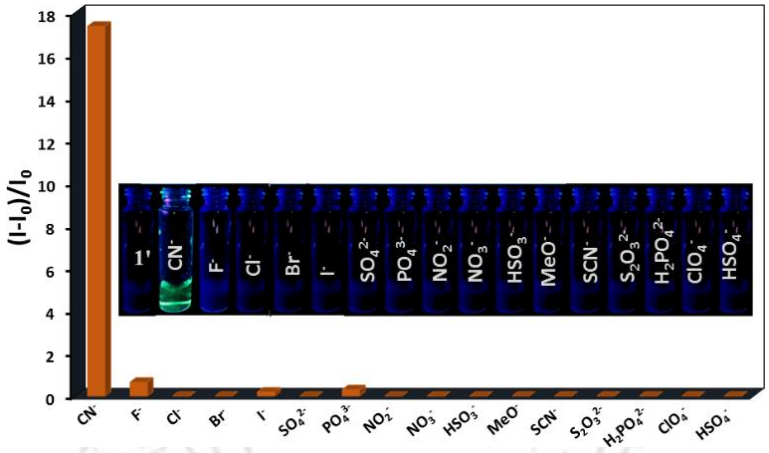

Figure 5.9 Relative fluorescence enhancement behavior of **7′** towards addition of different anions. Inset: naked-eye fluorogenic response of **7′** towards different anions.

5.3.6 Fluorescence intensity based sensing of CN^- ions

Due to the extreme toxicity of CN^- ions, a large number of fluorogenic probes have been developed in the past few decades for the sensing of CN^- ions.[16,28-30] Very recently, only a few MOF materials have been employed for the sensing of CN^- ions.[18] To check the hydrolytic stability of **7′**, we stirred the MOF material in water overnight. The recovered MOF material showed retention of its structural integrity after treatment with water, which was confirmed by the XRPD analysis (Figure 5.7). The non-toxicity and hydrolytic stability encouraged us to explore the applicability of the CAU-10-N_2H_3 material for the sensing of anions in pure aqueous medium.

Fluorescence titration experiments were carried out in order to serve this purpose. Thus, the emission spectra (λ_{ex} = 330 nm) of the stable aqueous suspension of **7′** were collected upon regular incremental addition of the sodium salts of different anions (Cl^-, I^-, F^-, Br^-, NO_3^-, NO_2^-, $H_2PO_4^-$, HSO_3^-, SO_4^{2-}, ClO_4^-, PO_4^{3-}, HSO_4^-, $S_2O_3^{2-}$, MeO^-, CN^- and SCN^-). Figure 5.8 shows that a drastic enhancement in the fluorescence intensity with a large blue-shift ($\Delta\lambda$ = 30 nm) in the emission band was noticed only after the addition of the CN^- ion. Negligible changes in the fluorescence intensity were observed for all the other 15 potentially intrusive anions (Figure 5.9). These observations unequivocally support that the CAU-10-N_2H_3 probe is highly selective for CN^- ions over other common competing anions. Interestingly, the development of green fluorescence was observed after the addition of CN^- solution to the aqueous suspension of **7′**, which can be easily visualized by the naked eye under a normal UV-lamp. Furthermore, the

XRPD pattern of **7′** was measured after the cyanide sensing experiment and no loss of crystallinity was observed (Figure 5.10). This observation confirms the structural integrity of the CAU-10-N_2H_3 material throughout the sensing event.

Time-dependent fluorescence investigations were carried out with different concentrations of CN^- ions in order to evaluate the response time of **7′** for the sensing of CN^- ions. We have monitored the fluorescence intensity of the CAU-10- N_2H_3 compound at a specific concentration of CN^- ions up to 15 min (Figure 5.11). The studies revealed that the compound showed a fast response time of approximately 2 min after the addition of CN^- solution.

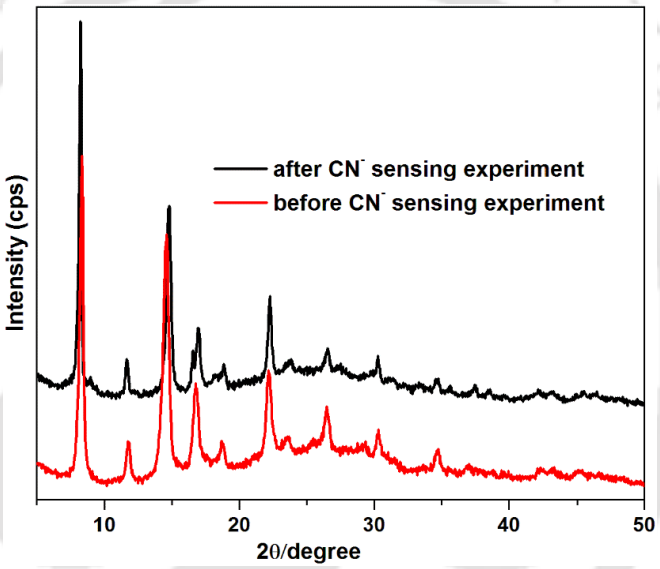

Figure 5.10 XRPD patterns of **7′** before and after the CN^- sensing experiment.

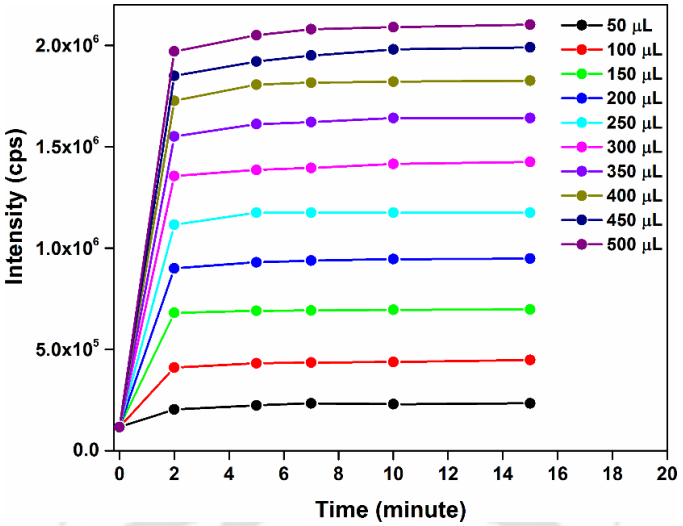

Figure 5.11 Time-dependent change in the fluorescence intensity of **7′** upon addition of different concentrations of CN^- ion.

For practical applications, it is desirable that the fluorescent probe should work effectively even in the presence of intrusive anions in complicated systems. To check the capability of the MOF material for the selective sensing of toxic CN^- ions, fluorescence titration experiments were carried out with **7′** after the addition of CN^- ions in the presence of other common interfering anions present in water. From Figure 5.12, it can be inferred that the detection ability of cyanide by **7′** was hardly influenced by the presence of other competitive anions. The relative fluorescence turn-on responses were found to be slightly lower with the co-existence of some anions like F^-, I^-, PO_4^{3-} and SO_4^{2-}. The F^-, PO_4^{3-} and SO_4^{2-} anions also have the affinity to form hydrogen bonding interactions with the acidic protons of receptor molecules.[31-33] Due to the competitive hydrogen bonding interactions, the relative fluorescence turn-on responses with the co-existence of these anions were found to be lower. On the other hand, the I^- ion is a well-known fluorescence quencher. The fluorescence quenching ability of the I^- ion is probably responsible for the comparatively lower fluorescence turn-on response. The outcomes of these fluorescence titration experiments substantiate that the hydrazine functionalized MOF material exhibits an exceptional selectivity towards CN^- ions and the co-existence of other common anions does not significantly interfere with the selectivity.

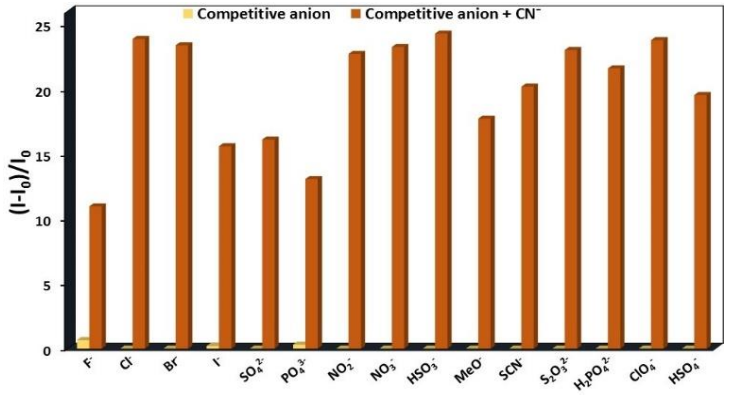

Figure 5.12 Enhancement of the fluorescence signal of **7′** in presence of an interfering anion, followed by the addition of CN^- solution.

The limit of detection (LOD) was calculated for this fluorogenic probe for CN^- ions. The LOD value was estimated to be 4.8×10^{-7} M (0.48 μM) by using the following equation at a signal-to-noise ratio of 3:[34]

$$LOD = 3\sigma/K$$

where σ indicates the standard deviation calculated from the initial intensity of the MOF material in the absence of CN^- solution and K stands for the slope of the linear curve which was obtained by plotting the fluorescence intensity of **7′** against the concentration of CN^- solution. The LOD value is lower than the World Health Organization (WHO) recommended concentration of CN^- ions in drinking water (2 μM).[35] Hence, a MOF-based water monitoring system can be developed by using the presented hydrazine-functionalized MOF material.

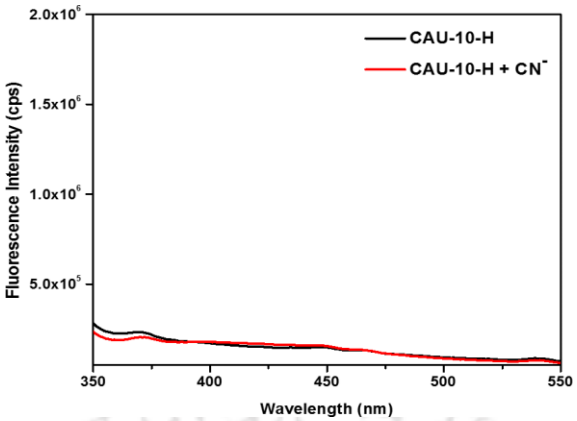

Figure 5.13 Change in the fluorescence intensity of CAU-10-H upon addition of 4 mM solution (500 µL) of aqueous CN^- solution.

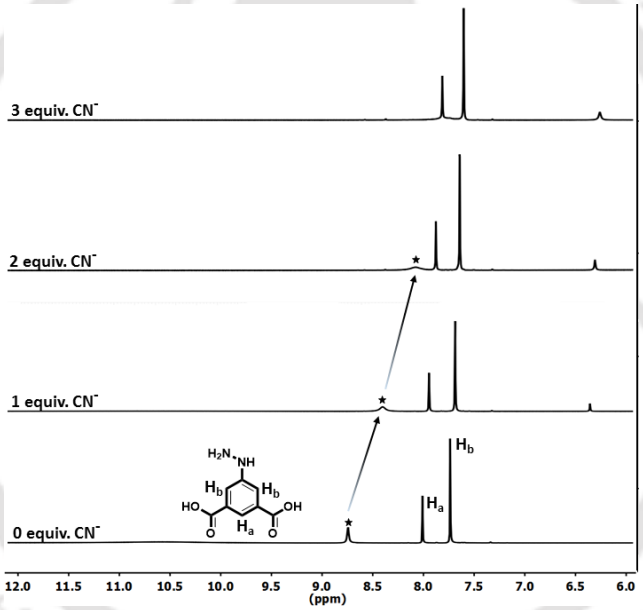

Figure 5.14 Stacked ^1H NMR spectra of the $H_2IPA\text{-}N_2H_3$ ligand upon the addition of CN^- solution in DMSO-d_6 at 25 °C.

5.3.7 Mechanism for the sensing of CN^- ions

The CN^- ion has the strong tendency to form hydrogen bonds with the acidic protons of sensor molecules.[36-38] Very recently, it has been demonstrated that the deprotonation of the acidic -NH proton of a carbazole-functionalized Z(IV) MOF by the CN^- ion can be utilized for the fluorescence turn-on sensing of the anion.[18] As a control experiment, unfunctionalized CAU-

10-H MOF was treated with the CN^- ion. No obvious change in the fluorescence intensity was recorded for the CAU-10-H MOF (Figure 5.13). This result affirms that the hydrazine-functionalized ligand present in the MOF system is responsible for sensing. To check the possibility of the cyanide-induced deprotonation mechanism for the presented MOF probe, NMR titration experiments were conducted with the free $H_2IPA\text{-}N_2H_3$ ligand in DMSO-d_6 upon addition of the aqueous solution of the CN^- ion.[39] With increasing concentration of the CN^- ion, the intensity of the peak at 8.7 ppm for the -NH proton decreased gradually and shifted towards the up-field region of the spectrum (Figure 5.14). After the addition of three equiv. of CN^- ion, the peak owing to the -NH proton disappeared, whereas a considerable upfield shift was observed for the peaks related to the aromatic protons. The disappearance of the peak due to the -NH proton and the drastic up-field shift of the corresponding peak affirm the cyanide-induced deprotonation of the -NH proton.

The cyanide induced deprotonation process can affect the electron transfer process throughout the MOF system. Initially, the photo-induced electron transfer (PET) process from the hydrazine moiety to the phenyl ring suppresses the fluorescence intensity of the MOF material. In the presence of the CN^- ion, the deprotonation-induced enhancement of the electron density throughout the framework prohibits the PET process, thus the fluorescence intensity of the MOF compound is enhanced. A similar fluorescence turn-on mechanism based on the inhibition of the electron transfer process has been proposed recently by Cao *et al.* for the selective detection of SO_2 gas by the amine functionalized MOF-5.[40]

5.3.8 Fluorescence lifetime based sensing of CN^- ions

Time-resolved photoluminescence (TRPL) decay experiments were performed with **7′** to examine its excited-state behavior as well as feasibility to act as a lifetime-based sensor for CN^- ions. The TRPL decay profiles of the MOF probe were measured in the absence and presence of CN^- ions (Figure 5.15). The compound showed a bi-exponential decay curve with two species with an average excited-state lifetime of 0.38 ns (Table 5.2). In the presence of the CN^- ion, the amplitude of the longer-lived component increased at the expense of the shorter-lived component and the average excited-state lifetime increased to 4.16 ns. The longer-lived species arises from the deprotonation of the -NH proton, which enhances the rate of radiative decay and

consequently boosts the fluorescence intensity of the MOF material.[37,40,41] The noticeable change in the fluorescence intensity after cyanide addition points out that the implementation of a lifetime-based fluorescence sensor for toxic CN^- ions can be achieved by this MOF material.

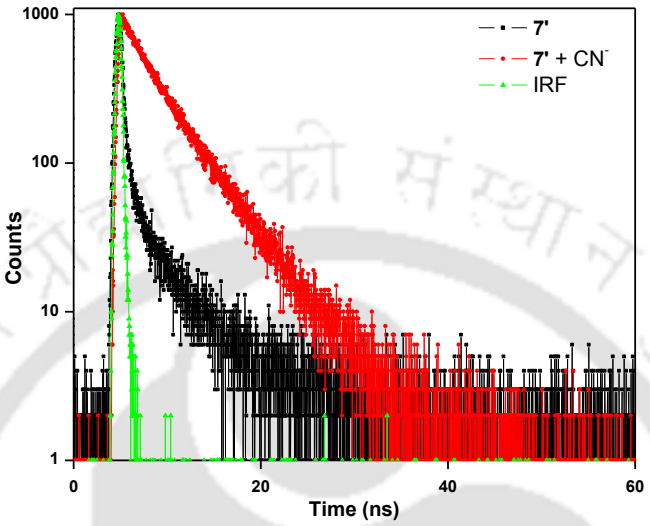

Figure 5.15 Lifetime decay profile of **7′** in presence of aqueous CN^- solution (λ_{ex} = 336 nm, monitored at 430 nm).

Table 5.2 Average excited-state lifetime (<τ>) values of **7′** before and after addition of CN^- solution (λ_{ex} = 336 nm).

Volume of CN^- solution added (μL)	a_1	a_2	τ_1 (ns)	τ_2 (ns)	<τ>* (ns)	χ^2
0	0.981	0.019	0.310	3.866	0.377	1.09
500	0.153	0.846	0.778	4.784	4.161	1.01

* $\langle\tau\rangle = a_1\tau_1 + a_2\tau_2$

5.3.9 Analysis of CN^- ions in real water samples

Encouraged by the excellent selectivity and sensitivity of **7′** towards CN^- sensing, we investigated the ability of the probe to detect CN^- ions in tap water and drinking water samples. Initially, no CN^- ion was found in either tap water or drinking water samples. Then, cyanide was spiked in the water samples and the spiked samples were used for the fluorescence sensing

experiments. The results obtained from these experiments are summarized in Table 5.2. The recovery for the cyanide sensing experiments ranges from 97.5 to 101.3% with very low RSD (n = 3; RSD = relative standard deviation) values, and suggests that **7′** has enormous potential for monitoring CN^- concentration in potable water.

Table 5.2 Estimation of CN^- concentrations in real water samples

Water sample	CN^- spiked (μM)	CN^- found (μM)	Recovery (%)	RSD (%)
Tap water	10	9.7	97	2.1
	40	39.5	98.7	1.3
Drinking water	10	10.3	103	1.8
	40	40.6	101.5	1.2

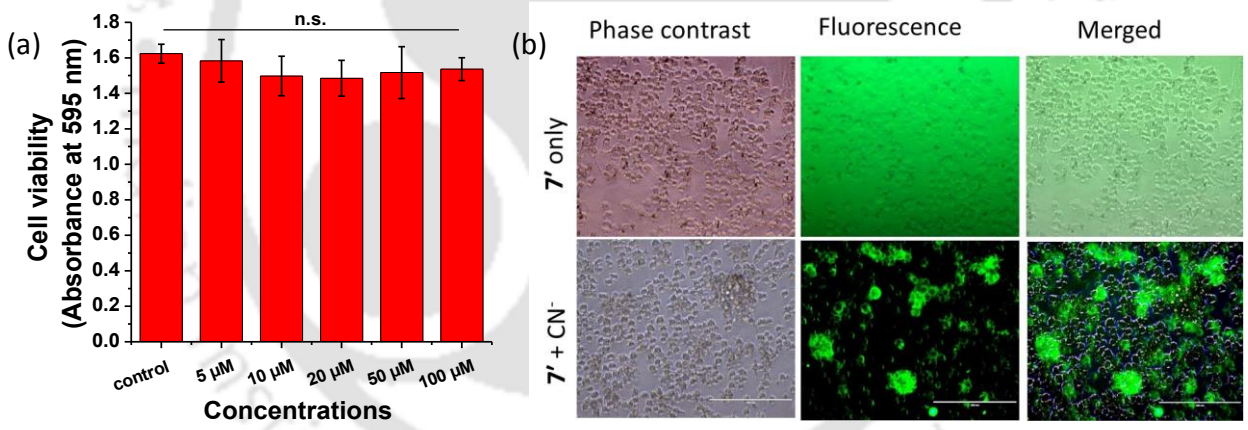

Figure 5.15 (a) Effect of different concentrations of **7′** on RAW 264.7 macrophages cultured in 96-well plates; Data represented as the average ± standard deviation, n = 3. (b) Live cell imaging of CN^- by **7′**. Phase contrast (first column), fluorescence (middle column) and merged images (third column) of **7′**-loaded RAW 264.7 macrophages before (above row) and after (bottom row) incubation with 15 μM NaCN solution for 15 min at 37 °C. Scale bar = 200 μm.

5.3.10 Live-cell imaging of CN^- ions

A cellular imaging experiment was conducted to demonstrate the CN^- sensing ability of **7′** in living cells. To use the MOF probe for cell imaging, it must be biocompatible. Therefore, an in vitro cell viability test was carried out with RAW 264.7 cells. The cells were treated for 72 h with five varying concentrations (5-100 μM) of **7′**. The data (shown in Figure 5.15a) demonstrated the cell viability as compared to the control sample (treated with PBS). The presence of **7′** had an almost negligible effect on cell viability. This cell viability experiment confirmed that the MOF probe **7′** is non-toxic to RAW 264.7 cells and it could be used for cell imaging investigation. As depicted in Figure 5.15b, the incubation of the RAW 264.7 cells with **7′** (25 μM) resulted in no fluorescence emission in the green fluorescence channel. In contrast, when the probe-loaded RAW 264.7 cells were treated with 15 μM CN^- solution, a bright green fluorescence signal was noticed. This observation is consistent with the results of the extracellular CN^- sensing experiment. From the results of live-cell imaging studies, it becomes inevitable that material **7′** can be used for monitoring cyanide toxicity inside the live cells.

5.4 Conclusions

In summary, we have shown the synthesis and systematic characterization of a hydrazine-functionalized Al(III) MOF namely CAU-10-N_2H_3 (**7**). The appropriate choice of a framework structure and functional group tethered with the ligand allowed us to utilize the material as a new sensor for the poisonous cyanide anion in aqueous medium. The activated material **7′** is capable of sensing CN^- ions even in the presence of other competitive anions present in water. The appearance of green fluorescence under UV light upon cyanide addition makes this material a naked-eye fluorescent sensor for CN^- ions in aqueous medium. The judicious design of a linker molecule with the acidic -NH proton facilitates the cyanide induced deprotonation pathway, which leads to the fluorescence turn-on signal of the MOF probe. In addition, the fluorescence lifetime measurements indicate that material **7′** can also be used as a lifetime-based sensor for CN^- ions. The CAU-10-N_2H_3 probe shows a very low detection limit of 0.48 μM, which is lower than the allowable cyanide concentration (2 μM) in drinking water according to the WHO. Fascinated by the sensitive detection of CN^- ions in aqueous medium, we performed spike-and-recovery experiments, which confirm that compound **7′** has the capability to detect cyanide in

environmental water samples. These results suggest that the CAU-10-N_2H_3 material can be used for controlling the quality of water samples. Furthermore, the live cell imaging experiments unambiguously demonstrate that probe **7′** is capable of sensing intracellular CN^- ions. Hence, the probe can be applied for monitoring cyanide toxicity in living cells.

5.5 References

1. K. N. Anjali, X. Shi, D. L. Harrison, J. E. Morningstar, S. Mahon, A. Chan, P. Sips, J. Lee, C. A. MacRae and G. R. Boss, *Cell Chem. Biol.*, 2017, **24**, 565-575.
2. F. Wang, L. Wang, X. Chen and J. Yoon, *Chem. Soc. Rev.*, 2014, **43**, 4312-4324.
3. W. H. Organization, Guidelines for drinking-water quality, World Health Organization, 2004.
4. H. L. Zhang, T. B. Wei, W. T. Li, W. J. Qu, Y. L. Leng, J. H. Zhang, Q. Lin, Y. M. Zhang and H. Yao, *Spectrochim. Acta, Part A*, 2017, **175**, 117-124.
5. J. Rocha, L. D. Carlos, F. A. A. Paz and D. Ananias, *Chem. Soc. Rev.*, 2011, **40**, 926-940.
6. T. Ebaston, G. Balamurugan and S. Velmathi, *Anal. Methods*, 2016, **8**, 6909-6915.
7. P. M. Reddy, S. R. Hsieh, C. J. Chang and J.-Y. Kang, *J. Hazard. Mater.*, 2017, **334**, 93 103.
8. Y. Y. Guo, X. L. Tang, F. P. Hou, J. Wu, W. Dou, W. W. Qin, J. X. Ru, G. L. Zhang, W. S. Liu and X. J. Yao, *Sens. Actuators, B*, 2013, **181**, 202-208.
9. E. Palomares, M. V. Martínez-Díaz, T. Torres and E. Coronado, *Adv. Funct. Mater.*, 2006, **16**, 1166-1170.
10. L. Basabe-Desmonts, D. N. Reinhoudt and M. Crego-Calama, *Chem. Soc. Rev.*, 2007, **36**, 993-1017.
11. S. M. Ng, M. Koneswaran and R. Narayanaswamy, *RSC Adv.*, 2016, **6**, 21624-21661.
12. L. E. Kreno, K. Leong, O. K. Farha, M. Allendorf, R. P. V. Duyne and J. T. Hupp, *Chem. Rev.*, 2011, **112**, 1105-1125.
13. L. Guo, M. Wang and D. Cao, *Small*, 2018, **14**, 1703822.
14. M. Wang, L. Guo and D. Cao, *Sens. Actuators, B*, 2018, **256**, 839-845.
15. Z. Xiang, C. Fang, S. Leng and D. Cao, *J. Mater. Chem. A*, 2014, **2**, 7662-7665.
16. A. Karmakar, N. Kumar, P. Samanta, A. V. Desai and S. K. Ghosh, *Chem. Eur. J.*, 2016, **22**, 864-868.
17. A. Karmakar, B. Joarder, A.Mallick, P. Samanta, A. V. Desai, S. Basu and S. K. Ghosh, *Chem. Commun.*, 2017, **53**, 1253-1256.

18. A. Das and S. Biswas, *Sens. Actuators, B*, 2017, **250**, 121-131.

19. H. Reinsch, M. A. v. d. Veen, B. Gil, B. Marszalek, T. Verbiest, D. D. Vos and N. Stock, *Chem. Mater.*, 2012, **25**, 17-26.

20. H. Jin, A. Wollbrink, R. Yao, Y. Li, J. Caro and W. Yang, *J. Membr. Sci.*, 2016, **513**, 40-46.

21. A. Coelho, Topas Academics 4.2, Coelho Software, Brisbane, 2007.

22. Materials Studio Version 5.0, Accelrys Inc., San Diego, 2009.

23. S. Nandi, H. Reinsch, S. Banesh, N. Stock, V. Trivedi and S. Biswas, *Dalton Trans.*, 2017, **46**, 12856-12864.

24. J. P. Kumar, R. Konwarh, M. Kumar, A. Gangrade and B. B. Mandal, *ACS Sustainable Chem. Eng.*, 2018, **6**, 1235-1245.

25. N. R. Dhumal, M. P. Singh, J. A. Anderson, J. Kiefer and H. J. Kim, *J. Phys. Chem. C*, 2016, **120**, 3295-3304.

26. H. Reinsch, S. Waitschat and N. Stock, *Dalton Trans.*, 2013, **42**, 4840-4847.

27. D. Fröhlich, S. K. Henninger and C. Janiak, *Dalton Trans.*, 2014, **43**, 15300-15304.

28. Y. Kim, H. S. Huh, M. H. Lee, I. L. Lenov, H. Zhao and F. P. Gabbaï, *Chem. -Eur. J.*, 2011, **17**, 2057-2062.

29. N. Busschaert, C. Caltagirone, W. V. Rossom and P. A. Gale, *Chem. Rev.*, 2015, **115**, 8038-8155.

30. A. K. Mahapatra, K. Maiti, S. K. Manna, R. Maji, C. D. Mukhopadhyay, B. Pakhira and S. Sarkar, *Chem. Asian J.*, 2014, **9**, 3623-3632.

31. B. Sui, B. Kim, Y. Zhang, A. Frazer and K. D. Belfield, *ACS Appl. Mater. Interfaces*, 2013, **5**, 2920-2923.

32. R. Dalapati and S. Biswas, *Sens. Actuators, B*, 2017, **239**, 759-767.

33. S. D. Padghan, R. S. Bhosale, N. V. Ghule, A. L. Puyad, S. V. Bhosale and S. V. Bhosale, *RSC Adv.*, 2016, **6**, 34376-34380.

34. L. Long, L. Wang, Y. Wu, A. Gong, Z. Da, C. Zhang and Z. Han, *Chem. -Asian J.*, 2014, **9**, 3291-3298.

35. M. La, Y. Hao, Z. Wang, G.-C. Han and L. Qu, *J. Anal. Methods Chem.*, 2016, **2016**, 1462013.

36. J. Jo and D. Lee, *J. Am. Chem. Soc.*, 2009, **131**, 16283-16291.

37. S. Saha, A. Ghosh, P. Mahato, S. Mishra, S. K. Mishra, E. Suresh, S. Das and A. Das, *Org. Lett.*, 2010, **12**, 3406-3409.

38. C. Zhang, C. Liu, B. Li, J. Chen, H. Zhang, Z. Hu and F. Yi, *New J. Chem.*, 2015, **39**, 1968-1973.

39. R. Chutia, S. K. Dey and G. Das, *Cryst. Growth Des.*, 2015, **15**, 4993-5001.

40. M. Wang, L. Guo and D. Cao, *Anal. Chem.*, 2018, **90**, 3608-3614.

41. A. K. Mahapatra, S. Mondal, S. K. Manna, K. Maiti, R. Maji, S. S. Ali, S. Mandal, M. Uddin and D. K. Maiti, *ChemistrySelect*, 2016, **1**, 375-383.

The classical MOFs developed in earlier years have attracted tremendous research attention because of their outstanding specific surface areas as well as tunable pore sizes. However, the hydrolytic stability of these MOFs was a huge challenge, as the MOF materials tend to undergo irreversible structural degradation in a water-containing environment. Therefore, the development of water-stable MOFs becomes necessary for the diverse applications of MOFs in humid conditions. The work presented in this thesis deals with the synthesis of water-stable MOF materials and their applications. The results obtained in the current thesis clearly indicate that the choice of metal ion and ligand is crucial for the physicochemical stability (air, water, acid-base, heat, etc.) of MOFs. The use of metal ions with higher oxidation states (e.g. Al(III), Zr(IV), Ce(IV)) along with carboxylic acid ligands has been demonstrated to be a successful approach for the preparation of water-stable MOFs. The high connectivity of metal clusters in the UiO and DUT type frameworks constructed with Al(III), Zr(IV) or Ce(IV) metal ion provides high thermal and chemical stability. The functional groups attached with the ligand molecules control the microenvironment of the MOF materials, which actually act as interaction sites during adsorption of gases and recognition sites during fluorescence sensing. The water-stable robust MOFs with enhanced performances will have great potentials in various industrial sectors over conventional porous materials (e.g. activated carbons, zeolites, etc.).

In Chapter 2, the solvothermal synthesis, characterization and sensing application of four isoreticular thienothiophene-based Zr(IV) MOF materials are presented. The hydrophobicity and fluorescence properties of all the MOF compounds can be tuned in a controlled way by altering methyl and phenyl groups to the thienothiophene-based ligands. The MOF materials retain their structural robustness upon treatment with water, acetic acid, NaOH (pH = 11) and 1 M HCl solutions, which was confirmed by XRPD measurements. The use of water-repellent methyl and phenyl groups enhances the hydrophobicity of MOF materials. The change of hydrophobic properties with changing the ligand functional group can directly understood from water adsorption and contact angle measurement. Apart from hydrophobicity, the fluorescence intensity of MOF material also influenced by the ligand substitution. All the water-stable and fluorescent MOF materials exhibited selective, fast, and sensitive sensing of Fe^{3+} ions in water through the fluorescence quenching mechanism. The trend in the quenching efficiency of the MOFs by Fe^{3+} can be correlated with the electron density available in their frameworks. The experimental investigation indicates that the transfer of electrons from the conjugated electron-rich

thienothiophene ligand moiety of MOFs to the half-filled 3d orbitals of Fe^{3+} ions causes the the fluorescence quenching of all MOF compounds. In contrast, the well-known electron acceptor methyl viologen (MV^{2+}) molecules show a reverse trend in the fluorescence quenching efficiencies of the MOF materials. This result suggests that both electronic and steric effects play decisive roles in the fluorescence quenching mechanism. Additionally, molecular logic gates could be designed to discriminate Fe^{3+} and Fe^{2+} ions by utilizing the diferent fluorescence responses of MOFs towards these ions. The high stability in water and reusability of Fe^{3+} sensing including the ability to discriminate between Fe^{3+} and Fe^{2+} ions through logic operations make the MOFs suitable for real-life applications.

In Chapter 3, the solvothermal synthesis and characterization of a Ce(IV)-based MOF material incorporating 3,4-dimethyl thieno[2,3-b]thiophene-2,5-dicarboxylic acid are presented. A through characterization was carried out by employing different methods like XRPD, XPS, FT-IR spectroscopy, TG and N_2 sorption experiments to ensure the phase purity of the MOF material. The material displayed high structural robustness in water, 1 M HCl and acetic acid, which was confirmed by XRPD measurements. The XPS study reveals the presence of both Ce(III) and Ce(IV) ions in the framework. Remarkably, the compound mimics the catalytic activity of biological oxidase enzymes due to the existence of redox-active cerium atoms in the framework. The excellent oxidase-like catalytic properties of the material were demonstrated by employing characteristic chromogenic peroxidase substrates: TMB and AzBTS. The oxidase-mimicking activity of the MOF allowed us to establish a colorimetric sensing platform for biothiols in NaAc buffer (0.2 M, pH = 4). The sensing ability of biothiols by the MOF enabled us to detect cysteine in human blood plasma. A significant heterogeneous catalytic performance of the mixed valence state Ce-MOF was also observed in the oxidation of thiol compounds using molecular oxygen. The MOF material is reusable, both as a heterogeneous catalyst and a colorimetric biosensor and retains its structural integrity. The high stability, low-cost and recyclability along with high biomimetic and heterogeneous catalytic activities make the MOF compound suitable for medical diagnostics, biological sample analysis as well as for oxidation catalysis in industry.

In Chapter 4, the synthesis, characterization and fluorogenic sensing potential of a dinitro-functionalized Zr(IV)-based MOF material called DUT-52-$(NO_2)_2$ are presented. The MOF acts as a colorimetric and fluorogenic turn-on probe for the sensing of H_2S under physiological

conditions (HEPES buffer, pH = 7.4, temperature = 37 °C). The MOF constructed from hexanuclear $[Zr_6O_4(OH)_4]^{12+}$ building units shows high stability in different solvents including water, 1M HCl and acetic acid. Based on its high stability in aqueous environment, the MOF material was used as a reaction-based colorimetric and fluorogenic turn-on probe for the sensing of H_2S. The MOF shows a turn-off fluorescence state due to the presence of strong electron withdrawing nitro functional groups. The H_2S-mediated reduction of nitro groups into amines increases electron density in the ligand and fluorescence turn-on state is achieved. The fluorescence titration experiments confirm that the reaction occurs selectively in presence of H_2S only. The MOF compound features significant capabilities for the highly selective and sensitive (detection limit: 20 μM) detection of H_2S. Additionally, the MOF probe shows visually detectable colorimetric and fluorogenic responses during the reaction-based sensing of H_2S under day light as well as under UV light. Based on the low toxicity of the compound, the probe could be used for the detection of H_2S in human blood plasma and as well as living cells. The aqueous medium stability and extraordinary selectivity for the detection of H_2S even in the existence of other interfering biomolecules and anions in biological system makes the MOF a potential candidate for the real-time monitoring of H_2S in aqueous media including biological systems.

The synthesis, characterization and fluorescence sensing application of an Al(III)-based MOF with CAU-10 topology are presented in Chapter 5. The hydrazine-functionalized Al(III) MOF namely CAU-10-N_2H_3 is able detect the toxic CN^- ions selectively even in the presence of other competitive anions present in water. The MOF constructed through the interconnection of cis-corner sharing $[AlO_6]$ octahedra with hydrazine-functionalized isophthalate ligand shows high hydrolytic stability. The hydrazine functional group attached with the ligand acts as a recognition site for anion. This material can act as a naked-eye fluorescent sensor for CN^- ions in aqueous medium, which is confirmed by the appearance of green fluorescence under UV light upon cyanide addition. The cyanide-induced deprotonation of the acidic -NH proton present in hydrazine-functional group was confirmed by ^1H NMR titration experiment. This deprotonation leads to the fluorescence turn-on signal of the MOF probe. Furthermore, the fluorescence lifetime measurements indicate that the MOF can also be used as a lifetime-based sensor for CN^- ions, as the lifetime of MOF changes drastically in presence of cyanide ion. A very low detection limit of 0.48 μM was obtained for this MOF, which is lower than the allowable cyanide concentration (2 μM) in drinking water according to the WHO. The spike-and-recovery experiments confirm that

Al(III) MOF has the ability to sense cyanide in real water samples, which can be used for controlling the quality of water samples. The cytocompatibility assay shows that this MOF is nontoxic to RAW 264.7 cells and it could be used for cell imaging study. The live cell imaging experiments with nontoxic Al(III) MOF clearly establish that the MOF is capable for the sensing of intracellular CN^- ions. These combined results suggest that water-stable, nontoxic hydrazine-functionalized Al(III) MOF namely CAU-10-N_2H_3 MOF can be used for the monitoring of cyanide toxicity in water as well as inside live cells.

There are still great challenges and opportunities for the development of robust and cost-effective MOFs with high performances and superior reusability for practical applications in aqueous medium. This thesis work is directed towards improving the hydrolytic stability of MOFs for subsequent practical applications. The thesis work demonstrates the design and synthesis of water-stable MOFs and their potential applications in chemical and biological sensing as well as heterogeneous catalysis.

Annexure I

JOHN WILEY AND SONS LICENSE TERMS AND CONDITIONS

Jan 22, 2019

This Agreement between Indian Institute of Technology -- RANA DALAPATI ("You") and John Wiley and Sons ("John Wiley and Sons") consists of your license details and the terms and conditions provided by John Wiley and Sons and Copyright Clearance Center.

License Number	4514240613078
License date	Jan 22, 2019
Licensed Content Publisher	John Wiley and Sons
Licensed Content Publication	Advanced Materials
Licensed Content Title	Preparation of Highly Moisture-Resistant Black-Colored Metal Organic Frameworks
Licensed Content Author	Seung Jae Yang, Chong Rae Park
Licensed Content Date	Jun 15, 2012
Licensed Content Volume	24
Licensed Content Issue	29
Licensed Content Pages	4
Type of use	Dissertation/Thesis
Requestor type	University/Academic
Format	Print and electronic
Portion	Figure/table
Number of figures/tables	1
Original Wiley figure/table number(s)	figure in introduction chapter
Will you be translating?	No
Title of your thesis / dissertation	Design and Synthesis of Water Stable Metal-Organic Framework for Catalysis and Fluorescence Sensing Applications
Expected completion date	May 2019
Expected size (number of pages)	220
Requestor Location	Indian Institute of Technology ROOM NO. S-130, BRAHMAPUTRA HOSTEL, IIT GUWAHATI GUWAHATI, ASSAM 781039 India Attn: Indian Institute of Technology
Publisher Tax ID	EU826007151
Total	0.00 USD
Terms and Conditions	

TERMS AND CONDITIONS

This copyrighted material is owned by or exclusively licensed to John Wiley & Sons, Inc. or one of its group companies (each a"Wiley Company") or handled on behalf of a society with which a Wiley Company has exclusive publishing rights in relation to a particular work

(collectively "WILEY"). By clicking "accept" in connection with completing this licensing transaction, you agree that the following terms and conditions apply to this transaction (along with the billing and payment terms and conditions established by the Copyright Clearance Center Inc., ("CCC's Billing and Payment terms and conditions"), at the time that you opened your RightsLink account (these are available at any time at http://myaccount.copyright.com).

Terms and Conditions

- The materials you have requested permission to reproduce or reuse (the "Wiley Materials") are protected by copyright.

- You are hereby granted a personal, non-exclusive, non-sub licensable (on a stand-alone basis), non-transferable, worldwide, limited license to reproduce the Wiley Materials for the purpose specified in the licensing process. This license, **and any CONTENT (PDF or image file) purchased as part of your order,** is for a one-time use only and limited to any maximum distribution number specified in the license. The first instance of republication or reuse granted by this license must be completed within two years of the date of the grant of this license (although copies prepared before the end date may be distributed thereafter). The Wiley Materials shall not be used in any other manner or for any other purpose, beyond what is granted in the license. Permission is granted subject to an appropriate acknowledgement given to the author, title of the material/book/journal and the publisher. You shall also duplicate the copyright notice that appears in the Wiley publication in your use of the Wiley Material. Permission is also granted on the understanding that nowhere in the text is a previously published source acknowledged for all or part of this Wiley Material. Any third party content is expressly excluded from this permission.

- With respect to the Wiley Materials, all rights are reserved. Except as expressly granted by the terms of the license, no part of the Wiley Materials may be copied, modified, adapted (except for minor reformatting required by the new Publication), translated, reproduced, transferred or distributed, in any form or by any means, and no derivative works may be made based on the Wiley Materials without the prior permission of the respective copyright owner.**For STM Signatory Publishers clearing permission under the terms of the STM Permissions Guidelines only, the terms of the license are extended to include subsequent editions and for editions in other languages, provided such editions are for the work as a whole in situ and does not involve the separate exploitation of the permitted figures or extracts,** You may not alter, remove or suppress in any manner any copyright, trademark or other notices displayed by the Wiley Materials. You may not license, rent, sell, loan, lease, pledge, offer as security, transfer or assign the Wiley Materials on a stand-alone basis, or any of the rights granted to you hereunder to any other person.

- The Wiley Materials and all of the intellectual property rights therein shall at all times remain the exclusive property of John Wiley & Sons Inc, the Wiley Companies, or their respective licensors, and your interest therein is only that of having possession of and the right to reproduce the Wiley Materials pursuant to Section 2 herein during the continuance of this Agreement. You agree that you own no right, title or interest in or to the Wiley Materials or any of the intellectual property rights therein. You shall have no rights hereunder other than the license as provided for above in Section 2. No right, license or interest to any trademark, trade name, service mark or other branding ("Marks") of WILEY or its licensors is granted hereunder, and you agree that you shall not assert any such right, license or interest with respect thereto

- NEITHER WILEY NOR ITS LICENSORS MAKES ANY WARRANTY OR REPRESENTATION OF ANY KIND TO YOU OR ANY THIRD PARTY, EXPRESS, IMPLIED OR STATUTORY, WITH RESPECT TO THE MATERIALS OR THE ACCURACY OF ANY INFORMATION CONTAINED IN THE MATERIALS, INCLUDING, WITHOUT LIMITATION, ANY IMPLIED WARRANTY OF MERCHANTABILITY, ACCURACY, SATISFACTORY QUALITY, FITNESS FOR A PARTICULAR PURPOSE, USABILITY, INTEGRATION OR NON-INFRINGEMENT AND ALL SUCH WARRANTIES ARE HEREBY EXCLUDED BY WILEY AND ITS LICENSORS AND WAIVED BY YOU.

- WILEY shall have the right to terminate this Agreement immediately upon breach of this Agreement by you.

- You shall indemnify, defend and hold harmless WILEY, its Licensors and their respective directors, officers, agents and employees, from and against any actual or threatened claims, demands, causes of action or proceedings arising from any breach of this Agreement by you.

- IN NO EVENT SHALL WILEY OR ITS LICENSORS BE LIABLE TO YOU OR ANY OTHER PARTY OR ANY OTHER PERSON OR ENTITY FOR ANY SPECIAL, CONSEQUENTIAL, INCIDENTAL, INDIRECT, EXEMPLARY OR PUNITIVE DAMAGES, HOWEVER CAUSED, ARISING OUT OF OR IN CONNECTION WITH THE DOWNLOADING, PROVISIONING, VIEWING OR USE OF THE MATERIALS REGARDLESS OF THE FORM OF ACTION, WHETHER FOR BREACH OF CONTRACT, BREACH OF WARRANTY, TORT, NEGLIGENCE, INFRINGEMENT OR OTHERWISE (INCLUDING, WITHOUT LIMITATION, DAMAGES BASED ON LOSS OF PROFITS, DATA, FILES, USE, BUSINESS OPPORTUNITY OR CLAIMS OF THIRD PARTIES), AND WHETHER OR NOT THE PARTY HAS BEEN ADVISED OF THE POSSIBILITY OF SUCH DAMAGES. THIS LIMITATION SHALL APPLY NOTWITHSTANDING ANY FAILURE OF ESSENTIAL PURPOSE OF ANY LIMITED REMEDY PROVIDED HEREIN.

- Should any provision of this Agreement be held by a court of competent jurisdiction to be illegal, invalid, or unenforceable, that provision shall be deemed amended to achieve as nearly as possible the same economic effect as the original provision, and the legality, validity and enforceability of the remaining provisions of this Agreement shall not be affected or impaired thereby.

- The failure of either party to enforce any term or condition of this Agreement shall not constitute a waiver of either party's right to enforce each and every term and condition of this Agreement. No breach under this agreement shall be deemed waived or excused by either party unless such waiver or consent is in writing signed by the party granting such waiver or consent. The waiver by or consent of a party to a breach of any provision of this Agreement shall not operate or be construed as a waiver of or consent to any other or subsequent breach by such other party.

- This Agreement may not be assigned (including by operation of law or otherwise) by you without WILEY's prior written consent.

- Any fee required for this permission shall be non-refundable after thirty (30) days from receipt by the CCC.

- These terms and conditions together with CCC's Billing and Payment terms and conditions (which are incorporated herein) form the entire agreement between you and WILEY concerning this licensing transaction and (in the absence of fraud) supersedes all prior agreements and representations of the parties, oral or written. This Agreement may not be amended except in writing signed by both parties. This Agreement shall be binding upon and inure to the benefit of the parties' successors, legal representatives, and authorized assigns.

- In the event of any conflict between your obligations established by these terms and conditions and those established by CCC's Billing and Payment terms and conditions, these terms and conditions shall prevail.

- WILEY expressly reserves all rights not specifically granted in the combination of (i) the license details provided by you and accepted in the course of this licensing transaction, (ii) these terms and conditions and (iii) CCC's Billing and Payment terms and conditions.

- This Agreement will be void if the Type of Use, Format, Circulation, or Requestor Type was misrepresented during the licensing process.

- This Agreement shall be governed by and construed in accordance with the laws of the State of New York, USA, without regards to such state's conflict of law rules. Any legal action, suit or proceeding arising out of or relating to these Terms and Conditions or the breach thereof shall be instituted in a court of competent jurisdiction in New York County in the State of New York in the United States of America and each party hereby consents and submits to the personal jurisdiction of such court, waives any objection to venue in such court and consents to service of process by registered or certified mail, return receipt requested, at the last known address of such party.

WILEY OPEN ACCESS TERMS AND CONDITIONS

Wiley Publishes Open Access Articles in fully Open Access Journals and in Subscription journals offering Online Open. Although most of the fully Open Access journals publish open access articles under the terms of the Creative Commons Attribution (CC BY) License only, the subscription journals and a few of the Open Access Journals offer a choice of Creative Commons Licenses. The license type is clearly identified on the article.

The Creative Commons Attribution License

The Creative Commons Attribution License (CC-BY) allows users to copy, distribute and transmit an article, adapt the article and make commercial use of the article. The CC-BY license permits commercial and non-

Creative Commons Attribution Non-Commercial License

The Creative Commons Attribution Non-Commercial (CC-BY-NC)License permits use, distribution and reproduction in any medium, provided the original work is properly cited and is not used for commercial purposes.(see below)

Creative Commons Attribution-Non-Commercial-NoDerivs License

The Creative Commons Attribution Non-Commercial-NoDerivs License (CC-BY-NC-ND) permits use, distribution and reproduction in any medium, provided the original work is properly cited, is not used for commercial purposes and no modifications or adaptations are made. (see below)

Use by commercial "for-profit" organizations

Use of Wiley Open Access articles for commercial, promotional, or marketing purposes requires further explicit permission from Wiley and will be subject to a fee.

Further details can be found on Wiley Online Library

http://olabout.wiley.com/WileyCDA/Section/id-410895.html

Other Terms and Conditions:

v1.10 Last updated September 2015

Questions? customercare@copyright.com or +1-855-239-3415 (toll free in the US) or +1-978-646-2777.

Annexure II

JOHN WILEY AND SONS LICENSE TERMS AND CONDITIONS

Jan 22, 2019

This Agreement between Indian Institute of Technology -- RANA DALAPATI ("You") and John Wiley and Sons ("John Wiley and Sons") consists of your license details and the terms and conditions provided by John Wiley and Sons and Copyright Clearance Center.

License Number	4514240404413
License date	Jan 22, 2019
Licensed Content Publisher	John Wiley and Sons
Licensed Content Publication	Chemistry - A European Journal
Licensed Content Title	An Ultrahydrophobic Fluorous Metal–Organic Framework Derived Recyclable Composite as a Promising Platform to Tackle Marine Oil Spills
Licensed Content Author	Soumya Mukherjee, Ankit M. Kansara, Debasis Saha, et al
Licensed Content Date	Jun 30, 2016
Licensed Content Volume	22
Licensed Content Issue	31
Licensed Content Pages	7
Type of use	Dissertation/Thesis
Requestor type	University/Academic
Format	Print and electronic
Portion	Figure/table
Number of figures/tables	1
Original Wiley figure/table number(s)	Figure in Inteoduction
Will you be translating?	No
Title of your thesis / dissertation	Design and Synthesis of Water Stable Metal-Organic Framework for Catalysis and Fluorescence Sensing Applications
Expected completion date	May 2019
Expected size (number of pages)	220
Requestor Location	Indian Institute of Technology ROOM NO. S-130, BRAHMAPUTRA HOSTEL, IIT GUWAHATI GUWAHATI, ASSAM 781039 India Attn: Indian Institute of Technology
Publisher Tax ID	EU826007151
Total	0.00 USD
Terms and Conditions	

TERMS AND CONDITIONS

This copyrighted material is owned by or exclusively licensed to John Wiley & Sons, Inc. or one of its group companies (each a"Wiley Company") or handled on behalf of a society with

which a Wiley Company has exclusive publishing rights in relation to a particular work (collectively "WILEY"). By clicking "accept" in connection with completing this licensing transaction, you agree that the following terms and conditions apply to this transaction (along with the billing and payment terms and conditions established by the Copyright Clearance Center Inc., ("CCC's Billing and Payment terms and conditions"), at the time that you opened your RightsLink account (these are available at any time at http://myaccount.copyright.com).

Terms and Conditions

- The materials you have requested permission to reproduce or reuse (the "Wiley Materials") are protected by copyright.
- You are hereby granted a personal, non-exclusive, non-sub licensable (on a stand-alone basis), non-transferable, worldwide, limited license to reproduce the Wiley Materials for the purpose specified in the licensing process. This license, **and any CONTENT (PDF or image file) purchased as part of your order,** is for a one-time use only and limited to any maximum distribution number specified in the license. The first instance of republication or reuse granted by this license must be completed within two years of the date of the grant of this license (although copies prepared before the end date may be distributed thereafter). The Wiley Materials shall not be used in any other manner or for any other purpose, beyond what is granted in the license. Permission is granted subject to an appropriate acknowledgement given to the author, title of the material/book/journal and the publisher. You shall also duplicate the copyright notice that appears in the Wiley publication in your use of the Wiley Material. Permission is also granted on the understanding that nowhere in the text is a previously published source acknowledged for all or part of this Wiley Material. Any third party content is expressly excluded from this permission.
- With respect to the Wiley Materials, all rights are reserved. Except as expressly granted by the terms of the license, no part of the Wiley Materials may be copied, modified, adapted (except for minor reformatting required by the new Publication), translated, reproduced, transferred or distributed, in any form or by any means, and no derivative works may be made based on the Wiley Materials without the prior permission of the respective copyright owner.**For STM Signatory Publishers clearing permission under the terms of the STM Permissions Guidelines only, the terms of the license are extended to include subsequent editions and for editions in other languages, provided such editions are for the work as a whole in situ and does not involve the separate exploitation of the permitted figures or extracts,** You may not alter, remove or suppress in any manner any copyright, trademark or other notices displayed by the Wiley Materials. You may not license, rent, sell, loan, lease, pledge, offer as security, transfer or assign the Wiley Materials on a stand-alone basis, or any of the rights granted to you hereunder to any other person.
- The Wiley Materials and all of the intellectual property rights therein shall at all times remain the exclusive property of John Wiley & Sons Inc, the Wiley Companies, or their respective licensors, and your interest therein is only that of having possession of and the right to reproduce the Wiley Materials pursuant to Section 2 herein during the continuance of this Agreement. You agree that you own no right, title or interest in or to the Wiley Materials or any of the intellectual property rights therein. You shall have no rights hereunder other than the license as provided for above in Section 2. No right, license or interest to any trademark, trade name, service mark or other branding ("Marks") of WILEY or its licensors is granted hereunder, and you agree that you shall not assert any such right, license or interest with respect thereto

- NEITHER WILEY NOR ITS LICENSORS MAKES ANY WARRANTY OR REPRESENTATION OF ANY KIND TO YOU OR ANY THIRD PARTY, EXPRESS, IMPLIED OR STATUTORY, WITH RESPECT TO THE MATERIALS OR THE ACCURACY OF ANY INFORMATION CONTAINED IN THE MATERIALS, INCLUDING, WITHOUT LIMITATION, ANY IMPLIED WARRANTY OF MERCHANTABILITY, ACCURACY, SATISFACTORY QUALITY, FITNESS FOR A PARTICULAR PURPOSE, USABILITY, INTEGRATION OR NON-INFRINGEMENT AND ALL SUCH WARRANTIES ARE HEREBY EXCLUDED BY WILEY AND ITS LICENSORS AND WAIVED BY YOU.

- WILEY shall have the right to terminate this Agreement immediately upon breach of this Agreement by you.

- You shall indemnify, defend and hold harmless WILEY, its Licensors and their respective directors, officers, agents and employees, from and against any actual or threatened claims, demands, causes of action or proceedings arising from any breach of this Agreement by you.

- IN NO EVENT SHALL WILEY OR ITS LICENSORS BE LIABLE TO YOU OR ANY OTHER PARTY OR ANY OTHER PERSON OR ENTITY FOR ANY SPECIAL, CONSEQUENTIAL, INCIDENTAL, INDIRECT, EXEMPLARY OR PUNITIVE DAMAGES, HOWEVER CAUSED, ARISING OUT OF OR IN CONNECTION WITH THE DOWNLOADING, PROVISIONING, VIEWING OR USE OF THE MATERIALS REGARDLESS OF THE FORM OF ACTION, WHETHER FOR BREACH OF CONTRACT, BREACH OF WARRANTY, TORT, NEGLIGENCE, INFRINGEMENT OR OTHERWISE (INCLUDING, WITHOUT LIMITATION, DAMAGES BASED ON LOSS OF PROFITS, DATA, FILES, USE, BUSINESS OPPORTUNITY OR CLAIMS OF THIRD PARTIES), AND WHETHER OR NOT THE PARTY HAS BEEN ADVISED OF THE POSSIBILITY OF SUCH DAMAGES. THIS LIMITATION SHALL APPLY NOTWITHSTANDING ANY FAILURE OF ESSENTIAL PURPOSE OF ANY LIMITED REMEDY PROVIDED HEREIN.

- Should any provision of this Agreement be held by a court of competent jurisdiction to be illegal, invalid, or unenforceable, that provision shall be deemed amended to achieve as nearly as possible the same economic effect as the original provision, and the legality, validity and enforceability of the remaining provisions of this Agreement shall not be affected or impaired thereby.

- The failure of either party to enforce any term or condition of this Agreement shall not constitute a waiver of either party's right to enforce each and every term and condition of this Agreement. No breach under this agreement shall be deemed waived or excused by either party unless such waiver or consent is in writing signed by the party granting such waiver or consent. The waiver by or consent of a party to a breach of any provision of this Agreement shall not operate or be construed as a waiver of or consent to any other or subsequent breach by such other party.

- This Agreement may not be assigned (including by operation of law or otherwise) by you without WILEY's prior written consent.

- Any fee required for this permission shall be non-refundable after thirty (30) days from receipt by the CCC.

- These terms and conditions together with CCC's Billing and Payment terms and conditions (which are incorporated herein) form the entire agreement between you and WILEY concerning this licensing transaction and (in the absence of fraud) supersedes all prior agreements and representations of the parties, oral or written. This Agreement may not be amended except in writing signed by both parties. This Agreement shall be binding upon and inure to the benefit of the parties' successors, legal representatives, and authorized assigns.

- In the event of any conflict between your obligations established by these terms and conditions and those established by CCC's Billing and Payment terms and conditions, these terms and conditions shall prevail.

- WILEY expressly reserves all rights not specifically granted in the combination of (i) the license details provided by you and accepted in the course of this licensing transaction, (ii) these terms and conditions and (iii) CCC's Billing and Payment terms and conditions.

- This Agreement will be void if the Type of Use, Format, Circulation, or Requestor Type was misrepresented during the licensing process.

- This Agreement shall be governed by and construed in accordance with the laws of the State of New York, USA, without regards to such state's conflict of law rules. Any legal action, suit or proceeding arising out of or relating to these Terms and Conditions or the breach thereof shall be instituted in a court of competent jurisdiction in New York County in the State of New York in the United States of America and each party hereby consents and submits to the personal jurisdiction of such court, waives any objection to venue in such court and consents to service of process by registered or certified mail, return receipt requested, at the last known address of such party.

WILEY OPEN ACCESS TERMS AND CONDITIONS

Wiley Publishes Open Access Articles in fully Open Access Journals and in Subscription journals offering Online Open. Although most of the fully Open Access journals publish open access articles under the terms of the Creative Commons Attribution (CC BY) License only, the subscription journals and a few of the Open Access Journals offer a choice of Creative Commons Licenses. The license type is clearly identified on the article.

The Creative Commons Attribution License

The Creative Commons Attribution License (CC-BY) allows users to copy, distribute and transmit an article, adapt the article and make commercial use of the article. The CC-BY license permits commercial and non-

Creative Commons Attribution Non-Commercial License

The Creative Commons Attribution Non-Commercial (CC-BY-NC)License permits use, distribution and reproduction in any medium, provided the original work is properly cited and is not used for commercial purposes.(see below)

Creative Commons Attribution-Non-Commercial-NoDerivs License

The Creative Commons Attribution Non-Commercial-NoDerivs License (CC-BY-NC-ND) permits use, distribution and reproduction in any medium, provided the original work is properly cited, is not used for commercial purposes and no modifications or adaptations are made. (see below)

Use by commercial "for-profit" organizations

Use of Wiley Open Access articles for commercial, promotional, or marketing purposes requires further explicit permission from Wiley and will be subject to a fee.

Further details can be found on Wiley Online Library

http://olabout.wiley.com/WileyCDA/Section/id-410895.html

Other Terms and Conditions:

v1.10 Last updated September 2015

Questions? customercare@copyright.com or +1-855-239-3415 (toll free in the US) or +1-978-646-2777.

Copyright Clearance Center

Note: Copyright.com supplies permissions but not the copyrighted content itself.

1 PAYMENT 2 REVIEW 3 CONFIRMATION

Step 3: Order Confirmation

Thank you for your order! A confirmation for your order will be sent to your account email address. If you have questions about your order, you can call us 24 hrs/day, M-F at +1.855.239.3415 Toll Free, or write to us at info@copyright.com. This is not an invoice.

Confirmation Number: 11784716
Order Date: 01/22/2019

If you paid by credit card, your order will be finalized and your card will be charged within 24 hours. If you choose to be invoiced, you can change or cancel your order until the invoice is generated.

Payment Information

RANA DALAPATI
Indian Institute of Technology
rana.dalapati@iitg.ac.in
+91 8721861596
Payment Method: n/a

Order Details

CrystEngComm

Order detail ID:	71776891
Order License Id:	4514240025066
ISSN:	1466-8033
Publication Type:	e-Journal
Volume:	
Issue:	
Start page:	
Publisher:	ROYAL SOCIETY OF CHEMISTRY
Author/Editor:	Royal Society of Chemistry (Great Britain)

Permission Status: Granted
Permission type: Republish or display content
Type of use: Thesis/Dissertation

Requestor type	Academic institution
Format	Print, Electronic
Portion	image/photo
Number of images/photos requested	1
The requesting person/organization	Rana Dalapati
Title or numeric reference of the portion(s)	Chapter 1
Title of the article or chapter the portion is from	NA

Editor of portion(s)	NA
Author of portion(s)	NA
Volume of serial or monograph	NA
Page range of portion	10
Publication date of portion	22-1-2019
Rights for	Main product
Duration of use	Life of current edition
Creation of copies for the disabled	yes
With minor editing privileges	yes
For distribution to	Worldwide
In the following language(s)	Original language of publication
With incidental promotional use	no
Lifetime unit quantity of new product	Up to 499
Title	Design and Synthesis of Water Stable Metal-Organic Framework for Catalysis and Fluorescence Sensing Applications
Institution name	n/a
Expected presentation date	May 2019

Note: This item will be invoiced or charged separately through CCC's **RightsLink** service. More info **$ 0.00**

This is not an invoice.

Total order items: 1 **Order Total: 0.00 USD**

Confirmation Number: 11784716

Special Rightsholder Terms & Conditions

The following terms & conditions apply to the specific publication under which they are listed

CrystEngComm
Permission type: Republish or display content
Type of use: Thesis/Dissertation

TERMS AND CONDITIONS

The following terms are individual to this publisher:

None

Other Terms and Conditions:

STANDARD TERMS AND CONDITIONS

1. Description of Service; Defined Terms. This Republication License enables the User to obtain licenses for republication of one or more copyrighted works as described in detail on the relevant Order Confirmation (the "Work(s)"). Copyright Clearance Center, Inc. ("CCC") grants licenses through the Service on behalf of the rightsholder identified on the Order Confirmation (the "Rightsholder"). "Republication", as used herein, generally means the inclusion of a Work, in whole or in part, in a new work or works, also as described on the Order Confirmation. "User", as used herein, means the person or entity making such republication.

2. The terms set forth in the relevant Order Confirmation, and any terms set by the Rightsholder with respect to a particular Work, govern the terms of use of Works in connection with the Service. By using the Service, the person transacting for a republication license on behalf of the User represents and warrants that he/she/it (a) has been duly authorized by the User to accept, and hereby does accept, all such terms and conditions on behalf of User, and (b) shall inform User of all such terms and conditions. In the event such person is a "freelancer" or other third party independent of User and CCC, such party shall be deemed jointly a "User" for purposes of these terms and conditions. In any event, User shall be deemed to have accepted and agreed to all such terms and conditions if User republishes the Work in any fashion.

3. Scope of License; Limitations and Obligations.

3.1 All Works and all rights therein, including copyright rights, remain the sole and exclusive property of the Rightsholder. The license created by the exchange of an Order Confirmation (and/or any invoice) and payment by User of the full amount set forth on that document includes only those rights expressly set forth in the Order Confirmation and in these terms and conditions, and conveys no other rights in the Work(s) to User. All rights not expressly granted are hereby reserved.

3.2 General Payment Terms: You may pay by credit card or through an account with us payable at the end of the month. If you and we agree that you may establish a standing account with CCC, then the following terms apply: Remit Payment to: Copyright Clearance Center, 29118 Network Place, Chicago, IL 60673-1291. Payments Due: Invoices are payable upon their delivery to you (or upon our notice to you that they are available to you for downloading). After 30 days, outstanding amounts will be subject to a service charge of 1-1/2% per month or, if less, the maximum rate allowed by applicable law. Unless otherwise specifically set forth in the Order Confirmation or in a separate written agreement signed by CCC, invoices are due and payable on "net 30" terms. While User may exercise the rights licensed immediately upon issuance of the Order Confirmation, the license is automatically revoked and is null and void, as if it had never been issued, if complete payment for the license is not received on a timely basis either from User directly or through a payment agent, such as a credit card company.

3.3 Unless otherwise provided in the Order Confirmation, any grant of rights to User (i) is "one-time" (including the editions and product family specified in the license), (ii) is non-exclusive and non-transferable and (iii) is subject to any and all limitations and restrictions (such as, but not limited to, limitations on duration of use or circulation) included in the Order Confirmation or invoice and/or in these terms and conditions. Upon completion of the licensed use, User shall either secure a new permission for further use of the Work(s) or immediately cease any new use of the Work(s) and shall render inaccessible (such as by deleting or by removing or severing links or other locators) any further copies of the Work (except for copies printed on paper in accordance with this license and still in User's stock at the end of such period).

3.4 In the event that the material for which a republication license is sought includes third party materials (such as photographs, illustrations, graphs, inserts and similar materials) which are identified in such material as having been used by permission, User is responsible for identifying, and seeking separate licenses (under this Service or otherwise) for, any of such third party materials; without a separate license, such third party materials may not be used.

3.5 Use of proper copyright notice for a Work is required as a condition of any license granted under the Service. Unless otherwise provided in the Order Confirmation, a proper copyright notice will read substantially as follows: "Republished with permission of [Rightsholder's name], from [Work's title, author, volume, edition number and year of copyright]; permission conveyed through Copyright Clearance Center, Inc. " Such notice must be provided in a reasonably legible font size and must be placed either immediately adjacent to the Work as used (for example, as part of a by-line or footnote

but not as a separate electronic link) or in the place where substantially all other credits or notices for the new work containing the republished Work are located. Failure to include the required notice results in loss to the Rightsholder and CCC, and the User shall be liable to pay liquidated damages for each such failure equal to twice the use fee specified in the Order Confirmation, in addition to the use fee itself and any other fees and charges specified.

3.6 User may only make alterations to the Work if and as expressly set forth in the Order Confirmation. No Work may be used in any way that is defamatory, violates the rights of third parties (including such third parties' rights of copyright, privacy, publicity, or other tangible or intangible property), or is otherwise illegal, sexually explicit or obscene. In addition, User may not conjoin a Work with any other material that may result in damage to the reputation of the Rightsholder. User agrees to inform CCC if it becomes aware of any infringement of any rights in a Work and to cooperate with any reasonable request of CCC or the Rightsholder in connection therewith.

4. Indemnity. User hereby indemnifies and agrees to defend the Rightsholder and CCC, and their respective employees and directors, against all claims, liability, damages, costs and expenses, including legal fees and expenses, arising out of any use of a Work beyond the scope of the rights granted herein, or any use of a Work which has been altered in any unauthorized way by User, including claims of defamation or infringement of rights of copyright, publicity, privacy or other tangible or intangible property.

5. Limitation of Liability. UNDER NO CIRCUMSTANCES WILL CCC OR THE RIGHTSHOLDER BE LIABLE FOR ANY DIRECT, INDIRECT, CONSEQUENTIAL OR INCIDENTAL DAMAGES (INCLUDING WITHOUT LIMITATION DAMAGES FOR LOSS OF BUSINESS PROFITS OR INFORMATION, OR FOR BUSINESS INTERRUPTION) ARISING OUT OF THE USE OR INABILITY TO USE A WORK, EVEN IF ONE OF THEM HAS BEEN ADVISED OF THE POSSIBILITY OF SUCH DAMAGES. In any event, the total liability of the Rightsholder and CCC (including their respective employees and directors) shall not exceed the total amount actually paid by User for this license. User assumes full liability for the actions and omissions of its principals, employees, agents, affiliates, successors and assigns.

6. Limited Warranties. THE WORK(S) AND RIGHT(S) ARE PROVIDED "AS IS". CCC HAS THE RIGHT TO GRANT TO USER THE RIGHTS GRANTED IN THE ORDER CONFIRMATION DOCUMENT. CCC AND THE RIGHTSHOLDER DISCLAIM ALL OTHER WARRANTIES RELATING TO THE WORK(S) AND RIGHT(S), EITHER EXPRESS OR IMPLIED, INCLUDING WITHOUT LIMITATION IMPLIED WARRANTIES OF MERCHANTABILITY OR FITNESS FOR A PARTICULAR PURPOSE. ADDITIONAL RIGHTS MAY BE REQUIRED TO USE ILLUSTRATIONS, GRAPHS, PHOTOGRAPHS, ABSTRACTS, INSERTS OR OTHER PORTIONS OF THE WORK (AS OPPOSED TO THE ENTIRE WORK) IN A MANNER CONTEMPLATED BY USER; USER UNDERSTANDS AND AGREES THAT NEITHER CCC NOR THE RIGHTSHOLDER MAY HAVE SUCH ADDITIONAL RIGHTS TO GRANT.

7. Effect of Breach. Any failure by User to pay any amount when due, or any use by User of a Work beyond the scope of the license set forth in the Order Confirmation and/or these terms and conditions, shall be a material breach of the license created by the Order Confirmation and these terms and conditions. Any breach not cured within 30 days of written notice thereof shall result in immediate termination of such license without further notice. Any unauthorized (but licensable) use of a Work that is terminated immediately upon notice thereof may be liquidated by payment of the Rightsholder's ordinary license price therefor; any unauthorized (and unlicensable) use that is not terminated immediately for any reason (including, for example, because materials containing the Work cannot reasonably be recalled) will be subject to all remedies available at law or in equity, but in no event to a payment of less than three times the Rightsholder's ordinary license price for the most closely analogous licensable use plus Rightsholder's and/or CCC's costs and expenses incurred in collecting such payment.

8. **Miscellaneous.**

8.1 User acknowledges that CCC may, from time to time, make changes or additions to the Service or to these terms and conditions, and CCC reserves the right to send notice to the User by electronic mail or otherwise for the purposes of notifying User of such changes or additions; provided that any such changes or additions shall not apply to permissions already secured and paid for.

8.2 Use of User-related information collected through the Service is governed by CCC's privacy policy, available online here: http://www.copyright.com/content/cc3/en/tools/footer/privacypolicy.html.

8.3 The licensing transaction described in the Order Confirmation is personal to User. Therefore, User may not assign or transfer to any other person (whether a natural person or an organization of any kind) the license created by the Order Confirmation and these terms and conditions or any rights granted hereunder; provided, however, that User may assign such license in its entirety on written notice to CCC in the event of a transfer of all or substantially all of User's rights in the new material which includes the Work(s) licensed under this Service.

8.4 No amendment or waiver of any terms is binding unless set forth in writing and signed by the parties. The Rightsholder and CCC hereby object to any terms contained in any writing prepared by the User or its principals, employees, agents or affiliates and purporting to govern or otherwise relate to the licensing transaction described in the Order Confirmation, which terms are in any way inconsistent with any terms set forth in the Order Confirmation and/or in these terms and conditions or CCC's standard operating procedures, whether such writing is prepared prior to, simultaneously with or subsequent to the Order Confirmation, and whether such writing appears on a copy of the Order Confirmation or in a separate instrument.

8.5 The licensing transaction described in the Order Confirmation document shall be governed by and construed under the law of the State of New York, USA, without regard to the principles thereof of conflicts of law. Any case, controversy, suit, action, or proceeding arising out of, in connection with, or related to such licensing transaction shall be brought, at CCC's sole discretion, in any federal or state court located in the County of New York, State of New York, USA, or in any federal or state court whose geographical jurisdiction covers the location of the Rightsholder set forth in the Order Confirmation. The parties expressly submit to the personal jurisdiction and venue of each such federal or state court.If you have any comments or questions about the Service or Copyright Clearance Center, please contact us at 978-750-8400 or send an e-mail to info@copyright.com.

v 1.1

Close

Confirmation Number: 11784716

Citation Information

Order Detail ID: 71776891

CrystEngComm by Royal Society of Chemistry (Great Britain) Reproduced with permission of ROYAL SOCIETY OF CHEMISTRY in the format Thesis/Dissertation via Copyright Clearance Center.

Close

Copyright Clearance Center

Note: Copyright.com supplies permissions but not the copyrighted content itself.

1 PAYMENT 2 REVIEW **3 CONFIRMATION**

Step 3: Order Confirmation

Thank you for your order! A confirmation for your order will be sent to your account email address. If you have questions about your order, you can call us 24 hrs/day, M-F at +1.855.239.3415 Toll Free, or write to us at info@copyright.com. This is not an invoice.

Confirmation Number: 11778142
Order Date: 12/31/2018

If you paid by credit card, your order will be finalized and your card will be charged within 24 hours. If you choose to be invoiced, you can change or cancel your order until the invoice is generated.

Payment Information

RANA DALAPATI
Indian Institute of Technology
rana.dalapati@iitg.ac.in
+91 8721861596
Payment Method: n/a

Order Details

Chemical Society reviews

Order detail ID:	71744022
Order License Id:	4499180405632
ISSN:	1460-4744
Publication Type:	e-Journal
Volume:	
Issue:	
Start page:	
Publisher:	ROYAL SOCIETY OF CHEMISTRY
Author/Editor:	Royal Society of Chemistry (Great Britain)

Permission Status: Granted
Permission type: Republish or display content
Type of use: Thesis/Dissertation

Requestor type	Academic institution
Format	Print, Electronic
Portion	image/photo
Number of images/photos requested	1
The requesting person/organization	RANA DALAPATI
Title or numeric reference of the portion(s)	Chapter 1, Figure 1.15
Title of the article or chapter the portion is from	Sensing

Editor of portion(s)	NA
Author of portion(s)	NA
Volume of serial or monograph	NA
Issue, if republishing an article from a serial	NO
Page range of portion	22-23
Publication date of portion	1/3/2019
Rights for	Main product
Duration of use	Current edition and up to 5 years
Creation of copies for the disabled	yes
With minor editing privileges	no
For distribution to	Worldwide
In the following language(s)	Original language of publication
With incidental promotional use	yes
Lifetime unit quantity of new product	Up to 499
Title	Design and Synthesis of Water Stable Metal-Organic Framework for Catalysis and Fluorescence Sensing Applications
Institution name	n/a
Expected presentation date	May 2019

Note: This item will be invoiced or charged separately through CCC's **RightsLink** service. More info **$ 0.00**

This is not an invoice.

Total order items: 1 **Order Total: 0.00 USD**

Confirmation Number: 11778142

Special Rightsholder Terms & Conditions

The following terms & conditions apply to the specific publication under which they are listed

Chemical Society reviews
Permission type: Republish or display content
Type of use: Thesis/Dissertation

TERMS AND CONDITIONS

The following terms are individual to this publisher:

None

Other Terms and Conditions:

STANDARD TERMS AND CONDITIONS

1. Description of Service; Defined Terms. This Republication License enables the User to obtain licenses for republication of one or more copyrighted works as described in detail on the relevant Order Confirmation (the "Work(s)"). Copyright Clearance Center, Inc. ("CCC") grants licenses through the Service on behalf of the rightsholder identified on the Order Confirmation (the "Rightsholder"). "Republication", as used herein, generally means the inclusion of a Work, in whole or in part, in a new work or works, also as described on the Order Confirmation. "User", as used herein, means the person or entity making such republication.

2. The terms set forth in the relevant Order Confirmation, and any terms set by the Rightsholder with respect to a particular Work, govern the terms of use of Works in connection with the Service. By using the Service, the person transacting for a republication license on behalf of the User represents and warrants that he/she/it (a) has been duly authorized by the User to accept, and hereby does accept, all such terms and conditions on behalf of User, and (b) shall inform User of all such terms and conditions. In the event such person is a "freelancer" or other third party independent of User and CCC, such party shall be deemed jointly a "User" for purposes of these terms and conditions. In any event, User shall be deemed to have accepted and agreed to all such terms and conditions if User republishes the Work in any fashion.

3. Scope of License; Limitations and Obligations.

3.1 All Works and all rights therein, including copyright rights, remain the sole and exclusive property of the Rightsholder. The license created by the exchange of an Order Confirmation (and/or any invoice) and payment by User of the full amount set forth on that document includes only those rights expressly set forth in the Order Confirmation and in these terms and conditions, and conveys no other rights in the Work(s) to User. All rights not expressly granted are hereby reserved.

3.2 General Payment Terms: You may pay by credit card or through an account with us payable at the end of the month. If you and we agree that you may establish a standing account with CCC, then the following terms apply: Remit Payment to: Copyright Clearance Center, 29118 Network Place, Chicago, IL 60673-1291. Payments Due: Invoices are payable upon their delivery to you (or upon our notice to you that they are available to you for downloading). After 30 days, outstanding amounts will be subject to a service charge of 1-1/2% per month or, if less, the maximum rate allowed by applicable law. Unless otherwise specifically set forth in the Order Confirmation or in a separate written agreement signed by CCC, invoices are due and payable on "net 30" terms. While User may exercise the rights licensed immediately upon issuance of the Order Confirmation, the license is automatically revoked and is null and void, as if it had never been issued, if complete payment for the license is not received on a timely basis either from User directly or through a payment agent, such as a credit card company.

3.3 Unless otherwise provided in the Order Confirmation, any grant of rights to User (i) is "one-time" (including the editions and product family specified in the license), (ii) is non-exclusive and non-transferable and (iii) is subject to any and all limitations and restrictions (such as, but not limited to, limitations on duration of use or circulation) included in the Order Confirmation or invoice and/or in these terms and conditions. Upon completion of the licensed use, User shall either secure a new permission for further use of the Work(s) or immediately cease any new use of the Work(s) and shall render inaccessible (such as by deleting or by removing or severing links or other locators) any further copies of the Work (except for copies printed on paper in accordance with this license and still in User's stock at the end of such period).

3.4 In the event that the material for which a republication license is sought includes third party materials (such as photographs, illustrations, graphs, inserts and similar materials) which are identified in such material as having been used by permission, User is responsible for identifying, and seeking separate licenses (under this Service or otherwise) for, any of such third party materials; without a separate license, such third party materials may not be used.

3.5 Use of proper copyright notice for a Work is required as a condition of any license granted under the Service. Unless otherwise provided in the Order Confirmation, a proper copyright notice will read substantially as follows: "Republished with permission of [Rightsholder's name], from [Work's title, author, volume, edition number and year of copyright]; permission conveyed through Copyright Clearance Center, Inc. " Such notice must be provided in a reasonably legible font size and must be placed either immediately adjacent to the Work as used (for example, as part of a by-line or footnote

but not as a separate electronic link) or in the place where substantially all other credits or notices for the new work containing the republished Work are located. Failure to include the required notice results in loss to the Rightsholder and CCC, and the User shall be liable to pay liquidated damages for each such failure equal to twice the use fee specified in the Order Confirmation, in addition to the use fee itself and any other fees and charges specified.

3.6 User may only make alterations to the Work if and as expressly set forth in the Order Confirmation. No Work may be used in any way that is defamatory, violates the rights of third parties (including such third parties' rights of copyright, privacy, publicity, or other tangible or intangible property), or is otherwise illegal, sexually explicit or obscene. In addition, User may not conjoin a Work with any other material that may result in damage to the reputation of the Rightsholder. User agrees to inform CCC if it becomes aware of any infringement of any rights in a Work and to cooperate with any reasonable request of CCC or the Rightsholder in connection therewith.

4. Indemnity. User hereby indemnifies and agrees to defend the Rightsholder and CCC, and their respective employees and directors, against all claims, liability, damages, costs and expenses, including legal fees and expenses, arising out of any use of a Work beyond the scope of the rights granted herein, or any use of a Work which has been altered in any unauthorized way by User, including claims of defamation or infringement of rights of copyright, publicity, privacy or other tangible or intangible property.

5. Limitation of Liability. UNDER NO CIRCUMSTANCES WILL CCC OR THE RIGHTSHOLDER BE LIABLE FOR ANY DIRECT, INDIRECT, CONSEQUENTIAL OR INCIDENTAL DAMAGES (INCLUDING WITHOUT LIMITATION DAMAGES FOR LOSS OF BUSINESS PROFITS OR INFORMATION, OR FOR BUSINESS INTERRUPTION) ARISING OUT OF THE USE OR INABILITY TO USE A WORK, EVEN IF ONE OF THEM HAS BEEN ADVISED OF THE POSSIBILITY OF SUCH DAMAGES. In any event, the total liability of the Rightsholder and CCC (including their respective employees and directors) shall not exceed the total amount actually paid by User for this license. User assumes full liability for the actions and omissions of its principals, employees, agents, affiliates, successors and assigns.

6. Limited Warranties. THE WORK(S) AND RIGHT(S) ARE PROVIDED "AS IS". CCC HAS THE RIGHT TO GRANT TO USER THE RIGHTS GRANTED IN THE ORDER CONFIRMATION DOCUMENT. CCC AND THE RIGHTSHOLDER DISCLAIM ALL OTHER WARRANTIES RELATING TO THE WORK(S) AND RIGHT(S), EITHER EXPRESS OR IMPLIED, INCLUDING WITHOUT LIMITATION IMPLIED WARRANTIES OF MERCHANTABILITY OR FITNESS FOR A PARTICULAR PURPOSE. ADDITIONAL RIGHTS MAY BE REQUIRED TO USE ILLUSTRATIONS, GRAPHS, PHOTOGRAPHS, ABSTRACTS, INSERTS OR OTHER PORTIONS OF THE WORK (AS OPPOSED TO THE ENTIRE WORK) IN A MANNER CONTEMPLATED BY USER; USER UNDERSTANDS AND AGREES THAT NEITHER CCC NOR THE RIGHTSHOLDER MAY HAVE SUCH ADDITIONAL RIGHTS TO GRANT.

7. Effect of Breach. Any failure by User to pay any amount when due, or any use by User of a Work beyond the scope of the license set forth in the Order Confirmation and/or these terms and conditions, shall be a material breach of the license created by the Order Confirmation and these terms and conditions. Any breach not cured within 30 days of written notice thereof shall result in immediate termination of such license without further notice. Any unauthorized (but licensable) use of a Work that is terminated immediately upon notice thereof may be liquidated by payment of the Rightsholder's ordinary license price therefor; any unauthorized (and unlicensable) use that is not terminated immediately for any reason (including, for example, because materials containing the Work cannot reasonably be recalled) will be subject to all remedies available at law or in equity, but in no event to a payment of less than three times the Rightsholder's ordinary license price for the most closely analogous licensable use plus Rightsholder's and/or CCC's costs and expenses incurred in collecting such payment.

8. **Miscellaneous.**

8.1 User acknowledges that CCC may, from time to time, make changes or additions to the Service or to these terms and conditions, and CCC reserves the right to send notice to the User by electronic mail or otherwise for the purposes of notifying User of such changes or additions; provided that any such changes or additions shall not apply to permissions already secured and paid for.

8.2 Use of User-related information collected through the Service is governed by CCC's privacy policy, available online here: http://www.copyright.com/content/cc3/en/tools/footer/privacypolicy.html.

8.3 The licensing transaction described in the Order Confirmation is personal to User. Therefore, User may not assign or transfer to any other person (whether a natural person or an organization of any kind) the license created by the Order Confirmation and these terms and conditions or any rights granted hereunder; provided, however, that User may assign such license in its entirety on written notice to CCC in the event of a transfer of all or substantially all of User's rights in the new material which includes the Work(s) licensed under this Service.

8.4 No amendment or waiver of any terms is binding unless set forth in writing and signed by the parties. The Rightsholder and CCC hereby object to any terms contained in any writing prepared by the User or its principals, employees, agents or affiliates and purporting to govern or otherwise relate to the licensing transaction described in the Order Confirmation, which terms are in any way inconsistent with any terms set forth in the Order Confirmation and/or in these terms and conditions or CCC's standard operating procedures, whether such writing is prepared prior to, simultaneously with or subsequent to the Order Confirmation, and whether such writing appears on a copy of the Order Confirmation or in a separate instrument.

8.5 The licensing transaction described in the Order Confirmation document shall be governed by and construed under the law of the State of New York, USA, without regard to the principles thereof of conflicts of law. Any case, controversy, suit, action, or proceeding arising out of, in connection with, or related to such licensing transaction shall be brought, at CCC's sole discretion, in any federal or state court located in the County of New York, State of New York, USA, or in any federal or state court whose geographical jurisdiction covers the location of the Rightsholder set forth in the Order Confirmation. The parties expressly submit to the personal jurisdiction and venue of each such federal or state court.If you have any comments or questions about the Service or Copyright Clearance Center, please contact us at 978-750-8400 or send an e-mail to info@copyright.com.

v 1.1

Close

Confirmation Number: 11778142

Citation Information

Order Detail ID: 71744022

Chemical Society reviews by Royal Society of Chemistry (Great Britain) Reproduced with permission of ROYAL SOCIETY OF CHEMISTRY in the format Thesis/Dissertation via Copyright Clearance Center.

Close

Journal Articles:

1. Fluorogenic Naked-Eye Sensing and Live-Cell Imaging of Cyanide by Hydrazine-Functionalized CAU-10 Metal-Organic Framework

   R. Dalapati, S. Nandi, H. Reinsch, B. K. Bhunia, B. B. Mandal, N. Stock, S. Biswas, *CrystEngComm*, 2018, **20**, 4194 - 4201.
2. Effect of Functional Groups in Aqueous-phase Selective Sensing of Fe(III) Ions by Thienothiophene-based Zirconium Metal-Organic Frameworks and Design of Molecular Logic Gates

   R. Dalapati, U. Koekcam-Demir, C. Janiak, S. Biswas, *Dalton Trans*., 2018, **47**, 1159.
3. A cerium-based Metal-organic Framework having Inherent Oxidase-like Activity Applicable for Colorimetric Sensing of Biothiols and Aerobic Oxidation of Thiols

   R. Dalapati, B. Sakthivel, A. Dhakshinamoorthy, S. Biswas, *CrystEngComm*, 2017, **19**, 5915.
4. A Dinitro-functionalized Zr(IV)-based Metal-Organic Framework as Colorimetric and Fluorogenic Probe for Highly Selective Detection of Hydrogen Sulphide

   R. Dalapati, S. N. Balaji, V. Trivedi, L. Khamari, S. Biswas, *Sens. Actuators, B*., 2017, **245**, 1039.
5. Post-synthetic Modification of a Metal-Organic Framework with Fluorescent-tag for Dual Naked-eye Sensing in Aqueous Medium

   R. Dalapati, S. Biswas, *Sens. Actuators, B*., 2017, **239**, 759.
6. A Highly Stable Dimethyl-functionalized Ce(IV)-based UiO-66 Metal-Organic Framework Material for Gas Sorption and Redox Catalysis

   R. Dalapati, B. Sakthivel, A. Dhakshinamoorthy, A. Buragohain, A. Bhunia, C. Janiak, S. Biswas, *CrystEngComm*, 2016, **18**, 7855.

Conferences Attended:

1. 25th ISCB International Conference (ISCBC-2019) Trends in Chemical and Biological Sciences: Impact on Health and Environment, Lucknow, India.
2. Conference on Frontiers in Chemical Sciences (FICS) -2018, Department of Chemistry, IIT Guwahati, Assam, India.

3. International Conference on Synthetic Potent Molecules and Its Application (ICSPMIA-2018), Sikkim Manipal Institute of Technology, Majitar, Sikkim, India.
4. 5th International Conference on Advanced Nanomaterials and Nanotechnology (ICANN-2017), Department of Chemistry, IIT Guwahati, Assam, India.
5. 29th Annual General Meeting of Materials Research Society of India and National Symposium on Advances in Functional and Exotic Materials, Bharathidasan University, Tiruchirappalli – 620024, India.
6. Conference on Frontiers in Chemical Sciences (FICS) -2016, Department of Chemistry, IIT Guwahati, Assam, India.

The End